nagra.

Arbeitsbericht NAB 21-20

TBO Marthalen-1-1: Data Report

Dossier VIII
Rock Properties, Porewater Characterisation and Natural Tracer Profiles

September 2021

U. Mäder, L. Aschwanden, L. Camesi,
T. Gimmi, A. Jenni, M. Kiczka, M. Mazurek,
D. Rufer, H.N. Waber, P. Wersin,
C. Zwahlen & D. Traber

National Cooperative
for the Disposal of
Radioactive Waste

Hardstrasse 73
P.O. Box 280
5430 Wettingen
Switzerland
Tel. +41 56 437 11 11

www.nagra.ch

nagra.

Arbeitsbericht NAB 21-20

TBO Marthalen-1-1: Data Report

Dossier VIII Rock Properties, Porewater Characterisation and Natural Tracer Profiles

September 2021

U. Mäder[1], L. Aschwanden[1], L. Camesi[1], T. Gimmi[1], A. Jenni[1], M. Kiczka[1], M. Mazurek[1], D. Rufer[1], H.N. Waber[1], P. Wersin[1], C. Zwahlen[1] & D. Traber[2]

[1] Rock-Water Interaction, Institute of Geological Sciences, University of Bern

[2] Nagra

Keywords:
MAR1-1, Zürich Nordost, TBO, deep drilling campaign, rock properties, petrophysical parameters, water content, porosity, mineralogy, clay content, clay mineral composition, sulphate minerals, porewater chemistry, natural tracer profiles

National Cooperative for the Disposal of Radioactive Waste

Hardstrasse 73
P.O. Box 280
5430 Wettingen
Switzerland
Tel. +41 56 437 11 11

www.nagra.ch

Nagra Arbeitsberichte ("Working Reports") present the results of work in progress that have not necessarily been subject to a comprehensive review. They are intended to provide rapid dissemination of current information.

This NAB aims at reporting drilling results at an early stage. Additional borehole-specific data will be published elsewhere.

In the event of inconsistencies between dossiers of this NAB, the dossier addressing the specific topic takes priority. In the event of discrepancies between Nagra reports, the chronologically later report is generally considered to be correct. Data sets and interpretations laid out in this NAB may be revised in subsequent reports. The reasoning leading to these revisions will be detailed there.

This Dossier was prepared by the Rock-Water Interaction Group of the University of Bern (authors are listed in the individual chapters). D. Traber was the responsible Nagra project manager.

The authors kindly acknowledge the laboratory work of:
P. Bähler, C. Pichler and P. Wanner efficiently produced a substantial part of the data presented in this report.
U. Eggenberger, J. Krbanjevic, M. Wolffers and J.W. Zucha provided data for mineralogical and elemental analyses as well as evaluation tools.
D. Rose, J. Richards and L. de Doliwa Zielinski performed the core sampling and processing of the lower half of the borehole.
P. Bähler and C. Pichler helped with core sampling for the upper half of the borehole.
Th. Siegenthaler expertly machined core samples for advective displacement experiments.
T. Oyama (CRIEPI, Japan) kindly collaborated in the context of porewater squeezing.

We also acknowledge the experimental and analytical work performed at Hydroisotop GmbH who performed a part of the isotope diffusive-exchange experiments.

We are also grateful for the excellent work of the drill-site team who reliably provided sealed and documented core samples according to our specifications.

N. Schwendener from IRM University of Bern provided X-ray CT scans of a substantial number of core samples, with support by L. Keller (ZHAW) for some of the CT sessions.

We thank P. Blaser and M. Unger for scientific editing and editorial work.

Text, clarity and discussions were improved by a thorough review by A. Gautschi.

Revised 3rd Feb. 2022: The layout of the title of Table 4.6-6 was corrected.

Table of Contents

List of Tables

List of Figures

Electronic Appendices

App. A Comprehensive data base with results of laboratory analyses (xls format)

App. B Detailed documentation of advective displacement experiments (xls format)

App. C Hydroisotop GmbH data report (pdf format)

Note: Appendix C is only included in the digital version of this report and can be found under the paper clip symbol. The Appendices A and B are available upon request.

1 Introduction

1.1 Context

To provide input for site selection and the safety case for deep geological repositories for radioactive waste, Nagra has drilled a series of deep boreholes ("Tiefbohrungen", TBO) in Northern Switzerland. The aim of the drilling campaign is to characterise the deep underground of the three remaining siting regions located at the edge of the Northern Alpine Molasse Basin (Fig. 1-1).

In this report, we present the results from the Marthalen-1-1 borehole.

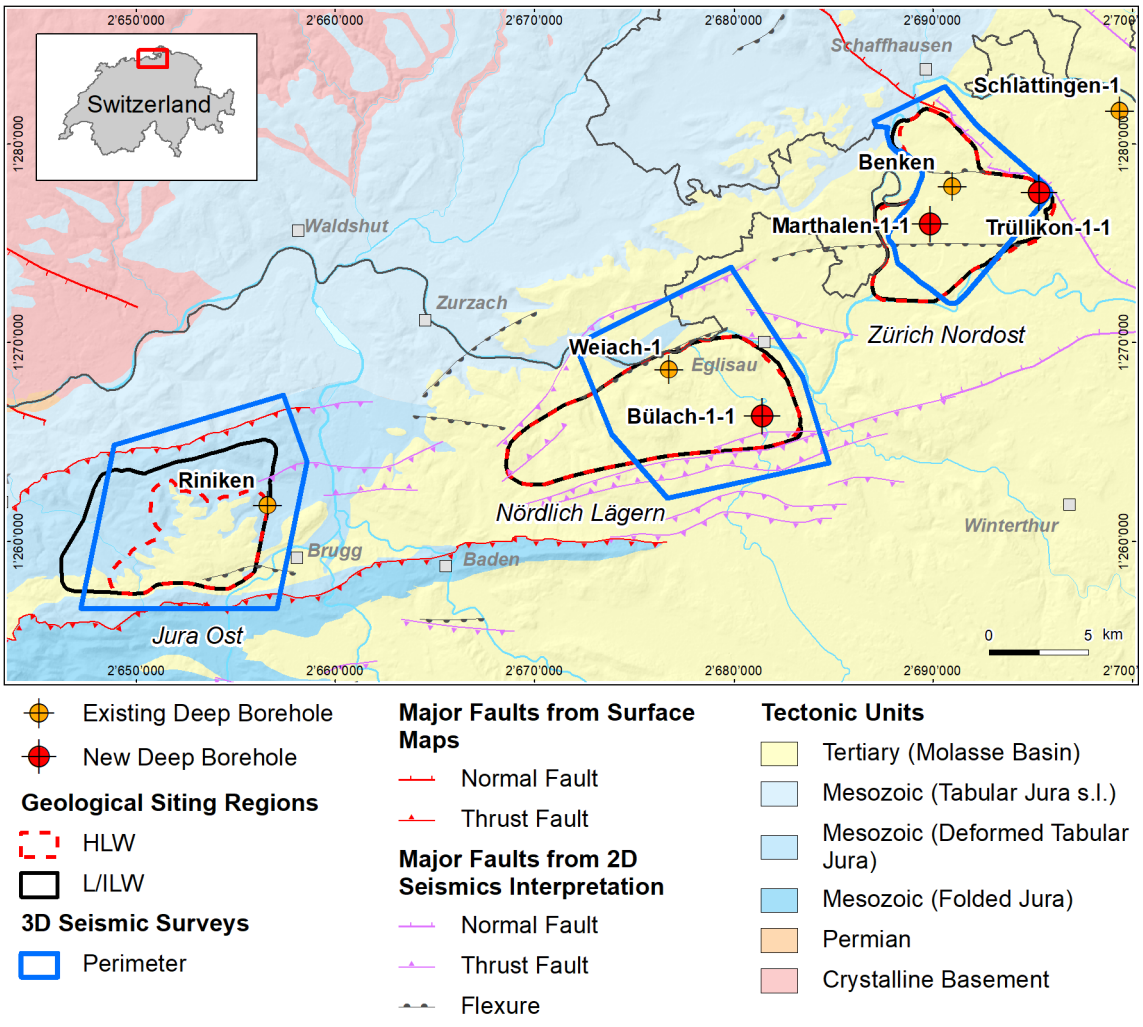

Fig. 1-1: Tectonic overview map with the three siting regions under investigation

1.2 Location and specifications of the borehole

The Marthalen-1-1 (MAR1-1) exploratory borehole is the third borehole drilled within the framework of the TBO project. The drill site is located in the western part of the Zürich Nordost siting region (Fig. 1-2). The vertical borehole reached a final depth of 1'099.25 m (MD)[1]. The borehole specifications are provided in Tab. 1-1.

Tab. 1-1: General information about the MAR1-1 borehole

Siting region	Zürich Nordost
Municipality	Marthalen (Canton Zürich / ZH), Switzerland
Drill site	Marthalen-1 (MAR1)
Borehole	Marthalen-1-1 (MAR1-1)
Coordinates	LV95: 2'689'889.946 / 1'275'956.932
Elevation	Ground level = top of rig cellar: 399.48 m above sea level (asl)
Borehole depth	1'099.25 m measured depth (MD) below ground level (bgl)
Drilling period	9th February 2020 – 14th July 2020 (spud date to end of rig release)
Drilling company	Daldrup & Söhne AG
Drilling rig	Wirth B 152t
Drilling fluid	Water-based mud with various amounts of different components such as[2]: 55 – 460 m: Bentonite & polymers 460 – 881 m: Potassium silicate & polymers 881 – 961 m: Sodium silicate & polymers 961 – 1'099.25 m: Sodium chloride & polymers

The lithostratigraphic profile and the casing scheme are shown in Fig. 1-3. The comparison of the core versus log depth[3] of the main lithostratigraphic boundaries in the MAR1-1 borehole is shown in Tab. 1-2.

[1] Measured depth (MD) refers to the position along the borehole trajectory, starting at ground level, which for this borehole is the top of the rig cellar. For a perfectly vertical borehole, MD below ground level (bgl) and true vertical depth (TVD) are the same. In all Dossiers depth refers to MD unless stated otherwise.

[2] For detailed information see Dossier I.

[3] Core depth refers to the depth marked on the drill cores. Log depth results from the depth observed during geophysical wireline logging. Note that the petrophysical logs have not been shifted to core depth, hence log depth differs from core depth.

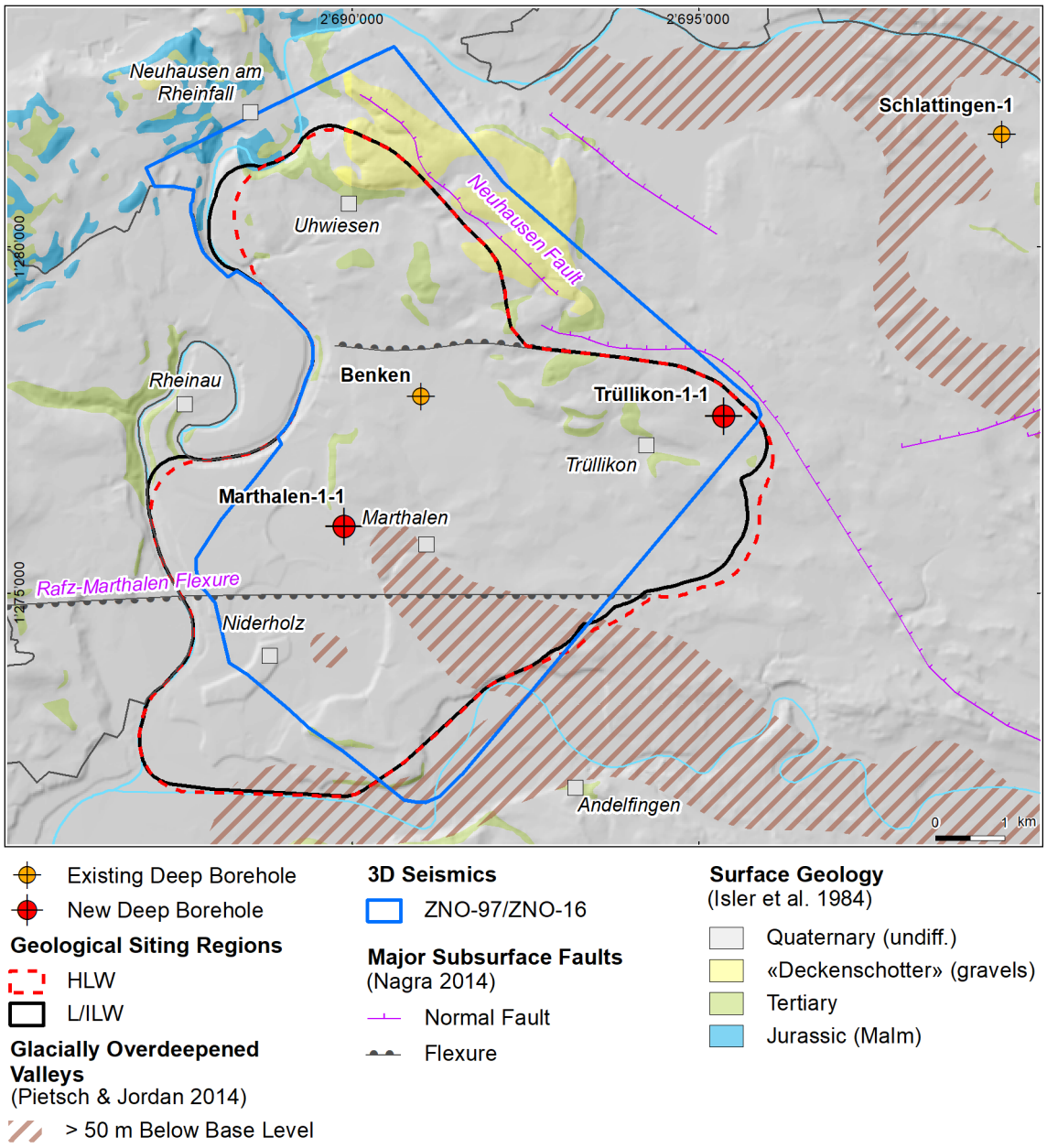

Fig. 1-2: Overview map of the investigation area in the Zürich Nordost siting region with the location of the MAR1-1 borehole in relation to the boreholes Benken, Schlattingen-1 and TRU1-1

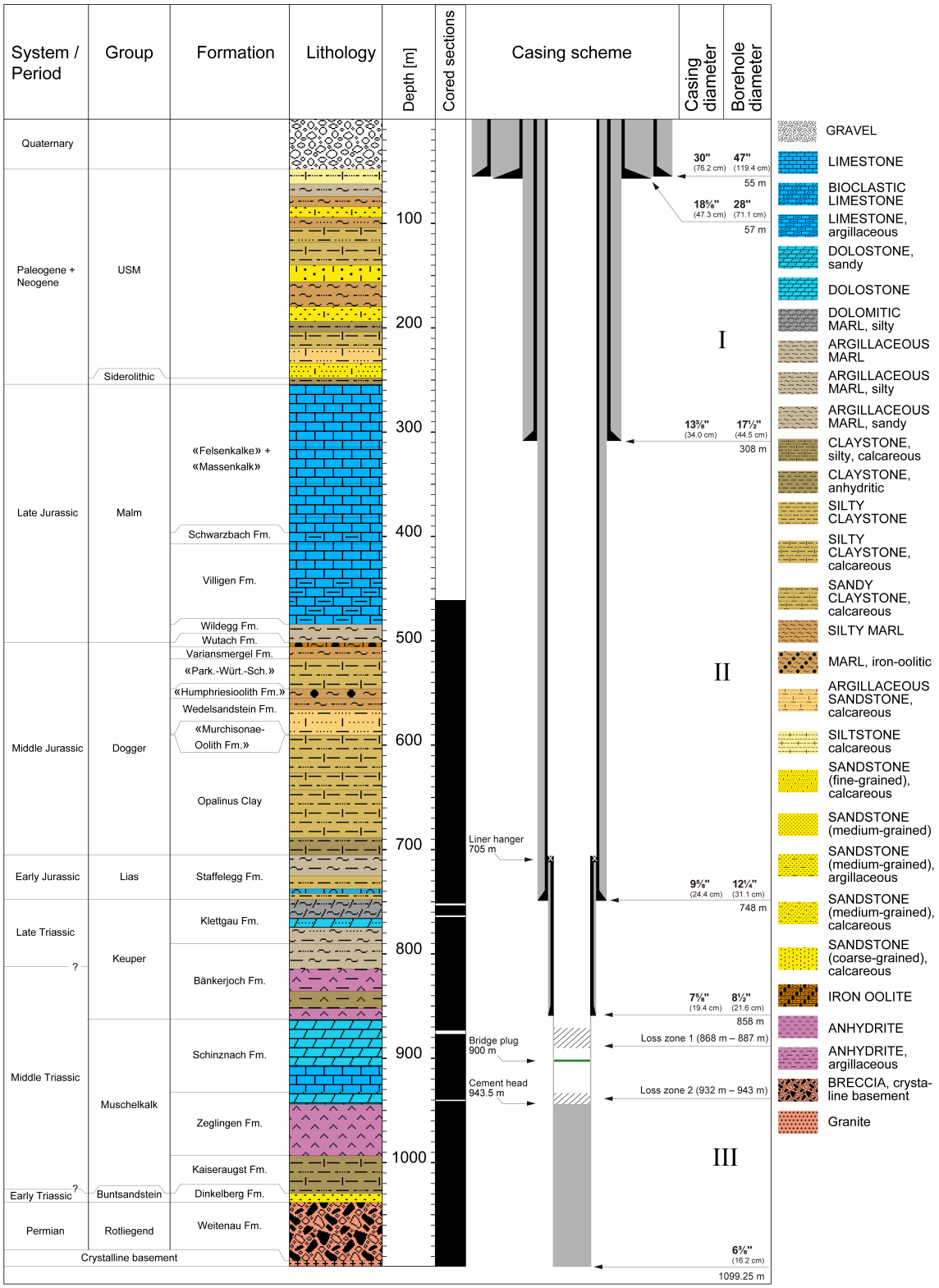

Fig. 1-3: Lithostratigraphic profile and casing scheme for the MAR1-1 borehole[4]

[4] For detailed information see Dossier I and III.

Tab. 1-2: Core and log depth for the main lithostratigraphic boundaries in the MAR1-1 borehole[5]

System / Period	Group	Formation	Core depth in m (MD)	Log depth in m (MD)	
Quaternary				**48**	—
Paleogene + Neogene	USM			248	—
	Siderolithic			**254**	—
Jurassic	Malm	«Felsenkalke» + «Massenkalk»		396.1	—
		Schwarzbach Formation		406.9	—
		Villigen Formation	484.02	484.22	—
		Wildegg Formation	501.80	501.92	—
	Dogger	Wutach Formation	505.75	506.03	—
		Variansmergel Formation	517.43	517.57	—
		«Parkinsoni-Württembergica-Schichten»	545.93	546.12	—
		«Humphriesioolith Formation»	555.23	555.47	—
		Wedelsandstein Formation	589.17	589.19	—
		«Murchisonae-Oolith Formation»	590.35	590.37	—
		Opalinus Clay	705.40	705.52	—
	Lias	Staffelegg Formation	**747.83**	**747.89**	—
Triassic	Keuper	Klettgau Formation	790.12	790.34	—
		Bänkerjoch Formation	862.52	862.77	—
	Muschelkalk	Schinznach Formation	932.24	932.47	—
		Zeglingen Formation	993.50	993.97	—
		Kaiseraugst Formation	1029.45	1029.95	—
	Buntsandstein	Dinkelberg Formation	**1037.98**	**1038.23**	—
Permian	Rotliegend	Weitenau Formation	**1094.08**	**1094.08**	—
		Crystalline Basement		1099.25 final depth	

[5] For details regarding lithostratigraphic boundaries see Dossier III and IV; for details about depth shifts (core goniometry) see Dossier V.

1.3 Documentation structure for the MAR1-1 borehole

NAB 21-20 documents the majority of the investigations carried out in the MAR1-1 borehole, including laboratory investigations on core material. The NAB comprises a series of stand-alone dossiers addressing individual topics and a final dossier with a summary composite plot (Tab. 1-3).

This documentation aims at early publication of the data collected in the MAR1-1 borehole. It includes most of the data available approximately one year after completion of the borehole. Some analyses are still ongoing (e.g. diffusion experiments, analysis of veins, hydrochemical interpretation of water samples) and results will be published in separate reports.

The current borehole report will provide an important basis for the integration of datasets from different boreholes. The integration and interpretation of the results in the wider geological context will be documented later in separate geoscientific reports.

Tab. 1-3: List of dossiers included in NAB 21-20

Black indicates the dossier at hand.

Dossier	Title	Authors
I	TBO Marthalen-1-1: Drilling	P. Hinterholzer-Reisegger & B. Garitte
II	TBO Marthalen-1-1: Core Photography	D. Kaehr & M. Gysi
III	TBO Marthalen-1-1: Lithostratigraphy	P. Jordan, P. Schürch, H. Naef, M. Schwarz, R. Felber, T. Ibele & M. Gysi
IV	TBO Marthalen-1-1: Microfacies, Bio- and Chemostratigraphic Analyses	S. Wohlwend, H.R. Bläsi, S. Feist-Burkhardt, B. Hostettler, U. Menkveld-Gfeller, V. Dietze & G. Deplazes
V	TBO Marthalen-1-1: Structural Geology	A. Ebert, L. Gregorczyk, E. Hägerstedt, S. Cioldi & M. Gysi
VI	TBO Marthalen-1-1: Wireline Logging and Micro-hydraulic Fracturing	J. Gonus, E. Bailey, J. Desroches & R. Garrard
VII	TBO Marthalen-1-1: Hydraulic Packer Testing	R. Schwarz, S.M.L. Hardie, H.R. Müller, S. Köhler & A. Pechstein
VIII	TBO Marthalen-1-1: Rock Properties, Porewater Characterisation and Natural Tracer Profiles	U. Mäder, L. Aschwanden, L. Camesi, T. Gimmi, A. Jenni, M. Kiczka, M. Mazurek, D. Rufer, H.N. Waber, P. Wersin, C. Zwahlen & D. Traber
IX	TBO Marthalen-1-1: Rock-mechanical and Geomechanical Laboratory Testing	E. Crisci, L. Laloui & S. Giger
X	TBO Marthalen-1-1: Petrophysical Log Analysis	S. Marnat & J.K. Becker
	TBO Marthalen-1-1: Summary Plot	Nagra

1.4 Scope and objectives of this dossier

The dossier at hand summarises the laboratory work of the Rock-Water Interaction Group (RWI) of the University of Bern, Institute of Geological Sciences, dedicated to rock and porewater characterisation of core materials obtained from the MAR1-1 borehole. The level of ambition is to document observations and measurements and to provide a quality-assured dataset. Closely related data obtained by other laboratories (e.g. data of stable water isotopes by Hydroisotop GmbH, CEC data by PSI) are integrated with our data.

Data are evaluated and discussed to some degree, including consistency and plausibility checks. An in-depth discussion, sophisticated modelling efforts and regional comparisons with data from other sites are beyond the scope of this report. Additional data obtained by other groups (e.g. hydraulic tests, groundwater sampling, geophysical borehole and core logging, structural logging) are considered in several cases but not in a comprehensive way. An integrated interpretation of all available data is deferred to a later stage of the TBO programme, when results from several boreholes can be synthesised for a siting region.

Throughout this report, rock samples used for analysis are identified by their mid-sample depth in m.

Note that in this report «Brauner Dogger» is used for the Dogger units overlying the Opalinus Clay *sensu lato*. In the Sectoral Plan Stages 1 and 2, «Brauner Dogger» is referred to the clay-rich rock sequence only (Nagra 2008).

2 Geoscientific data of interest and drilling conditions

Urs Mäder, Lukas Aschwanden

2.1 Geological information

As illustrated in Fig. 1-1, the MAR1-1 borehole is located in the south-central part of the Zürich Nordost siting region, which belongs tectonically to the autochthonous eastern Tabular Jura. The major tectonic structures in the area are the NW-SE trending Neuhausen Fault to the north-east of the region and the Rafz – Marthalen Flexure (Fig. 1-2). The Neuhausen Fault zone runs parallel to the Bonndorf – Hegau – Bodensee Graben that is known to cut the entire Mesozoic sediment stack. The Rafz – Marthalen Flexure is an E-W striking structure in the southern part of the region that is possibly associated with the northern margin of a Permo-Carboniferous trough.

A lithostratigraphic profile of the borehole is shown in Fig. 1-3. The Molasse section was percussion-drilled, and core drilling started in the limestones of the Malm. A continuous core profile is available to the final depth in the top of the crystalline basement, below the Permian.

2.2 Hydrogeological conditions

Ten hydraulic packer tests were conducted in the MAR1-1 borehole (Dossier VII), and selected results for the more permeable sections are summarised in Tab. 2.2-1. Hydraulic conductivities for the clay-rich section «Brauner Dogger» to Staffelegg Formation range from 3×10^{-14} to 1×10^{-13} m/s (best estimates). Enhanced hydraulic conductivities were identified in the Malm and Muschelkalk aquifers. The Keuper section is not very transmissive ($K = 3 \times 10^{-10}$ m/s) and did not yield sufficient groundwater for sampling, but its presence as an aquifer-like feature is evident in porewater chemical profiles.

Tab. 2.2-1: Results of selected hydraulic packer tests (aquifers only)

The best estimates for transmissivity T, hydraulic conductivity K and hydraulic head are indicated. Data are from Dossier VII.

Top [m MD]	**Bottom** [m MD]	**Length** [m]	**Geological units**	**T** [m^2/s]	**K** [m/s]	**Head** [m asl]
335.63	352.62	16.99	«Felsenkalke» + «Massenkalk» (Malm aquifer)	2×10^{-07}	1×10^{-08}	376
755.15	789.13	33.98	Klettgau Fm. (Keuper)	1×10^{-08}	3×10^{-10}	426
821.20	877.00	55.80	Schinznach Fm. (Muschelkalk aquifer)	8×10^{-05}	1×10^{-06}	383

Fluid logging was performed across the borehole section of the Malm aquifer (Dossier VII) to identify major inflow zones. Major inflows were inferred to occur from 318 – 328 m, and one with highest transmissivity from a narrower zone at 350 m.

2.3 Groundwater samples

Groundwater samples with variable degrees of drilling-fluid contamination were obtained from the Malm and Muschelkalk aquifers, but sampling was not possible for the Keuper aquifer (Tab. 2.2-1). For the present report, values for the chemically conservative parameters Cl and Br and the water-isotope ratios $\delta^{18}O$ and $\delta^{2}H$ are of interest, as these serve as boundary conditions for the porewater data. These values were corrected by Lorenz et al. (2021) for drilling fluid contamination and are reproduced in Tab. 2.3-1 along with information on the chemical water type and mineralisation of the groundwaters.

Tab. 2.3-1: Conservative parameters for waters from the Malm and Muschelkalk aquifers, measured values and corrected for drilling fluid contamination

Values represent analytical results of groundwater sampled towards the end of the pumping test and values corrected for contamination by drilling fluid (Lorenz et al. 2021). The chemical type relates to the measured fluid and does not necessarily correspond to the true groundwater type. Aquifer zone: interval used for plotting in depth profiles; adjusted for Muschelkalk interval to exclude the Bänkerjoch Formation.

Parameter		**Unit**	**Malm aquifer**	**Muschelkalk aquifer**
Chemical type	measured		Na-Cl-SO_4	K-Ca-SO_4
Mineralisation	measured	[g/L]	4.4	3.0
Chloride (Cl^-)	measured	[mg/L]	1'800	16.0
Chloride (Cl^-)	corrected	[mg/L]	1'910	8.7 – 21.9
Bromide (Br^-)	measured	[mg/L]	4.4	0.04
Bromide (Br^-)	corrected	[mg/L]	4.4	0.01 – 0.05
$\delta^{18}O$ of water	measured	[‰$_{VSMOW}$]	-8.63	-12.53
$\delta^{18}O$ of water	corrected	[‰$_{VSMOW}$]	-8.72	-12.43
$\delta^{2}H$ of water	measured	[‰$_{VSMOW}$]	-68.0	-90.0
$\delta^{2}H$ of water	corrected	[‰$_{VSMOW}$]	-68.5	-90.2 – -88.3
Test zone	depth	[m]	335.63 – 352.62	821.2 – 877.0
Aquifer zone	depth	[m]	335.63 – 352.62	862.52 – 877.0
Hydraulic conductivity, K		[m/s]	1×10^{-08}	1×10^{-06}

2.4 Structural logging

The results of structural core logging are documented in Dossier V, where the following features are distinguished:

- fault planes and fault zones (structures with shear indications)
- brittle extensional fractures (structures without shear or slip indications, e.g. fractures, tension gashes/veins and joints)
- stylolites
- open pores

The majority of all structures are found in the Keuper and in the Muschelkalk (Dossier V). A number of larger fault zones, i.e. zones with high densities of fault planes, were defined and are listed in Tab. 2.4-1.

Tab. 2.4-1: Fault zones in the cored section of the MAR1-1 borehole

From Dossier V.

Top [m MD]	**Bottom** [m MD log depth]	**Thickness** [m]	**Unit**
555.67	556.64	0.97	Wedelsandstein Fm.
606.28	606.43	0.15	Opalinus Clay
620.88	621.90	1.02	Opalinus Clay
676.49	676.52	0.03	Opalinus Clay
754.90	755.51	0.61	Klettgau Fm.
756.40	756.48	0.08	Klettgau Fm.
776.92	777.28	0.36	Klettgau Fm.
778.00	779.20	1.20	Klettgau Fm.
787.43	787.47	0.04	Klettgau Fm.
795.49	795.98	0.49	Bänkerjoch Fm.
804.98	805.21	0.23	Bänkerjoch Fm.
808.00	808.34	0.34	Bänkerjoch Fm.
815.22	815.44	0.22	Bänkerjoch Fm.
816.05	816.38	0.33	Bänkerjoch Fm.
817.76	818.38	0.62	Bänkerjoch Fm.
843.19	843.35	0.26	Bänkerjoch Fm.
941.68	941.73	0.05	Zeglingen Fm.
942.78	943.00	0.22	Zeglingen Fm.
943.58	944.46	0.88	Zeglingen Fm.
945.50	950.73	5.23	Zeglingen Fm.
950.73	950.91	0.18	Zeglingen Fm.
950.91	951.70	0.79	Zeglingen Fm.
1'010.49	1'010.63	0.14	Kaiseraugst Fm.
1'022.11	1'022.37	0.26	Kaiseraugst Fm.
1'022.67	1'022.83	0.16	Kaiseraugst Fm.
1'094.12	1'099.25	5.13	Crystalline basement

2.5 Drilling conditions and drilling muds

The drilling history of MAR1-1 comprises considerable losses of drilling mud at two depth intervals, and the use of four different kinds of drilling mud: bentonite polymer, potassium silicate, sodium silicate and saturated salt mud (Dossier I). Key information is listed in Tab. 2.5-1. The composition of the different drilling muds is given in Tab. 2.5-2. A total of 1'709 m^3 drilling fluid (50% silicate drilling fluid, 10% spacers and LCM (lost-circulation material added for blockage) pills and approximately 40% of sodium chloride) were lost in the two main fracture zones mentioned above, within the Schinznach Formation (Stamberg Member; 867.6 – 887.2 m)

and a zone comprising the very base of the Schinznach Formation (Leutschenberg and Kienberg Members) and the top of the Zeglingen Formation ('Dolomitzone'; 932.2 – 942.6 m). Drilling operations were hampered by these mud losses and many core-loss operations with various blocking materials had to be undertaken. Apart from mineral/solid/fiber additives, these materials also contain Xanthan gum, for example, and other conditioners for density and viscosity/rheology.

The borehole was cored below 460 m using a wireline coring technique with an inner core barrel and plastic liner. The main coring diameter was 6⅜", with a core diameter of 95 mm. The borehole is essentially vertical, with a total step-out of only 16 m N and E at final depth that occurred below 400 m. The last coring section, from 954 m to 1'099 m was retrieved and mapped but not sampled on-site and was therefore not analysed as part of our geochemical programme. There were no significant occurrences of hydrocarbon gases detected during continuous monitoring.

Tab. 2.5-1: Drilling muds and depth intervals, events and fracture zones

Depth interval [m MD]	**Geological unit**	**Drilling mud**	**Comments**
309 – 460	Malm	Bentonite+polymer	Destructive drilling
460 – 750	Malm – top Keuper	Potassium silicate	Exchange of bent+polymer by freshwater, then by K-silicate
750 – 869.8	Keuper – Schinznach Fm.	Potassium silicate	Total mud loss
869.8 – 877	Schinznach Fm.	Potassium silicate	Dynamic mud loss 320 – 650 l/min; fracture zone with vertical fractures; loss-control operations
877 – 881.5	Schinznach Fm.	Potassium silicate	Still dynamic losses; very limited core recovery; running out of K-silicate mud; stop of coring
881.5 – 881.9	Schinznach Fm.	Sodium silicate	Substitute K-silicate by Na-silicate; continued losses; more loss-control
881 – 888	Schinznach Fm.	Sodium silicate	Still losses; more loss-control
888 – 932	Schinznach Fm. – top Zeglingen Fm.	Sodium silicate	Increase in losses at 932 m; loss-control continued
932 – 961	Top Zeglingen Fm. – «Sulfatzone»	Sodium silicate	Continued losses
961	«Sulfatzone» of Muschelkalk	Sodium silicate / saturated salt	Sudden increase of Cl in drilling mud, from 3 g/l to 13 g/l; switch to saturated salt mud
961 – 1'054	«Sulfatzone» – Weitenau Fm.	saturated salt	Dynamic losses 60 – 100 l/min; provisional final depth
1'054 – 1'099	Weitenau Fm. – Crystalline Basement	saturated salt	Dynamic losses to end depth
867.6 – 887.2	Schinznach Fm.		**Upper loss zone**; determined by imaging and core material
932.2 – 942.6	Schinznach Fm. / Zeglingen Fm.		**Lower loss zone**; determined by imaging and core material

Tab. 2.5-2: Composition of drilling muds

Average analyses of selected components of fluid samples taken for the groundwater sampling campaigns. See Lorenz et al. (2021) for complete analyses.

Parameter	**Units**	**Bentonite + polymer**	**K-silicate**	**K-silicate**
Depth	[m]	380	460	842
pH [1]		9.3 – 10	12.5 – 13.5	12.5 – 13.5
pH		9.7	12.94	12.95
EC	[µS/cm]	11'900	104'000	105'500
uranine	[ppb]	1'050	714	1'560
TOC	[mg/L]	3'400	2'300	3'130
Na	[mg/L]	3'360	1'630	1'830
K	[mg/L]	33.8	120'000	117'000
NH_4	[mg/L]	< 1	~ 1	< 1
Ca	[mg/L]	108	270	400
Si	[mg/L]	176	65'000	74'400
Cl	[mg/L]	1'760	730	590
SO_4	[mg/L]	2.4	91	2'200
NO_3	[mg/L]	< 1	7.8	4.9

[1] Preparation of fresh drilling mud (Dossier I).

3 Sampling and applied methods

3.1 Sampling strategy

Martin Mazurek & Urs Mäder

A suite of different sample types as defined by Rufer (2019) were investigated, and Tab. 3.1-1 provides a summary. All samples arrived at RWI in a state according to the instructions, i.e. no single sample was inflated or showed other evidence of loss of tightness of the wrapping. Some samples had bedding-parallel fractures that were created after on-site conditioning.

Tab. 3.1-1: Sample types and sampling strategy

Sample type	**Main study targets**	**Sampling (by on-site team)**
PW (pore-water chemistry), RP (various rock properties)	Characterisation of rock and porewater	Sample lithology representative of the current lithofacies and the sampled core section (usually 3 m). Sampling with a regular spacing, in order to obtain a representative dataset
SQ (squeezing)	Characterisation of porewater chemistry	Focussed on clay-rich lithologies due to methodological constraints
AD (advective displacement)	Characterisation of porewater chemistry	Focussed on clay-rich lithologies due to methodological constraints
OD (out-diffusion)	Out-diffusion experiments (diffusion coefficient for Cl^-, Cl^- concentration in bulk porewater)	Focussed on clay-poor lithologies due to methodological constraints. Experiments are not part of this investigation
NG (noble gas analysis)	Concentrations and isotopic compositions of dissolved noble and reactive gases	Sampling with a regular spacing, with situational tightening of the sampling interval close to potentially water-conducting features. Reported separately.
GM (geomechanics)	Mineralogy and grain density of samples studied for their geo-mechanical properties by other laboratories	Representative sampling of the most relevant lithologies within the Opalinus Clay and the overlying Wedelsandstein Fm.
V (vein studies)	Petrography, structure and geochemistry of veins	Opportunistic sampling at later stages

3.2 Laboratory programme

Urs Mäder

A total of 193 core segments were prepared on-site and designated for our studies, not including samples for geomechanical tests (15 GM samples) and 50 samples for noble-gas analyses (NG) that are still ongoing. These latter two sample types followed separate workflows, but some supporting measurements were performed in our laboratories (e.g. mineralogy, water content, density). A substantial subset of theses 193 samples were analysed for geochemical and petro-physical characterisation (porewater: PW, RP), squeezing (SQ), advective displacement (AD) and

out-diffusion experiments (OD). The latter were not part of the standard Nagra investigations but were carried out on our own terms (part of a M.Sc. Thesis) and as a supplementary study in progress. Samples for vein studies (V) were sub-sampled later from lithologies containing veins and related features. In total, 215 samples were investigated in the RWI laboratories as part of the standard programme, and Tab. 3.2-1 provides an overview. In Tab. 3.2-2, the analytical programme for the various sample types is shown in more detail. BET analyses were not performed for the MAR1-1 programme.

Tab. 3.2-1: Numbers of samples analysed for the different geological units

In the case of the NG samples, the number refers to the number of samples for which samples had be prepared for outgassing. OD samples are noz counted as they are not part of the standard programme for MAR1-1.

Unit	**PW, RP**	**SQ**	**AD**	**OD**	**NG**	**GM**	**V**	**Total**
Malm	6				5		2	13
«Brauner Dogger»	25	2	2		8	1		38
Opalinus Clay	38	3	2		11	14	6	74
Staffelegg Fm.	14	1	2		4		4	25
Klettgau Fm.	7		1		4		1	13
Bänkerjoch Fm.	7	2			5			14
Schinznach Fm.	7			(4 *)	5		2	14
Zeglingen Fm.	7				4			11
Kaiseraugst Fm.	3	1	1		2		2	9
Dinkelberg Fm.				(1 **)				0
Weitenau Fm.	2			(4 **)	2			4
All	**116**	**9**	**8**	**(9)**	**50**	**15**	**17**	**215**

* Experiments carried out as part of a completed M.Sc. Thesis.

** Experiments carried out, but analytical work not yet decided on.

Tab. 3.2-2: Analytical programme performed for the different sample types

××= standard programme, × = selected samples only, calc. = calculated.

Method	**PW, RP**	**SQ**	**AD**	**OD**	**NG**	**GM**	**V**
Bulk mineralogical composition including CNS analysis	××	××	××	××		××	
Clay mineralogy	×		××	×			
Bulk wet density	××		calc.	calc.			
Grain density	××		calc.	×		××	
Water content	××	××	××	××	××		
Cation-exchange properties (Ni-en method)			××				
Aqueous extraction	××	××	××	××			
Pore-water squeezing		××					
Advective displacement of porewater			××				
Out-diffusion				××			
Stable water isotopes	××	××	××	×			
Dissolved noble gases					××		
Dissolved reactive gases					×		

3.3 Analytical methods

Martin Mazurek

Experimental procedures, analytical methods and data processing, including error calculations, are documented in Waber (ed.) (2020) and are not repeated here. Any deviations or more details are given in the respective Chapter 4 sections.

3.4 Methods of raw-data processing

Thomas Gimmi & Martin Mazurek

Approaches and formalisms to evaluate and process measured data are also documented in Waber (ed.) (2020), including formalisms for the quantification of propagated errors. This information is not repeated here, but additional information is provided for situations where the current practice is not documented or deviates from that described in Waber (ed.) (2020).

Corrections for high salinities were not required for this dataset. Such corrections were developed for saline samples from the BUL1-1 dataset and are documented in Mazurek et al. (2021).

The evaluation of diffusive-exchange experiments for obtaining the ratios of stable isotopes of water was slightly adjusted compared to the documentation in Waber (ed.) (2020). This revised procedure is documented in Chapter 3 of the BUL1-1 data report by Mazurek et al. (2021).

4 Results

4.1 Documentation of measured and calculated data

Martin Mazurek, Lukas Aschwanden & Urs Mäder

Raw data collected by the two different laboratories (University of Bern, Hydroisotop GmbH) in the framework of the analytical programme of MAR are organised in a FileMaker data base, including raw-data files (e.g. XRD quantification not corrected for C/N/S analysis), graphics (e.g. XRD patterns) and photographs. The main purpose of this data base is to ensure the full documentation and traceability of original and derived data presented in this report. From this data base, the relevant data were exported into a comprehensive Excel sheet, which is attached as Appendix A (Excel file). The full dataset for advective displacement experiments are provided as Appendix B (Excel file). The full dataset of Hydroisotop GmbH is provided in their data report in the electronic Appendix C.

The objective of the Excel summary sheet is not to fully document all analyses made but, per parameter and sample, to indicate the best or most representative value in case multiple measurements were made, and to list parameters calculated from the original measurements. For example, only one composition is given for squeezed and advectively displaced porewaters in a sample, even though multiple aliquots were collected and analysed. Explanatory notes for this sheet follow here.

Measurements on cation exchange capacity and selectivity were mostly performed by PSI. This data is partially integrated into Chapter 5.7, with reference to a stand-alone data report issued by PSI, and along with our own measurements on few selected samples. These data are also integrated in the Excel summary sheet in Appendix A.

Bulk mineralogy (X-ray diffraction and CNS analysis)

- Contents of minerals not detected by X-ray diffraction are set to 0, as the actual detection limits are difficult to quantify. 'tr' = present in trace amounts.
- Clay-mineral content is not measured directly but is calculated by difference to 100%.
- Pyrite content is calculated from the measured S content, assuming that pyrite is the main S reservoir in the rock. This is not the case in anhydrite-bearing rocks, which are typically free of pyrite. Here, the S is used to calculate the content of anhydrite.
- Column 'Füchtbauer name' refers to the nomenclature of clastic rocks as defined in Naef et al. (2019). Names are listed only for rock compositions that have < 10 wt.-% minerals not represented in the Füchtbauer triangle (i.e. minerals other than clays, calcite, dolomite/ ankerite, siderite, quartz, K-feldspar, plagioclase). In particular, this means that evaporitic rocks are not given a Füchtbauer name. If a rock contains ≥ 90 wt.-% minerals represented in the Füchtbauer triangle but also contains anhydrite, this is stated in brackets.

Clay mineral groups

- All data refer to wt.-% of the total rock.
- Illite/smectite ML (85-90) refers to a mixed-layer phase with 85 – 90% illite layers, Chl/Sm ML (85-95) designates a chlorite-smectite mixed-layer phase with 85 – 95% chlorite (analogous for the other listed mixed-layer phases).

End-member clays

- All data refer to wt.-% of the total rock.
- Illite, smectite and chlorite partially occur in mixed-layer phases. Here, the respective total contents of the end-members are calculated. For example, if a sample contains 10 wt.-% illite and 8 wt.-% illite/smectite mixed layers containing 75% illite, the end-member illite content would be 16 wt.-%.

Petrophysical parameters

- Bulk wet density was measured, and bulk dry density was calculated using equation 5-14 in Waber (ed.) (2020).
  - Pycnometer porosity was calculated from densities using equation 5-16 in Waber (ed.) (2020).
  - Water content (dry) was calculated from water content (wet) using $w_d = w_w/(1-w_w)$.
  - Water-loss porosity was calculated using bulk wet density (equation 5-9 in Waber ed. 2020) or grain density (equation 5-7 in Waber ed. 2020).
  - The formalisms to calculate water content from isotope diffusive-exchange experiments are detailed in Mazurek et al. (2021).

Chloride and bromide from aqueous extracts recalculated to porewater concentrations using water content

- Concentrations are given relative to bulk porewater as well as relative to various assumptions regarding anion accessibility in the pore space. The calculation is made using equation 6-1 in in Waber (ed.) (2020). The variants pertaining to the dependence of anion accessibility on the clay-mineral content are discussed in Chapter 5.

Errors

- The error columns refer to analytical uncertainty or instrument precision for measured parameters and to propagated errors for calculated parameters, following the formalisms documented in Waber (ed.) (2020).

4.2 Mineralogical composition

Martin Mazurek, Lukas Aschwanden & Urs Mäder

4.2.1 Whole rock data

A total of 108 mineralogical analyses were performed in the section Malm – Permian. The full dataset is documented in Appendix A, and Tab. 4.2-1 provides formation-specific summaries. The depth trends for the most relevant minerals are shown graphically in Fig. 4.2-1, and a representation in the Füchtbauer triangle is given in Fig. 4.2-3. Clay-mineral contents are low in the Malm but become substantially larger, even though heterogeneous, in the underlying «Brauner Dogger». The Wedelsandstein Formation is particularly rich in quartz, but the clay-mineral content may exceed 50 wt.-% in some beds. In the Opalinus Clay, clay-mineral contents are mostly > 40 wt.-% and tend to increase with depth. Again, more heterogeneity characterises the Staffelegg Formation and the underlying Triassic. In the Triassic, the highly variable contents of anhydrite and dolomite are the main contributors to the lithological heterogeneity. One sample from the Gansingen Member of the Klettgau Formation contains 10 wt.-% celestite in diagenetic concretions. The Schinznach Formation consists of almost pure carbonates, with variable ratios of calcite to dolomite. The Permian Weitenau Formation is dominated by clastic minerals, i.e. quartz, feldspars and clay minerals, and thus corresponds to argillaceous siltstones/sandstones/ conglomerates in the Füchtbauer nomenclature.

The depth profiles of the contents of S and N (based on CNS analysis) are shown in Fig. 4.2-2. S contents are below detection in the limestones of the Villigen Formation, the dolostones and limestones of the Schinznach Formation (except in the sample from the Asp Member, the former 'Lettenkohle', with a particularly high S content) and the argillaceous siltstones of the Weitenau Formation (the former 'Rotliegendes'). These units have in common that the depositional environment was not strongly reducing or even oxidising, such that no early diagenetic precipitation of pyrite occurred. In clay-bearing to clay-rich units («Brauner Dogger» to Staffelegg Formation, Kaiseraugst Formation), S contents typically vary in the range 0.1 – 1 wt.-% and can be attributed to diagenetic pyrite. The one high value in the Staffelegg Formation comes from the Rietheim Member ('Posidonienschiefer') and correlates with the high content of organic C in this sample. All other samples with high S contents are due to the presence of anhydrite in the Klettgau, Bänkerjoch and Zeglingen Formations.

The contents of N are < 0.08 wt.-%, except for 2 high values in the Rietheim Member of the Staffelegg Formation. A positive correlation is identified between the N and C(org) contents, which suggests an association of N to the organic matter. Values above the detection limit of 0.01 wt.-% are limited to the Dogger – Lias section, plus one single value in the uppermost Bänkerjoch Formation.

Tab. 4.2-1: Bulk-rock mineralogy: formation-specific means, medians, standard devations and ranges [wt.-%]

For the calculation of statistical parameters, values below detection were set to 0. In several cases, systematic depth trends of mineral contents are observed (see below). This means that in these cases the data do not follow a Gaussian distribution, which is a pre-requisite for the calculation of meaningful standard deviations. In such cases, the ranges (also listed) are more meaningful.

Formation (number of analyses)	**Member**		**S** [wt.-%]	**N** [wt.-%]	**C(inorg)** [wt.-%]	**C(org)** [wt.-%]	**Quartz** [wt.-%]	**K-feldspar** [wt.-%]	**Plagioclase** [wt.-%]	**Calcite** [wt.-%]	**Dolomit/Ank.erite** [wt.-%]	**Siderite** [wt.-%]	**Anhydrite** [wt.-%]	**Celestite** [wt.-%]	**Pyrite** [wt.-%]	**Clay minerals** [wt.-%]
Villigen Fm. (3)		Mean	0.00	0.00	11.01	0.29	0.7	0.7	0.0	91.0	0.7	0.0	0.0	0.0	0.0	6.7
		Median	0.00	0.00	11.27	0.27	0.0	0.0	0.0	93.9	0.0	0.0	0.0	0.0	0.0	5.8
		Stdev	0.00	0.00	0.61	0.13	1.2	1.2	0.0	6.4	1.3	0.0	0.0	0.0	0.0	2.8
		Min	0.00	0.00	10.32	0.17	0.0	0.0	0.0	83.6	0.0	0.0	0.0	0.0	0.0	4.4
		Max	0.00	0.00	11.45	0.44	2.0	2.0	0.0	95.4	2.2	0.0	0.0	0.0	0.0	9.8
Wildegg Fm. (3)		Mean	0.20	0.00	7.48	0.40	7.0	3.7	1.0	56.6	5.3	0.0	0.0	0.0	0.4	25.7
		Median	0.29	0.00	7.58	0.40	6.0	4.0	1.0	57.0	5.7	0.0	0.0	0.0	0.5	24.9
		Stdev	0.18	0.00	0.27	0.03	2.6	0.6	0.0	6.4	4.0	0.0	0.0	0.0	0.3	2.0
		Min	0.00	0.00	7.18	0.37	5.0	3.0	1.0	50.0	1.1	0.0	0.0	0.0	0.0	24.1
		Max	0.32	0.00	7.69	0.43	10.0	4.0	1.0	62.8	9.1	0.0	0.0	0.0	0.6	28.0
Variansmergel Fm. (4)		Mean	0.67	0.03	2.73	0.82	16.8	5.3	1.8	21.3	1.3	0.0	0.0	0.0	1.3	51.5
		Median	0.68	0.04	1.98	0.77	17.0	5.5	2.0	16.5	1.0	0.0	0.0	0.0	1.3	55.1
		Stdev	0.19	0.02	1.81	0.15	3.7	1.0	0.5	14.9	1.6	0.0	0.0	0.0	0.3	10.9
		Min	0.45	0.00	1.53	0.68	12.0	4.0	1.0	9.1	0.0	0.0	0.0	0.0	0.8	35.8
		Max	0.88	0.04	5.43	1.04	21.0	6.0	2.0	43.1	3.3	0.0	0.0	0.0	1.6	60.2
«Parkinsoni-Württ.-Sch.» (11)		Mean	0.68	0.01	2.99	0.70	20.2	5.8	2.6	22.3	2.0	0.2	0.0	0.0	1.3	45.0
		Median	0.63	0.00	2.59	0.70	18.0	6.0	3.0	18.6	2.7	0.0	0.0	0.0	1.2	50.4
		Stdev	0.25	0.02	1.01	0.16	6.0	0.8	0.5	8.6	1.5	0.6	0.0	0.0	0.5	11.4
		Min	0.18	0.00	1.87	0.44	16.0	4.0	2.0	12.7	0.0	0.0	0.0	0.0	0.3	23.2
		Max	1.05	0.05	5.10	0.90	37.0	7.0	3.0	39.0	4.0	2.1	0.0	0.0	2.0	56.9
«Humphriesiool. Fm.» (1)		Mean	0.00	0.00	7.39	0.29	19.0	4.0	1.0	61.6	0.0	0.0	0.0	0.0	0.0	14.1
Wedelsandstein Fm. (12)		Mean	0.43	0.01	2.07	0.53	40.2	6.6	3.5	17.1	0.2	0.0	0.0	0.0	0.7	31.1
		Median	0.43	0.00	1.74	0.59	38.5	7.0	4.0	14.3	0.0	0.0	0.0	0.0	0.8	28.7
		Stdev	0.25	0.02	0.79	0.21	9.4	1.0	0.8	6.5	0.4	0.0	0.0	0.0	0.5	11.1
		Min	0.00	0.00	1.14	0.00	23.3	4.9	2.0	9.5	0.0	0.0	0.0	0.0	0.0	17.6
		Max	0.95	0.04	3.64	0.74	58.0	8.0	4.0	30.3	1.1	0.0	0.0	0.0	1.8	55.7
'Murch.-Oolith Fm.' (1)		Mean	0.61	0.03	0.91	1.16	39.0	5.0	4.0	7.0	0.0	0.7	0.0	0.0	1.1	42.1
Opalinus Clay (25)	All	Mean	0.45	0.05	1.32	1.11	21.4	5.4	2.6	9.2	0.1	2.0	0.0	0.0	0.8	57.5
		Median	0.39	0.06	1.19	1.16	22.4	5.0	3.0	7.8	0.0	2.5	0.0	0.0	0.7	57.4
		Stdev	0.22	0.02	0.60	0.18	4.4	0.7	1.3	4.9	0.4	1.8	0.0	0.0	0.4	8.1
		Min	0.16	0.00	0.65	0.78	13.0	4.0	0.0	3.3	0.0	0.0	0.0	0.0	0.3	35.3
		Max	1.06	0.07	3.07	1.41	28.0	7.0	4.0	23.7	2.1	5.3	0.0	0.0	2.0	69.8
Opalinus Clay (7)	Sub-unit with silty calcareous beds	Mean	0.54	0.05	1.63	1.07	23.8	5.4	2.3	13.0	0.3	0.3	0.0	0.0	1.0	52.7
		Median	0.46	0.05	1.24	1.01	25.0	5.2	2.8	10.3	0.0	0.0	0.0	0.0	0.9	55.4
		Stdev	0.28	0.01	0.95	0.16	3.3	0.5	1.1	7.0	0.8	0.8	0.0	0.0	0.5	10.5
		Min	0.23	0.03	0.78	0.88	17.2	5.0	0.0	6.5	0.0	0.0	0.0	0.0	0.4	35.3
		Max	1.06	0.07	3.07	1.28	27.0	6.0	3.0	23.7	2.1	2.2	0.0	0.0	2.0	66.6

Tab. 4.2-1: continued

Formation (number of analyses)	**Member**		**S** [wt.-%]	**N** [wt.-%]	**C(inorg)** [wt.-%]	**C(org)** [wt.-%]	**Quartz** [wt.-%]	**K-feldspar** [wt.-%]	**Plagioclase** [wt.-%]	**Calcite** [wt.-%]	**Dolomit/Ank.erite** [wt.-%]	**Siderite** [wt.-%]	**Anhydrite** [wt.-%]	**Celestite** [wt.-%]	**Pyrite** [wt.-%]	**Clay minerals** [wt.-%]
Opalinus Clay (3)	Upper silty sub-unit	Mean	0.53	0.05	1.17	1.13	24.3	6.0	3.7	9.0	0.0	0.9	0.0	0.0	1.0	54.0
		Median	0.54	0.05	1.19	1.16	23.0	6.0	4.0	9.9	0.0	0.0	0.0	0.0	1.0	55.3
		Stdev	0.16	0.01	0.13	0.06	3.2	1.0	0.6	2.4	0.0	1.6	0.0	0.0	0.3	4.4
		Min	0.37	0.04	1.03	1.06	22.0	5.0	3.0	6.3	0.0	0.0	0.0	0.0	0.7	49.2
		Max	0.68	0.06	1.29	1.16	28.0	7.0	4.0	10.8	0.0	2.7	0.0	0.0	1.3	57.6
Opalinus Clay (10)	Mixed clay-silt-carbonate sub-unit	Mean	0.34	0.06	1.14	1.18	21.9	5.5	2.6	6.7	0.0	3.2	0.0	0.0	0.6	58.2
		Median	0.29	0.06	1.09	1.26	22.5	5.7	3.0	7.4	0.0	3.3	0.0	0.0	0.5	57.1
		Stdev	0.16	0.02	0.35	0.20	3.6	0.6	1.4	2.3	0.0	1.4	0.0	0.0	0.3	6.3
		Min	0.16	0.00	0.65	0.78	17.0	4.5	0.0	3.3	0.0	0.0	0.0	0.0	0.3	48.1
		Max	0.61	0.07	1.78	1.41	26.8	6.0	4.0	10.2	0.0	5.3	0.0	0.0	1.1	69.8
Opalinus Clay (5)	Clay-rich sub-unit	Mean	0.50	0.05	1.30	1.00	15.3	4.7	2.1	8.7	0.0	2.4	0.0	0.0	0.9	64.8
		Median	0.62	0.06	1.24	0.97	15.0	5.0	2.3	7.8	0.0	2.9	0.0	0.0	1.2	65.6
		Stdev	0.21	0.03	0.50	0.18	2.2	0.4	1.2	3.7	0.0	1.4	0.0	0.0	0.4	3.0
		Min	0.25	0.00	0.85	0.79	13.0	4.0	0.0	5.8	0.0	0.0	0.0	0.0	0.5	59.7
		Max	0.72	0.07	2.13	1.25	19.0	5.0	3.0	15.1	0.0	3.7	0.0	0.0	1.4	67.1
Staffelegg Fm. (10)		Mean	0.60	0.05	2.32	1.78	17.6	3.7	2.0	18.2	0.2	0.8	0.0	0.0	1.1	54.5
		Median	0.34	0.04	0.96	0.87	17.0	4.0	2.0	6.3	0.0	0.5	0.0	0.0	0.6	53.0
		Stdev	0.90	0.07	2.65	2.15	8.4	1.8	1.2	21.9	0.7	1.1	0.0	0.0	1.7	17.0
		Min	0.14	0.00	0.00	0.35	7.0	0.0	0.0	0.0	0.0	0.0	0.0	0.0	0.3	33.1
		Max	3.11	0.19	6.42	6.74	31.0	6.0	4.0	51.0	2.4	2.9	0.0	0.0	5.8	84.2
Klettgau Fm. (8)		Mean	0.61	0.00	3.98	0.13	17.6	6.0	3.3	6.5	26.0	0.0	1.6	1.3	0.0	38.9
		Median	0.00	0.00	3.55	0.11	13.0	5.0	4.0	0.5	23.6	0.0	0.0	0.0	0.0	37.6
		Stdev	1.69	0.00	4.09	0.08	12.4	6.7	2.2	10.6	22.1	0.0	4.5	3.7	0.0	17.2
		Min	0.00	0.00	0.00	0.05	7.0	0.0	0.0	0.0	0.0	0.0	0.0	0.0	0.0	5.8
		Max	4.80	0.00	10.91	0.28	44.0	16.0	6.0	29.9	56.1	0.0	12.7	10.3	0.1	56.4
Bänker-joch Fm. (9)		Mean	8.16	0.00	1.39	0.16	5.3	2.6	0.6	0.5	10.1	0.0	34.4	0.0	0.1	46.1
		Median	7.00	0.00	0.31	0.10	3.0	0.0	0.0	0.0	2.4	0.0	29.7	0.0	0.0	52.5
		Stdev	8.42	0.01	1.77	0.12	4.9	4.0	0.9	1.0	13.4	0.0	36.0	0.0	0.2	19.1
		Min	0.00	0.00	0.03	0.05	0.0	0.0	0.0	0.0	0.0	0.0	0.0	0.0	0.0	10.4
		Max	21.00	0.03	5.06	0.37	13.7	9.5	2.0	2.4	38.9	0.0	89.2	0.0	0.5	67.2
Schinz-nach Fm. (7)	All	Mean	0.58	0.00	10.28	0.36	5.6	0.0	0.0	22.4	58.2	0.0	0.0	0.0	1.1	12.4
		Median	0.00	0.00	12.01	0.22	2.0	0.0	0.0	0.0	67.7	0.0	0.0	0.0	0.0	3.7
		Stdev	1.54	0.00	4.54	0.40	9.5	0.0	0.0	32.2	39.5	0.0	0.0	0.0	2.9	23.0
		Min	0.00	0.00	0.05	0.11	1.0	0.0	0.0	0.0	0.0	0.0	0.0	0.0	0.0	0.0
		Max	4.07	0.00	12.88	1.26	27.0	0.0	0.0	81.7	98.9	0.0	0.0	0.0	7.6	64.1
Schi Fm., Asp Mb. (1)		Mean	4.07	0.00	0.05	1.26	27.0	0.0	0.0	0.0	0.0	0.0	0.0	0.0	7.6	64.1
Schinz-nach Fm. (3)	Stamberg Mb.	Mean	0.00	0.00	12.12	0.26	2.3	0.0	0.0	0.0	93.0	0.0	0.0	0.0	0.0	4.4
		Median	0.00	0.00	12.05	0.22	3.0	0.0	0.0	0.0	92.5	0.0	0.0	0.0	0.0	4.3
		Stdev	0.00	0.00	0.73	0.08	1.2	0.0	0.0	0.0	5.6	0.0	0.0	0.0	0.0	4.5
		Min	0.00	0.00	11.43	0.21	1.0	0.0	0.0	0.0	87.8	0.0	0.0	0.0	0.0	0.0
		Max	0.00	0.00	12.88	0.36	3.0	0.0	0.0	0.0	98.9	0.0	0.0	0.0	0.0	8.9

Tab. 4.2-1: continued

Formation (number of analyses)	**Member**		**S** [wt.-%]	**N** [wt.-%]	**C(inorg)** [wt.-%]	**C(org)** [wt.-%]	**Quartz** [wt.-%]	**K-feldspar** [wt.-%]	**Plagioclase** [wt.-%]	**Calcite** [wt.-%]	**Dolomit/Ank.erite** [wt.-%]	**Siderite** [wt.-%]	**Anhydrite** [wt.-%]	**Celestite** [wt.-%]	**Pyrite** [wt.-%]	**Clay minerals** [wt.-%]
Schinznach Fm. (3)	Liedertswil, Leutschenberg & Kienberg Mb.	Mean	0.00	0.00	11.84	0.17	1.7	0.0	0.0	52.3	42.7	0.0	0.0	0.0	0.0	3.1
		Median	0.00	0.00	12.01	0.16	2.0	0.0	0.0	48.0	48.0	0.0	0.0	0.0	0.0	2.9
		Stdev	0.00	0.00	0.36	0.05	0.6	0.0	0.0	27.5	28.0	0.0	0.0	0.0	0.0	0.5
		Min	0.00	0.00	11.43	0.11	1.0	0.0	0.0	27.3	12.5	0.0	0.0	0.0	0.0	2.8
		Max	0.00	0.00	12.09	0.22	2.0	0.0	0.0	81.7	67.7	0.0	0.0	0.0	0.0	3.7
Zeglingen Fm. (7)	All	Mean	16.29	0.00	2.30	0.06	1.0	0.0	0.1	0.0	17.5	0.0	69.2	0.0	0.0	12.1
		Median	18.00	0.00	0.73	0.05	0.0	0.0	0.0	0.0	5.6	0.0	76.4	0.0	0.0	5.2
		Stdev	7.50	0.00	4.44	0.04	1.5	0.0	0.4	0.0	34.2	0.0	31.8	0.0	0.0	11.6
		Min	0.00	0.00	0.12	0.02	0.0	0.0	0.0	0.0	0.0	0.0	0.0	0.0	0.0	1.1
		Max	22.00	0.00	12.35	0.14	4.0	0.0	1.0	0.0	94.8	0.0	93.4	0.0	0.0	27.9
Zegl. Fm., 'Dol.-Z.' (1)		Mean	0.00	0.00	12.35	0.14	4.0	0.0	0.0	0.0	94.8	0.0	0.0	0.0	0.0	1.1
Zeglingen Fm. (6)	«Obere Sulfatzone»	Mean	19.00	0.00	0.62	0.05	0.5	0.0	0.2	0.0	4.6	0.0	80.7	0.0	0.0	14.0
		Median	19.00	0.00	0.57	0.05	0.0	0.0	0.0	0.0	4.4	0.0	80.7	0.0	0.0	10.0
		Stdev	2.37	0.00	0.37	0.02	0.8	0.0	0.4	0.0	3.1	0.0	10.0	0.0	0.0	11.5
		Min	16.00	0.00	0.12	0.02	0.0	0.0	0.0	0.0	0.0	0.0	67.9	0.0	0.0	3.3
		Max	22.00	0.00	1.07	0.06	2.0	0.0	1.0	0.0	8.2	0.0	93.4	0.0	0.0	27.9
Kaiseraugst Fm. (5)		Mean	0.19	0.00	4.60	0.27	18.3	3.5	3.1	36.2	1.4	0.8	0.0	0.0	0.4	36.2
		Median	0.10	0.00	4.32	0.27	14.3	3.0	4.0	32.5	0.0	1.2	0.0	0.0	0.2	39.3
		Stdev	0.22	0.00	1.70	0.16	12.5	1.2	2.1	15.1	2.6	0.7	0.0	0.0	0.4	17.1
		Min	0.00	0.00	2.32	0.06	8.0	2.0	0.0	18.1	0.0	0.0	0.0	0.0	0.0	10.4
		Max	0.48	0.00	6.87	0.49	40.0	5.3	5.0	57.2	5.9	1.5	0.0	0.0	0.9	55.7
Weitenau Fm. (2)		Mean	0.00	0.00	0.67	0.06	45.5	13.0	5.5	5.0	0.5	0.0	0.0	0.0	0.0	30.4
		Median	0.00	0.00	0.67	0.06	45.5	13.0	5.5	5.0	0.5	0.0	0.0	0.0	0.0	30.4
		Stdev	0.00	0.00	0.62	0.02	6.4	1.4	7.8	4.4	0.7	0.0	0.0	0.0	0.0	5.1
		Min	0.00	0.00	0.23	0.04	41.0	12.0	0.0	1.9	0.0	0.0	0.0	0.0	0.0	26.8
		Max	0.00	0.00	1.11	0.07	50.0	14.0	11.0	8.1	1.0	0.0	0.0	0.0	0.0	34.0

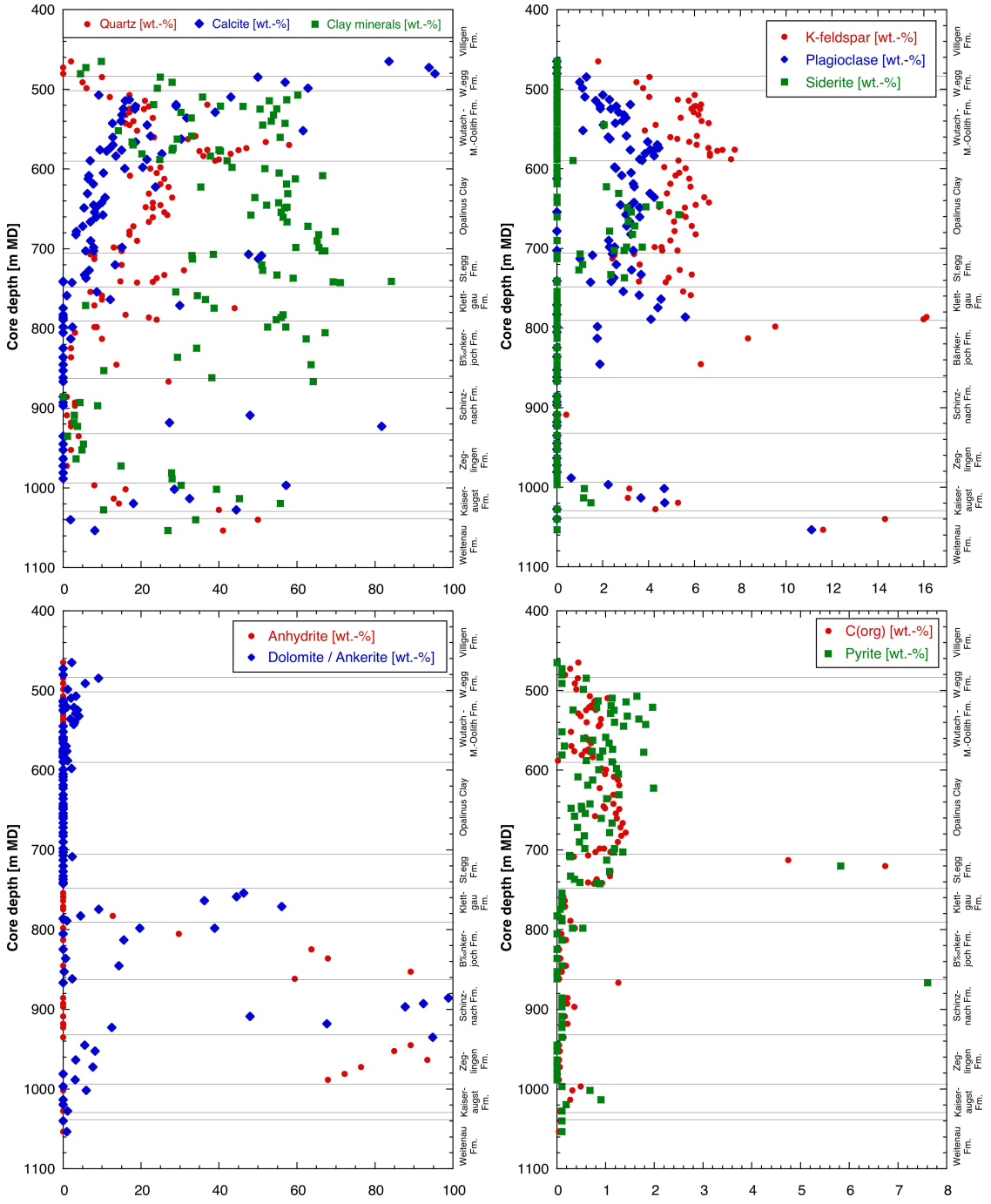

Fig. 4.2-1: Mineral contents in the bulk rock as a function of depth

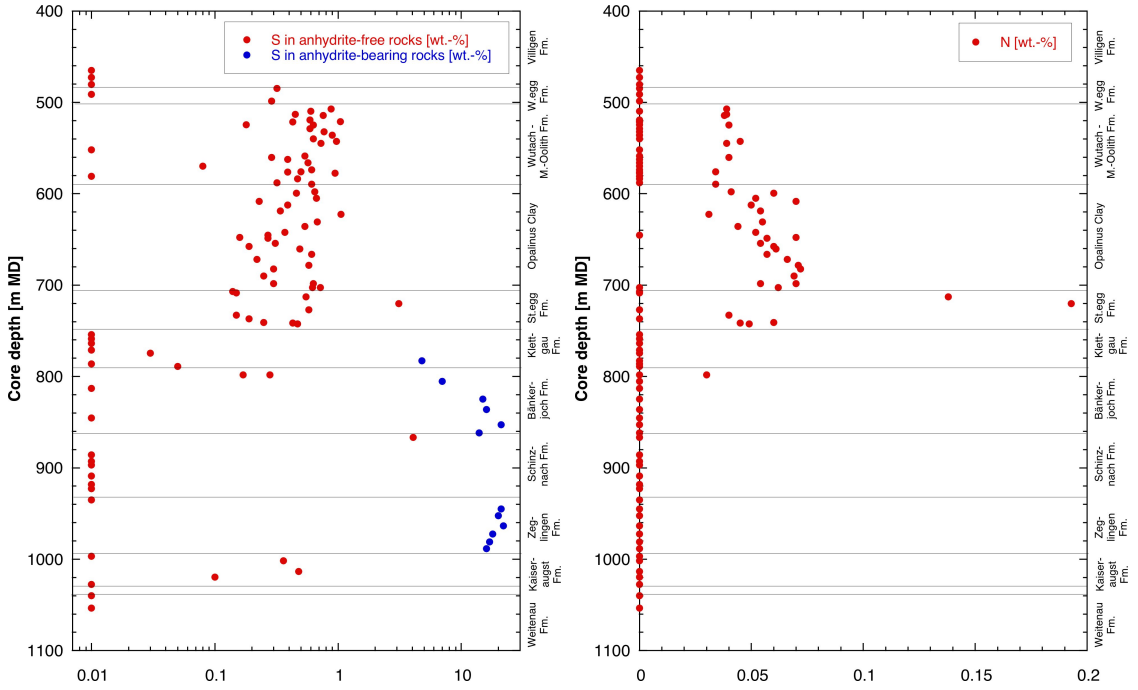

Fig. 4.2-2: Contents of S and N in the bulk rock as a function of depth

S contents below the detection limit of 0.05 wt.-% are represented by data points shown at 0.01 wt.-%. N contents below the detection limit of 0.01 wt.-% are represented by data points shown at 0 wt.-%.

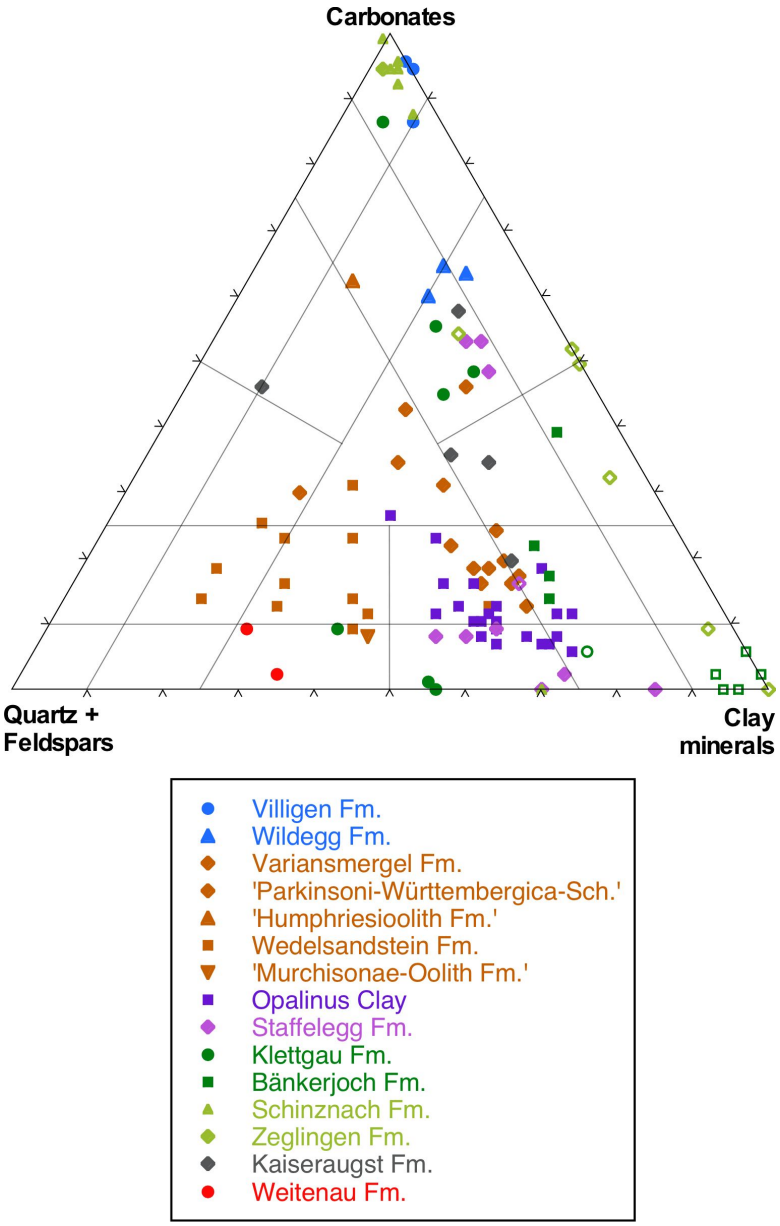

Fig. 4.2-3: Mineralogical composition of studied samples in the Füchtbauer triangle

Open symbols indicate samples containing > 10 wt.-% minerals other than those represented by the Füchtbauer triangle (which are clays, calcite, dolomite/ankerite, siderite, quartz, K-feldspar, plagioclase). In case of the samples from the Staffelegg Formation, these phases are pyrite and organic C. In case of the Triassic samples, anhydrite is the main additional phase.

A closer look at the clay-rich section Staffelegg Formation – Opalinus Clay – »Brauner Dogger»

The graphs shown in Fig. 4.2-4 indicate some systematic depth trends in particular of quartz, feldspars, clay-mineral and calcite contents, whereas most other minerals show less systematic variability.

Staffelegg Formation

- Clay-mineral contents decrease substantially upwards. In contrast, quartz and feldspars increase upwards systematically in the lower part (Schambelen Member – Frick Member), and this trend is reversed at least for quartz (at lower contents) in the upper part (Rietheim Member – Gross Wolf Member). These trends are analogous to those identified in the Trüllikon-1 profile (Aschwanden et al. 2021), even though slightly less well defined. The existence of two cycles is also seen in the depth profile of the quartz/clay ratio.
- The Rietheim Member (formerly 'Posidonienschiefer') is characterised by a strong positive excursion of the contents of C(org) and pyrite, pointing to highly reducing conditions during deposition. The highest N contents are also found in this unit.

Opalinus Clay

Informal sub-units within the Opalinus Clay were defined by Mazurek & Aschwanden (2020) on a regional basis. This scheme was successfully applied to the MAR1-1 core (Dossier III), and the sub-unit boundaries are included in Fig. 4.2-4.

- The base of the Opalinus Clay correlates with the onset of more homogeneous mineral contents, in contrast to a substantial scatter in the underlying Staffelegg Formation. Clay-mineral contents show a marked discontinuity towards higher values at the base, from where an upward trend of slightly decreasing clay-mineral contents reaching to the top of the mixed clay-silt-carbonate sub-unit is seen. Quartz and plagioclase contents show a reverse trend. A further subdivision of the mixed clay-silt-carbonate sub-unit as in Trüllikon-1-1 (TRU1-1) is not evident. Siderite contents increase upwards in the clay-rich sub-unit at the base of the Opalinus Clay.
- Unlike in the TRU1-1 core, no well-defined trends can be seen in the uppermost two sub-units. Exceptions include decreasing feldspar contents in the two uppermost sub-units and decreasing clay-mineral and increasing calcite contents in the upper half of the sub-unit with silty calcareous beds.

«Brauner Dogger»

- The mineralogical composition is more heterogeneous in comparison to the Opalinus Clay. The only clear trends include the upward decrease of feldspars in the section Wedelsandstein Formation – «Humphriesioolith Formation» and another cycle of decreasing feldspar contents in the «Parkinsoni-Württembergica-Schichten» and the Variansmergel Formation.

Conclusion

A number of mineralogical discontinuities and changes in depth trends were identified and correlate well with the lithostratigraphic subdivision defined in Dossier III. The trends are similar to, even though often less well defined than, those identified in the TRU1-1 core.

Quartz and clay-mineral contents show the most pronounced trends and discontinuities in their depth profiles. As the depth trends of quartz and clay minerals are often inverse, the ratio quartz/ clay minerals highlights the depositional cycles that govern the mineralogical composition, as shown in Fig. 4.2-4d. Last, let us note that at least the lower two sub-units of the Opalinus Clay are not zones with constant properties but rather zones with constant trends, i.e. depositional cycles.

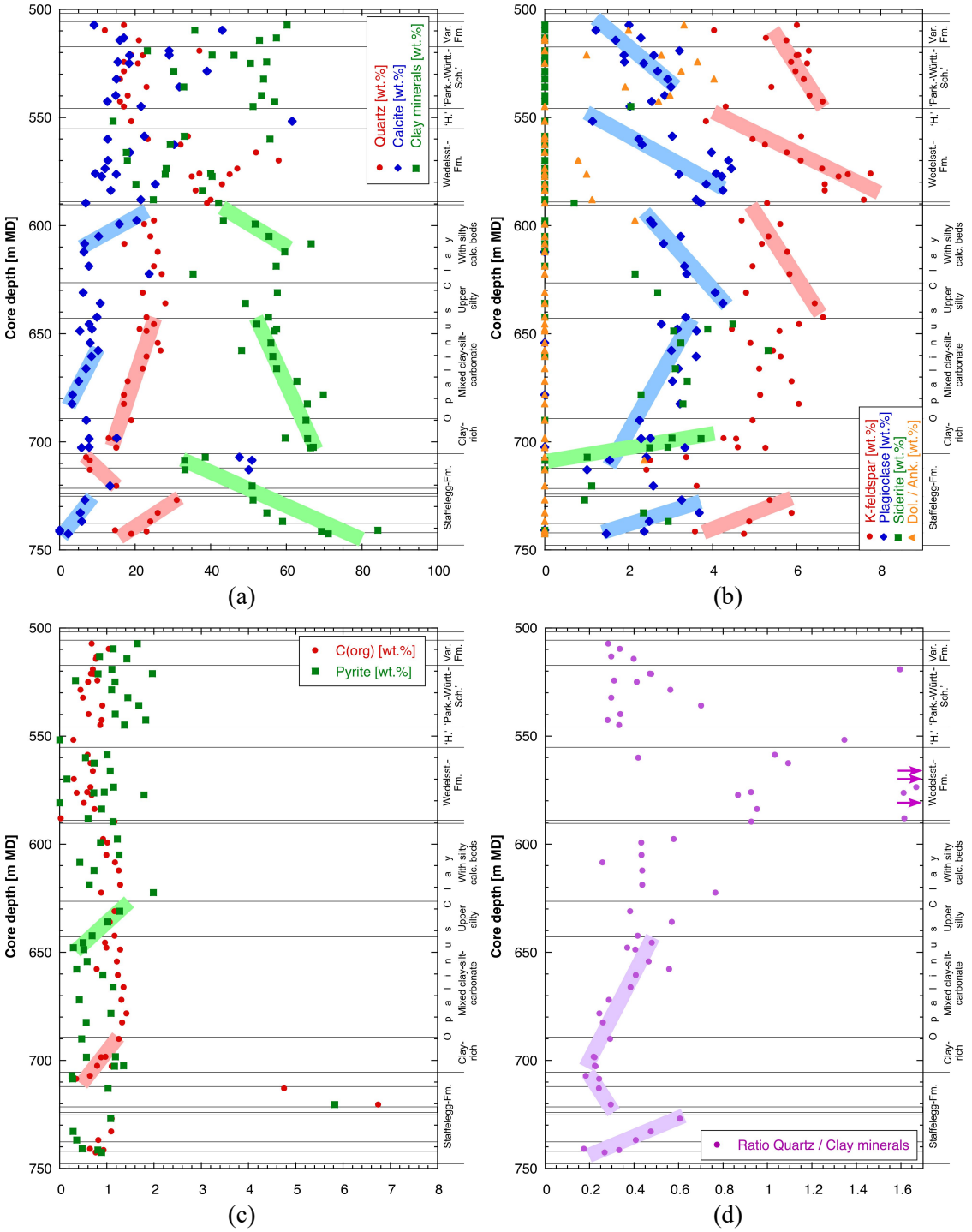

Fig. 4.2-4: Depth trends of mineral contents in the bulk rock in the Lias – Dogger interval

Coloured bars highlight systematic trends. Detailed lithostratigraphic subdivision according to Dossier III. Pink arrows in graph (d) indicate high values that are outside the plotted range.

4.2.2 Clay minerals

A total of 32 mineralogical analyses of the clay fraction were performed in the section Malm – Muschelkalk. The full dataset is documented in Appendix A, and Tab. 4.2-2 provides formation-specific summaries, normalising the contents of individual clay phases to the sum of all clay minerals.

The identified clay-mineral species include illite, smectite, illite/smectite mixed layers, kaolinite, chlorite and chlorite/smectite mixed layers. The identification of chlorite/smectite mixed layers in all samples is in contrast with previous data from northern Switzerland where this mineral was rarely reported (Mazurek 2017). However, this is not a real difference but due to the improved methodology of the evaluation of X-ray patterns that was applied for the TBO campaign (details in Waber ed. 2020). Because the chlorite/smectite mixed-layer phase contains 85 – 95% chlorite layers, its XRD reflections are close to those of pure chlorite. The new methodology also allows to better resolve the fraction of smectite layers in the illite/smectite mixed-layer phase. As seen in Tab. 4.2-2, illite-rich mixed layers dominate, but minor amounts of illite-poorer mixed layers also occur. Given the fact that the contents of mixed-layer phases and the smectite fractions in these are known, the end-member compositions of illite, smectite, chlorite and kaolinite (whether in mixed layers or as a discrete phase) can be calculated and are also listed in Tab. 4.2-2.

Depth trends are shown graphically in Fig. 4.2-5 for individual clay phases (a) and end-member clays (b). The depth plot of the latter is less noisy than that of the individual clay minerals. The content of the smectite end-member remains remarkably constant over the whole profile, and chlorite also varies only to a limited degree. The observed variability is mainly due to a variable ratio of the illite and kaolinite end-members. The two available analyses from the Triassic indicate a strong dominance of the illite end-member and low kaolinite contents. On the other hand, the Opalinus Clay has the lowest ratio of the illite to kaolinite end-members.

Tab. 4.2-2: Mineralogical composition of the clay fraction: formation-specific means, medians, standard deviations and ranges

In some cases, systematic depth trends of clay-mineral contents are observed. This means that in these cases the data do not follow a Gaussian distribution, which is a pre-requisite for the calculation of meaningful standard deviations. In such cases, the ranges (also listed) are more meaningful.

Formation (number of analyses)	**Member**		**Individual clay phases** [wt.-% of clay fraction]										**End-member clays** [wt.-% of clay fraction]			
			Illite	**Ill/Sm ML (85-90)**	**Ill/Sm ML (75-80)**	**Ill/Sm ML (50-70)**	**Ill/Sm ML (20-40)**	**Total Ill/Sm**	**Smectite**	**Kaolinite**	**Chlorite**	**Chl/Sm ML (85-95)**	**Illite**	**Smectite**	**Kaolinite**	**Chlorite**
Variansm. Fm. (1)		Mean	33.8	4.0	17.8	1.2	0.0	23.1	0.0	33.8	3.2	6.2	52.3	5.4	33.8	8.6
«Parkinsoni-Württ.-Sch.» (4)		Mean	37.4	12.2	11.6	2.8	0.1	26.7	0.0	25.4	3.4	5.3	58.9	6.3	25.4	9.7
		Median	37.5	12.5	11.6	1.8	0.0	25.8	0.0	26.0	3.7	6.0	59.2	5.9	26.0	9.7
		Stdev	1.9	6.1	5.9	2.1	0.2	2.2	0.0	3.5	1.0	2.3	3.2	1.1	3.5	0.5
		Min	35.2	6.0	6.0	1.6	0.0	25.1	0.0	21.0	2.0	2.0	55.1	5.4	21.0	9.1
		Max	39.6	18.0	17.1	6.0	0.4	30.0	0.0	28.7	4.3	7.1	62.0	8.0	28.7	10.2
Wedelsandstein Fm. (5)		Mean	43.5	3.5	26.0	3.2	0.0	32.8	0.1	10.9	6.2	6.0	68.8	8.3	10.9	12.0
		Median	42.9	1.0	24.1	3.5	0.0	34.4	0.0	9.5	5.2	5.8	67.8	7.8	9.5	11.0
		Stdev	4.9	4.5	5.5	1.5	0.1	6.1	0.2	4.9	1.8	1.7	3.6	1.0	4.9	3.0
		Min	38.0	0.0	21.1	0.9	0.0	22.7	0.0	5.0	5.0	4.0	64.3	7.4	5.0	8.6
		Max	51.3	10.2	34.0	5.0	0.2	39.0	0.5	17.8	9.1	7.8	74.0	10.0	17.8	16.1
Opalinus Clay (12)	All	Mean	31.8	10.4	10.8	2.1	0.0	23.3	0.0	33.8	4.3	6.6	50.5	5.3	33.9	10.3
		Median	31.2	8.9	10.8	1.9	0.0	23.6	0.0	33.6	4.3	6.7	50.6	5.4	33.6	10.3
		Stdev	1.8	4.2	4.5	1.0	0.0	1.9	0.0	2.3	1.2	0.7	2.0	0.3	2.3	1.0
		Min	29.4	5.3	0.0	1.1	0.0	20.3	0.0	28.3	2.3	5.7	47.8	4.7	28.3	7.8
		Max	35.4	20.3	18.3	4.2	0.0	26.0	0.1	36.8	6.6	7.6	55.2	5.7	36.8	11.6
Opalinus Clay (3)	Sub-unit with silty calcar-eous beds	Mean	33.5	7.5	14.1	1.5	0.0	23.1	0.0	31.7	5.6	6.1	52.1	5.3	31.7	10.9
		Median	33.9	8.4	14.0	1.5	0.0	24.3	0.0	33.4	5.8	5.8	50.9	5.5	33.4	10.9
		Stdev	2.1	1.9	4.1	0.4	0.0	2.4	0.0	3.0	1.1	0.6	2.7	0.5	3.0	0.7
		Min	31.3	5.3	10.0	1.1	0.0	20.3	0.0	28.3	4.4	5.7	50.2	4.7	28.3	10.2
		Max	35.4	8.8	18.3	1.9	0.0	24.8	0.0	33.5	6.6	6.7	55.2	5.6	33.5	11.6
Opalinus Clay (2)	Upper silty sub-unit	Mean	31.9	17.4	3.5	3.9	0.0	24.7	0.0	33.9	2.6	7.0	51.9	5.4	33.9	8.8
		Median	31.9	17.4	3.5	3.9	0.0	24.7	0.0	33.9	2.6	7.0	51.9	5.4	33.9	8.8
		Stdev	1.2	4.1	4.9	0.4	0.0	0.3	0.0	2.3	0.4	1.0	1.3	0.4	2.3	1.4
		Min	31.0	14.5	0.0	3.6	0.0	24.5	0.0	32.2	2.3	6.3	51.0	5.1	32.2	7.8
		Max	32.8	20.3	6.9	4.2	0.0	24.9	0.0	35.5	2.9	7.6	52.8	5.7	35.5	9.8
Opalinus Clay (4)	Mixed clay-silt-carbon-ate sub-unit	Mean	30.7	10.6	11.9	1.8	0.0	24.2	0.0	34.0	4.4	6.4	50.2	5.4	34.1	10.3
		Median	30.1	9.8	11.7	1.5	0.0	24.1	0.0	33.6	4.1	6.4	50.6	5.5	33.6	10.3
		Stdev	1.6	2.6	1.3	0.9	0.0	1.7	0.0	2.0	0.6	0.5	1.1	0.3	1.9	0.7
		Min	29.4	8.5	10.6	1.1	0.0	22.6	0.0	32.0	4.0	5.8	48.7	5.0	32.3	9.4
		Max	33.0	14.3	13.4	3.0	0.0	26.0	0.1	36.8	5.3	7.0	51.1	5.6	36.8	11.1

Tab. 4.2-2: continued

Formation (number of analyses)	**Member**		**Individual clay phases** [wt.-% of clay fraction]										**End-member clays** [wt.-% of clay fraction]			
			Illite	**Ill/Sm ML (85-90)**	**Ill/Sm ML (75-80)**	**Ill/Sm ML (50-70)**	**Ill/Sm ML (20-40)**	**Total Ill/Sm**	**Smectite**	**Kaolinite**	**Chlorite**	**Chl/Sm ML (85-95)**	**Illite**	**Smectite**	**Kaolinite**	**Chlorite**
Opalinus Clay (3)	Clay-rich sub-unit	Mean	31.4	8.5	10.9	2.0	0.0	21.5	0.0	35.6	4.2	7.3	48.5	5.2	35.8	10.6
		Median	31.0	8.5	10.4	2.0	0.0	21.4	0.0	35.9	4.5	7.3	48.4	5.2	35.9	10.9
		Stdev	1.1	2.6	2.8	0.1	0.0	0.5	0.0	0.6	0.9	0.3	0.7	0.2	0.4	0.8
		Min	30.5	6.0	8.4	1.9	0.0	21.0	0.0	35.0	3.2	7.0	47.8	5.0	35.4	9.7
		Max	32.6	11.1	14.0	2.1	0.0	22.0	0.0	36.0	5.0	7.6	49.2	5.4	36.0	11.2
Staffelegg Fm. (8)		Mean	34.8	16.9	6.8	3.1	0.0	26.8	0.0	26.3	4.8	7.3	56.5	5.9	26.2	11.4
		Median	34.6	18.5	3.8	2.9	0.0	26.5	0.0	27.2	5.1	7.0	55.9	6.0	27.0	11.3
		Stdev	3.6	6.8	7.9	2.2	0.0	2.5	0.0	3.2	1.6	1.7	3.8	0.7	3.2	1.5
		Min	30.1	6.0	0.0	0.0	0.0	23.8	0.0	20.3	2.6	4.7	50.7	4.6	20.3	9.4
		Max	42.4	27.0	20.0	5.5	0.0	32.2	0.1	29.3	6.7	9.7	62.0	6.6	29.3	14.2
Klettgau Fm. (1)		Mean	52.0	27.0	1.0	1.0	0.0	30.0	1.0	6.0	4.0	4.0	75.0	0.0	6.0	12.0
Kaiseraugst Fm. (1)		Mean	59.0	31.0	0.0	0.0	0.0	31.0	0.0	2.0	4.0	3.0	86.2	5.2	2.0	6.6

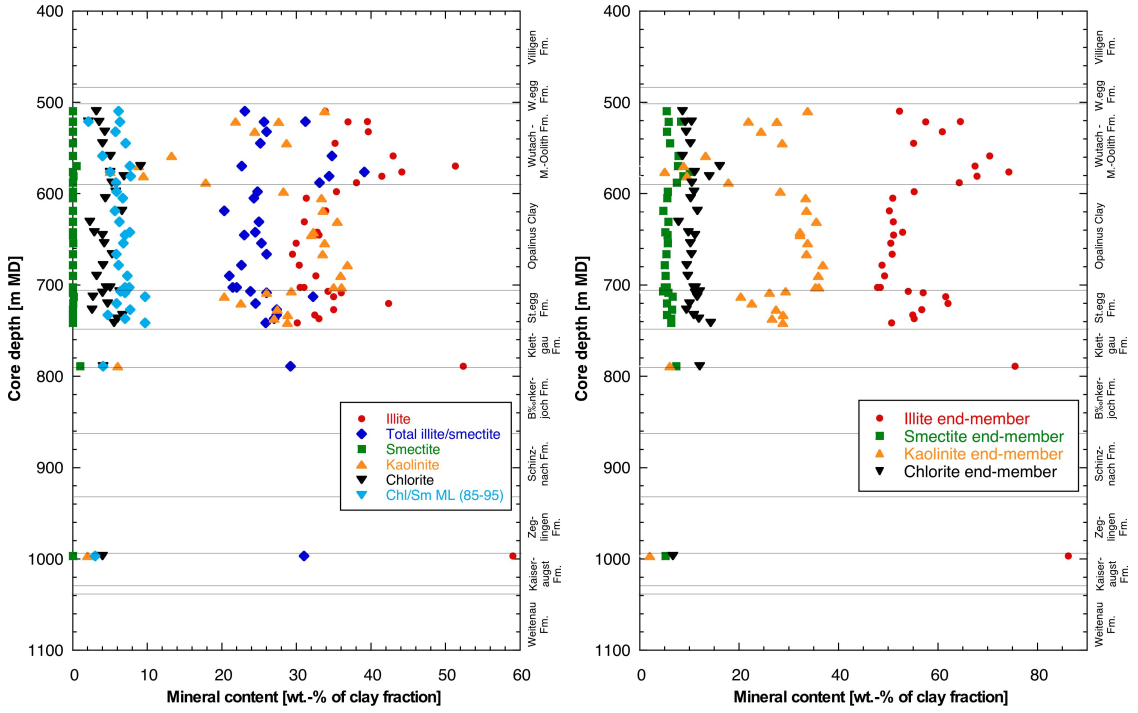

(a) (b)

Fig. 4.2-5: Mineralogical composition of the clay fraction as a function of depth; (a) individual clay minerals, (b) end-member clays

Detailed lithostratigraphic subdivision according to Dossier III.

A closer look at the clay-rich section Staffelegg Formation – Opalinus Clay – «Brauner Dogger»

The composition of the clay fraction shows some depth trends (Figs. 4.2-6 and 4.2-7). In the Staffelegg Formation, chlorite and chlorite/illite mixed layers decrease upwards and then remain at a constant level higher up. In the lower part of the Staffelegg Formation, the ratio illite to kaolinite end-member increases, whereas a systematic upward decrease is seen in the Gross Wolf Member, the uppermost sub-unit of the Staffelegg Formation. The relative contents of end-member clays remain remarkably constant throughout the Opalinus Clay. The ratio illite to kaolinite end-member increases sharply in the Wedelsandstein Formation and becomes more heterogeneous in comparison to the Opalinus Clay. The very high value in the centre of the Wedelsandstein Formation corresponds to an analogous finding in the TRU1-1 core (Aschwanden et al. 2021). The relative proportion of the smectite end-member in the Wedelsandstein Formation (7 – 10 wt.-% of total clay minerals) is higher than in other units.

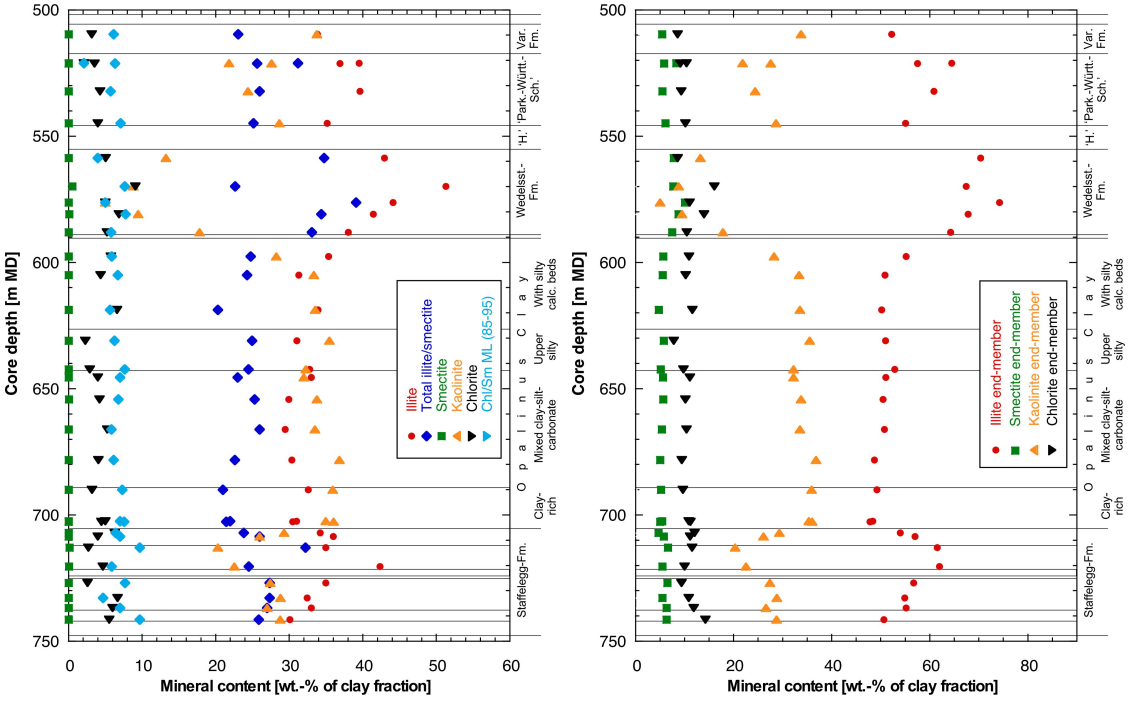

Fig. 4.2-6: Mineralogical composition of the clay fraction as a function of depth in the Lias – Dogger interval; (a) individual clay minerals, (b) end-member clays

Detailed lithostratigraphic subdivision according to Dossier III.

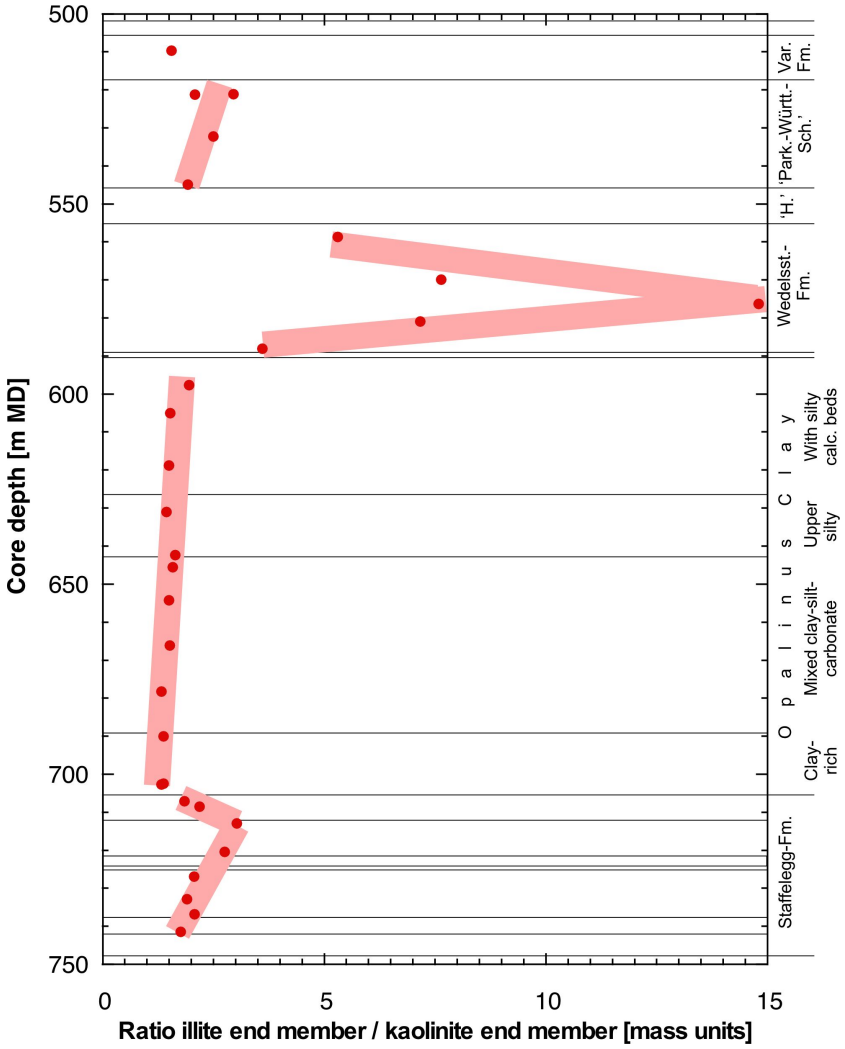

Fig. 4.2-7: Ratio of the illite to kaolinite end-member clays as a function of depth

Red bars highlight systematic trends. Detailed lithostratigraphic subdivision according to Dossier III.

4.3 Petrophysical parameters

Martin Mazurek & Lukas Aschwanden

Petrophysical parameters were obtained by 3 laboratories, and the acquired parameters are listed in Tab. 4.3-1. Given the fact that the methodologies applied at all laboratories were identical, the respective datasets are fully comparable and therefore not reported separately in tables and graphics. The formalisms to calculate additional parameters from measured data (such as porosity) are detailed in Waber (ed.) (2020). Formation-specific statistical data are summarised in Tab. 4.3-2, and the full dataset is documented in Appendix A. Note that, given the absence of density data for samples studied by Hydroisotop GmbH and CRIEPI, water-loss porosity was calculated assuming a grain density of 2.7 g/cm^3. The uncertainty related to this assumption is small.

Tab. 4.3-1: Analytical programme for petrophysical measurements

Parameter	**University of Bern**	**Hydroisotop GmbH**	**CRIEPI**
Bulk wet density	86		
Grain density	88		
Gravimetric water content	101	23	9
Water content from isotope mass balance	57	23	
N_2 adsorption isotherm	31		

Tab. 4.3-2: Summary of measured and calculated petrophysical data

Listed water contents (wet) are averages of measurements performed on 3 subsamples (exception: 1 subsample for CRIEPI). n = number of samples per geological unit.

Formation	Member		Bulk wet density [g/cm³]	Bulk dry density, calculated [g/cm³]	Grain density [g/cm³]	Pycnometer porosity [–]	Gravimetry				Isotope mass balance		
							Water content (wet) (105 °C) [wt.-%]	Water content (dry) (105 °C) [wt.-%]	Water-loss porosity using bulk wet density [–]	Water-loss porosity using grain density [–]	Water content (wet) based on isotope diff. exch. [wt.-%]	Porosity based on isotope diff. exch. using bulk wet density [–]	Porosity based on isotope diff. exch. using grain density [–]
Villigen Fm.		Mean	2.673	2.644	2.709	0.024	1.079	1.093	0.029	0.029	1.076	0.029	0.029
		Median	2.680	2.658	2.712	0.021	0.820	0.827	0.022	0.022	0.870	0.023	0.023
		Stdev	0.014	0.029	0.012	0.007	0.586	0.601	0.015	0.015	0.495	0.013	0.013
		Min	2.657	2.611	2.696	0.020	0.668	0.672	0.018	0.018	0.717	0.019	0.019
		Max	2.681	2.663	2.719	0.032	1.750	1.781	0.046	0.046	1.641	0.044	0.043
		n	3	3	3	3	3	3	3	3	3	3	3
Wildegg Fm.		Mean	2.582	2.496	2.706	0.078	3.351	3.468	0.087	0.086	3.822	0.099	0.097
		Median	2.583	2.494	2.704	0.079	3.330	3.445	0.086	0.085	3.919	0.101	0.099
		Stdev	0.002	0.007	0.011	0.002	0.231	0.247	0.006	0.005	0.343	0.009	0.008
		Min	2.580	2.490	2.696	0.075	3.132	3.233	0.081	0.081	3.441	0.089	0.088
		Max	2.584	2.503	2.718	0.079	3.592	3.726	0.093	0.092	4.105	0.106	0.103
		n	3	3	3	3	3	3	3	3	3	3	3
Varians-mergel Fm.		Mean	2.542	2.431	2.709	0.103	5.315	5.636	0.111	0.131	6.295	0.135	0.153
		Median	2.542	2.431	2.709	0.103	5.894	6.263	0.111	0.145	6.694	0.135	0.162
		Stdev	0.096	0.144	0.006	0.051	1.597	1.755	0.048	0.037	1.449	0.035	0.032
		Min	2.474	2.328	2.705	0.066	2.960	3.050	0.077	0.076	4.228	0.110	0.107
		Max	2.610	2.533	2.713	0.139	6.513	6.967	0.146	0.158	7.566	0.160	0.181
		n	2	2	2	2	4	4	2	4	4	2	4
«Parkinsoni-Württ.-Sch.»		Mean	2.505	2.376	2.717	0.125	5.163	5.452	0.129	0.128	5.769	0.149	0.142
		Median	2.498	2.364	2.712	0.130	5.497	5.817	0.132	0.136	5.724	0.142	0.141
		Stdev	0.030	0.051	0.011	0.018	0.876	0.970	0.021	0.020	0.755	0.010	0.017
		Min	2.471	2.314	2.706	0.093	3.695	3.837	0.094	0.094	4.262	0.141	0.107
		Max	2.554	2.460	2.736	0.147	6.361	6.793	0.157	0.156	6.568	0.162	0.160
		n	6	6	6	6	11	11	6	11	9	5	9
«Humphriesioolith Fm.»		Mean	2.605	2.531	2.717	0.068	2.839	2.922	0.074	0.074	3.218	0.084	0.083
		n	1	1	1	1	1	1	1	1	1	1	1

Tab. 4.3-2: continued

Formation	Member		Bulk wet density [g/cm³]	Bulk dry density, calculated [g/cm³]	Grain density [g/cm³]	Pycnometer porosity [–]	Gravimetry				Isotope mass balance		
							Water content (wet) (105 °C) [wt.-%]	Water content (dry) (105 °C) [wt.-%]	Water-loss porosity using bulk wet density [–]	Water-loss porosity using grain density [–]	Water content (wet) based on isotope diff. exch. [wt.-%]	Porosity based on isotope diff. exch. using bulk wet density [–]	Porosity based on isotope diff. exch. using grain density [–]
Wedel-sandstein Fm.		Mean	2.494	2.384	2.687	0.113	4.661	4.899	0.109	0.116	5.002	0.121	0.124
		Median	2.515	2.417	2.689	0.102	4.617	4.841	0.111	0.115	4.801	0.117	0.120
		Stdev	0.042	0.063	0.007	0.023	0.986	1.086	0.024	0.023	1.068	0.030	0.024
		Min	2.427	2.296	2.675	0.094	3.198	3.304	0.080	0.082	3.269	0.082	0.083
		Max	2.530	2.440	2.695	0.144	6.260	6.678	0.143	0.153	6.782	0.166	0.164
		n	7	7	7	7	12	12	7	12	10	6	10
«Murchisonae-Oolith Fm.»		Mean					4.292	4.484		0.108	4.748		0.119
		n	0	0	0	0	1	1	0	1	1	0	1
Opalinus Clay	All	Mean	2.517	2.402	2.692	0.108	4.693	4.927	0.115	0.117	5.200	0.124	0.129
		Median	2.517	2.402	2.691	0.106	4.773	5.012	0.115	0.119	5.249	0.124	0.130
		Stdev	0.020	0.034	0.013	0.012	0.535	0.585	0.015	0.012	0.613	0.010	0.014
		Min	2.489	2.357	2.675	0.082	2.750	2.828	0.070	0.071	3.721	0.117	0.094
		Max	2.562	2.492	2.720	0.131	5.694	6.038	0.134	0.140	6.340	0.131	0.155
		n	20	20	22	20	43	43	20	43	21	2	21
Opalinus Clay	Sub-unit with silty calcareous beds	Mean	2.524	2.420	2.691	0.102	4.683	4.919	0.104	0.117	5.399	0.124	0.133
		Median	2.525	2.412	2.688	0.102	4.863	5.112	0.113	0.121	5.304	0.124	0.131
		Stdev	0.025	0.046	0.017	0.014	0.759	0.827	0.021	0.018	0.520	0.010	0.012
		Min	2.492	2.368	2.675	0.082	2.750	2.828	0.070	0.071	4.618	0.117	0.116
		Max	2.562	2.492	2.713	0.120	5.694	6.038	0.124	0.140	6.340	0.131	0.155
		n	5	5	6	5	12	12	5	12	7	2	7
Opalinus Clay	Upper silty sub-unit	Mean	2.527	2.419	2.690	0.101	4.251	4.441	0.108	0.107	4.283		0.108
		Median	2.524	2.421	2.687	0.098	4.463	4.671	0.113	0.112	4.535		0.114
		Stdev	0.007	0.010	0.009	0.006	0.357	0.389	0.010	0.008	0.488		0.011
		Min	2.521	2.408	2.684	0.097	3.738	3.883	0.097	0.095	3.721		0.094
		Max	2.535	2.427	2.700	0.108	4.498	4.710	0.114	0.113	4.593		0.115
		n	3	3	3	3	6	6	3	6	3	0	3

Tab. 4.3-2: continued

Formation	Member		Bulk wet density [g/cm³]	Bulk dry density, calculated [g/cm³]	Grain density [g/cm³]	Pycnometer porosity [–]	Gravimetry				Isotope mass balance		
							Water content (wet) (105 °C) [wt.-%]	Water content (dry) (105 °C) [wt.-%]	Water-loss porosity using bulk wet density [–]	Water-loss porosity using grain density [–]	Water content (wet) based on isotope diff. exch. [wt.-%]	Porosity based on isotope diff. exch. using bulk wet density [–]	Porosity based on isotope diff. exch. using grain density [–]
Opalinus Clay	Mixed clay-silt-carbonate sub-unit	Mean	2.518	2.401	2.691	0.107	4.660	4.890	0.117	0.116	5.140		0.128
		Median	2.517	2.400	2.691	0.108	4.634	4.859	0.116	0.116	5.118		0.127
		Stdev	0.021	0.031	0.011	0.011	0.376	0.414	0.011	0.009	0.352		0.008
		Min	2.489	2.357	2.678	0.093	4.101	4.276	0.104	0.103	4.544		0.114
		Max	2.549	2.444	2.715	0.122	5.377	5.683	0.134	0.132	5.679		0.140
		n	8	8	9	8	17	17	8	17	8	0	8
Opalinus Clay	Clay-rich sub-unit	Mean	2.499	2.370	2.697	0.121	5.108	5.383	0.129	0.127	5.811		0.143
		Median	2.500	2.371	2.693	0.120	5.083	5.355	0.129	0.126	5.846		0.144
		Stdev	0.004	0.005	0.016	0.007	0.168	0.187	0.002	0.004	0.546		0.012
		Min	2.494	2.363	2.682	0.115	4.871	5.120	0.126	0.121	5.249		0.130
		Max	2.502	2.374	2.720	0.131	5.360	5.664	0.131	0.133	6.339		0.155
		n	4	4	4	4	8	8	4	8	3	0	3
Staffelegg Fm.		Mean	2.495	2.382	2.658	0.104	4.198	4.407	0.113	0.104	3.954		0.098
		Median	2.508	2.384	2.693	0.096	4.570	4.789	0.116	0.114	4.812		0.120
		Stdev	0.072	0.076	0.084	0.017	1.530	1.644	0.023	0.037	2.179		0.053
		Min	2.377	2.255	2.487	0.080	0.573	0.576	0.081	0.015	0.628		0.017
		Max	2.575	2.484	2.717	0.128	6.020	6.406	0.150	0.147	6.357		0.155
		n	9	9	9	9	17	17	9	17	7	0	7
Klettgau Fm.		Mean	2.585	2.472	2.758	0.104	4.453	4.684	0.114	0.112	5.652	0.144	0.140
		Median	2.562	2.428	2.744	0.108	4.778	5.017	0.123	0.121	5.425	0.139	0.136
		Stdev	0.119	0.155	0.075	0.032	1.556	1.658	0.039	0.038	0.713	0.018	0.017
		Min	2.489	2.356	2.675	0.030	0.774	0.780	0.022	0.022	5.056	0.126	0.125
		Max	2.860	2.838	2.927	0.132	5.731	6.079	0.146	0.143	6.783	0.173	0.166
		n	8	8	8	8	8	8	8	8	5	5	5
Bänker-joch Fm.		Mean	2.772	2.703	2.850	0.054	3.274	3.454	0.069	0.082	3.476	0.091	0.087
		Median	2.799	2.764	2.885	0.042	5.236	5.525	0.035	0.131	3.629	0.094	0.093
		Stdev	0.179	0.244	0.094	0.056	2.664	2.831	0.069	0.066	3.080	0.080	0.075
		Min	2.534	2.390	2.734	0.000	0.150	0.150	0.004	0.004	0.311	0.009	0.009
		Max	2.943	2.938	2.942	0.130	5.780	6.135	0.144	0.142	6.436	0.176	0.160
		n	7	7	7	7	9	9	7	9	6	6	6

Tab. 4.3-2: continued

Formation	Member		Bulk wet density [g/cm³]	Bulk dry density, calculated [g/cm³]	Grain density [g/cm³]	Pycnometer porosity [–]	Gravimetry				Isotope mass balance		
							Water content (wet) (105 °C) [wt.-%]	Water content (dry) (105 °C) [wt.-%]	Water-loss porosity using bulk wet density [–]	Water-loss porosity using grain density [–]	Water content (wet) based on isotope diff. exch. [wt.-%]	Porosity based on isotope diff. exch. using bulk wet density [–]	Porosity based on isotope diff. exch. using grain density [–]
Schinznach Fm.	All	Mean	2.708	2.671	2.791	0.043	1.398	1.426	0.038	0.038	1.924	0.051	0.051
		Median	2.729	2.691	2.818	0.045	1.393	1.413	0.038	0.038	1.639	0.044	0.045
		Stdev	0.059	0.079	0.064	0.027	0.934	0.960	0.025	0.025	0.866	0.021	0.020
		Min	2.584	2.518	2.676	0.001	0.138	0.138	0.004	0.004	1.237	0.034	0.034
		Max	2.759	2.751	2.853	0.078	2.557	2.624	0.066	0.066	2.897	0.075	0.074
		n	7	7	7	7	7	7	7	7	3	3	3
Schinznach Fm., Asp Mb.		Mean	2.584	2.518	2.676	0.059	2.557	2.624	0.066	0.066	2.897	0.075	0.074
		n	1	1	1	1	1	1	1	1	1	1	1
Schinznach Fm.	Stamberg Mb.	Mean	2.718	2.669	2.840	0.060	1.797	1.832	0.049	0.049	1.438	0.039	0.040
		Median	2.710	2.663	2.838	0.058	1.747	1.778	0.047	0.048	1.438	0.039	0.040
		Stdev	0.029	0.044	0.013	0.018	0.564	0.585	0.015	0.015	0.284	0.007	0.008
		Min	2.693	2.629	2.828	0.043	1.260	1.276	0.035	0.035	1.237	0.034	0.034
		Max	2.750	2.715	2.853	0.078	2.385	2.443	0.064	0.065	1.639	0.044	0.045
		n	3	3	3	3	3	3	3	3	2	2	2
Schinznach Fm.	Liedertswil, Leutschenberg & Kienberg Mb.	Mean	2.740	2.724	2.781	0.021	0.613	0.620	0.017	0.017			
		Median	2.733	2.729	2.794	0.016	0.307	0.308	0.008	0.009			
		Stdev	0.016	0.030	0.044	0.022	0.681	0.692	0.019	0.019			
		Min	2.729	2.691	2.732	0.001	0.138	0.138	0.004	0.004			
		Max	2.759	2.751	2.818	0.045	1.393	1.413	0.038	0.038			
		n	3	3	3	3	3	3	3	3	0	0	0
Zeglingen Fm.	All	Mean	2.870	2.834	2.930	0.034	1.443	1.573	0.036	0.036	3.757	0.093	0.091
		Median	2.947	2.945	2.948	0.004	0.170	0.170	0.005	0.005	0.580	0.017	0.017
		Stdev	0.186	0.268	0.043	0.081	3.361	3.701	0.082	0.082	5.786	0.141	0.137
		Min	2.450	2.228	2.850	0.000	0.033	0.033	0.001	0.001	0.256	0.008	0.008
		Max	2.956	2.952	2.962	0.218	9.058	9.960	0.222	0.221	10.435	0.256	0.249
		n	7	7	7	7	7	7	7	7	3	3	3
Zeglingen Fm., «Dolomitzone»		Mean	2.450	2.228	2.850	0.218	9.058	9.960	0.222	0.221	10.435	0.256	0.249
		n	1	1	1	1	1	1	1	1	1	1	1

Tab. 4.3-2: continued

Formation	Member		Bulk wet density [g/cm³]	Bulk dry density, calculated [g/cm³]	Grain density [g/cm³]	Pycnometer porosity [–]	Gravimetry				Isotope mass balance		
							Water content (wet) (105 °C) [wt.-%]	Water content (dry) (105 °C) [wt.-%]	Water-loss porosity using bulk wet density [–]	Water-loss porosity using grain density [–]	Water content (wet) based on isotope diff. exch. [wt.-%]	Porosity based on isotope diff. exch. using bulk wet density [–]	Porosity based on isotope diff. exch. using grain density [–]
Zeglingen Fm.	«Obere Sulfatzone»	Mean	2.940	2.935	2.944	0.003	0.174	0.175	0.005	0.005	0.418	0.012	0.012
		Median	2.947	2.945	2.953	0.003	0.121	0.121	0.004	0.004	0.418	0.012	0.012
		Stdev	0.018	0.022	0.027	0.003	0.150	0.151	0.004	0.004	0.229	0.007	0.007
		Min	2.910	2.900	2.891	0.000	0.033	0.033	0.001	0.001	0.256	0.008	0.008
		Max	2.956	2.952	2.962	0.009	0.360	0.361	0.011	0.011	0.580	0.017	0.017
		n	6	6	6	6	6	6	6	6	2	2	2
Kaiseraugst Fm.		Mean	2.611	2.544	2.717	0.064	2.731	2.817	0.067	0.071	2.661	0.070	0.069
		Median	2.617	2.531	2.717	0.073	3.177	3.281	0.077	0.083	3.050	0.080	0.079
		Stdev	0.026	0.045	0.027	0.022	1.010	1.055	0.028	0.026	1.832	0.048	0.047
		Min	2.575	2.504	2.694	0.031	0.986	0.996	0.026	0.026	0.666	0.018	0.018
		Max	2.635	2.609	2.741	0.077	3.380	3.498	0.088	0.087	4.268	0.112	0.109
		n	4	4	4	4	5	5	4	5	3	3	3
Weitenau Fm.		Mean	2.528	2.459	2.666	0.078	2.702	2.777	0.068	0.069	2.942	0.074	0.075
		Median	2.528	2.459	2.666	0.078	2.702	2.777	0.068	0.069			
		Stdev	0.009	0.015	0.014	0.001	0.239	0.252	0.006	0.006			
		Min	2.521	2.449	2.656	0.077	2.533	2.599	0.064	0.065			
		Max	2.534	2.470	2.676	0.078	2.871	2.956	0.072	0.073			
		n	2	2	2	2	2	2	2	2	1	1	1

4.3.1 Water content

The distribution of gravimetric water content in the studied section Malm–Permian is shown in Fig. 4.3-1. Note that the error bars on gravimetric water content reflect the variability among 3 aliquots of the samples, i.e. they are a measure of the lithological heterogeneity of the sample on the cm-scale. Water content is low in the Villigen Formation and increases abruptly to 3.1 – 3.6 wt.-% in the Wildegg Formation. In the underlying «Brauner Dogger», values tend to be higher but the spread is substantial (2.8 – 7.6 wt.-%), illustrating the lithological heterogeneity of this unit. Water content in the Opalinus Clay is more homogeneous, and the systematic trends that can be observed are further discussed below. A sharp discontinuity towards lower values can be seen at the top of the Staffelegg Formation, with a clear increasing trend with depth. Water content remains relatively high until the upper half of the Bänkerjoch Formation but drops to lower and more scattered values in the underlying section of this unit, which is lithologically heterogeneous and contains anhydrite beds. The dolostones and limestones of the Schinznach Formation show generally low but variable water contents. The uppermost sample from the Zeglingen Formation ('Dolomit der Anhydritgruppe') is a dolostone with abundant dissolution features on the cm-scale, which is reflected by its high and locally quite variable water content. The rest of the Zeglingen Formation is dominated by anhydrite-rich lithologies with low water contents. The generally marly to silty lithologies of the Kaiseraugst and Weitenau Formations yield water contents in the range 2 – 4 wt.-%, except for a limestone sample with a lower value.

Water contents from gravimetry and from isotope diffusive exchange correlate well (Fig. 4.3-2), but the latter shows values that are consistently higher, about $13\%_{rel}$ on the average. Some samples that slightly deviate from the regression line tend to have larger errors, reflecting sample heterogeneity.

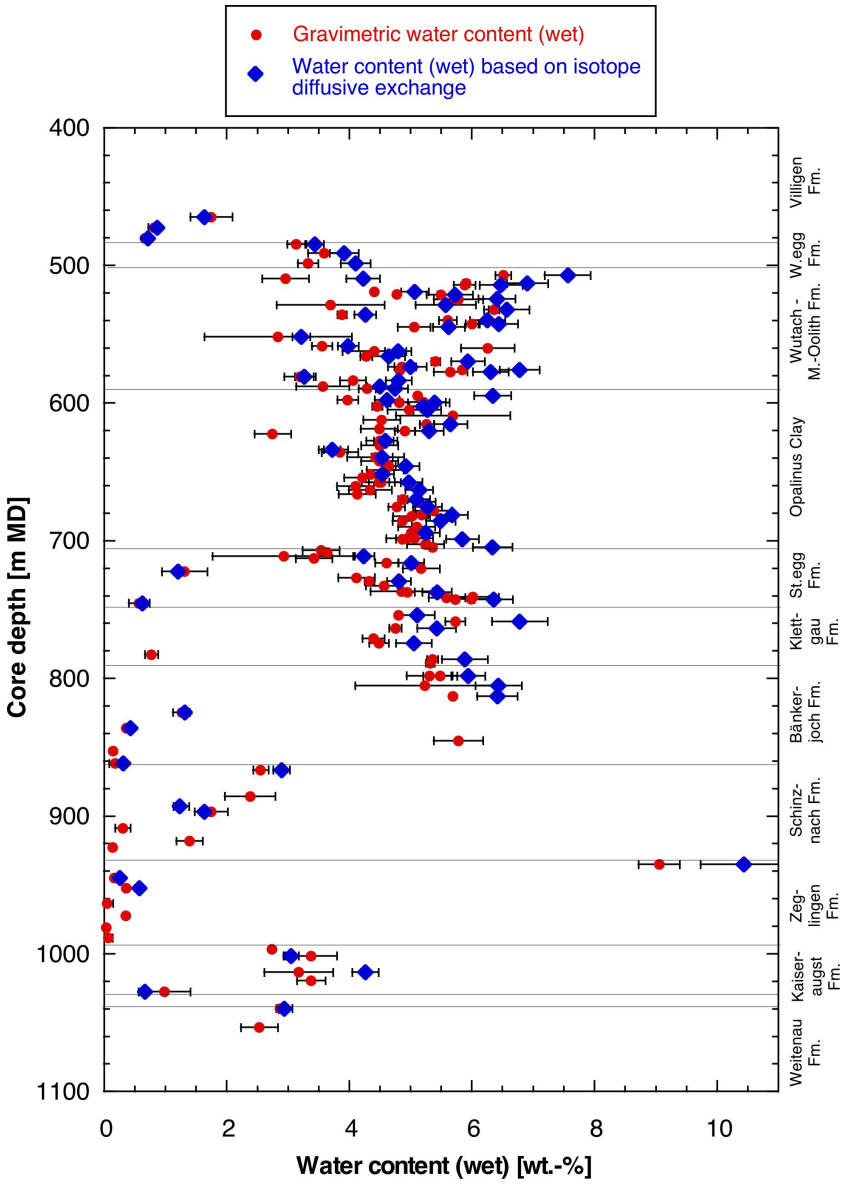

Fig. 4.3-1: Water content as a function of depth

Black bars for gravimetric water content indicate 1σ variability among 3 aliquots of the same sample. Black bars for water content from isotope diffusive exchange represent the propagated analytical error.

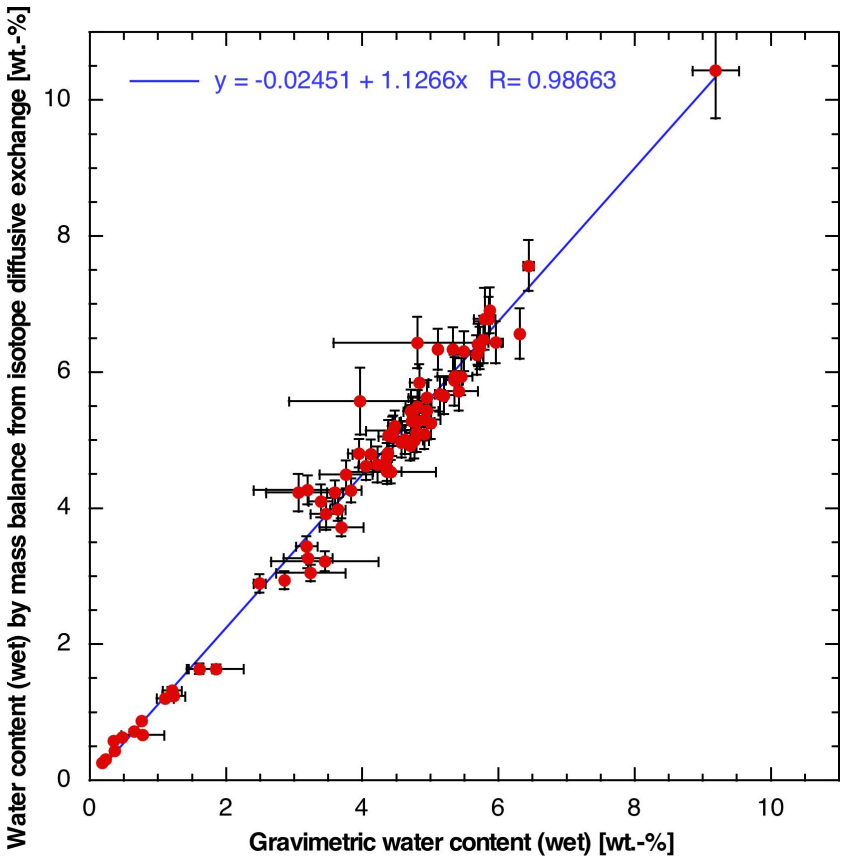

Fig. 4.3-2: Correlation of water contents based on gravimetry and on isotope diffusive exchange

Black bars for gravimetric water content indicate 1σ variability among 2 aliquots of the same sample. Note that only the 2 gravimetric water contents obtained from the aliquots used for the isotope diffusive-exchange experiments are considered in this graph, so the correlation refers to identical sample materials. This is particularly important for anhydrite-bearing samples, given the fact that only the anhydrite-poorest portions of such samples were used for diffusive-exchange experiments. Black bars for water content from isotope diffusive exchange represent the propagated analytical error.

A closer look at the clay-rich Lias – Dogger section

As shown in Fig. 4.3-3, water contents in the Staffelegg Formation, in the Opalinus Clay and in large parts of the Wedelsandstein Formation show systematic depth trends. These are similar for gravimetric water content and that obtained from isotope mass balance (except in the 'Mixed clay-silt-carbonate sub-unit' of the Opalinus Clay). Two distinct cycles of water contents decreasing upwards can be identified in the Staffelegg Formation, analogous to the findings for borehole TRU1-1 (Aschwanden et al. 2021). In the Opalinus Clay, at least 3 different trends can be identified and differ somewhat from those seen at TRU1-1. In the upper half of the Wedelsandstein Formation, a clear upward trend of decreasing water content can be identified, while no evident trend was observed at TRU1-1.

The observed trends of the water content correlate reasonably well with those identified for clay-mineral contents (Section 4.2.1, Fig. 4.2-4). In particular, a positive correlation can be identified with the clay-mineral content and a negative correlation with the ratio quartz/clay minerals. It is evident that a substantial part of the porewater is related to the presence of clay minerals. In detail,

some differences exist, e.g. in the Staffelegg Formation where two cycles of water content are decreasing upwards (Fig. 4.3-3), whereas only one cycle of decreasing clay-mineral content is suggested by mineralogical data (Fig. 4.2-4).

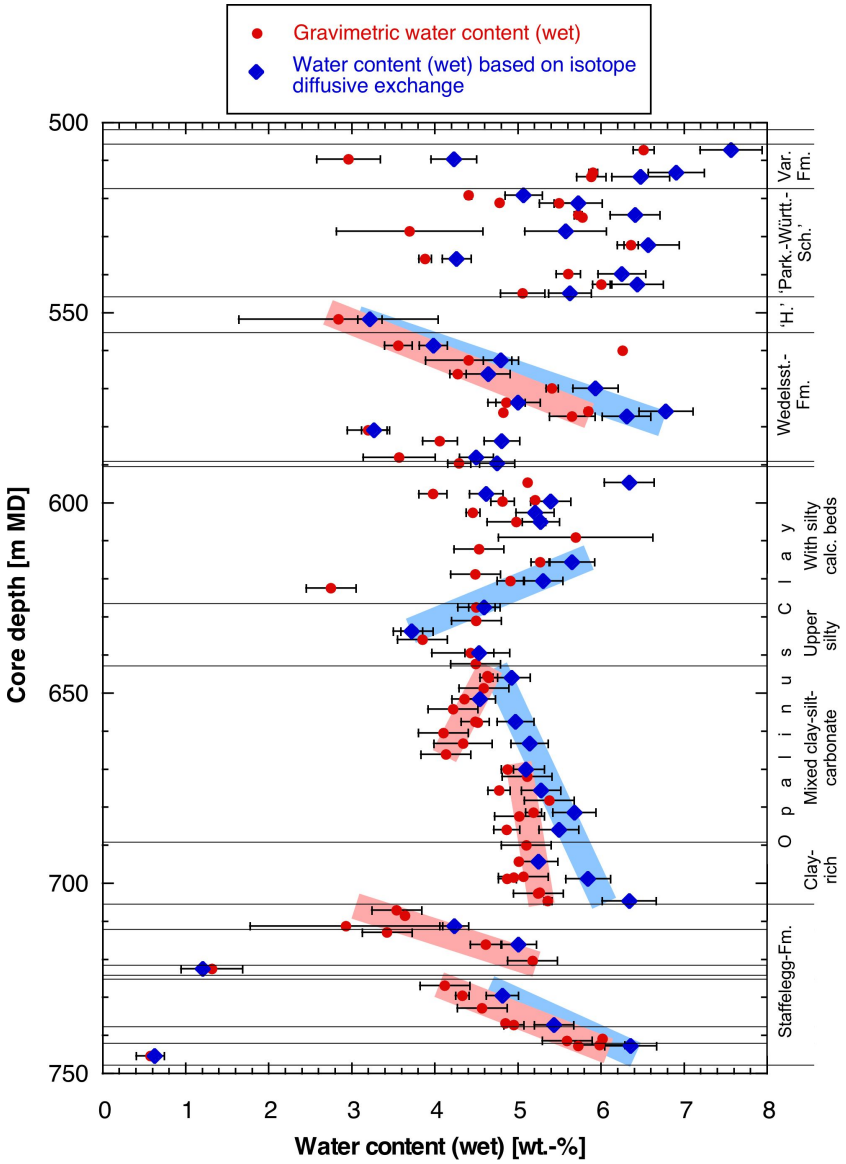

Fig. 4.3-3: Water content (wet) as a function of depth in the Lias – Dogger interval

Black bars for gravimetric water content indicate 1σ variability among 3 aliquots of the same sample. Black bars for water content from isotope diffusive exchange represent the propagated analytical error.

4.3.2 Grain density

The grain-density profile is shown in Fig. 4.3-4 (note that no data are available for samples analysed at Hydroisotop GmbH). Throughout the Malm, Dogger and Lias units, values are around 2.7 g/cm^3, with only limited scatter. The only conspicuous excursion is identified in the Rietheim Member of the Staffelegg Formation ('Posidonienschiefer'), where high contents of organic matter (C_{org} = 4.8 – 6.7 wt.-%) lead to markedly lower grain-density values.

In the underlying Triassic section comprising the Klettgau Formation to the Zeglingen Formation, values become larger, as does variability. This reflects the lithological heterogeneity, in particular the variable contents of dolomite and anhydrite with their high mineral densities. Fig. 4.3-5 shows the correlation between grain density and dolomite/ankerite contents. Grain density increases linearly with dolomite concentration, and outliers are due to the presence of anhydrite. In the Kaiseraugst and Weitenau Formations at the base of the profile, grain density lies again around 2.7 g/cm^3.

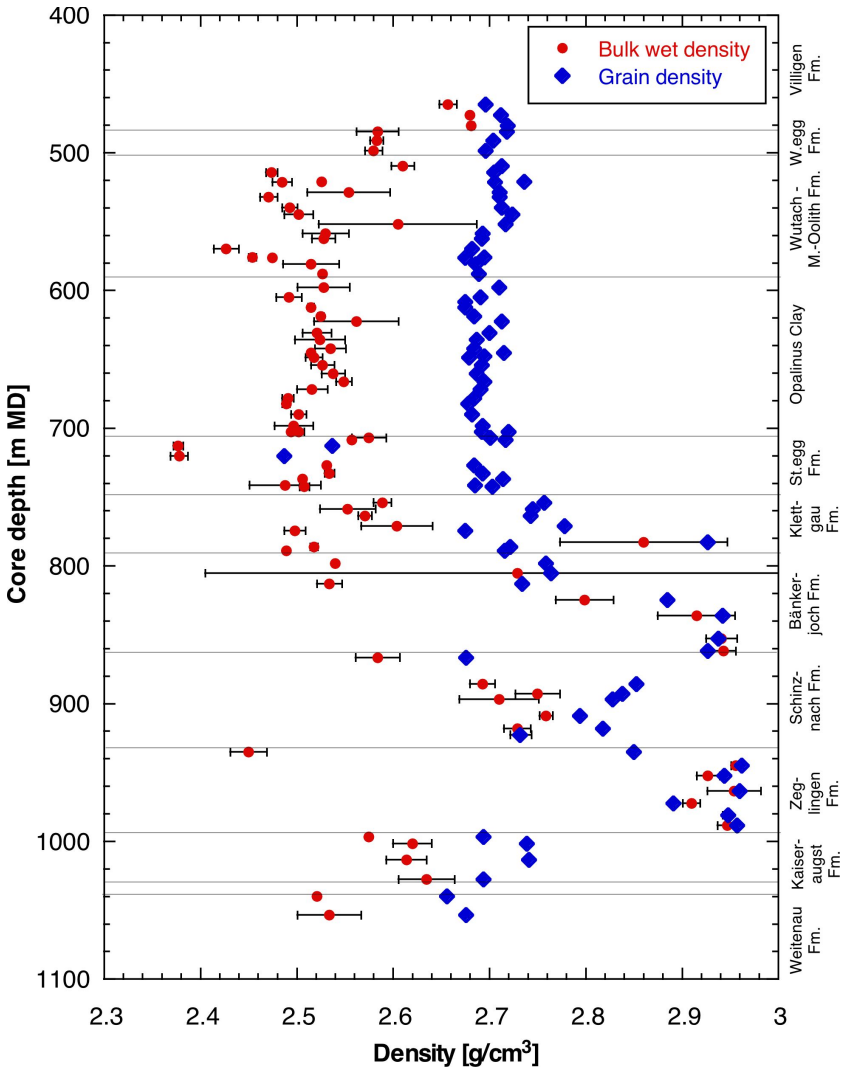

Fig. 4.3-4: Depth profile of bulk wet and grain densities

Black bars for bulk wet density indicate 1σ variability among 3 pieces of the same sample. Analytical error bars for grain density are smaller than the symbol size.

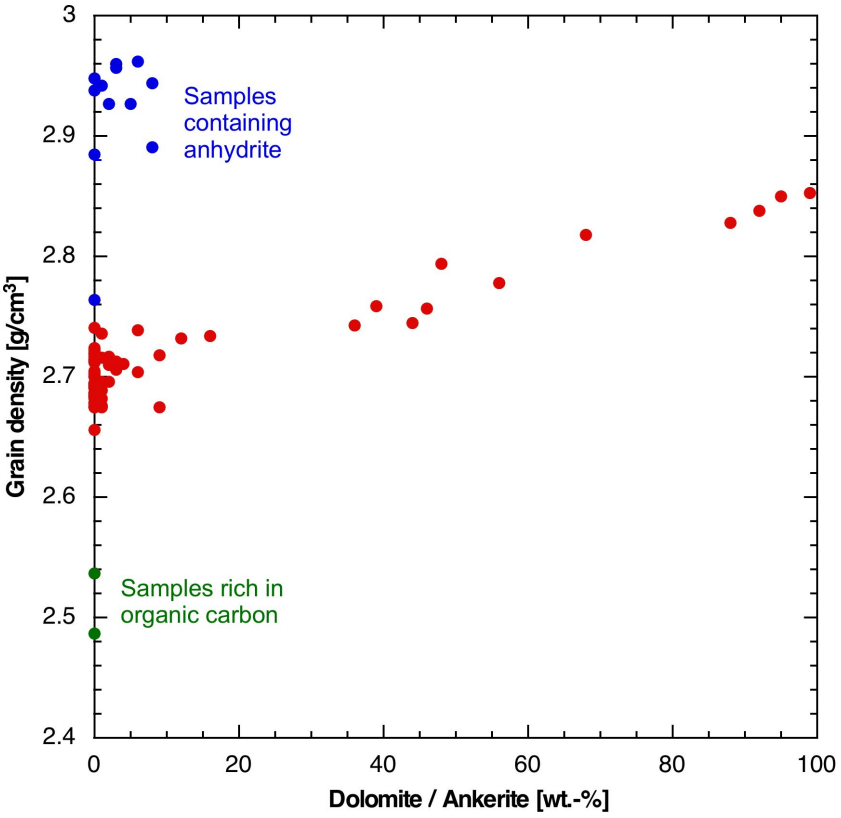

Fig. 4.3-5: Grain density as a function of the contents of dolomite/ankerite

Blue points are from Keuper and Muschelkalk units. Green points are from the Rietheim Member of the Staffelegg Formation.

4.3.3 Bulk wet density

Data are shown in Fig. 4.3-4 as a function of depth. Large error bars for some samples reflect heterogeneity on the cm scale.

4.3.4 Porosity

Three different approaches were used to constrain rock porosity (for details see Waber ed. 2020):

- *Water-loss porosity:* calculation from the gravimetric water content using either bulk wet or grain density
- *Porosity from isotope diffusive exchange:* calculation from the water content obtained by mass balance using either bulk wet or grain density
- *Pycnometer porosity:* calculation from bulk dry and grain densities; bulk dry density is calculated from bulk wet density and water content

Water-loss porosity and porosity from isotope diffusive exchange were calculated using bulk wet density by default. If the latter was not available, grain density was used, by which full water saturation of the pore space is assumed. The graphic in Fig. 4.3-6 shows that the two densities yield near-identical porosities, so the choice of the type of density for the calculation incurs no additional uncertainty.

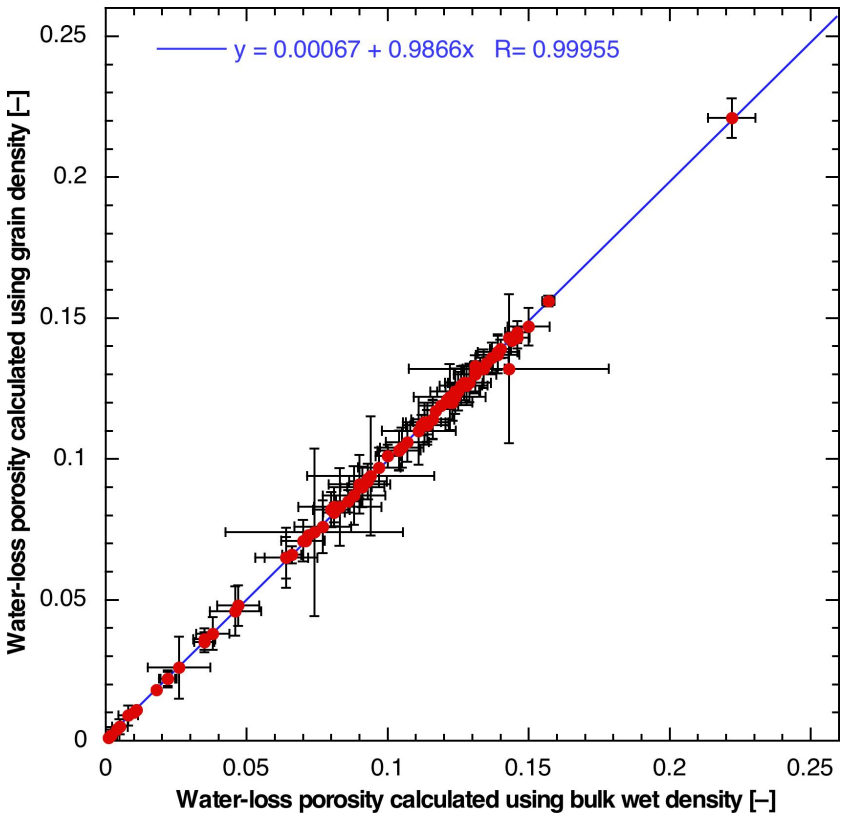

Fig. 4.3-6: Water-loss porosity calculated from gravimetric water content using either bulk wet or grain density

Bars indicate propagated errors, which are dominated by local heterogeneity of water content.

Comparison of porosities obtained by different methods

- An excellent linear correlation is observed between water-loss porosity and porosity from isotope diffusive exchange (Fig. 4.3-7). The latter yields about 11%$_{rel}$ higher values. Some samples that slightly deviate from the regression line tend to have larger errors on water-content porosity, reflecting sample heterogeneity.
- A slightly less good linear correlation is found between pycnometer porosity and porosity from isotope diffusive exchange (Fig. 4.3-8). The latter yields about 14%$_{rel}$ higher values. One outlier, sample 805.16 from the Bänkerjoch Formation, is heterogeneous on the cm scale, containing clay-rich and anhydrite-rich domains (Fig. 4.3-9). This heterogeneity explains the deviation from the regression line and the very large error bar on pycnometer porosity.
- The correlation between water-loss and pycnometer porosity is shown in Fig. 4.3-10. Again, sample 805.16 is an outlier. Excluding this sample yields a slope for the regression line of about 0.92.

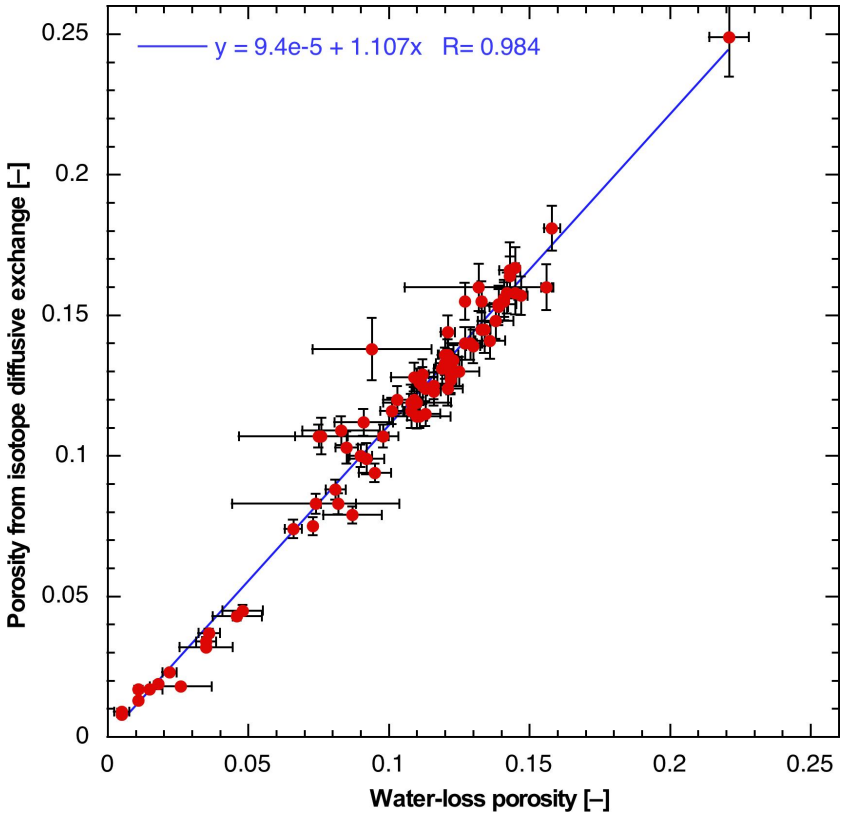

Fig. 4.3-7: Correlation of water-loss porosity and porosity from isotope diffusive exchange

Bars indicate propagated errors. Note that only the gravimetric water contents obtained from the aliquots used for the isotope diffusive-exchange experiments are considered for the x axis of this graph, so the correlation refers to identical sample materials. In the absence of grain-density data for the Hydroisotop GmbH samples, a value of 2.7 g/cm^3 was used.

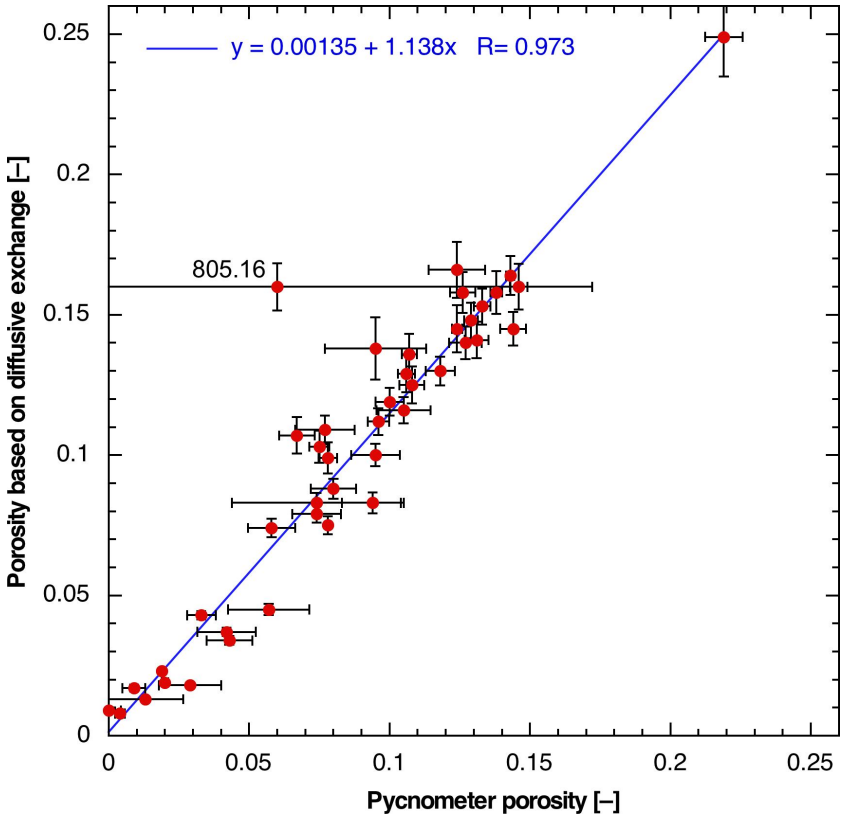

Fig. 4.3-8: Correlation of pycnometer porosity and porosity from isotope diffusive exchange
Bars indicate propagated errors. Outlier 805.16 was excluded from the regression line.

805.16 (Bänkerjoch Formation)

935.12 (Zeglingen Formation)

Fig. 4.3-9: Illustrations of heterogeneous samples

Left: Sample comprising clay-rich and anhydritic domains. Right: Dolostone containing horizons with macropores (dissolution features). Width of photographs is 10 cm.

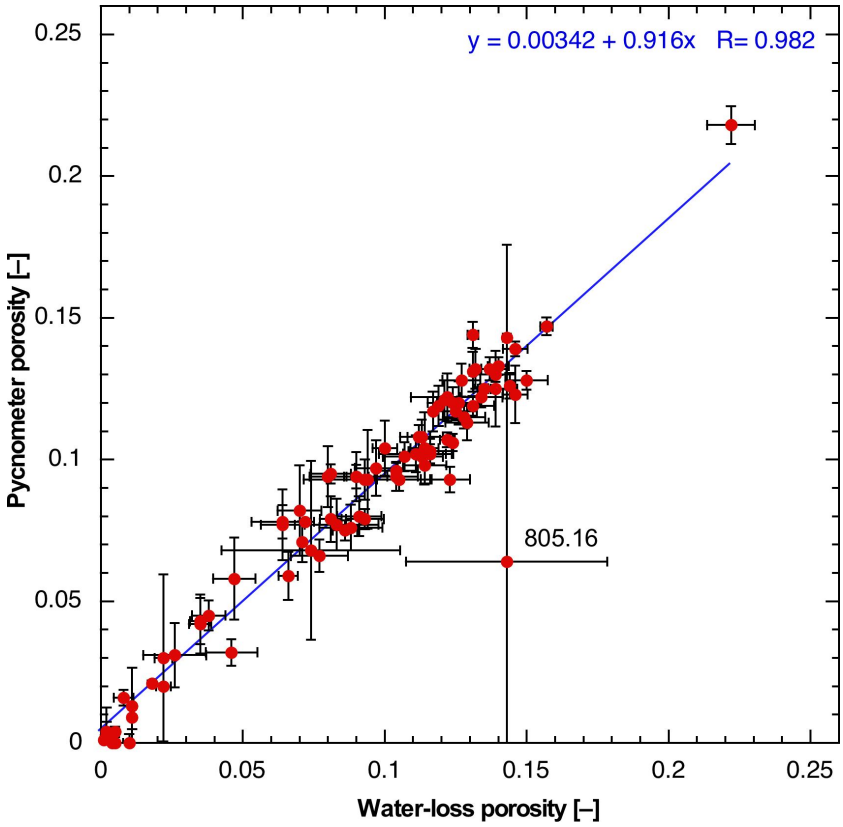

Fig. 4.3-10: Correlation of water-loss and pycnometer porosity

Bars indicate propagated errors. One outlier was excluded from the regression line.

Depth trends

In Fig. 4.3-11, porosity is shown as a function of depth. The shape of the profile is similar to that of water content (Fig. 4.3-1), including the systematic trends in the Lias – Dogger section (Fig. 4.3-3). The comments made on the distribution of water content with depth (Section 4.3.1) also apply to porosity.

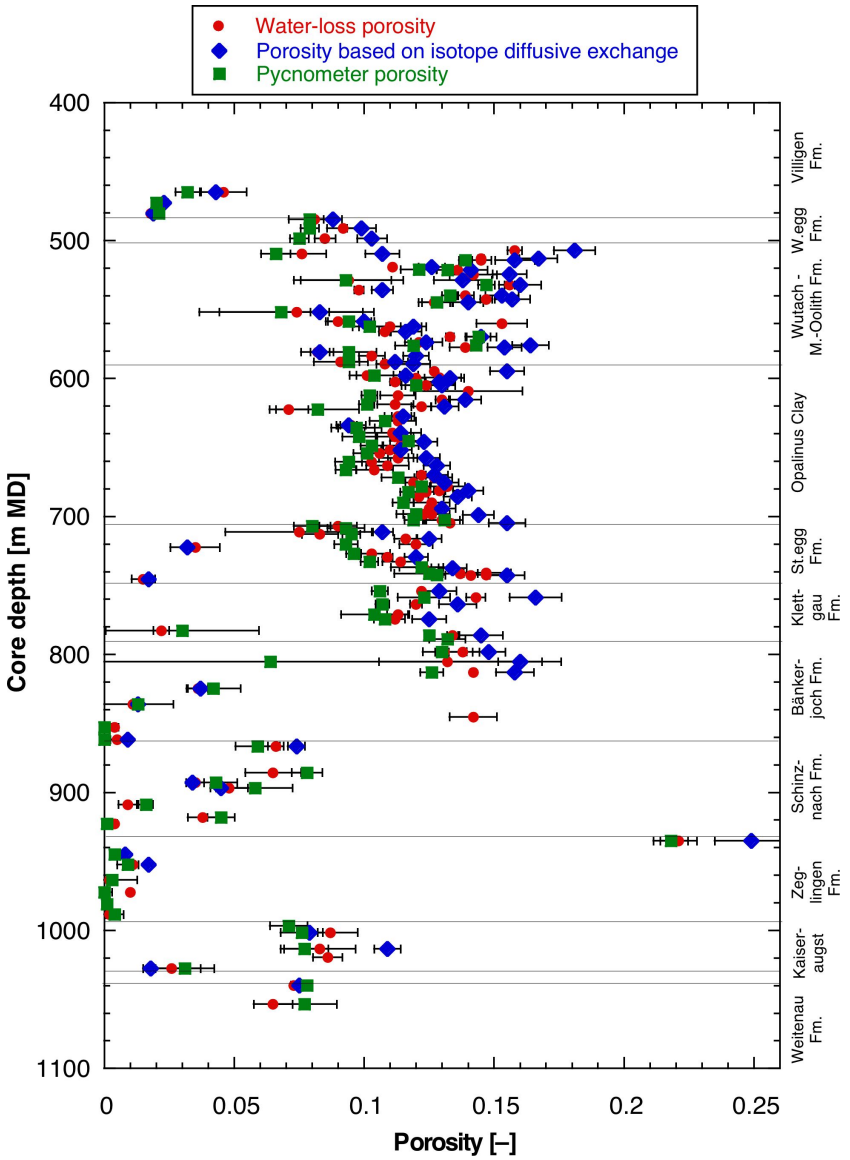

Fig. 4.3-11: Depth trends of porosities obtained by different methods

Porosity as a function of mineralogical composition

The correlation of porosity with clay-mineral content is shown in Fig. 4.3-12. When considering all available data (Fig. 4.3-12a), a general positive correlation can be identified, but scatter is substantial. When only samples from the Malm – Dogger – Lias section are considered, i.e. when the mineralogically and texturally more heterogeneous samples from the Triassic are excluded, a more systematic correlation is obtained (Fig. 4.3-12b). The slope of the data is steeper for clay-mineral contents in the range 0 – 30 wt.-% and becomes flatter at higher clay-mineral contents.

In the Triassic, a number of highly porous samples with low clay-mineral contents are found in dolomite-rich lithologies. These were affected by diagenetic dissolution to some degree, either during the process of dolomitisation or at later stages. Thus, their porosity is not the result of compaction and cementation alone. On the other hand, the presence of anhydrite tends to reduce porosity for a given clay-mineral content. Fig. 4.3-13 illustrates that porosity tends to reach values < 0.02 for anhydrite-rich samples.

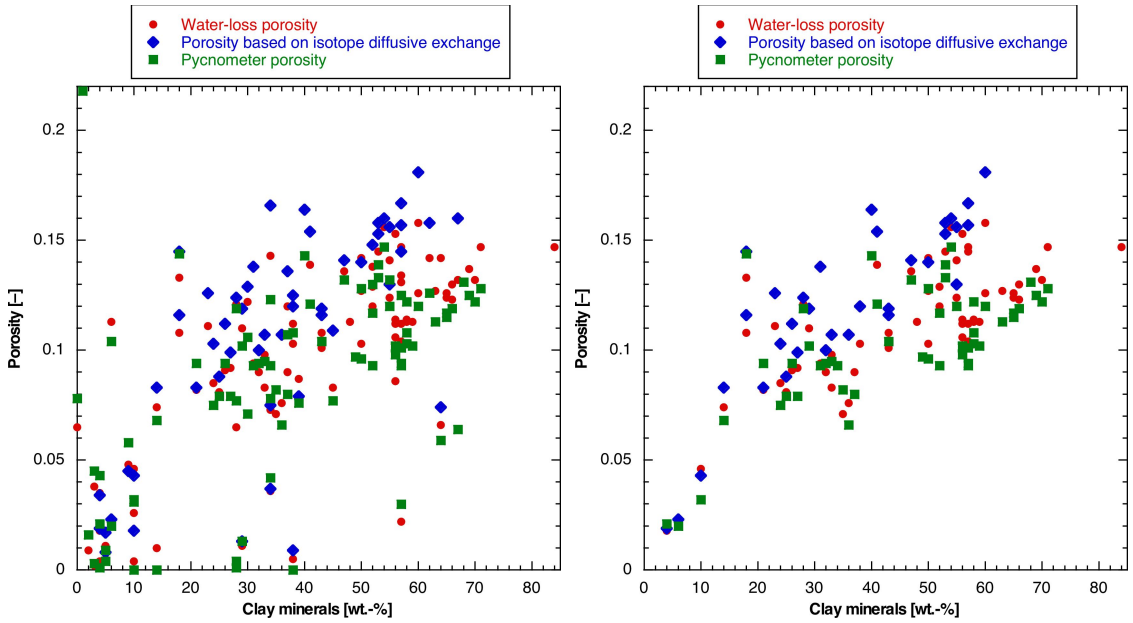

Fig. 4.3-12: Porosity as a function of clay-mineral content; (a) all data, (b) data from the section Malm – Dogger – Lias

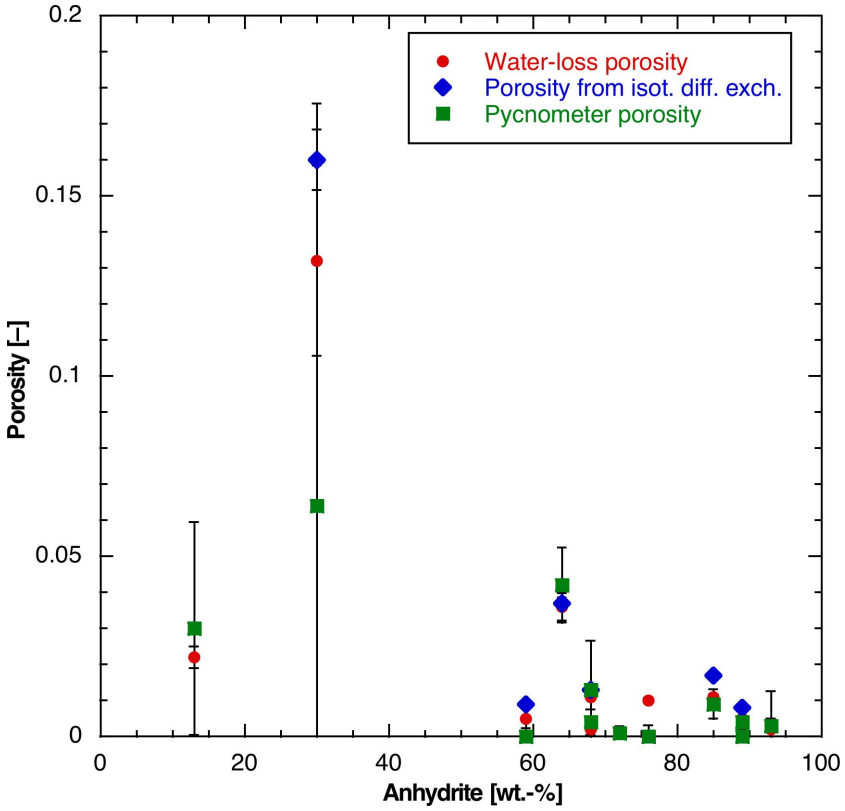

Fig. 4.3-13: Porosity of anhydrite-bearing samples

Bars indicate propagated errors. The sample with 13 wt.-% anhydrite also contains 10 wt.-% celestite (see Section 4.2-1).

4.4 Data from aqueous extraction tests

Carmen Zwahlen

Aqueous extraction (AqEx) tests are a simple but useful method to improve the understanding of the porewater – rock system across a sequence of sedimentary rocks if carried out at regular intervals. In this Section we present the data from aqueous extraction tests performed at a solid to liquid ratio of approximately 1. The data is discussed further in chapter 5. The full dataset can be found in Appendix A and details about the method are given in Waber (ed.) (2020).

4.4.1 Sample material and overview of analytical work

A total of 86 moisture-preserved drill core samples (PW and AD) from the Malm to the Rotliegendes and 10 dried drill core samples from the Schinznach and Zeglingen Formation were subjected to aqueous extraction tests. Additionally, the data of the extract solutions were used to model the mineral saturation states and the partial pressure of CO_2. These parameters were calculated with the PHREEQC Version 3 code (Parkhurst & Appelo 2013) and the PSI/Nagra thermodynamic database (Thoenen et al. 2014) assuming a temperature of 25 °C.

Tab. 4.4-1 Summary of analytical work performed on samples for aqueous extraction tests from the different geological formations (excluding duplicate and post-mortem extracts of AD and SQ experiments; *cf.* Sections 4.7.4 and 4.6.5)

Sample type: PW/RP: porewater sample, AD: Advective displacement sample, AqEx: aqueous extraction tests, S/L: solid to liquid ratio.

Group	**Formation**	**Sample type**	**AqEx at S/L 1, pH, Alkalinity, Cations, Anions**
Malm	Villigen Fm.	PW	3
Malm	Wildegg Fm.	PW	3
Dogger	Variansmergel	PW	2
Dogger	«Parkinsoni-Württembergica- Sch.»	PW, AD	6
Dogger	«Humphriesioolith Fm.»	PW	1
Dogger	Wedelsandstein	PW, AD	7
Dogger	Opalinus Clay	PW, AD	20
Lias	Staffelegg Fm.	PW, AD	9
Keuper	Klettgau Fm.	PW, AD	8
Keuper	Bänkerjoch Fm.	PW	7
Muschelkalk	Schinznach Fm.	PW	10
Muschelkalk	Zeglingen Fm.	PW	14
Muschelkalk	Kaiseraugst Fm.	PW, AD	4
Rotliegend	Weitenau Fm.	PW	2
Total		PW, AD	96

4.4.2 Aqueous extraction tests at a S/L of 1

Ion concentrations in aqueous extracts have a limited significance if they are not recalculated to porewater concentrations, either to the measured water content or additionally corrected for anion exclusion. For chemically conservative compounds this recalculation is established in Chapter 5. Thus, in this Section only ion ratios are presented as they are independent of the recalculation formalisms, except for Cl and Br.

4.4.2.1 Contamination by drilling fluid

During sample preparation approximately 1.5 cm of rim material is removed from the drill core samples to avoid contamination by the drilling fluid. However, in porous and permeable rocks such as e.g. dolostones or sandstones, the drilling fluid might reach the central parts of the drill core. This was already observed in a few samples from the Bülach-1-1 (BUL1-1) and TRU1-1 boreholes (Mazurek et al. 2021, Aschwanden et al. 2021).

The drilling fluid used in the section from the Dogger to the Schinznach Formation was a potassium silicate mud down to a depth of approximately 880 m and was then gradually or completely replaced by sodium silicate mud (see Section 2.5). It remains unclear to which extent the K-silicate drilling fluid still affected the borehole below 880 m: either from extensive fluid losses further up in the borehole or by using remaining K-silicate drilling mud. Both drilling muds are highly alkaline and characterised by a high Si and K or Na concentration. The concentration of Si and K in the hyperalkaline K-silicate mud is extreme (ca. 40 g/L Si, 70 g/L K, mostly balanced by OH, Section 2.5) and only a small portion is required to affect an entire aqueous extract. The K-silicate drilling mud contains SO_4, Cl, Br and Na concentrations that do not differ much from porewater concentrations and thus bear much less potential to contaminate the aqueous extracts (ca. 1.2 g/L SO_4, 4.9 g/L Cl and 4.4 g/L Na, Section 2.5).

In this borehole we identified 8 samples from the Bänkerjoch, Schinznach and Zeglingen Formation that show evidence for contamination by the drilling fluid for selective components (Tab. 4.4-2). All these samples exhibit a high Si concentration and most of them have a close to zero or positive saturation index for quartz along with a low quartz content of the rock (Tab. 4.4-2). Aqueous extracts are unlikely to reach equilibrium with the barely soluble quartz and clay minerals during the 24 h reaction time and, hence, this indicates that the Si derives from the drilling fluid. The molar Na/K ratio is below or close to 1 in most of the contaminated samples, where the K-silicate drilling fluid was used (above or close to 880 m depth), which is hard to reach through evolving a marine porewater in the corresponding formations, or by later processes (Tab. 4.4-2). Additionally, some of the contaminated samples have elevated alkalinity and pH values pointing towards contamination by the drilling fluid (Tab. 4.4-2). Most of the contaminated samples are dolostones with a high porosity and likely also elevated permeability. Two contaminated samples are clay- and anhydrite-rich and likely much less permeable. It remains unclear how the drilling mud enters the interior of these samples, but the contamination could be induced during sample preparation by accidentally mixing in rim fragments into the material used for aqueous extraction.

Tab. 4.4-2: List of 8 samples and their geochemical characteristics which classify them as contaminated by the drilling fluid

The drilling fluid is characterised by a high Si concentration, pH, alkalinity and a high K concentration above 880 m. Below 880 m depth the drilling fluid is Na- and Si-rich but might still contain portions of K drilling mud (see Section 2.5). The abbreviations are Bä: Bänkerjoch Formation, Sc: Schinznach Formation, Ze: Zeglingen Formation and alk:. alkalinity.

Depth [m]	**Fm.**	**Füchtbauer name**	**WC_{wet}** [wt.-%]	**Qz** [wt.-%]	**Si** [mg/L]	**SI Qz**	**Na/K** [mol/mol]	**pH**	**alk.** [meq/L]
805.16	Bä	No Füchtbauer name (Anhydrite & Clay rich)	5.236	3	8.1	0.2	17.6	7.7	0.6
861.68	Bä	No Füchtbauer name (Anhydrite & Clay rich)	0.184	tr	4.1	-0.1	1.1	8.1	0.5
866.43	Sc	Very sandy/silty claystone	2.557	27	8.4	0.2	0.8	7.7	0.9
885.59	Sc	Dolostone	2.385	1	48.1	0.7	0.4	9.8	8.5
892.99	Sc	Dolostone	1.26	3	3.7	-0.2	2.8	8.9	2.3
896.73	Sc	Dolostone	1.747	3	5.2	0.0	4.2	8.7	2.2
918.04	Sc	Dolostone	1.393	2	17.3	0.3	23.9	9.6	2.9
935.12	Ze	Dolostone	9.058	4	144.0	0.5	1.2	10.6	20.9

It is conspicuous that all samples from the Schinznach Formation are aligned along a different linear trend with higher Br/Cl ratios than seawater (Fig. 4.4-1), but there is no explanation for this to be a contamination issue at this stage even though these samples were classified as contaminated based on their Si concentration, pH and alkalinity. For Br, Cl, Na and SO_4 the maximal estimated proportion of contamination lies within the analytical uncertainty, except for the Cl concentration of a dolostone sample at 935.12 m with a potential uncertainty of 7 to 14%. This estimation is based on the Si and K concentrations of the drilling mud and the assumption that all measured Si and K derives from the drilling mud. Note that calculations are made with the same drilling mud analysis from 842 m depth despite a drilling mud change at 880 m depth. All samples that show indications for contamination by the drilling fluid are highlighted with red circles in Figs. 4.4-4 and 4.4-5.

4.4.2.2 Anions

The Cl concentrations in the aqueous extracts range between 2.2 and 380 mg/L and reach maximal values in the Kaiseraugst Formation. The Br concentrations vary from below the limit of detection to 0.54 mg/L in the Schinznach Formation.

Most of the samples from the Villigen Formation to the Weitenau Formation exhibit a molar Br/Cl ratio below the seawater ratio and follow a linear trend with a slope of a third of the latter (Fig. 4.4-1). Despite the scatter, the Kaiseraugst Formation appears to have distinctly lower Br/Cl ratios. The samples from the Schinznach Formation form an exception and plot along a linear trend above the seawater ratio.

The depth profile of the Br/Cl ratio (Fig. 4.4-2) displays a smooth trend with slightly decreasing Br/Cl ratios from the Villigen Formation to the base of the Staffelegg Formation. From the Klettgau Formation downwards, the Br/Cl ratios vary more strongly and reach high values in the Bänkerjoch and the Schinznach Formation before attaining a minimum at the base of the Zeglingen Formation.

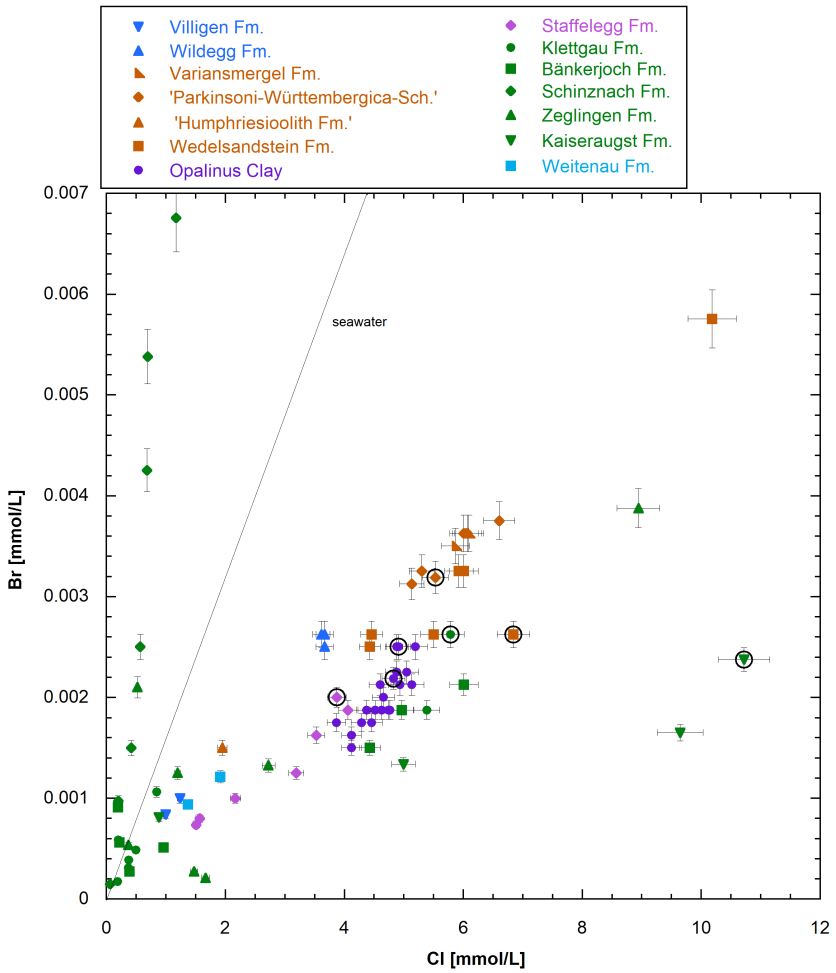

Fig. 4.4-1: Molar Br versus Cl concentrations in aqueous extracts at a S/L ratio of about 1 AD samples are marked with black circles.

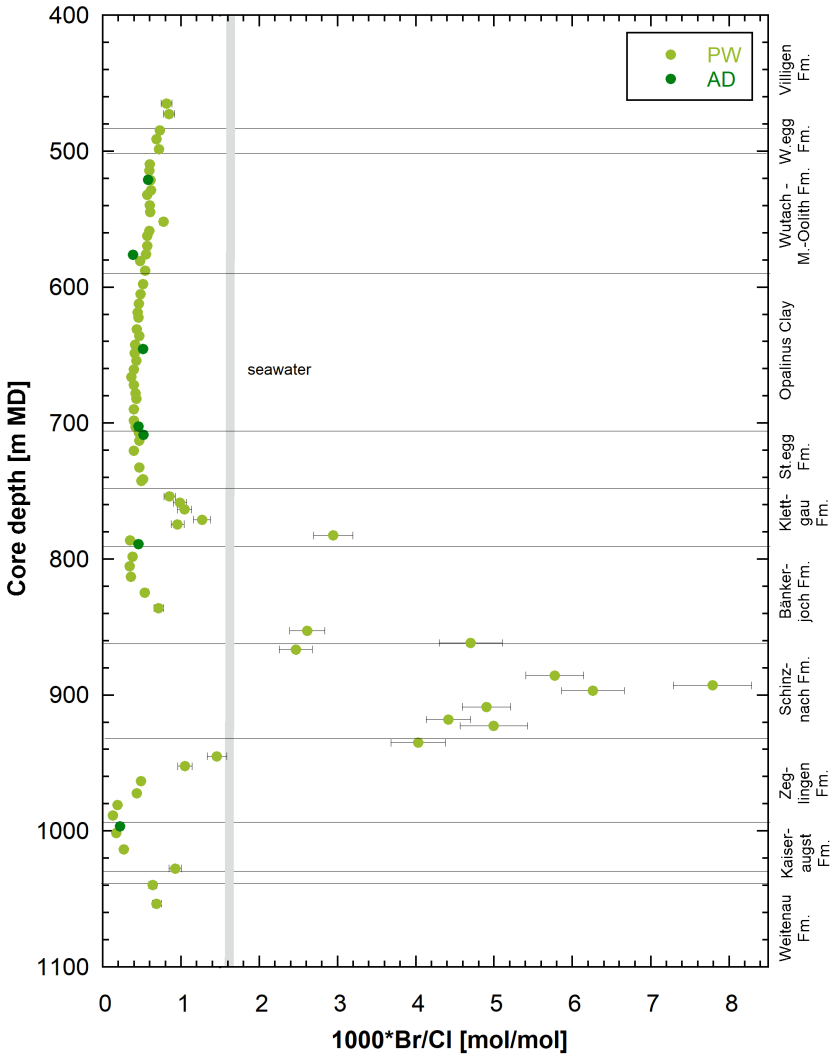

Fig. 4.4-2: Depth profile of the molar Br/Cl ratio in aqueous extracts at a S/L ratio of about 1

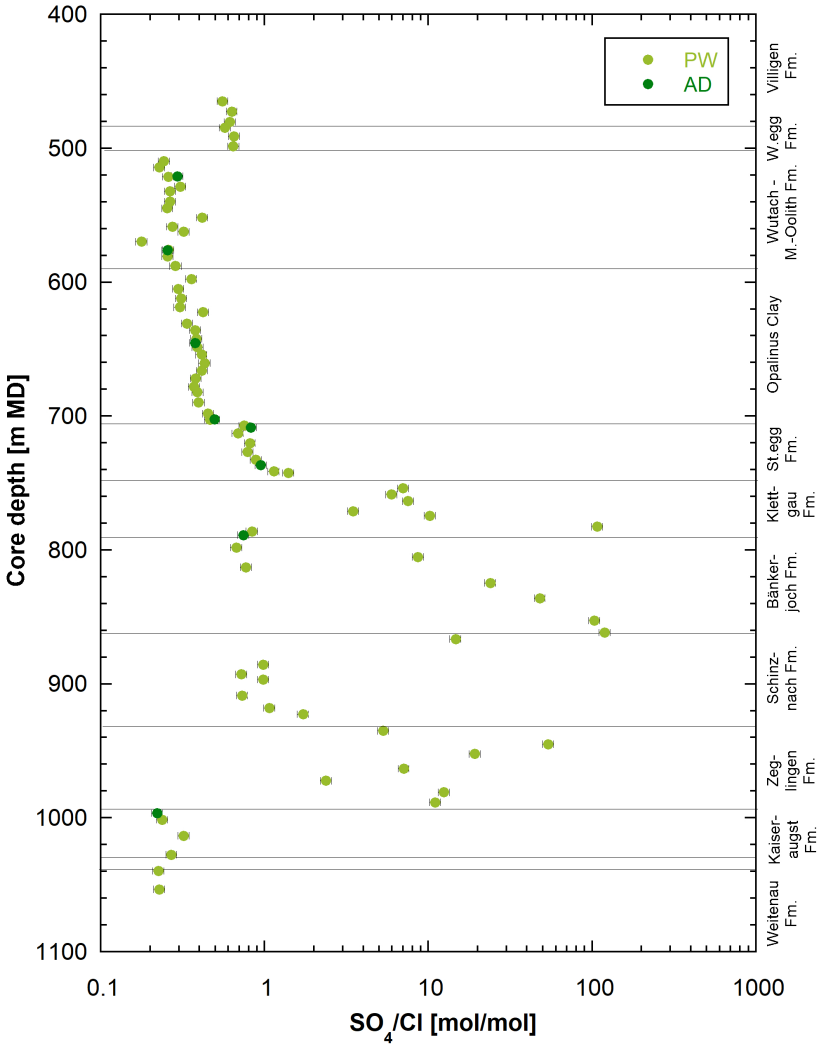

Fig. 4.4-3: Depth profile of SO_4/Cl molar concentration ratio in aqueous extracts at a S/L ratio of about 1

The SO_4 varies between 23 and 443 mg/L with the exception of anhydrite bearing samples from the Klettgau, Bänkerjoch and Zeglingen Formation where concentrations range between 1'750 up to 3'680 mg/L. The depth profile of the SO_4/Cl ratio in aqueous extract solutions presents a near-constant value in the Villigen and Wildegg Formations and a sharp step-like change to lower values in the Wutach Formation and below. This shift arises from a sharp decrease in the SO_4 concentrations, apparent when bulk porewater concentrations are compared to each other (see Figs. 4.4-7 and 5.3-1). At this position in the depth profile, there is a lithological change manifested by an increasing clay, quartz and pyrite content and a decreasing calcite content. However, there is no obvious link between this lithological change and the shift in the SO_4/Cl ratios. Sample preparation issues, such as the release of fluid inclusions, that are abundant in calcite, cannot explain the shift since this would lead to lower rather than higher ratios. Also, analytical issues can be excluded.

Subsequently, the ratio increases slightly in a smooth trend from the top of the Wutach Formation throughout the «Brauner Dogger», Opalinus Clay and the Staffelegg Formation. A local maximum with substantial scatter is evident in the Klettgau Formation where the sample with the highest value contains anhydrite. Towards the base of the Klettgau Formation and top of Bänkerjoch Formation a local minimum is reached. In the lower half of the Bänkerjoch Formation and the Zeglingen Formation many samples contain anhydrite which leads to locally higher SO_4/Cl ratios with significant scatter. Ratios are lower in the dolomitic and calcareous units of the Schinznach Formation between the anhydritic units. Further below, ratios are low and less variable in the Kaiseraugst and Weitenau Formation, similar to those in the Dogger.

The F concentrations in aqueous extracts range between 0.2 and 7.5 mg/L across the whole depth profile (not shown) with the highest values being in the Wildegg, Staffelegg and Klettgau Formations. The alkalinity varies between 0.3 and 5.3 meq/L when excluding the contaminated samples (alkalinity affected by OH). The pH is fairly constant from the Villigen to the Staffelegg Formation and continues with more scatter down to the Weitenau Formation. The values range from 7.0 up to 9.3, disregarding likely contaminated samples with high dissolved Si concentrations > 10 mg/L (Tab. 4.4-2).

4.4.2.3 Cations

The Na concentrations vary between 5 and 1'174 mg/L with maximal values reached in the Bänkerjoch Formation before the switchover to the Na silicate drilling fluid. The Na/Cl ratios show little variability throughout the Malm and Dogger section of the depth profile. The ratios increase in the Staffelegg Formation until reaching a maximum in the Klettgau Formation. The Na/Cl ratios scatter from the base of the Klettgau Formation downwards around the values measured in the Malm and Dogger section of the borehole with a few exceptions in the Bänkerjoch and Zeglingen Formation.

The K concentrations range from 1.78 mg/L in the Schinznach Formation up to 470 mg/L in the Zeglingen Formation, where the drilling fluid is dominated by a Na silicate mud. The Na/K ratios present a complex depth profile with the highest ratios in the Staffelegg and Klettgau Formation. The very low Na/K ratios observed in the top of Schinznach Formation (below or close to 880 m depth) are indicative for drilling fluid contamination (elevated K) as discussed in detail in Section 4.4.2.1. Most of the AD samples plot below the neighbouring PW samples. The samples with the largest discrepancy are located in the «Brauner Dogger» in the K-silicate fluid section and contain a low Na concentration rather than a high K concentration (Section 4.7.4), implying that there are no contamination issues with these samples. The Sr concentrations differ between 0.029 and 13.6 mg/L and maximal values are measured in the Bänkerjoch Formation. The Sr/Cl ratios (not shown) plot in a narrow range throughout the Malm, Dogger and Lias sections with a couple of outliers. In the underlying formations the Sr concentration varies over several orders of magnitude. This can be explained by the release of Sr from the dissolution of anhydrite during aqueous extraction. Celestite was detected in an anhydrite-bearing sample from the Klettgau Formation.

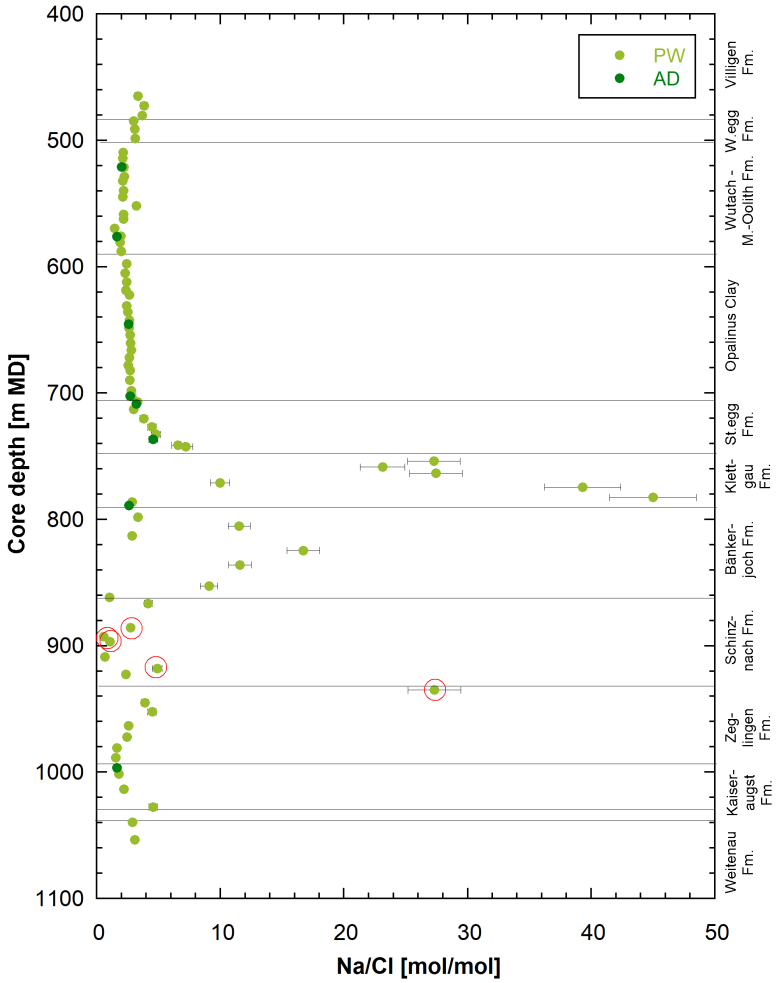

Fig. 4.4-4: Depth profile of the Na/Cl molar concentration ratio in aqueous extracts at a S/L ratio of about 1

The samples with red circles show indications of contamination by the Na -silicate drilling fluid.

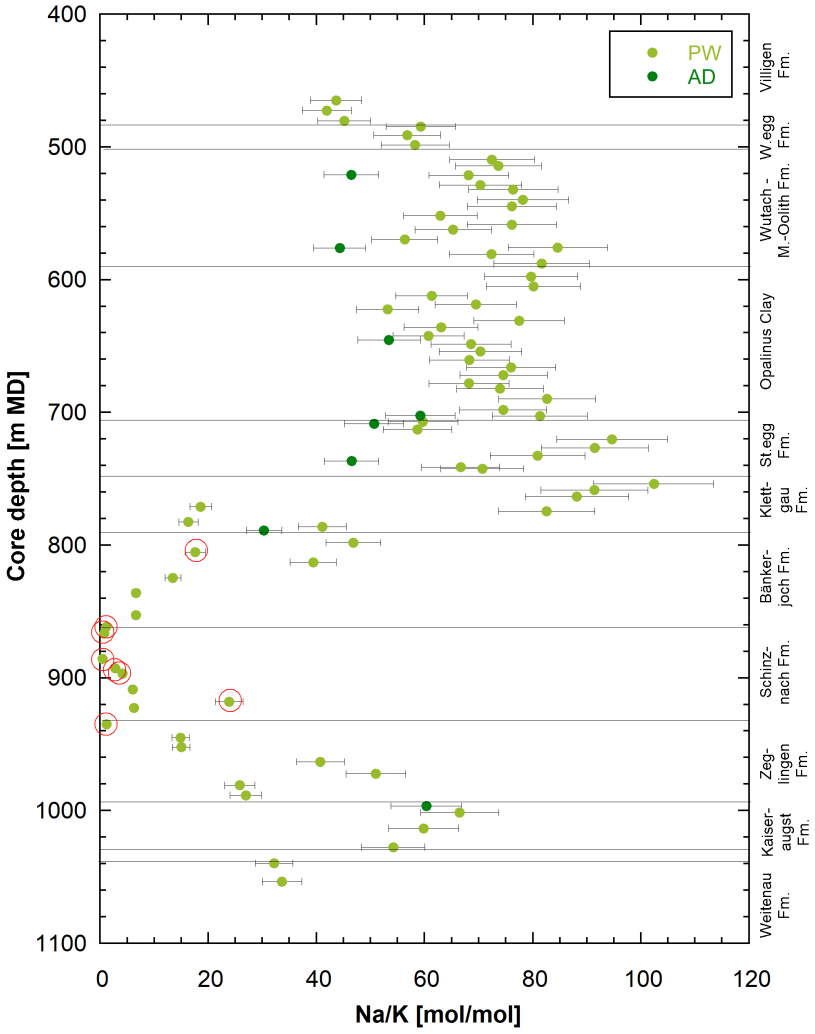

Fig. 4.4-5: Depth versus Na/K molar concentration ratio in aqueous extracts at a S/L ratio of about 1

The samples with red circles show indications of contamination by the K- and/or Na-silicate drilling fluid.

4.4.2.4 Saturation indices

Most aqueous extract solutions from the Malm, Dogger and Lias are saturated or close to saturation with respect to calcite, but mostly undersaturated with respect to dolomite (disordered and ordered) (Tab. 4.4-3). The saturation indices for calcite vary from the Klettgau to the Weitenau Formation from -0.8 to 1.0, with distinct oversaturation reached in many samples from all these formations. Calcite oversaturation is expected for anhydrite-bearing samples where dissolution of Ca-sulphate is producing excess Ca that cannot be precipitated as calcite sufficiently fast. All considerably undersaturated samples with respect to calcite don't contain detectable amounts of calcite with the exception of the samples at 678 and 996 m depth which contain 3 and 57 wt.-%, respectively, despite showing an undersaturation of -0.3. This might be caused by calcite dissolution during the aqueous extraction leading to a pCO_2 level below atmospheric concentrations and a subsequent decrease in pH due to CO_2 equilibration during filtration and titration. Contamination by K, Na and Si from drilling muds (Sections above) is not

expected to significantly affect calculations, except in case of pH and alkalinity (total titrated alkalinity interpreted as carbonate alkalinity for speciation calculations), or where significant additional K or Na uptake may liberate Ca-Mg-Sr-Na or K from the clay exchanger.

The sulphate minerals gypsum, anhydrite and celestite are undersaturated by 2 to 4 orders of magnitude in all extract solutions from the Malm to the Lias and in the Schinznach, Kaiseraugst and Weitenau Formation. The samples that contain anhydrite in the Klettgau, Bänkerjoch and Zeglingen Formation are saturated with respect to gypsum and close to saturation with respect to anhydrite. Two samples in the Klettgau and Bänkerjoch Formation reached celestite saturation even though only one of them has detectable levels of celestite in the XRD analysis.

Quartz saturation or oversaturation is reached in most of the samples which are contaminated by the drilling fluid despite a dilution factor of 20 to 30 (Tab. 4.4-3).

Tab. 4.4-3 Saturation indices for calcite, dolomite (disordered and ordered), gypsum, anhydrite, celestite and quartz at a S/L 1, pH and partial pressure of CO_2

Mineral saturation indices were calculated with the PHREEQC Version 3 code (Parkhurst & Appelo 2013) and the PSI/Nagra thermodynamic database (Thoenen et al. 2014) assuming a temperature of 25 °C. Note that a few samples lack a SI for dolomite due to Mg concentrations below the limit of detection. For all AD samples (521.06 m, 576.32 m, 645.48 m, 702.40 m, 708.51 m, 736.79 m, 788.85 m and 996.55 m) the carbonate system is defined through the total inorganic carbon concentration instead of the alkalinity. The abbreviations are Ma: Malm, Bd: «Brauner Dogger», Op: Opalinus Clay, St: Staffelegg Fm., Kl: Klettgau Fm., Bä: Bänkerjoch Fm., Sc: Schinznach Fm., Ze: Zeglingen Fm., Ka: Kaiseraugst Fm., We: Weitenau Fm., Cc: Calcite, Do: Dolomite, Gy: Gypsum, An: Anhydrite, Ce: Celestite, Qz: Quartz; dis: disordered, ord: ordered.

Fm.	**Depth** [m]	**S/L**	**SI Cc**	**SI Do (dis)**	**SI Do (ord)**	**SI Gy**	**SI An**	**SI Ce**	**SI Qz**	**pH**	**log(pCO_2)** [bar]
Ma	464.92	0.97	0.35	-0.22	0.33	-3.15	-3.37	-2.89		9.60	-4.76
Ma	472.60	0.98	0.18	-0.54	0.01	-3.18	-3.40	-2.91		9.32	-4.38
Ma	480.48	0.96	0.17	-0.64	-0.09	-3.19	-3.42	-2.94		9.34	-4.40
Ma	484.71	0.93	-0.05	-0.85	-0.30	-2.68	-2.91	-2.26		8.75	-3.52
Ma	491.19	0.93	-0.04	-0.84	-0.29	-2.58	-2.80	-2.13		8.74	-3.54
Ma	498.58	0.94	0.05	-0.69	-0.14	-2.53	-2.75	-2.10		8.76	-3.55
Bd	509.68	0.95	0.24	-0.33	0.22	-2.80	-3.02	-2.42		8.93	-3.65
Bd	514.32	0.89	0.02	-0.83	-0.28	-2.78	-3.01	-2.41		8.65	-3.34
Bd	521.06	0.93	0.16	-0.54	0.01	-2.81	-3.03	-2.43		9.06	-3.91
Bd	521.29	0.89	0.04	-0.76	-0.21	-2.85	-3.08	-2.49		8.77	-3.49
Bd	528.63	0.92	-0.03	-0.87	-0.32	-2.76	-2.99	-2.37		8.72	-3.47
Bd	532.18	0.88	0.18	-0.42	0.13	-2.71	-2.94	-2.29		8.88	-3.62
Bd	539.84	0.89	0.12	-0.55	0.00	-2.77	-3.00	-2.35		8.83	-3.55
Bd	544.94	0.90	0.07	-0.64	-0.09	-2.79	-3.01	-2.37		8.79	-3.52

Tab. 4.4-3: continued

Fm.	**Depth** [m]	**S/L**	**SI Cc**	**SI Do (dis)**	**SI Do (ord)**	**SI Gy**	**SI An**	**SI Ce**	**SI Qz**	**pH**	**log(pCO_2)** [bar]
Bd	551.76	0.95	0.34	-0.22	0.33	-3.14	-3.36	-2.92		9.37	-4.27
Bd	558.62	0.93	0.07	-0.77	-0.22	-3.00	-3.22	-2.67		9.06	-3.92
Bd	562.53	0.95	0.13	-0.58	-0.03	-2.93	-3.16	-2.58		9.19	-4.12
Bd	569.87	0.90	-0.07	-0.95	-0.40	-2.32	-2.55	-1.40		8.55	-3.60
Bd	575.90	0.89	-0.01	-0.88	-0.33	-2.85	-3.07	-2.51		8.93	-3.81
Bd	576.32	0.91	0.07	-0.72	-0.17	-2.77	-3.00	-2.33		9.18	-4.25
Bd	580.89	0.94	0.03	-0.82	-0.27	-2.91	-3.13	-2.49		9.09	-4.05
Bd	588.03	0.93	0.15	-0.54	0.01	-2.78	-3.00	-2.29		9.08	-3.98
Op	597.66	0.92	0.13	-0.61	-0.06	-2.73	-2.95	-2.39		8.87	-3.61
Op	605.04	0.90	0.08	-0.69	-0.14	-2.80	-3.02	-2.49		8.79	-3.49
Op	612.16	0.92	0.09	-0.66	-0.11	-2.87	-3.09	-2.54		8.85	-3.53
Op	618.77	0.91	-0.10	-1.04	-0.49	-2.81	-3.04	-2.49		8.56	-3.20
Op	622.45	0.94	0.02	-0.89	-0.34	-2.81	-3.03	-2.51		8.83	-3.59
Op	630.96	0.92	0.02	-0.86	-0.31	-2.79	-3.01	-2.50		8.73	-3.41
Op	635.90	0.92	0.00	-0.88	-0.33	-2.78	-3.01	-2.43		8.74	-3.44
Op	642.38	0.91	0.00	-0.85	-0.30	-2.83	-3.05	-2.53		8.75	-3.43
Op	645.48	0.96	0.01	-0.88	-0.33	-2.70	-2.92	-2.40		8.65	-3.30
Op	648.73	0.92	0.05	-0.82	-0.27	-2.74	-2.96	-2.46		8.73	-3.40
Op	654.25	0.92	-0.05	-1.03	-0.48	-2.73	-2.95	-2.44		8.62	-3.29
Op	660.46	0.92	-0.02	-0.96	-0.41	-2.80	-3.03	-2.49		8.74	-3.43
Op	666.13	0.92	0.02	-0.82	-0.27	-2.80	-3.03	-2.54		8.74	-3.40
Op	671.90	0.90	0.06	-0.72	-0.17	-2.75	-2.97	-2.48		8.72	-3.35
Op	678.24	0.90	-0.33	-1.56	-1.01	-2.68	-2.91	-2.44		8.29	-2.94
Op	682.31	0.90	-0.06	-1.06	-0.51	-2.72	-2.94	-2.50		8.53	-3.13
Op	689.93	0.90	0.01	-0.83	-0.28	-2.73	-2.95	-2.47		8.65	-3.27
Op	698.24	0.90	0.02	-0.82	-0.27	-2.69	-2.92	-2.48		8.69	-3.34
Op	702.40	0.92	-0.01	-0.91	-0.36	-2.65	-2.88	-2.44		8.63	-3.28
Op	702.63	0.90	-0.02	-0.98	-0.43	-2.56	-2.78	-2.34		8.63	-3.34
St	707.11	0.93	-0.13	-1.20	-0.65	-2.51	-2.74	-2.24		8.60	-3.38
St	708.51	0.92	-0.01	-0.93	-0.38	-2.36	-2.59	-2.03		8.75	-3.62
St	712.92	0.93	-0.01	-0.93	-0.38	-2.37	-2.60	-1.98		8.68	-3.53
St	720.33	0.90	0.00	-0.92	-0.37	-2.76	-2.98	-2.55		8.91	-3.63
St	726.88	0.92	-0.05	-1.07	-0.52	-3.05	-3.27	-2.88		8.96	-3.65
St	732.78	0.91	-0.10	-1.14	-0.59	-2.93	-3.15	-2.80		8.75	-3.36
St	736.79	0.91	0.02	-0.95	-0.40	-2.86	-3.09	-2.77		8.97	-3.70
St	741.38	0.89	0.03	-0.86	-0.31	-2.98	-3.21	-2.95		8.87	-3.44
St	742.48	0.88	-0.10	-1.17	-0.62	-2.87	-3.09	-2.82		8.68	-3.24
Kl	754.10	0.91	0.30	-0.12	0.43	-2.99	-3.21	-2.85		9.49	-4.25
Kl	758.60	0.89	0.53	0.12	0.67	-2.57	-2.79	-2.68		9.23	-3.87

Tab. 4.4-3: continued

Fm.	**Depth** [m]	**S/L**	**SI Cc**	**SI Do (dis)**	**SI Do (ord)**	**SI Gy**	**SI An**	**SI Ce**	**SI Qz**	**pH**	**log(pCO_2)** [bar]
Kl	763.57	0.94	0.29	-0.17	0.38	-2.93	-3.16	-2.81		9.46	-4.22
Kl	771.18	0.91	0.35	0.53	1.08	-2.71	-2.93	-2.53		9.60	-4.65
Kl	774.47	0.91	0.11	-0.69	-0.14	-3.28	-3.50			9.66	-4.60
Kl	782.61	0.49	0.59	0.03	0.58	0.01	-0.22	0.05		8.14	-3.64
Kl	786.21	0.87	-0.41	-1.68	-1.13	-2.31	-2.54	-1.83		8.80	-4.06
Kl	788.85	0.90	0.31	-0.40	0.15	-2.30	-2.52	-2.30		9.31	-4.40
Bä	798.23	0.88	0.56	0.44	0.99	-2.46	-2.69	-2.47		9.14	-3.76
Bä	805.16	0.88	0.02	-1.19	-0.64	0.11	-0.12	-0.07	0.21	7.74	-3.31
Bä	812.97	0.87	-0.11	-0.93	-0.38	-2.34	-2.57	-2.29		8.71	-3.55
Bä	824.70	0.96	0.13	-1.19	-0.64	0.06	-0.16	-0.09		7.82	-3.49
Bä	836.13	0.98	0.56	-0.57	-0.02	0.08	-0.15	0.02		8.03	-3.62
Bä	852.75	0.99	0.73	-0.33	0.22	0.15	-0.07	-0.15		8.27	-3.92
Bä	861.68	0.97	0.54	-0.42	0.13	0.17	-0.05	-0.21	-0.10	8.05	-3.69
Sc	866.43	0.93	-0.46	-1.76	-1.21	-1.89	-2.12	-2.08	0.22	7.72	-2.98
Sc	885.59	0.95	0.68	1.86	2.41	-3.40	-3.62	-3.41	0.66	9.79	-4.43
Sc	892.99	0.97	0.55	1.38	1.93	-2.68	-2.90	-2.68	-0.19	8.88	-3.80
Sc	896.73	0.96	0.44	1.03	1.58	-2.47	-2.69	-2.51	-0.02	8.70	-3.63
Sc	908.68	0.99	0.37	1.01	1.56	-3.05	-3.27	-3.52	-0.69	9.25	-4.51
Sc	918.04	1.00	0.66	1.79	2.34	-3.06	-3.29	-3.41	0.30	9.62	-4.66
Sc	922.60	1.00	0.03	-0.36	0.19	-2.75	-2.97	-2.92	-0.07	8.79	-4.15
Ze	935.12	0.94							0.52	10.62	-5.60
Ze	945.09	1.03	-0.44	-3.35	-2.80	0.11	-0.11	-0.22	-0.66	7.27	-3.07
Ze	952.33	1.00	0.85	-0.45	0.10	0.15	-0.07	-0.17	-0.46	8.44	-4.11
Ze	963.33	0.99	0.98	-0.28	0.27	0.07	-0.16	-0.27		8.66	-4.40
Ze	972.31	0.98	1.00	0.08	0.63	-0.01	-0.23	-0.25		8.63	-4.19
Ze	981.01	1.00	-0.76	-4.19	-3.64	0.07	-0.15	-0.27		6.99	-2.83
Ze	988.60	0.98	-0.83	-4.28	-3.73	0.07	-0.15	-0.20		6.98	-2.88
Ka	996.55	0.92	-0.27	-1.64	-1.09	-2.63	-2.85	-2.66		8.60	-3.49
Ka	1'001.49	0.92	0.07	-0.90	-0.35	-2.64	-2.86	-2.57		8.87	-3.69
Ka	1'013.57	0.92	0.07	-0.97	-0.42	-2.96	-3.18	-2.94		9.07	-3.88
Ka	1'027.56	0.97	0.27	-0.71	-0.16	-4.00	-4.23			9.80	-4.84
We	1'039.68	0.94	0.68	0.92	1.47	-3.22	-3.44	-2.76		9.56	-4.51
We	1'053.55	0.95	0.32	-0.37	0.18	-3.63	-3.85	-3.44		9.53	-4.52

4.4.3 Chloride and bromide concentrations in bulk porewater

The formalisms to recalculate Cl and Br concentrations in aqueous extracts to concentrations in bulk porewater are given in Waber (ed.) (2020). In clay-free rocks, this recalculation to water content delivers the porewater concentrations of Cl and Br directly. In clay-bearing rocks, this recalculation additionally has to account for the anion-exclusion effect in order to result in porewater concentrations. The derivation of the Cl- and Br-accessible porosity proportion and calculation of porewater concentrations is established in Chapter 5.

The recalculation of Cl and Br concentrations in aqueous extracts to concentrations in bulk porewater (Figs. 4.4-6 and 4.4-7) requires the knowledge of the water content of the rocks, which is obtained by calculating the average of the three gravimetric water contents (one regular sample and two subsamples used for diffusive-exchange experiments). Additional aqueous extraction tests were carried out on the dried regular water content subsample of the deepest three Schinznach Formation samples and all Zeglingen Formation samples in order to reduce the uncertainty regarding the variability of the water contents.

The depth profiles of Cl and Br concentrations in bulk porewater cover a large range of 0.1 to 94.4 g/kg_{H2O} and 0.3 to 59.3 mg/kg_{H2O}, respectively (Figs. 4.4-6 and 4.4-7). The AD aqueous extract samples fit well into the concentration profile of the PW aqueous extracted samples. Both, the Cl and Br concentrations, present constant values in the Malm and «Brauner Dogger» section and a general decreasing trend from the Opalinus Clay Formation down to the Staffelegg Formation (Figs. 4.4-6 and 4.4-7), reaching a minimum in the Klettgau Formation, the location of the not so prominent Keuper aquifer. At greater depths, a large variability in concentrations extends to the Weitenau Formation. A limited excursion to higher chloride concentrations occurs in the anhydrite-bearing rocks of the Bänkerjoch Formation, and much more prominently in the Zeglingen Formation comprising similar lithologies. Lower values are reached towards the base of the Kaiseraugst Formation and the Weitenau Formation below. Trends in Br below 800 m do not closely correlate with chloride trends, with a prominent zone of rather high Br concentrations across the dolomites and limestones of the Schinznach Formation (see also Fig. 4.4-1). At this stage, these observed trends should be treated with care because the recalculated Cl and Br concentrations still need to be corrected for anion accessibility, which, as mentioned above, is further investigated in Chapter 5.

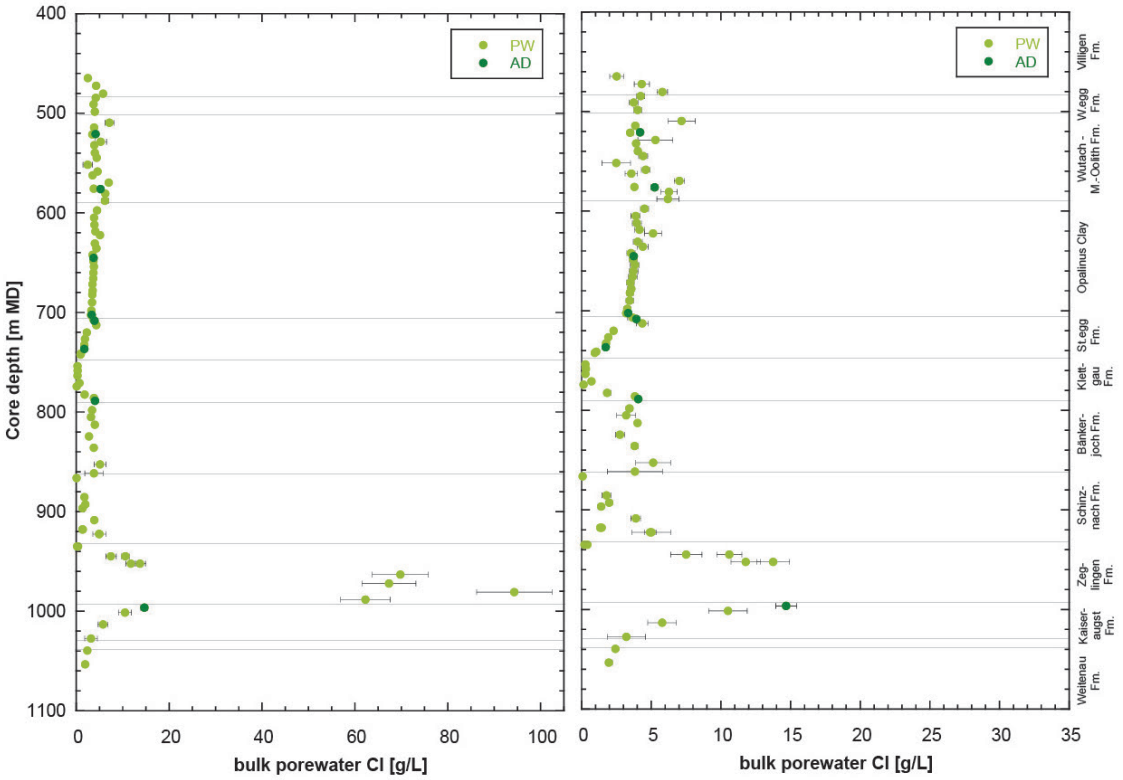

Fig. 4.4-6: Bulk porewater Cl concentrations versus depth from aqueous extracts
Left graph; expanded concentration scale.

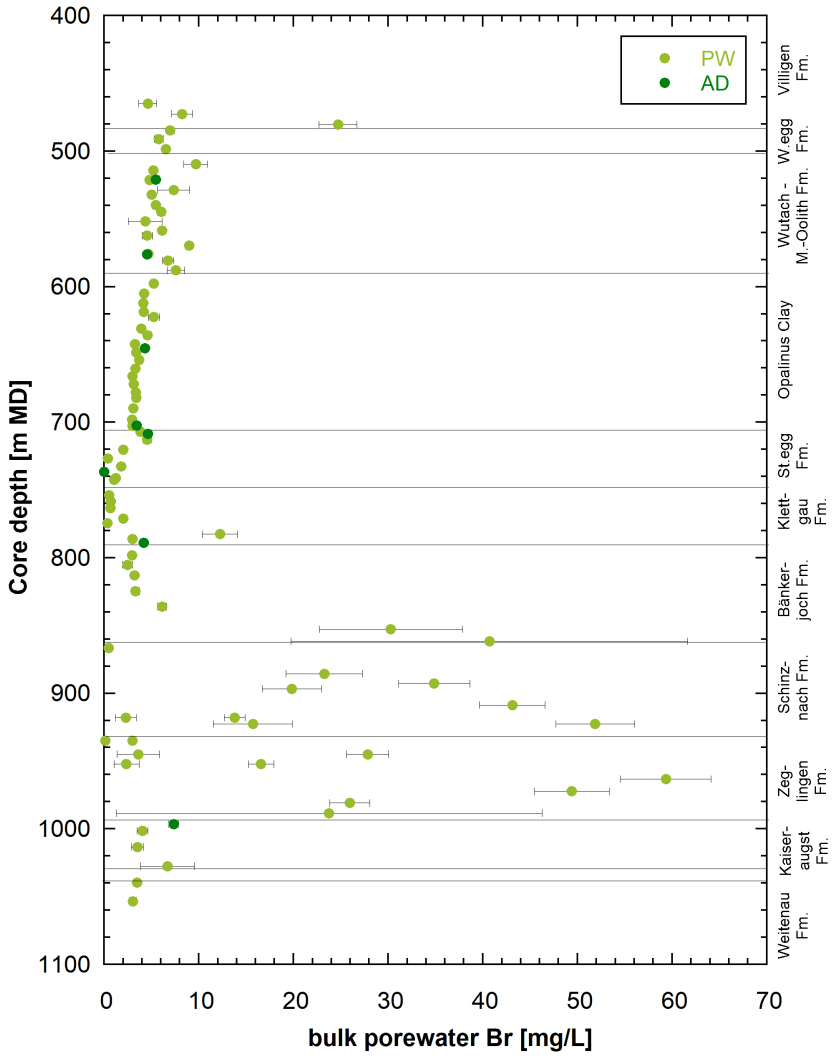

Fig. 4.4-7: Bulk porewater Br concentrations versus depth from aqueous extracts

4.5 Data from cation-exchange extraction measurements

Paul Wersin

Seven samples used for advective displacement experiments (AD samples) were analysed at Uni Bern with the nickel ethylenediamine (Ni-en) extraction method to determine the cation exchange capacity (CEC) and the composition of the clay exchanger (for methodology see Waber ed. 2020). Material from end pieces above and below the AD core was mixed to obtain a representative sample for Ni-en extraction. A larger number of samples were studied by the team at PSI using the CsCl extraction method (Marques Fernandes & Baeyens *in prep.*). The objective of the Ni-en extraction study was (i) to help to analyse the AD data (Section 4.7) and (ii) to compare and verify the PSI study with an alternative method.

The CEC can be derived in two ways: (1) From the consumption of the index cation (Ni in this case) during extraction and (2) from the sum of extracted cations (ΣCAT). Note that the latter includes (i) the exchangeable cations, (ii) cations dissolved in the porewater and (iii) cations released from potentially dissolving minerals (e.g. carbonates, sulphates) during extraction. Thus, in principle, the CEC derived from the sum of cations requires correction from contributions of (ii) and (iii). Corrected CEC and exchangeable cation data are discussed in Section 5.7, where the data from Uni Bern is also compared with that of PSI. The analysis does not include ammonium, NH_4^+, known to be present in small but measurable amounts (e.g. < 1 to 3 mg/L in aqueous extracts, at S/L ≈ 1, Section 4.7).

Tab. 4.5-1 shows the Ni consumption and extracted cation data (Na, K, Ca, Mg, Sr, Ba, Fe) for solid/liquid ratios (S/L) around 1[6]. Anion data (Cl, Br, SO_4, NO_3) is depicted in Tab. 4.5-2. Note that Ni nitrate was added to the samples, which explains the high NO_3 contents.

Tab. 4.5-1: Cation data from Ni-en extracts at a S/L ratio around 1 (Uni Bern data)

Type	Depth [m]	Formation	S/L [g/g]	Na	K	Ca	Mg	Sr	Ba	Fe	ΣCAT	Ni cons.
AD	521.06	«Parkinsoni-Württemb.-Sch.»	0.886	41.5	6.2	30.7	14.6	0.9	0.005	< 0.001	93.9	98.4
AD	576.32	Wedelsandstein Fm.	0.907	35.0	5.3	27.4	12.1	0.9	0.017	0.0012	80.7	85.0
AD	645.48	Opalinus Clay	0.913	47.1	6.3	32.5	14.2	0.8	0.012	< 0.001	101.0	106.9
AD	702.40	Opalinus Clay	0.884	56.6	6.8	43.9	16.1	0.9	0.009	< 0.001	124.3	126.2
AD	708.51	Staffelegg Fm.	0.964	32.2	4.1	24.0	10.1	0.6	0.010	0.0012	71.0	67.2
AD	736.79	Staffelegg Fm.	0.904	59.7	7.6	39.3	12.6	0.7	0.005	< 0.001	119.9	120.3
AD	996.55	Kaiseraugst Fm.	0.887	43.2	6.3	17.6	4.7	0.2	0.003	< 0.001	71.9	66.1

[6] A water mass equal to the mass of the wet rock was added, leading to S/L (mass of dry rock /[mass of added water + porewater]) slightly below 1.

Tab. 4.5-2: Anion data from Ni-en extracts at a S/L ratio around 1 (Uni Bern data)

Type	**Depth** [m]	**Formation**	**S/L** [g/g]	**F**	**Cl**	**Br**	**NO_3** [a]	**SO_4**
				[meq/$kg_{dry\ rock}$]				
AD	521.06	«Parkinsoni-Württembergica-Sch.»	0.886	0.05	5.3	0.003	227.2	2.5
AD	576.32	Wedelsandstein Fm.	0.907	0.03	6.9	0.005	222.0	2.8
AD	645.48	Opalinus Clay	0.913	0.03	4.7	0.002	220.8	2.6
AD	702.40	Opalinus Clay	0.884	0.06	4.8	< 0.002	226.2	3.5
AD	708.51	Staffelegg Fm.	0.964	0.03	4.2	< 0.002	218.0	4.2
AD	736.79	Staffelegg Fm.	0.904	0.08	2.3	< 0.002	224.4	3.2
AD	996.55	Kaiseraugst Fm.	0.887	0.02	11.2	< 0.002	238.9	3.7

[a] Nitrate is part of the added Ni-en stock solution

The CEC derived from Ni consumption of the AD samples varies in the range 66 – 126 meq/kg_{rock}, similar to the uncorrected sum of cations. Note that the sum of cations needs to be corrected for CEC as outlined in Section 5.7. The depth profiles of Ni consumption and ΣCAT data both show consistent trends (Fig. 4.5-1). The CEC data show a positive correlation with the clay-mineral content (Fig. 4.5-2). At a low clay-mineral content (i.e. < 40 wt.-%), however, there appears to be more scatter. The scatter in CEC at a low clay-mineral content is further discussed in Section 5.7.2.

Na and Ca are the main extracted cations, followed by Mg and K (Tab. 4.5-1). The Ca/Na ratio (eq/eq) is constant for the six samples down to the Staffelegg Formation, with values of 0.7 – 0.8. The lowermost sample from the Kaiseraugst Formation displays a lower Ca/Na ratio of 0.4. Mg correlates with Ca, thus the ratio (Ca+Mg)/Na shows the same trend as the Ca/Na ratio. The K/Na ratio exhibits a narrow range of 0.12 – 0.15 for all samples. The Sr/Na ratio ranges from 0.01 to 0.02 within the «Brauner Dogger» – Staffelegg Formation sequence and exhibits a low value of 0.004 in the Kaiseraugst Formation.

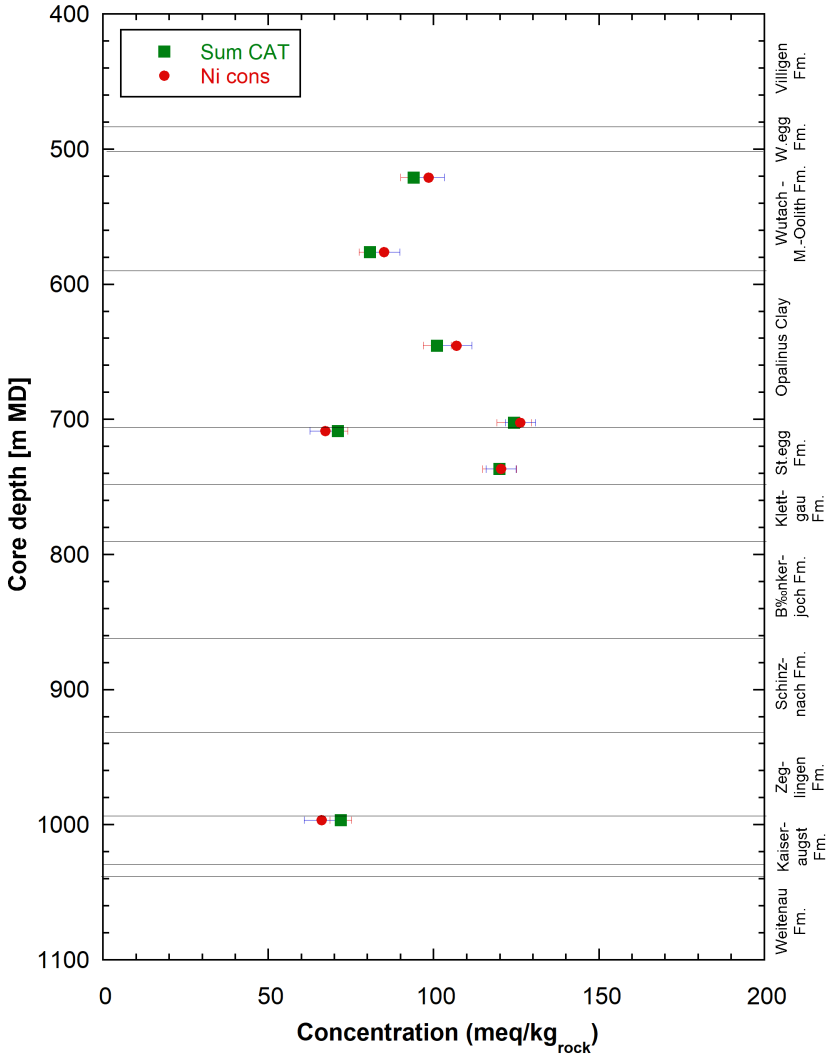

Fig. 4.5-1: Depth profile of Ni consumption and sum of cations (uncorrected, Uni Bern data)
Errors reflect propagated analytical uncertainties.

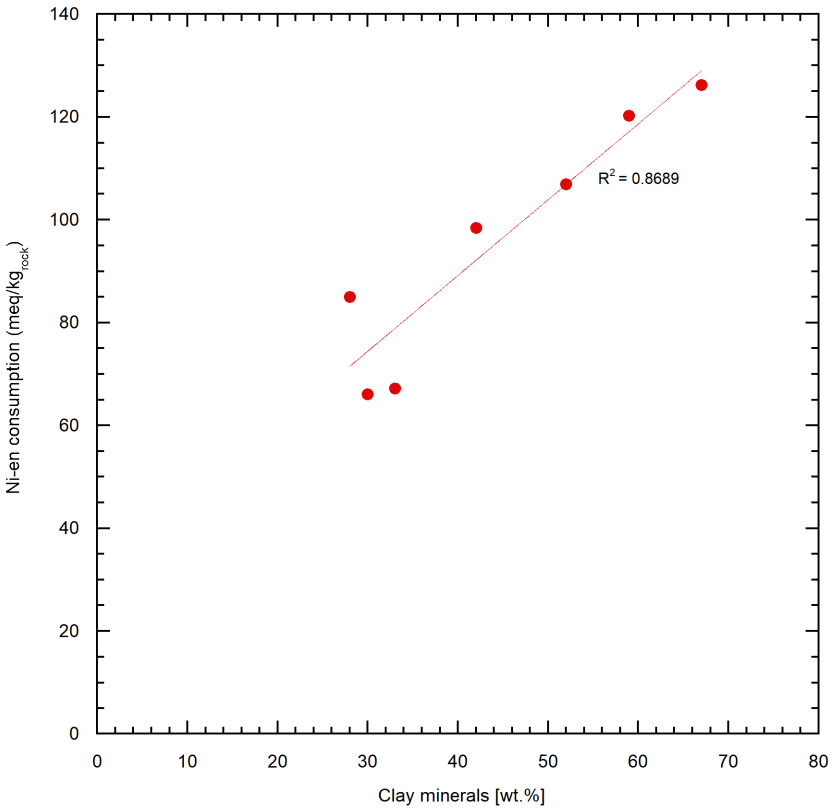

Fig. 4.5-2: Ni consumption vs. clay-mineral content (Uni Bern data)

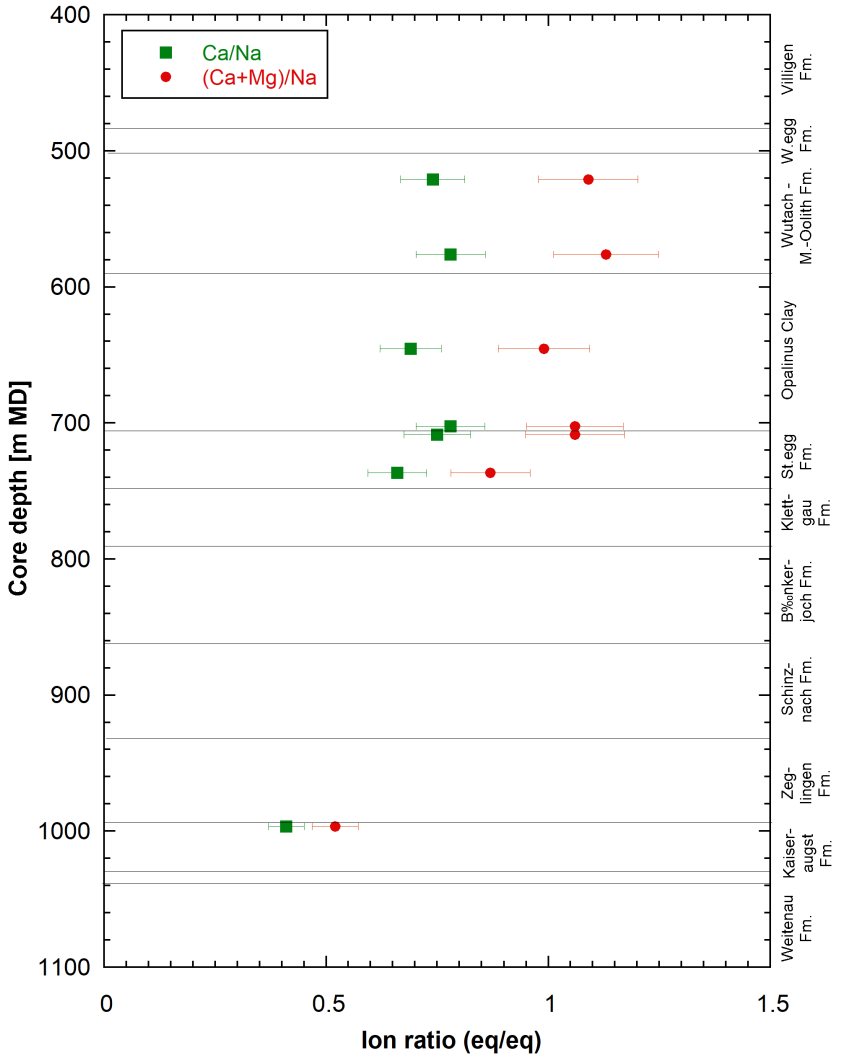

Fig. 4.5-3: Depth profiles of Ca/Na and (Ca+Mg)/Na ratios in Ni-en extracts (Uni Bern data)
Errors reflect propagated analytical uncertainties.

Speciation calculations on the Ni-en extracts were carried out with the PHREEQC Version 3 code (Parkhurst & Appelo 2013) and the PSI/Nagra thermodynamic database (Thoenen et al. 2014) assuming a temperature of 25 °C. The ethylene diamine complexes were taken from the MINTEC database (Allison et al. 1991) and included in the calculations. The concentration of ethylene diamine in the extracts, which was not analysed, was constrained by charge balance. The dissolved carbonate concentration (not measured) was constrained by assuming calcite equilibrium. The calculated TIC values are low, in the range of 0.09 – 0.27 mM (Tab. 4.5-3). The calculated partial pressures of CO_2 (pCO_2) and saturation indices for selected minerals are depicted in Tab. 4.5-3. The Ni-en extracts are clearly undersaturated with regard to the carbonate minerals dolomite and strontianite. They are also undersaturated with regard to the sulphate minerals gypsum and celestite but oversaturated with regard to barite.

Tab. 4.5-3: Calculated saturation indices of selected minerals, TIC and log(pCO_2) for Ni-en extract solutions

Calcite saturation was assumed in the calculations

Type	**Depth** [m]	**Formation**	**log(pCO_2)** [bar]	**TIC** [mol/kg_w]	**Gypsum**	**Celestite**	**Barite**	**Dolomite (ord)**	**Dolomite (dis)**	**Strontianite**
AD	521.06	«Parkinsoni-Württembergica-Sch.»	-4.63	1.27E-04	-1.46	-0.92	0.15	-0.19	-0.74	-0.72
AD	576.32	Wedelsandstein Fm.	-4.59	1.38E-04	-1.43	-0.88	0.76	-0.22	-0.77	-0.72
AD	645.48	Opalinus Clay	-4.48	1.18E-04	-1.36	-0.81	0.68	-0.20	-0.75	-0.72
AD	702.40	Opalinus Clay	-4.47	9.32E-05	-1.34	-0.95	0.76	-0.21	-0.76	-0.88
AD	708.51	Staffelegg Fm.	-4.67	1.43E-04	-1.39	-0.92	0.54	-0.23	-0.78	-0.80
AD	736.79	Staffelegg Fm.	-4.58	9.59E-05	-1.40	-0.95	0.48	-0.28	-0.83	-0.81
AD	996.55	Kaiseraugst Fm.	-4.16	2.72E-04	-1.47	-1.41	0.20	-0.44	-0.99	-1.20

4.6 Data from squeezing experiments

Martin Mazurek

A set of 9 samples from the interval «Brauner Dogger» – Muschelkalk were subjected to porewater squeezing. The mineralogical composition of the samples is listed in Tab. 4.6-1. The following observations can be made:

- Clay-mineral contents are ≥ 48 wt.-% for all samples.
- Sample 740.87 from the Staffelegg Formation contains only trace amounts of calcite and no other carbonates; it is exceptionally rich in clay minerals and devoid of feldspars.
- Calcite is the main carbonate mineral, except in the two samples from the Bänkerjoch Formation where dolomite/ankerite dominate.

Tab. 4.6-1: Mineralogical composition of samples subjected to squeezing experiments

tr = trace, empty field = mineral not identified.

Depth [m]	**Formation**	**Member**	**S** [wt.-%]	**C(inorg)** [wt.-%]	**C(org)** [wt.-%]	**Quartz** [wt.-%]	**K-feldspar** [wt.-%]	**Plagioclase** [wt.-%]	**Calcite** [wt.-%]	**Dolomite / Ank.** [wt.-%]	**Siderite** [wt.-%]	**Pyrite** [wt.-%]	**Clay minerals** [wt.-%]
524.95	«Parkinsoni-Württemb.-Sch.»		0.63	2.21	0.60	21	6	2	18	tr		1.2	50
560.01	Wedelsandstein Fm.		0.29	1.53	0.54	23	5	2	13	tr		0.5	56
599.33	Opalinus Clay	'Sub-unit with silty calcareous beds'	0.46	1.90	1.01	22	6	3	16			0.9	52
657.71	Opalinus Clay	'Mixed clay-silt-carbonate sub-unit'	0.19	1.78	0.78	27	5	3	10	tr	5	0.4	48
698.47	Opalinus Clay	'Clay-rich sub-unit'	0.30	1.32	0.88	15	5	2	8		4	0.6	66
740.87	Staffelegg Fm.	Beggingen Mb.	0.25	0.10	0.64	15			tr			0.5	84
798.00	Bänkerjoch Fm.		0.28	2.85	0.34	9	10	2	2	20		0.5	57
845.18	Bänkerjoch Fm.		< 0.05	1.87	0.19	14	6	2		14		< 0.1	64
1'019.57	Kaiseraugst Fm.	'Wellen-mergel'	0.10	2.32	0.20	14	5	5	18	tr	1	0.2	56

4.6.1 Mass recovery

The water masses obtained by squeezing are listed in Tab. 4.6-2 and shown graphically in Fig. 4.6-1 as a function of the squeezing pressure. The total mass recovery correlates with the initial water content of the sample (Fig. 4.6-2). The latter was measured at CRIEPI on the cut-off materials adjacent to the squeezed rock pieces. Samples yielded first water aliquots at 200 MPa, except for 3 samples where 300 MPa were required to extract the first waters. On the other hand, no evident correlation is found between mass recovery and the contents of clay or other minerals. Thus, other sample characteristics, such as microfabric, must play a role regarding squeezability.

Given the fact that a sufficient water mass was obtained in the pressure range 200 – 400 MPa, the experiments were terminated at this pressure, i.e. no waters were squeezed at the highest pressure of 500 MPa.

Tab. 4.6-2: Water masses squeezed at different pressure steps

The initial water content was measured at CRIEPI on cut-off materials adjacent to the squeezed core, and this value was used here to calculate the initial mass of porewater in the sample. "-": pressure step not applied.

Depth [m]	**Formation**	**Initial sample mass (CRIEPI)** [g]	**Initial wet water content (CRIEPI)** [wt.-%]	**Mass of porewater prior to squeezing (CRIEPI)** [g]	**Mass squeezed at P =**						**Total mass squeezed** [g]
					100 MPa [g]	**150 MPa** [g]	**200 MPa** [g]	**300 MPa** [g]	**400 MPa** [g]	**500 MPa** [g]	
524.95	«Parkinsoni-Württembergica-Sch.»	405.31	5.78	23.42	0	-	2.19	2.16	1.31	-	5.66
560.01	Wedelsandstein Fm.	418.28	6.26	26.19	0	-	2.89	2.35	1.38	-	6.62
599.33	Opalinus Clay	420.15	5.21	21.87	0	-	0.71	1.36	1.60	-	3.67
657.71	Opalinus Clay	423.32	4.52	19.13	0	-	0	0.79	1.12	-	1.91
698.47	Opalinus Clay	394.89	4.95	19.55	0	-	1.41	1.68	1.15	-	4.24
740.87	Staffelegg Fm.	390.71	6.02	23.51	0	-	1.59	1.29	0.81	-	3.69
798.00	Bänkerjoch Fm.	407.03	5.31	21.61	0	-	1.22	1.48	1.38	-	4.08
845.18	Bänkerjoch Fm.	454.79	5.78	26.29	0	-	0	0.87	1.32	-	2.19
1'019.57	Kaiseraugst Fm.	381.35	3.38	12.88	0	-	0	0.94	0.90	-	1.84

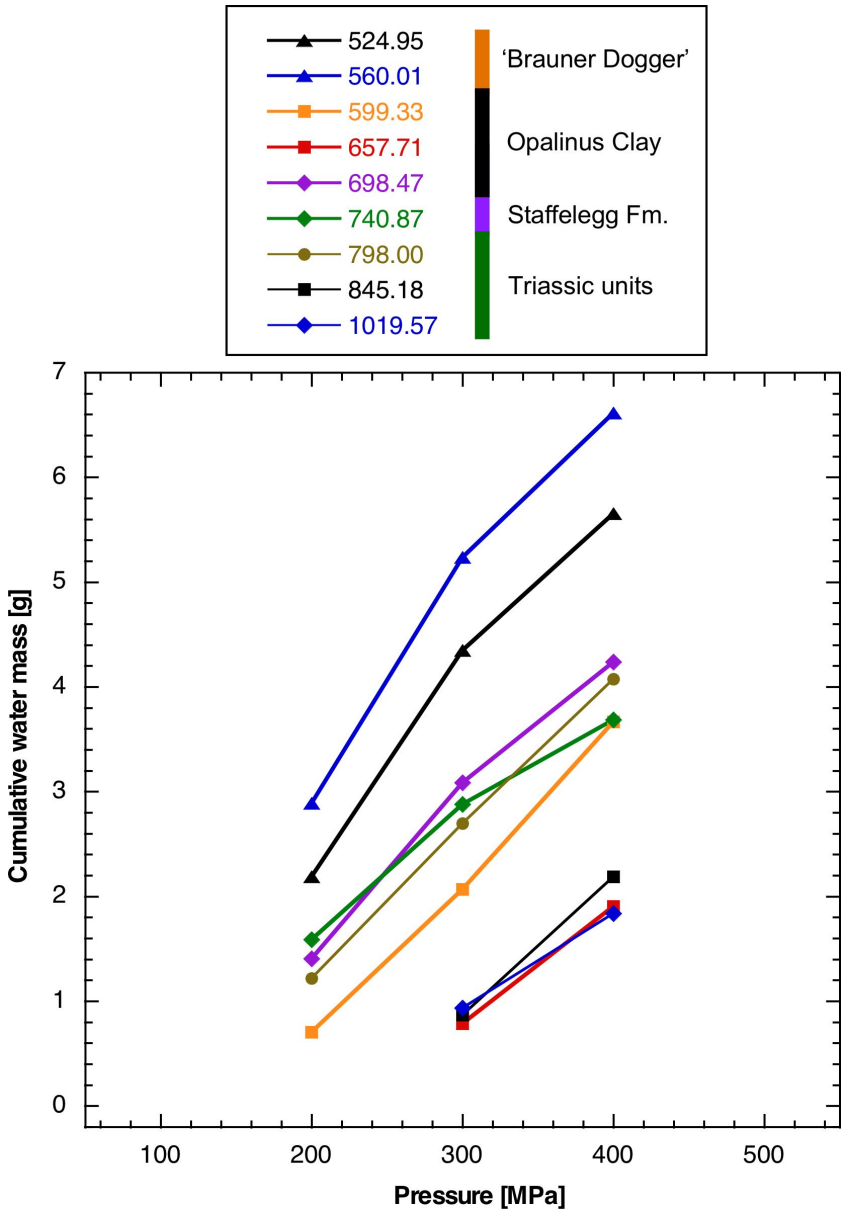

Fig. 4.6-1: Cumulative water masses obtained by squeezing as a function of the squeezing pressure

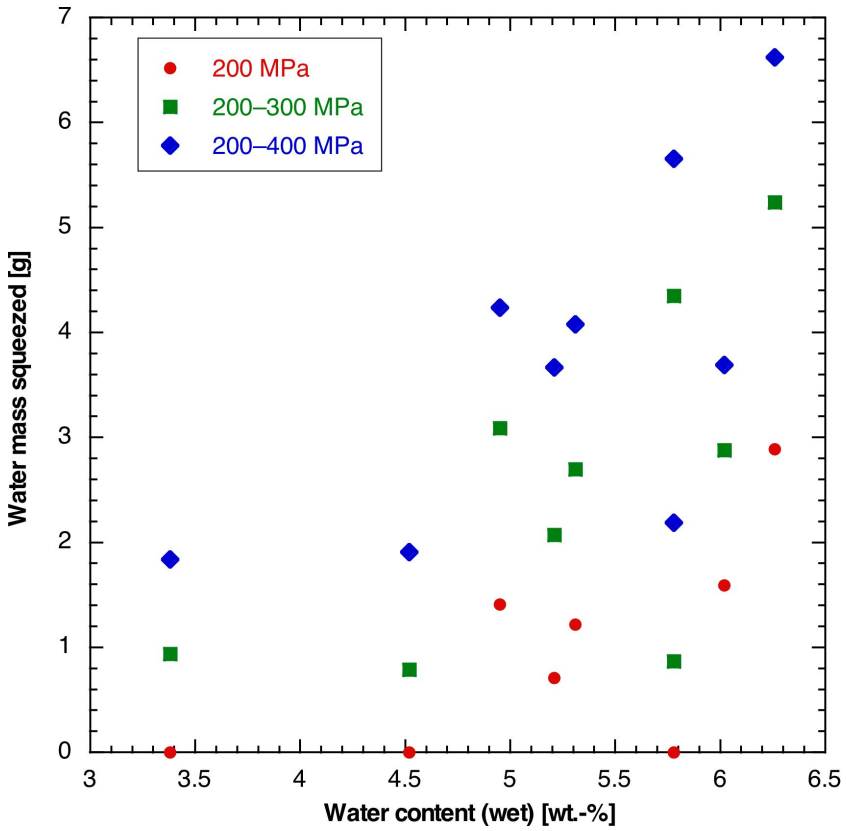

Fig. 4.6-2: Correlation of the original water content and the water mass obtained by squeeezing

4.6.2 Chemical composition of squeezed waters

Given the fact that the effects of artefacts (ion filtration, enhanced mineral dissolution) increase with squeezing pressure, only waters obtained during the first two pressure steps were analysed. The first squeezed aliquot yielded > 0.7 g water in all cases, from which a complete dataset (major-ion composition, TIC/TOC, pH, water isotopes) could be obtained. This is a success that has not been realised in full in previous campaigns with cores from BUL1-1 (Mazurek et al. 2021) and from TRU1-1 (Aschwanden et al. 2021). In addition, Si concentrations were analysed for the majority of the samples, motivated by the fact that K-silicate and Na-silicate drilling mud was used (Section 2.5) and so Si could potentially provide information about potential sample contamination by drilling fluid.

The chemical compositions of squeezed waters are listed in Tab. 4.6-3 and shown graphically as a function of squeezing pressure in Fig. 4.6-3. All waters are dominated by Na and Cl. The concentrations of monovalent ions (Na, K, Cl, Br, NO_3) generally decrease with squeezing pressure, likely due to ion-filtration effects that become important at higher pressures (Mazurek et al. 2015). Sample 845.18 from the Bänkerjoch Formation is exceptional in that the concentrations of most solutes show only marginal evolution (or even a slight increase for K, Br, TIC) with squeezing pressure. The mineralogical composition (Tab. 4.6-1) shows no distinctive features explaining this finding. Further, the NO_3 contents of two samples from the Opalinus Clay also slightly increase with squeezing pressure. Ca, Mg and Sr remain near-constant with pressure or increase slightly, the latter being considered to be due to the dissolution of carbonate minerals that becomes important at higher pressures. SO_4 concentrations remain constant within analytical error for most samples.

As discussed in Mazurek et al. (2015) and Rufer & Mazurek (2018), the composition of the first water aliquot recovered from a sample is considered to be closest to that of the porewater, and these analyses are highlighted by bold print in Tab. 4.6-3. F concentrations, in particular in the first squeezed aliquots, are contaminated by F leached from the fiberglass filters and so are not representative of the porewater. For clarity, the subset of the data that is considered to be useful for further interpretation is summarised in Tab. 4.6-4.

Tab. 4.6-3: Chemical composition of squeezed waters: full dataset

Bold print indicates the selected ("best") aliquots. F concentrations, in particular in the first squeezed aliquots, are contaminated by F leached from the fiberglass filters and so are not representative of the porewater. n.a. = no analysis.

Depth [m]	**Formation**	**Pressure** [MPa]	**Squeezing time** [d]	**Mass squeezed** [g]	**Na** [mg/L]	**NH_4** [mg/L]	**K** [mg/L]	**Ca** [mg/L]	**Mg** [mg/L]	**Sr** [mg/L]	**Ba** [mg/L]	**Si** [mg/L]	**F** [mg/L]	**Cl** [mg/L]	**Br** [mg/L]	**NO_3** [mg/L]	**SO_4** [mg/L]	**pH**	**TIC** [mg/L]	**TOC** [mg/L]	**TDS** [mg/L]	**Charge balance** [%]
524.95	«Parkinsoni-Württemb.-Sch.»	200	2	2.19	3'969	< 10	70.6	553	191	26.1	< 0.25	33.8	8.1	6'507	8.59	8.19	1'248	8.41	31.1	99.8	12'881	1.3
		300	3	2.16	3'392	< 10	44.9	588	202	27.7	< 0.25	32.5	4.5	5'667	7.39	7.09	1'261	8.32	27.6	63.0	11'438	1.7
560.01	Wedelsand-stein Fm.	200	2	2.89	3'765	< 10	69.8	566	180	26.1	0.26	31.5	7.2	6'170	7.91	8.61	1'283	8.50	25.7	96.5	12'342	1.4
		300	3	2.35	3'013	< 10	59.4	589	197	27.6	< 0.25	31.8	4.1	5'204	6.20	5.20	1'251	8.39	22.5	61.5	10'565	1.1
599.33	Opalinus Clay	200	3	0.71	4'460	< 10	80.6	635	194	22.0	< 0.25	38.2	11.2	7'291	8.87	20.60	1'341	8.33	38.9	187.0	14'488	1.3
		300	3	1.36	4'140	< 10	56.4	653	209	25.4	< 0.25	32.4	4.8	6'863	8.22	11.33	1'465	8.36	29.1	98.0	13'716	1.1
657.71	Opalinus Clay	300	3	0.79	4'608	< 10	78.3	666	164	18.8	< 0.25	37.9	8.0	7'216	7.91	13.34	1'786	8.57	32.2	150.4	14'918	1.1
		400	3	1.12	3'632	< 10	46.4	703	194	17.8	< 0.25	36.2	5.1	6'105	6.62	14.13	1'656	8.37	29.5	114.2	12'680	0.2
698.47	Opalinus Clay	200	3	1.41	3'859	< 10	58.4	713	203	18.0	< 0.25	37.0	9.4	6'440	6.29	17.56	1'981	8.40	44.8	174.8	13'746	-1.2
		300	3	1.68	3'409	< 10	37.4	725	206	19.1	< 0.25	33.8	4.7	5'494	5.73	19.56	1'948	8.35	33.8	104.5	12'178	0.9
740.87	Staffelegg Fm.	200	3	1.59	2'576	< 10	41.8	220	62	4.3	< 0.25	38.9	12.4	2'520	2.58	14.01	2'455	8.66	44.6	129.5	8'303	1.0
		300	3	1.29	2'008	< 10	20.7	231	71	5.0	< 0.25	36.6	6.0	1'971	1.99	3.88	2'186	8.60	31.8	58.1	6'761	0.5
798.00	Bänkerjoch Fm.	200	3	1.22	5'465	n.a.	107.5	904	192	14.3	n.a.	n.a.	10.9	6'664	6.69	6.89	4'582	8.59	11.6	103.1	18'115	2.8
		300	2	1.48	4'566	n.a.	64.2	858	194	15.1	n.a.	n.a.	5.6	5'554	5.73	2.97	4'100	8.71	11.3	48.1	15'471	3.2
845.18	Bänkerjoch Fm.	300	2	0.87	3'326	n.a.	107.4	938	362	16.0	n.a.	n.a.	9.6	4'679	4.95	4.75	3'856	8.54	12.1	97.1	13'462	2.4
		400	2	1.32	3'297	n.a.	111.4	930	354	15.6	n.a.	n.a.	6.7	4'674	5.06	3.67	3'863	8.58	14.9	66.2	13'402	1.9
1019.57	Kaiseraugst Fm.	300	2	0.94	7'785	n.a.	115.1	1'234	134	31.9	n.a.	n.a.	10.4	12'950	4.45	8.41	1'609	8.38	< 10	119.7	24'047	1.8
		400	2	0.90	7'444	n.a.	79.5	1'348	134	34.5	n.a.	n.a.	5.4	11'851	3.87	3.47	1'703	8.28	< 10	55.4	22'712	4.4

Tab. 4.6-4: Chemical composition of squeezed waters: summary of selected analyses to be used for interpretation

n.a. = no analysis.

Depth [m]	**Formation**	**Pressure** [MPa]	**Squeezing time** [d]	**Mass squeezed** [g]	**Na** [mg/L]	**K** [mg/L]	**Ca** [mg/L]	**Mg** [mg/L]	**Sr** [mg/L]	**Ba** [mg/L]	**Si** [mg/L]	**Cl** [mg/L]	**Br** [mg/L]	**NO_3** [mg/L]	**SO_4** [mg/L]	**pH**	**TIC** [mg/L]	**TOC** [mg/L]
524.95	«Park.-Württ.-Sch.»	200	2	2.19	3'969	70.6	553	191	26.1	< 0.25	33.8	6'507	8.59	8.19	1'248	8.41	31.1	99.8
560.01	Wedel-ssst. Fm.	200	2	2.89	3'765	69.8	566	180	26.1	0.26	31.5	6'170	7.91	8.61	1'283	8.50	25.7	96.5
599.33	Opalinus Clay	200	3	0.71	4'460	80.6	635	194	22.0	< 0.25	38.2	7'291	8.87	20.60	1'341	8.33	38.9	187.0
657.71	Opalinus Clay	300	3	0.79	4'608	78.3	666	164	18.8	< 0.25	37.9	7'216	7.91	13.34	1'786	8.57	32.2	150.4
698.47	Opalinus Clay	200	3	1.41	3'859	58.4	713	203	18.0	< 0.25	37.0	6'440	6.29	17.56	1'981	8.40	44.8	174.8
740.87	Staffel-egg Fm.	200	3	1.59	2'576	41.8	220	62	4.3	< 0.25	38.9	2'520	2.58	14.01	2'455	8.66	44.6	129.5
798.00	Bänker-joch Fm.	200	3	1.22	5'465	107.5	904	192	14.3	n.a.	n.a.	6'664	6.69	6.89	4'582	8.59	11.6	103.1
845.18	Bänker-joch Fm.	300	2	0.87	3'326	107.4	938	362	16.0	n.a.	n.a.	4'679	4.95	4.75	3'856	8.54	12.1	97.1
1'019.57	Kaiser-augst Fm.	300	2	0.94	7'785	115.1	1'234	134	31.9	n.a.	n.a.	12'950	4.45	8.41	1'609	8.38	< 10	119.7

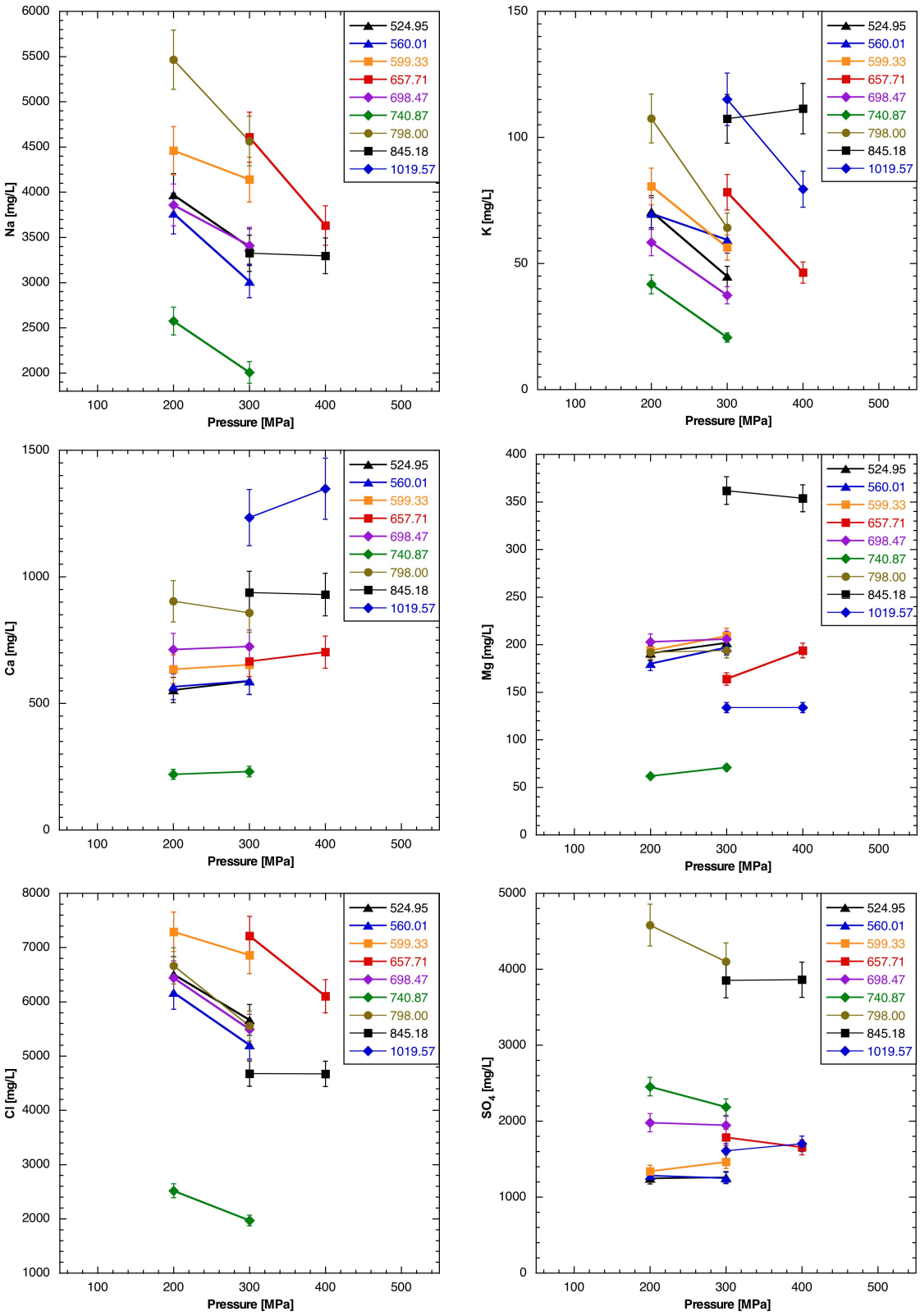

Fig. 4.6-3: Ion concentrations in squeezed waters as a function of squeezing pressure
Bars indicate analytical errors of ion-chromatography analysis.

4.6.3 Depth trends

Some observations can be noted for the interval between the top of the «Brauner Dogger» and the Keuper aquifer located in the upper part of the Klettgau Formation. Only 3 samples were investigated at deeper levels, where depth trends can only be identified by integrating information from other methods (Chapter 5). Depth profiles based on squeezing data are illustrated in Fig. 4.6-4.

- Na, K, Ca, Cl and Br increase slightly with depth and show a maximum in the Opalinus Clay. Concentrations then drop substantially towards the Keuper aquifer.
- The Br/Cl ratio decreases with depth in the interval «Brauner Dogger» – Opalinus Clay. This trend appears to be broken below the Opalinus Clay. All values are substantially below the modern seawater range of $1.52 \times 10^{-3} – 1.60 \times 10^{-3}$ in molar units (Morris & Riley 1966, Davis et al. 1998, Alcala & Custodio 2004, 2008, Millero 2014).
- SO_4 concentration increases with depth but, in contrast to the ions above, keeps doing so even in the sample from the Staffelegg Formation, leading to a SO_4/Cl ratio that sharply increases towards the Keuper aquifer. In the «Brauner Dogger», the molar SO_4/Cl ratio is only slightly higher than in modern seawater (0.0516 – 0.0518) in molar units (Morris & Riley 1966, Millero 2014).
- Mg shows no evident depth trend above the Keuper aquifer.

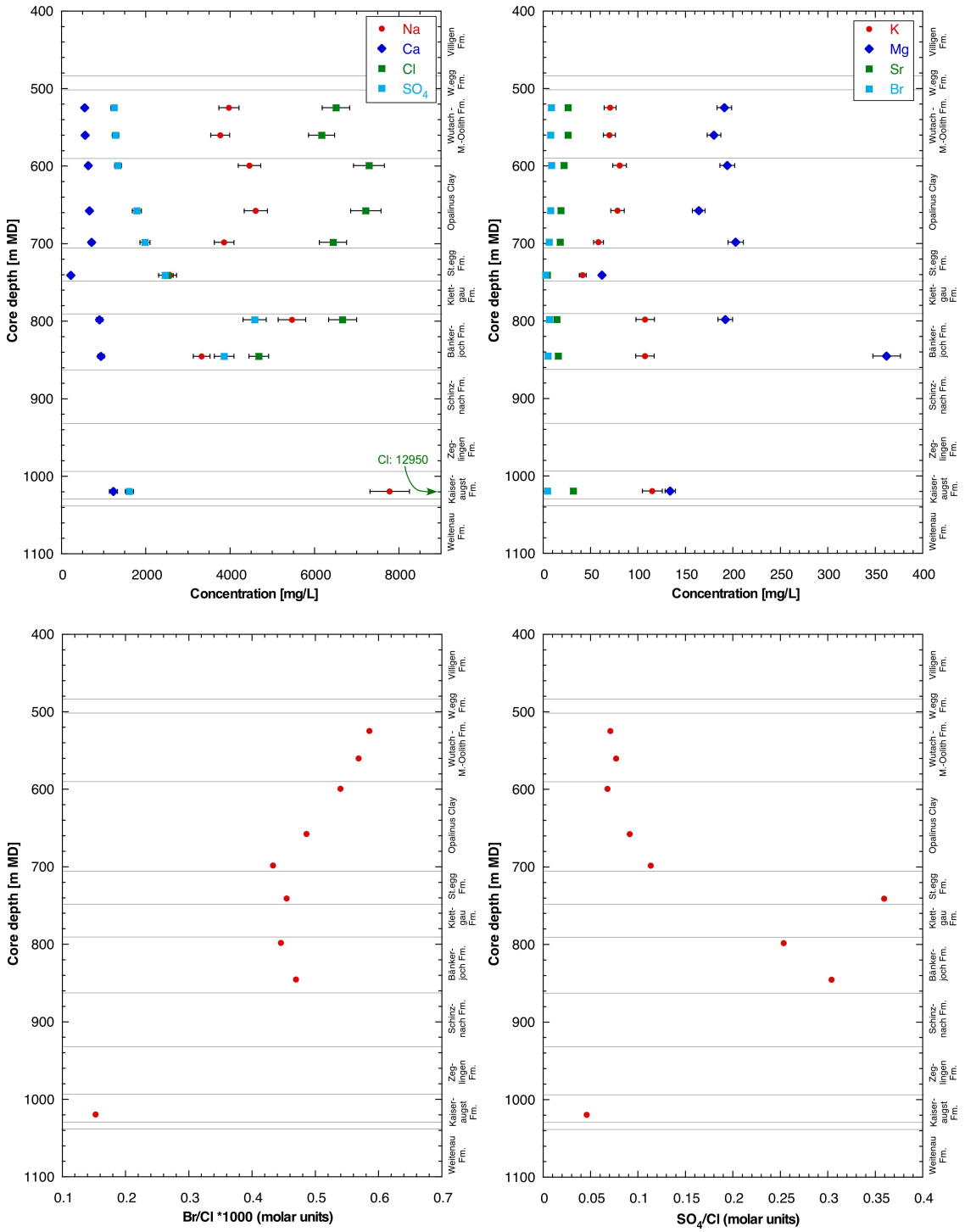

Fig. 4.6-4: Depth trends of ion concentrations and ion ratios in squeezed waters

Only the selected aliquots are shown for each sample. Bars indicate analytical errors of ion-chromatography analysis.

4.6.4 Geochemical modelling and mineral saturation states

Mineral saturation indices for squeezed waters were calculated using PHREEQC V3 and the PSI/Nagra thermodynamic data base at 25 °C (Thoenen et al. 2014) and are shown in Tab. 4.6-5.

- Squeezed waters are strongly oversaturated with respect to calcite and dolomite, a feature already known from previous studies (e.g. Mazurek et al. 2015). The oversaturation is possibly due to the fact that mineral solubility at high pressures during squeezing is higher than at atmospheric pressure. Further, outgassing of CO_2 during the squeezing process increases the pH and the saturation indices of calcite and dolomite (Tournassat et al. 2015). Further outgassing may take place in the headspace of the sample vials during sample storage. The comparatively low calculated pCO_2 suggest that some outgassing may have taken place, which also affects pH. However, this nevertheless does not markedly affect the obtained major-ion composition due to the large buffering capacity of the rock-water system in clay-rich lithologies. Last, lattice defects in carbonate minerals induced by deformation during squeezing might increase the solubility of these minerals. On the other hand, outgassing into the external atmosphere during sample storage in glass vessels is not considered to contribute to the low pCO_2, given the fact that there is no evidence for leakages.
- The waters are close to saturation with respect to celestite (except for the sample from the Staffelegg Formation, which shows undersaturation).
- Saturation indices for strontianite decrease with depth. Slight oversaturation is observed for the Dogger units, evolving towards undersaturation in the Triassic.
- The waters are undersaturated with respect to gypsum in samples from the Dogger and Liassic but close to saturation in the underlying Triassic units.
- Using the data from Tab. 4.6-3, squeezed waters are strongly oversaturated with respect to fluorite, which is a consequence of the contamination of F concentrations by the filter material. Therefore, no F data are listed in Tab. 4.6-4.

Si concentrations were determined for a subset of the squeezed waters («Brauner Dogger» to Staffelegg Formation; Tab. 4.6-3). All values are remarkably high, and both quartz and chalcedony are oversaturated (Tab. 4.6-5). The question arises whether oversaturation is due to contamination by the K-silicate drilling fluid or due to other reasons. Na/K ratios in waters squeezed at the lowermost pressure step in this depth interval are similar, which speaks against contamination (unless the degree of contamination would be the same in all samples, which appears unlikely). The same is true for the Si/Cl ratio (except for sample 740.87). An alternative explanation would be enhanced solubility of quartz due to lattice dislocations generated by deformation during squeezing. A definitive answer could be provided by Si analysis of waters squeezed from samples that were not drilled with a silicate-based drilling fluid, such as those from the BUL1-1 borehole.

Tab. 4.6-5: Mineral saturation indices for squeezed waters

Bold print indicates the selected ('best') aliquots.

Depth [m]	**Formation**	**Pressure** [MPa]	**pH**	**TIC** [M]	**log(pCO_2)** [bar]	**SI Calcite**	**SI Aragonite**	**SI Dolomite (ordered)**	**SI Dolomite (disordered)**	**SI Strontianite**	**SI Gypsum**	**SI Anhydrite**	**SI Celestite**	**SI Fluorite**	**SI Quartz**	**SI Chalcedony**
524.95	«Parkinsoni-Württemb.-Sch.»	**200**	**8.41**	**2.62E-03**	**-3.40**	**1.31**	**1.16**	**2.49**	**1.94**	**0.43**	**-0.48**	**-0.70**	**-0.09**	**0.99**	**0.81**	**0.62**
		300	8.32	2.32E-03	-3.35	1.21	1.06	2.29	1.74	0.33	-0.44	-0.65	-0.04	0.52	0.79	0.60
560.01	Wedel-sandstein Fm.	**200**	**8.50**	**2.17E-03**	**-3.58**	**1.32**	**1.17**	**2.47**	**1.92**	**0.43**	**-0.45**	**-0.67**	**-0.07**	**0.91**	**0.78**	**0.58**
		300	8.39	1.89E-03	-3.51	1.19	1.05	2.24	1.69	0.32	-0.42	-0.64	-0.03	0.45	0.79	0.59
599.33	Opalinus Clay	**200**	**8.33**	**3.29E-03**	**-3.22**	**1.37**	**1.23**	**2.57**	**2.02**	**0.37**	**-0.42**	**-0.64**	**-0.16**	**1.32**	**0.87**	**0.67**
		300	8.36	2.46E-03	-3.38	1.29	1.14	2.41	1.86	0.33	-0.37	-0.59	-0.06	0.59	0.80	0.60
657.71	Opalinus Clay	**300**	**8.57**	**2.72E-03**	**-3.57**	**1.51**	**1.36**	**2.74**	**2.19**	**0.41**	**-0.29**	**-0.51**	**-0.12**	**1.04**	**0.85**	**0.66**
		400	8.37	2.49E-03	-3.38	1.33	1.19	2.44	1.89	0.19	-0.28	-0.49	-0.15	0.68	0.84	0.65
698.47	Opalinus Clay	**200**	**8.40**	**3.78E-03**	**-3.24**	**1.53**	**1.38**	**2.84**	**2.29**	**0.38**	**-0.21**	**-0.43**	**-0.09**	**1.20**	**0.85**	**0.66**
		300	8.35	2.85E-03	-3.30	1.38	1.23	2.54	1.99	0.25	-0.20	-0.42	-0.06	0.61	0.81	0.62
740.87	Staffelegg Fm.	**200**	**8.66**	**3.74E-03**	**-3.46**	**1.29**	**1.14**	**2.35**	**1.80**	**0.04**	**-0.51**	**-0.73**	**-0.49**	**1.03**	**0.85**	**0.66**
		300	8.60	2.67E-03	-3.53	1.14	1.00	2.10	1.55	-0.07	-0.48	-0.71	-0.43	0.45	0.83	0.64
798.00	Bänker-joch Fm.	**200**	**8.59**	**9.83E-04**	**-4.05**	**1.11**	**0.97**	**1.87**	**1.32**	**-0.23**	**0.14**	**-0.08**	**0.06**	**1.35**		
		300	8.71	9.56E-04	-4.19	1.20	1.05	2.07	1.52	-0.10	0.10	-0.12	0.07	0.77		
845.18	Bänker-joch Fm.	**300**	**8.54**	**1.02E-03**	**-3.97**	**1.13**	**0.99**	**2.18**	**1.63**	**-0.18**	**0.12**	**-0.10**	**0.07**	**1.23**		
		400	8.58	1.26E-03	-3.93	1.25	1.11	2.41	1.86	-0.07	0.12	-0.10	0.06	0.92		
1'019.57	Kaiser-augst Fm.	**300**	**8.38**	**4.26E-04***	**-4.22**	**0.77**	**0.62**	**0.91**	**0.36**	**-0.37**	**-0.15**	**-0.36**	**-0.02**	**1.52**		
		400	8.28	4.26E-04*	-4.11	0.71	0.57	0.76	0.21	-0.43	-0.10	-0.31	0.04	0.98		

* Measured TIC is < 10 mg/; 5 mg/L were assumed for the calculation.

4.6.5 Water content and aqueous extraction of squeezed core material

After the squeezing experiment, each core was dried at 105 °C, from which the mass of water remaining in the sample was obtained. The dry core was then subjected to aqueous extraction, from which the mass of Cl remaining in the sample could be calculated. The results are summarised in Tab. 4.6-6. Given the fact that oven-drying was performed with air, some degree of rock oxidation occurred. Therefore, results are only given for the conservative constituents Cl and Br.

Tab. 4.6-6: Water contents and results of aqueous-extraction tests on previously squeezed samples

Depth [m]	**Formation**	**Water content (wet) of squeezed sample** [wt.-%]	**Mass of porewater in squeezed sample** [g]	**Aqueous extraction of squeezed sample**				
				Mass of dry rock [g]	**Mass of added water** [g]	**S/L** [g/g]	**Cl** [mg/L$_{extract\ solution}$]	**Br** [mg/L$_{extract\ solution}$]
524.95	«Parkinsoni-Württembergica-Sch.»	4.19	16.69	30.08	29.88	1.007	124	0.11
560.01	Wedelsandstein Fm.	4.39	18.01	30.06	29.88	1.006	115	0.10
599.33	Opalinus Clay	3.86	15.98	30.12	29.82	1.010	124	0.10
657.71	Opalinus Clay	3.46	14.48	30.09	29.83	1.009	103	0.07
698.47	Opalinus Clay	3.85	15.04	30.09	29.87	1.008	97.8	0.07
740.87	Staffelegg Fm.	4.61	17.74	29.97	29.84	1.004	44.6	0.04
798.00	Bänkerjoch Fm.	4.73	19.15	29.96	29.89	1.002	143	0.12
845.18	Bänkerjoch Fm.	5.45	24.71	28.88	29.83	0.968	133	0.13
1'019.57	Kaiseraugst Fm.	3.27	12.46	29.95	29.80	1.005	204	0.08

4.6.6 Chloride-accessible porosity

Combining the data for squeezed waters (Tab. 4.6-3) and for the samples after squeezing (Tab. 4.6-6) permits the reconstruction of the total Cl and water inventories, therefore also the initial Cl concentrations in the bulk porewater. Assuming that the squeezed water represents the composition of the anion-accessible water, the Cl-accessible porosity fraction f_{Cl} can be calculated. The formalism is detailed in Mazurek et al. (2021).

The volume of the water remaining in the sample after squeezing is obtained from the water content of the squeezed core, assuming a porewater density of 1 g/cm^3. Note that the formalism also assumes that the dead volume of the squeezing system is negligible. While the dead volume is indeed likely small, a sensitivity calculation was performed on its impact. Assuming a dead volume of 1 mL results is an anion-accessible porosity fraction that is 0.01 – 0.04 higher than the value without consideration of a dead volume. The most strongly expressed shift is found in

samples where only a small water volume was squeezed, while it becomes insignificant for samples with a good water yield.

The Cl-accessible porosity fraction is finally obtained from:

$$f_{Cl} = \frac{C_{Cl\ in\ bulk\ pore\ water}}{C_{Cl\ in\ squeezed\ water}}$$

The resulting Cl-accessible porosity fractions are listed in Tab. 4.6-7 and shown as a function of the clay-mineral content in Fig. 4.6-5. The mean value for f_{Cl} is 0.48, which is slightly higher than the value obtained for samples from the TRU1-1 borehole (Aschwanden et al. 2021), distinctly lower than in the BUL1-1 borehole (Mazurek et al. 2021) and slightly lower than existing data from Mont Terri (Pearson et al. 2003) and Schlattingen (Mazurek et al. 2015). Note that the very clay-rich (84 wt.-%) sample from the Staffelegg Formation also shows the lowest anion accessibility. See Chapter 5.1 and 5.2 for a more in-depth discussion of fCl and its consequences.

The results cover a limited range from 0.42 – 0.53 for the chloride-accessible porosity proportion for clay-rich samples (48 – 84 wt.-% clay minerals), despite quite a range of experimental bounding parameters: squeezed first aliquots of 3 – 11% of the porewater inventory, and a Cl concentration range of 2.5 – 13 g/L. This attests a certain robustness to the method.

Tab. 4.6-7: Cl-accessible porosity fractions derived from squeezing and aqueous-extraction experiments

Depth [m]	**Formation**	**Member**	**Cl-accessible porosity fraction f_{Cl}** [-]
524.95	«Parkinsoni-Württem-bergica-Sch.»		0.51
560.01	Wedelsandstein Fm.		0.49
599.33	Opalinus Clay	'Sub-unit with silty calcareous beds'	0.44
657.71	Opalinus Clay	'Mixed clay-silt-carbonate sub-unit'	0.46
698.47	Opalinus Clay	'Clay-rich sub-unit'	0.44
740.87	Staffelegg Fm.	Beggingen Mb.	0.42
798.00	Bänkerjoch Fm.		0.46
845.18	Bänkerjoch Fm.		0.55
1'019.57	Kaiseraugst Fm.	'Wellenmergel'	0.53

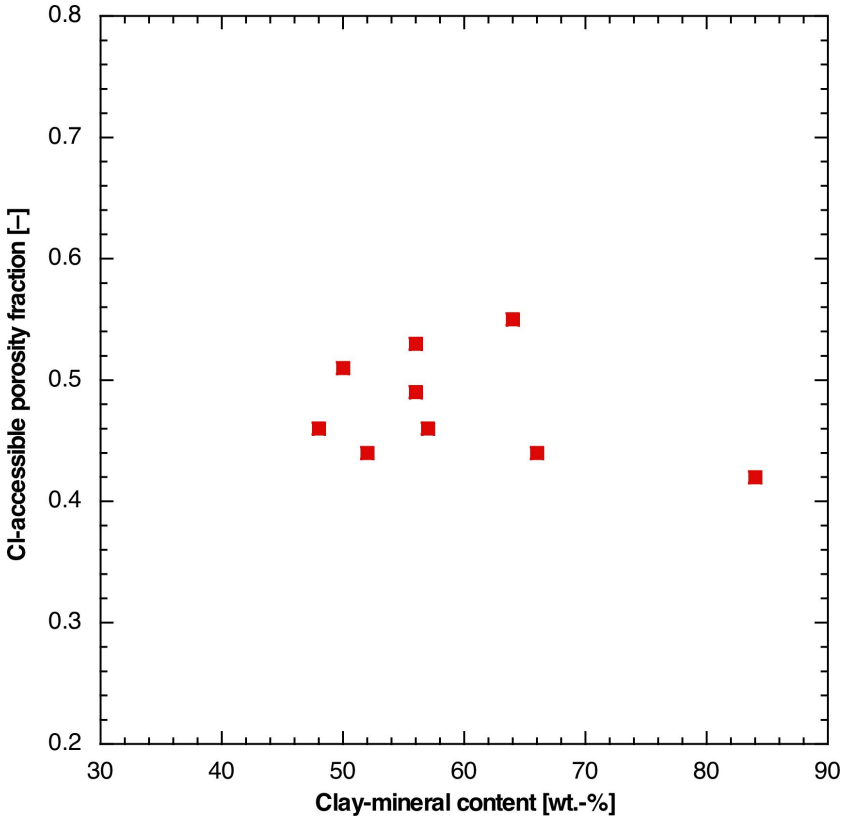

Fig. 4.6-5: Cl-accessible porosity fractions derived from squeezing experiments as a function of the clay-mineral content

4.6.7 Composition of stable isotopes of squeezed waters

Results of analyses of stable water isotopes are listed in Tab. 4.6-8 and shown as a function of depth in Fig. 4.6-6. The following observations can be made:

- Within any sample, the variation of the δ values with squeezing pressure is small (often within analytical error). In most cases, the δ values become marginally more negative with increasing pressure.
- Both $\delta^{18}O$ and $\delta^{2}H$ are near-constant in the «Brauner Dogger» and then decrease systematically with depth.
- In a plot $\delta^{18}O$ vs. $\delta^{2}H$ (Fig. 4.6-7), the shallower samples are located on the right side of the global ($\delta^{2}H = 8\ \delta^{18}O + 10$) and the local ($\delta^{2}H = 7.55\ \delta^{18}O + 4.8$) meteoric water lines. In the Staffelegg Formation and deeper, data lie slightly to the left of the meteoric water lines. The deepest sample from the Kaiseraugst Formation is located on the GMWL and LMWL within error.
- The same information is illustrated in Fig. 4.6-8 by the depth trend of deuterium excess ($\delta^{18}O - 8\ \delta^{2}H$), which increases systematically with depth until the Staffelegg Formation, followed by a slight decrease towards deeper levels.

Tab. 4.6-8: Composition of stable isotopes of squeezed waters

The aliquots selected for interpretation are shown in bold.

Depth [m]	**Formation**	**Pressure** [MPa]	**$\delta^{18}O$** [‰ VSMOW]	**$\delta^{2}H$** [‰ VSMOW]	**D excess** [‰]
524.95	«Parkinsoni-Württembergica-Schichten»	**200**	**-4.25**	**-41.7**	**-7.7**
781.25	«Humphriesioolith Fm.»	300	-4.35	-41.7	-6.9
560.01	Wedelsandstein Fm.	**200**	**-4.58**	**-42.1**	**-5.5**
904.86	Opalinus Clay	300	-4.71	-42.1	-4.4
599.33	Opalinus Clay	**200**	**-4.40**	**-39.6**	**-4.5**
959.22	Staffelegg Fm.	300	-4.42	-39.7	-4.4
657.71	Opalinus Clay	**300** 400	**-4.86** -5.07	**-39.9** -40.4	**-1.1** 0.2
698.47	Opalinus Clay	**200** 300	**-6.09** -6.13	**-43.8** -44.0	**4.9** 5.0
740.87	Staffelegg Fm.	**200** 300	**-7.72** -7.88	**-49.3** -50.1	**12.4** 12.9
798.00	Bänkerjoch Fm.	**200** 300	**-7.24** -7.38	**-47.1** -47.3	**10.9** 11.7
845.18	Bänkerjoch Fm.	**300** 400	**-8.72** -8.83	**-58.0** -58.6	**11.7** 12.0
1'019.57	Kaiseraugst Fm.	**300** 400	**-9.72** -9.76	**-70.0** -70.0	**7.7** 8.1

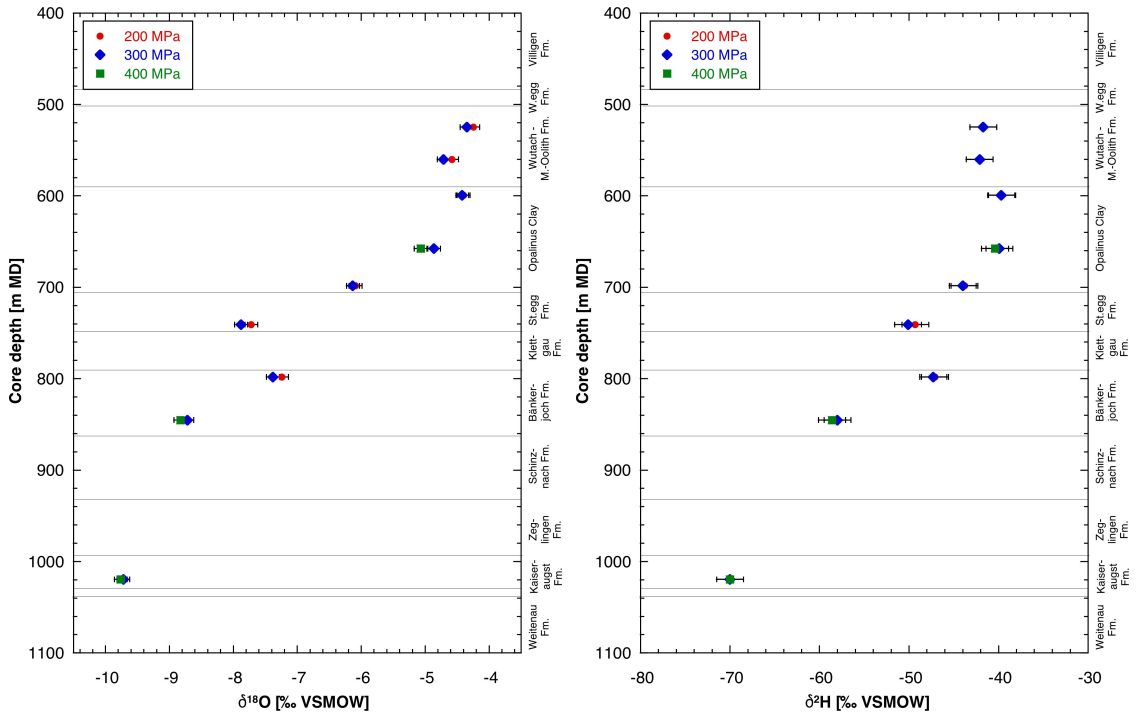

Fig. 4.6-6: Depth trends of $\delta^{18}O$ and $\delta^{2}H$ in squeezed waters

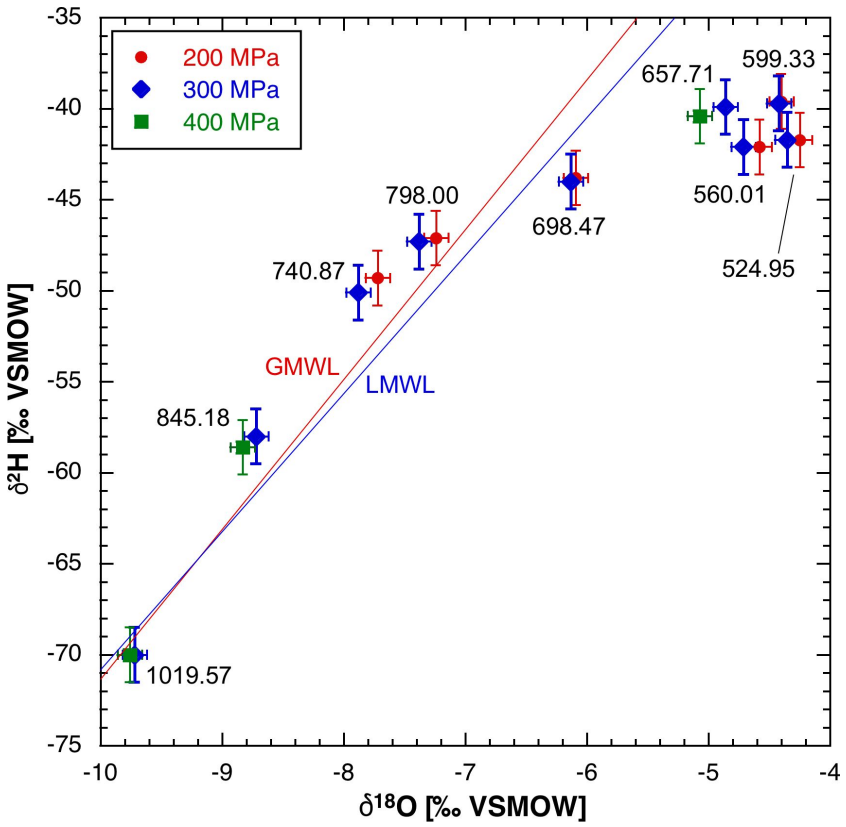

Fig. 4.6-7: Plot of $\delta^{18}O$ vs. $\delta^{2}H$ for squeezed waters

GMWL = Global Meteoric Water Line, LMWL = Local Meteoric Water Line.

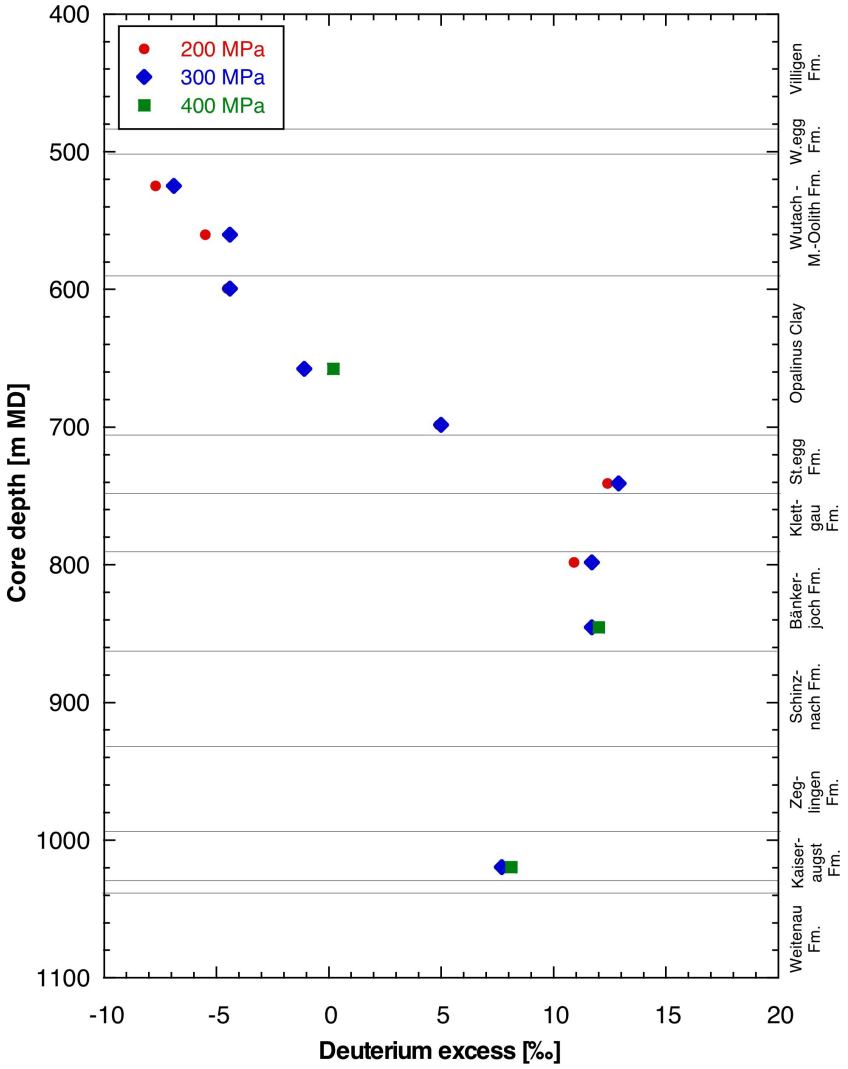

Fig. 4.6-8: Depth trend of deuterium excess in squeezed waters

4.7 Data from advective displacement experiments

Andreas Jenni, Mirjam Kiczka, Urs Mäder & H. Niklaus Waber

Advective displacement (AD) experiments are a methodology for a comprehensive physico-chemical characterisation, including porewater chemistry and certain transport properties (details in method report, Waber ed. 2020). This Section presents summary data, and details, where important, with short comments. The full datasets are provided in Appendix B. Integration of the data into context and depth profiles is included in Chapter 5.

Eight samples from the clay-rich confining units were processed. All experiments were successful, subjected to a similar analytical program, with differences mainly related to the duration of each experiment (numbers of sampled fluid aliquots). The extent of pre and post-mortem characterisation of core material was optimised based on gained experience from former BUL1-1 and TRU1-1 investigations. The programme fulfilled the planned work, but partially provided longer periods of advective displacement than requested and included more experiments than originally foreseen. The duration of the percolation period was 62 – 291 days, transporting 0.4 –1.4 pore volumes of fluid.

A feature not observed in boreholes BUL1-1 and TRU1-1 are very large nitrate concentrations eluted initially during advective displacement of samples from the Staffelegg Formation and below (less so for the deepest sample from the Kaiseraugst Formation). This is discussed in Section 4.7.5.4, and further below.

4.7.1 Sample material and overview of analytical work

The eight sample cores (Fig. 4.7-1) span more than 200 m of clay-rich confining units (521 – 737 m depth), from the «Parkinsoni-Württembergica-Schichten» («Brauner Dogger») to the Staffelegg Formation and include two samples of Opalinus Clay. In addition, two deeper samples from the Klettgau and Kaiseraugst Formation were processed.

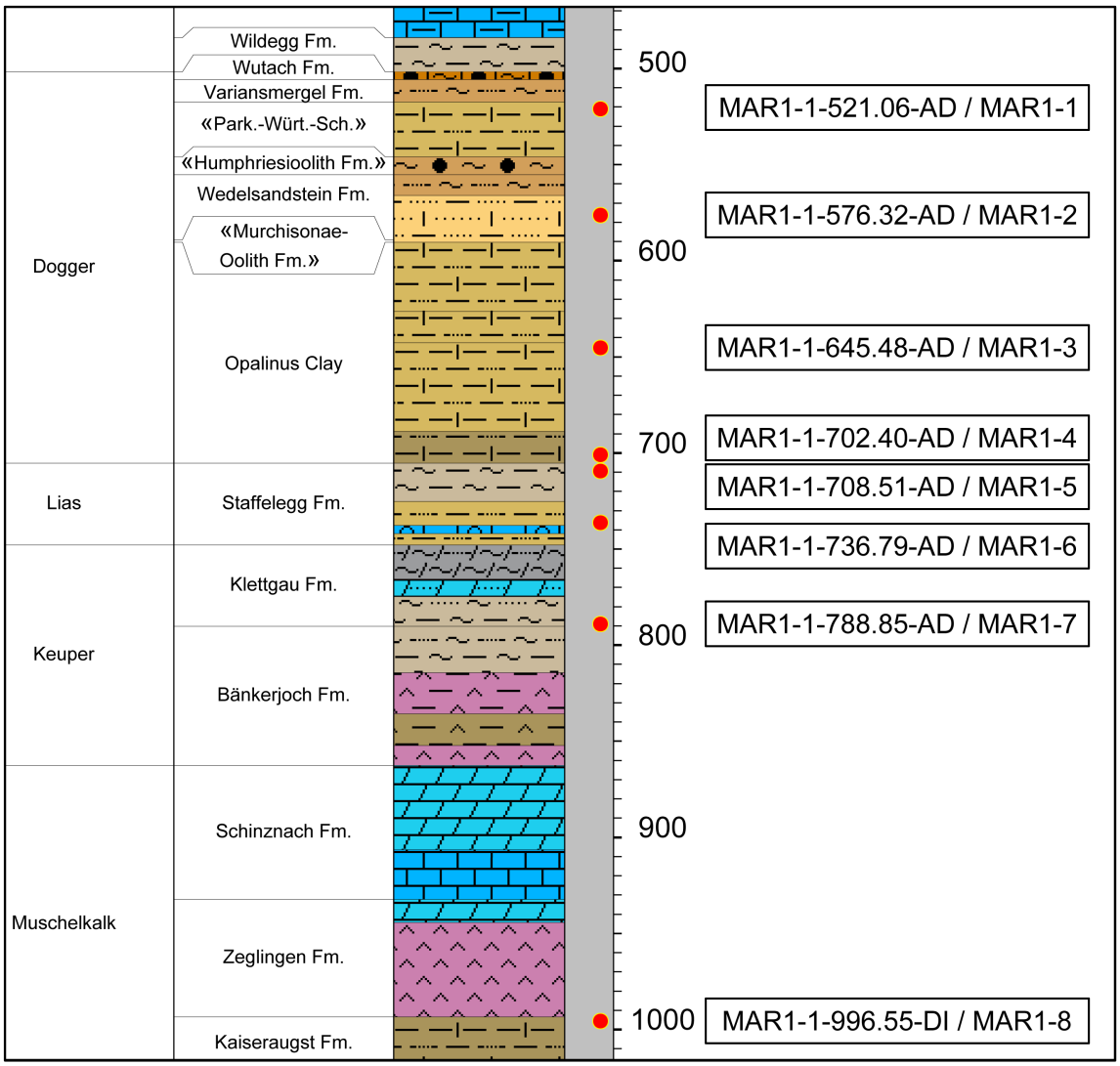

Fig. 4.7-1: Location of samples used for advective displacement experiments (red dots)
Short labels are consecutively numbered laboratory abbreviations.

X-ray computed tomography (CT) was performed on a medical scanner (Waber ed. 2020) for sample selection (Fig. 4.7-2), detection of disturbing features (fractures, pyrite accumulations, macro-fossils, etc.). Dry cutting was used for obtaining a central core segment for AD experiments, and adjacent 1 or 2 discs for accompanying characterisation (green in Fig. 4.7-2). The central core segment (yellow in Fig. 4.7-2) was turned on a lathe to 80 mm diameter. Tab. 4.7-1 lists all analytical work performed on the eight samples.

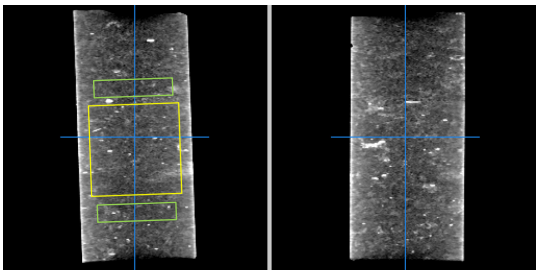
MAR1-1-521.06-AD («Park.-Württ.-Sch.»)

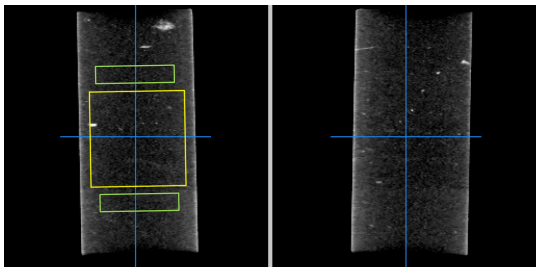
MAR1-1-576.32-AD (Wedelsandstein Fm.)

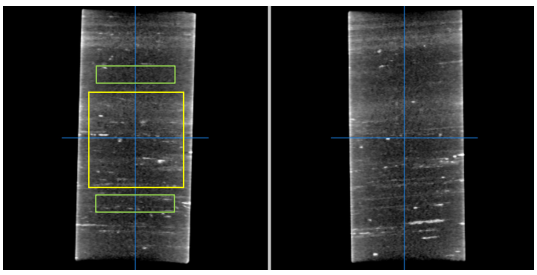
MAR1-1-645.48-AD (Opalinus Clay)

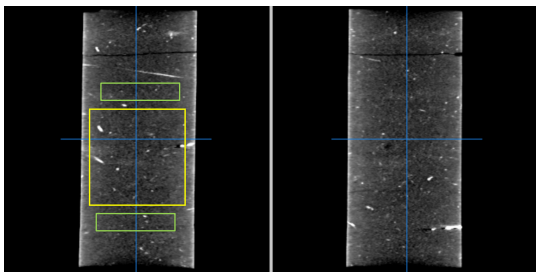
MAR1-1-702.40-AD (Opalinus Clay)

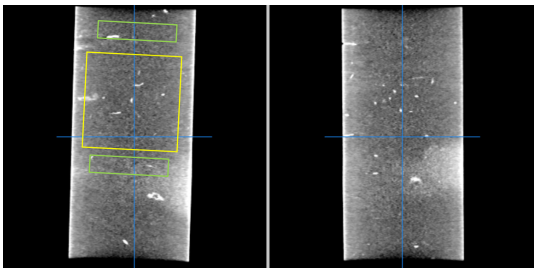
MAR1-1-708.51-AD (Staffelegg Fm./Gr.W. Mb.)

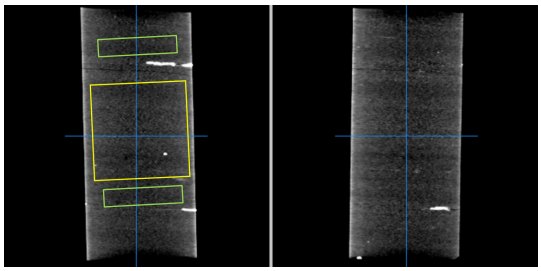
MAR1-1-736.79-AD (Staffelegg Fm./Frick Mb.)

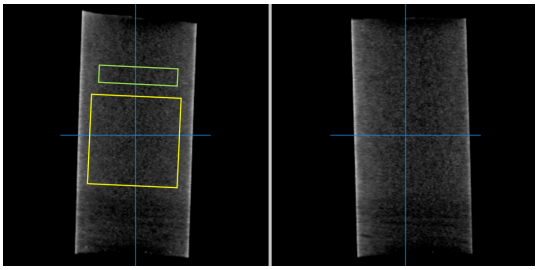
MAR1-1-788.85-AD (Klettgau Fm./Ergolz Mb.)

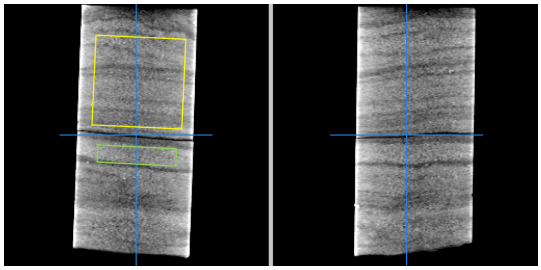
MAR1-1-996.55-AD (Kaiseraugst Fm./ 'Orbicul.')

Fig. 4.7-2: X-ray CT images of AD samples

Central sections parallel to core axis at right angle. Grey scale range setting is 1'700 – 2'500 HU. Yellow segments are used for advective displacement, green segments for pre-characterisation. Low X-ray absorbance represents clay/quartz-rich sections (darker grey), slightly lighter grey indicates carbonate-richer parts, siderite is brighter, and pyrite is white (strongest absorbance). Black lines/gaps represent fractures.

Tab. 4.7-1: Summary of analytical work perfomed on samples for advective displacement experiments

Parameter	**MAR1-1**	**MAR1-2**	**MAR1-3**	**MAR1-4**	**MAR1-5**	**MAR1-6**	**MAR1-7**	**MAR1-8**
Sample ID RWI	MAR1-1-521.06-AD	MAR1-1-576.32-AD	MAR1-1-645.48-AD	MAR1-1-702.40-AD	MAR1-1-708.51-AD	MAR1-1-736.79-AD	MAR1-1-788.85-AD	MAR1-1-996.55-DI
Lab sample ID	MAR1-1xx-AD	MAR1-2xx-AD	MAR1-3xx-AD	MAR1-4xx-AD	MAR1-5xx-AD	MAR1-6xx-AD	MAR1-7xx-AD	MAR1-8xx-AD
Depth [m]	521.06	576.32	645.48	702.40	708.51	736.79	788.85	996.55
Geol. unit	«Parkinsoni-Württem-bergica-Sch.»	Wedel-sandstein Fm.	Opalinus Clay	Opalinus Clay	Staffelegg Fm.	Staffelegg Fm.	Klettgau Fm.	Kaiser-augst Fm.
Member					Gross Wolf Mb.	Frick Mb.	Ergolz Mb.	Orbicularis-mergel
AD_exp	y	y	y	y	y	y	y	y
Pre_WC	1+1	1+1	1+1	1+1	1+1	1+1	1 (top)	2 (base)
Pre_M	y	y	y	y	y	y	y	y
Pre_V,A,L	y	y	y	y	y	y	y	y
Pre_Min	1	1	1	1	1	1	1	1
Pre_Clay	1	1	1	1	1	1	1	1
Pre_AqEx	1+1	1+1	1+1	1+1	1+1	1+1	1 (top)	1 (base)
Pre_Ni-en	ave	ave	ave	ave	ave	ave	n	1 (base)
Post_WC	5	5	5	5	5	5	5	5
Post_M	y	y	y	y	y	y	y	y
Post_V,A,L	y	y	y	y	y	y	y	y
Post_AqEx	1+1	1+1	1+1	5	1+1	1+1	1+1	1+1
Post_Ni-en	1+1	1+1	1+1	1+1	1+1	1+1	1+1	1+1

y = yes = done; n = no = not done; integer numbers refer to the number of samples processed; +: samples from above (left number) and below (right number) a core were processed; 2: duplicate samples; ave = average; Pre: sample pre-characterisation; Post: post-mortem characterisation; WC: water content; M: mass; V,A,L: core volume, sectional area and length; Min: mineralogy; Clay: clay mineralogy; AqEx: aqueous extracts; Ni-en: cation selectivity with Ni-en method; Post_WC: post-mortem water content determined along a profile with 5 segments; AD_exp: complete analysis of fluid sample aliquots collected during advective displacement.

4.7.2 Conditions of advective displacement experiments

Sample preparation was performed according to Waber (ed.) (2020). The overview table (Tab. 4.7-2) presents some experiment specific parameters such as sample processing dates, storage time and other characteristic times like arrival of first fluid drop and its electric conductivity. Numbers of samples taken and analysed are listed as well as average pressures for confining and injection. The number of pore volumes percolated are based on the water content determined from pre-characterisation. Confining pressure was set to 58 – 62 bar, pressurised by Ar on water, and 47 – 48 bar for infiltration of the artificial porewater (APW) by He pressure. The hydraulic gradients are large, 5'000 – 7'000 m_{H2O}/m (sample dimensions are in Tab. 4.7-4). Experiments were started within 9 – 30 days of sample delivery, except MAR1-8 was processed after more than 3 months (vacuum sealed, cold storage). The time until arrival of a first fluid drop at the electric conductivity cell (outflow, before sampling syringe) was 2 – 20 days after start of infiltration.

Tab. 4.7-2: Conditions of advective displacement experiments.

Parameter	**MAR1-1**	**MAR1-2**	**MAR1-3**	**MAR1-4**	**MAR1-5**	**MAR1-6**	**MAR1-7**	**MAR1-8**
Depth [m]	521.06	576.32	645.48	702.40	708.51	736.79	788.85	996.55
Geol. unit	«Parkinsoni-Württem-bergica-Sch.»	Wedel-sandstein Fm.	Opalinus Clay	Opalinus Clay	Staffelegg Fm.	Staffelegg Fm.	Klettgau Fm.	Kaiseraugst Fm.
Drilled	3/8/2020	3/10/2020	3/14/2020	3/17/2020	3/18/2020	3/19/2020	5/21/2020	6/27/2020
Delivered	3/16/2020	3/16/2020	4/6/2020	4/6/2020	4/6/2020	4/6/2020	6/2/2020	7/6/2020
Prep_AD	3/26/2020	3/26/2020	4/29/2020	4/29/2020	5/6/2020	5/6/2020	6/11/2020	10/15/2020
Injection	3/27/2020	3/27/2020	4/30/2020	4/30/2020	5/7/2020	5/7/2020	6/12/2020	10/17/2020
First drop	4/15/2020	3/29/2020	5/14/2020	5/14/2020	5/15/2020	5/18/2020	6/17/2020	10/29/2020
Days to first drop	19.5	2.4	14.3	14.2	7.4	10.1	5.2	11.6
Initial gas [ml]	6.6	0.1	9.3	4.0	3.9	0.0	16.4	4.5
End_AD	1/12/2021	6/10/2020	11/5/2020	1/12/2021	7/9/2020	7/9/2020	8/18/2020	1/12/2021
Duration [d]	291.0	75.5	188.7	256.7	62.6	62.4	66.7	86.9
Pore-volumes	0.4	1.3	0.9	1.4	0.6	0.4	1.0	0.5
EC_initial (25 °C) (max. in 1st 24h) [mS/cm]	18.67	ca. 23	23.92	25.78	29.17	21.15	19.35	60.31
Filter	single PEEK	single PEEK	single PEEK	single PEEK	single PEEK	single PEEK	single PEEK	single PEEK
AD-samples	10	15	14	21	10	8	13	9
AD-samp_chem	9	14	13	20	8	7	11	5
AD-samp_isotopes	9	14	13	20	9	7	12	4
in-line pH	5	7	7	11	5	4	6	4
P_Conf [bar]	59	58	59	61	60	58	59	59
P_Inf [bar]	47	47	47	47	48	48	47	47
Gradient [mH2O/m]	5'850	5'549	5'591	5'848	5'750	5'809	5'900	5'940

4.7.3 Mineralogy and petrophysical properties

Mineralogy was determined on the sum of subsamples cut adjacent to the core segment used for the AD experiments (Tab. 4.7-1). Values for subsamples (Tab. 4.7-3) are plotted in Section 4.2 and cover a range of clay-mineral contents from 29 – 67 wt.-%, calcite contents of 0 – 57 wt.-%, and quartz contents of 8 – 45 wt.-%. Most samples contain pyrite, between 0.1 and 2 wt.-%, only in MAR1-2 and MAR1-8 no pyrite was detected. Of the clays, the dominant minerals are illite (12 – 29 wt.-%), illite/smectite mixed layers (9 – 17 wt.-%), and kaolinite (1 – 24 wt.-%). The ratio of (illite/smectite+smectite)/(total_clay) is rather uniform in the range 0.22 – 0.39.

Included are also carbon and sulphur analysis, and nitrogen was below a detection limit of 0.01 wt.-% in all samples. Pyrite contents are moderately low because pyrite-rich lithologies were avoided based on X-ray CT characterisation (Fig. 4.7-2). More details, including end-member clays, are included in Appendix C.

A plethora of petrophysical parameters may be derived from sample dimensions, mass, water content, and changes in these parameters determined before and after an AD experiment (Tab. 4.7-4). Derived quantities include porosity, bulk density, grain density, water uptake during the experiments, and unsaturated porosity (saturation ratio). The relationships are given in Waber (ed.) (2020). Note that the water content determined for pre-characterisation is based on 2 sub-samples adjacent to the AD core segment (except MAR1-7 and MAR1-8, with too short core segments), but it is determined for post-mortem characterisation along a 5-sample profile of the entire AD core segment itself. Accounting for the usually observed slight core volume expansion during an AD experiment, one can derive a corrected initial water content, as well as any unsaturated (gas-filled) porosity fraction.

Core volume is seen to increase by 0.1 – 1.0% (Tab. 4.7-4) during AD experiments (except MAR1-8 showing virtually no volume change), accompanied by a water uptake of 2.0 – 5.4 g. Accounting for volume expansion, there remains a small water uptake that must reflect an initially small volume of unsaturated porosity, ranging from 1.0 to 2.7 mL, or a saturation ratio in the range 0.98 – 0.92. The initial state is essentially saturated for all samples within measurement uncertainty.

There are significant differences in water content measured in adjacent samples (pre-characterisation) and in the core itself (post-mortem) of 5 – 13%, even when accounting for core expansion (Fig. 4.7-3). This leads to different values of bulk wet density, water-loss porosity and grain density (assuming saturated conditions) derived from pre-characterisation and post-mortem data. This spread is significantly larger than measurement uncertainties and illustrates that the largest contribution to uncertainty is sample heterogeneity for parameters that depend on water content. In contrast, measurements on replicate samples agree well within measurement uncertainty. Differences in water content commonly correlate with differences in the clay-mineral content, such that this heterogeneity is mainly an issue of lamination in fine-grained sediments.

Tab. 4.7-3: Mineralogy of advective displacement samples, including C, S and N analyses
Average values of subsamples (see text).

Parameter	**Unit**	**MAR1-1**	**MAR1-2**	**MAR1-3**	**MAR1-4**	**MAR1-5**	**MAR1-6**	**MAR1-7**	**MAR1-8**
Depth	[m]	521.06	576.32	645.48	702.40	708.51	736.79	788.85	996.55
Geol. unit		«Parkinsoni-Württem-bergica-Sch.»	Wedel-sandstein Fm.	Opalinus Clay	Opalinus Clay	Staffelegg Fm.	Staffelegg Fm.	Klettgau Fm.	Kaiser-augst Fm.
S	[wt.-%]	1.0	0.4	0.3	0.7	0.1	0.2	0.1	b.d.
C(inorg)	[wt.-%]	3.9	1.8	1.4	1.2	6.4	1.0	b.d.	6.9
C(org)	[wt.-%]	0.7	0.4	1.0	0.8	0.3	0.8	0.3	0.5
N	[wt.-%]	b.d.	b.d.	b.d.	b.d.	b.d.	b.d.	b.d.	b.d.
Quartz	[wt.-%]	19	45	25	15	8	24	24	8
K-feldspar	[wt.-%]	6	7	6	5	3	5	16	2
Plagioclase	[wt.-%]	2	3	3	b.d.	2	2	4	2
Calcite	[wt.-%]	31	14	8	8	51	6	b.d.	57
Dolomite / Ankerite	[wt.-%]	1	1	b.d.	b.d.	2	b.d.	11	b.d.
Siderite	[wt.-%]	b.d.	b.d.	4	3	b.d.	3	b.d.	b.d.
Anhydrite	[wt.-%]	b.d.	b.d.	b.d.	b.d.	b.d.	b.d.	b.d.	b.d.
Celestite	[wt.-%]	b.d.	b.d.	b.d.	b.d.	b.d.	b.d.	b.d.	b.d.
Pyrite	[wt.-%]	2	b.d.	0.5	1	0.3	0.4	0.1	b.d.
Clay minerals	**[wt.-%]**	**38**	**29**	**52**	**67**	**33**	**59**	**56**	**30**
Illite	[wt.-%]	14	13	17	21	12	19	29	18
Illite/smectite ML (85-90)	[wt.-%]	7	0	5	4	7	4	15	9
Illite/smectite ML (75-80)	[wt.-%]	2	10	6	9	b.d.	12	1	b.d.
Illite/smectite ML (50-70)	[wt.-%]	2	1	2	1	1	1	1	b.d.
Illite/smectite ML (20-40)	[wt.-%]	b.d.	b.d.	b.d.	b.d.	b.d.	b.d.	b.d.	b.d.
Smectite	[wt.-%]	b.d.	b.d.	b.d.	b.d.	b.d.	b.d.	0.6	b.d.
Kaolinite	[wt.-%]	7.9	1.4	16.7	23.5	8.6	15.9	3.3	0.6
Chlorite	[wt.-%]	0.8	1.4	2.1	3.4	1.3	3.5	2.2	1.2
Chl/Sm ML (85-95)	[wt.-%]	0.8	1.4	2.1	3.4	1.3	3.5	2.2	1.2
Total illite/smectite	[wt.-%]	**11**	**11**	**12**	**15**	**9**	**16**	**17**	**9**
(tot_ill/sm+sm)/ (total_clay)		0.30	0.39	0.23	0.22	0.26	0.27	0.30	0.31
(tot_ill+ill/sm+sm)/ (total_clay)		0.68	0.83	0.56	0.53	0.62	0.60	0.82	0.90

Tab. 4.7-4: Core dimensions and derived petrophysical parameters

Parameter	**Unit**	**MAR1-1**	**MAR1-2**	**MAR1-3**	**MAR1-4**	**MAR1-5**	**MAR1-6**	**MAR1-7**	**MAR1-8**
Depth	[m]	521.06	576.32	645.48	702.40	708.51	736.79	788.85	996.55
Geol. Unit		«Parkinsoni-Württem-bergica-Sch.»	Wedelsand-stein Fm.	Opalinus Clay	Opalinus Clay	Staffelegg Fm.	Staffelegg Fm.	Klettgau Fm.	Kaiseraugst Fm.
Pre_Core_M	**[g]**	**1'015.19**	**1'049.45**	**1'066.10**	**1'006.63**	**1'064.35**	**1'037.37**	**999.17**	**1'020.85**
Pre_Core_DM	[cm]	8.01	8.02	8.01	8.00	8.01	8.01	8.01	8.02
Pre_Core_L	[cm]	7.98	8.41	8.42	8.03	8.27	8.22	7.97	7.85
Pre_Core_A	[cm^2]	50.36	50.45	50.34	50.30	50.34	50.34	50.41	50.50
Pre_Core_V	[cm^3]	401.87	424.07	423.90	403.63	416.22	413.95	401.49	396.50
Post_Core_M	**[g]**	**1'017.19**	**1'053.10**	**1'070.60**	**1'011.76**	**1'066.80**	**1'042.78**	**1'003.24**	**1'023.08**
Post_Core_DM	[cm]	8.01	8.02	8.01	8.02	8.01	8.02	8.03	8.02
Post_Core_L	[cm]	7.99	8.42	8.48	8.07	8.28	8.28	7.97	7.84
Post_Core_A	[cm^2]	50.37	50.48	50.38	50.50	50.43	50.51	50.63	50.56
Post_Core_V	[cm^3]	402.39	425.00	427.26	407.50	417.65	418.09	403.40	396.27
Delta_M	**[g]**	**2.00**	**3.65**	**4.50**	**5.13**	**2.45**	**5.41**	**4.07**	**2.23**
Delta_Core_DM	[cm]	0.001	0.002	0.003	0.016	0.007	0.013	0.018	0.005
Delta_Core_L	[cm]	0.008	0.014	0.061	0.044	0.015	0.055	0.002	-0.014
Delta_Core_A	[cm^2]	0.013	0.025	0.038	0.204	0.082	0.167	0.227	0.063
Delta_Core_V	[cm^3]	**0.516**	**0.931**	**3.366**	**3.863**	**1.432**	**4.137**	**1.907**	**-0.226**
Delta_Core_V-%	[%]	0.128	0.220	0.794	0.957	0.344	0.999	0.475	-0.057
Pre_Bulk_WD	**[g/cm^3]**	**2.526**	**2.475**	**2.515**	**2.494**	**2.557**	**2.506**	**2.489**	**2.575**
Post_Bulk_WD	**[g/cm^3]**	**2.528**	**2.478**	**2.506**	**2.483**	**2.554**	**2.494**	**2.487**	**2.582**
Delta_Bulk_WD	[g/cm^3]	0.002	0.003	-0.009	-0.011	-0.003	-0.012	-0.002	0.007
Delta_Bulk_WD-%	[%]	0.069	0.128	-0.369	-0.443	-0.114	-0.474	-0.067	0.276
Pre_GD	**[g/cm^3]**	**2.736**	**2.675**	**2.715**	**2.720**	**2.717**	**2.714**	**2.716**	**2.694**
Post_GD	**[g/cm^3]**	**2.726**	**2.689**	**2.717**	**2.724**	**2.730**	**2.731**	**2.724**	**2.713**
Delta_GD	[g/cm^3]	-0.010	0.015	0.002	0.004	0.013	0.016	0.008	0.018
Corr_Pre_GD	**[g/cm^3]**	**2.714**	**2.670**	**2.709**	**2.714**	**2.723**	**2.721**	**2.707**	**2.694**
Pre_WCw		**0.0478**	**0.0482**	**0.0463**	**0.0526**	**0.0364**	**0.0485**	**0.0532**	**0.0274**
Post_WCw		**0.0453**	**0.0505**	**0.0491**	**0.0563**	**0.0398**	**0.0548**	**0.0553**	**0.0296**
Delta_WCw		-0.0025	0.0023	0.0027	0.0037	0.0034	0.0063	0.0021	0.0022
Corr_Pre_WCw		**0.0434**	**0.0472**	**0.0451**	**0.0515**	**0.0376**	**0.0499**	**0.0515**	**0.0275**
Pre_H2O_Core	**[g]**	**48.51**	**50.63**	**49.40**	**52.99**	**38.75**	**50.33**	**53.18**	**27.96**
Post_H2O_Core	**[g]**	**46.11**	**53.21**	**52.55**	**56.98**	**42.47**	**57.16**	**55.51**	**30.27**
Delta_H2O_Core	[g]	-2.41	2.58	3.15	3.99	3.71	6.83	2.33	2.31
Corr_Pre_H2O_Core	**[g] or [mL]**	**44.10**	**49.56**	**48.05**	**51.85**	**40.02**	**51.76**	**51.43**	**28.04**
Unsat_Vol	[g] or [mL]	1.49	2.72	1.13	1.27	1.02	1.27	2.17	2.46
Pore_Vol_tot	[mL]	45.59	52.28	49.18	53.12	41.04	53.02	53.60	30.50
Sat_ratio		**0.97**	**0.95**	**0.98**	**0.98**	**0.98**	**0.98**	**0.96**	**0.92**

Tab. 4.7-4: continued

Parameter	Unit	MAR1-1	MAR1-2	MAR1-3	MAR1-4	MAR1-5	MAR1-6	MAR1-7	MAR1-8
Pre_Poro_WL		**0.1207**	**0.1194**	**0.1165**	**0.1313**	**0.0931**	**0.1216**	**0.1325**	**0.0705**
Post_Poro_WL		**0.1146**	**0.1252**	**0.1230**	**0.1398**	**0.1017**	**0.1367**	**0.1376**	**0.0764**
Delta_Poro_WL		-0.0061	0.0058	0.0064	0.0086	0.0086	0.0151	0.0052	0.0059
Delta_Poro_WL-%	[%]	-5.0800	4.8622	5.5342	6.5148	9.2096	12.4402	3.8893	8.3206
Corr_Pre_Poro_WL		**0.1097**	**0.1169**	**0.1133**	**0.1285**	**0.0962**	**0.1250**	**0.1281**	**0.0707**
Corr_Pre_Poro_tot		**0.1134**	**0.1233**	**0.1160**	**0.1316**	**0.0986**	**0.1281**	**0.1335**	**0.0769**

L = length; _A = area; _V = volume; _M = mass; WD = wet density; GD = grain density; WCw = water content rel. to wet mass; _WL = water loss

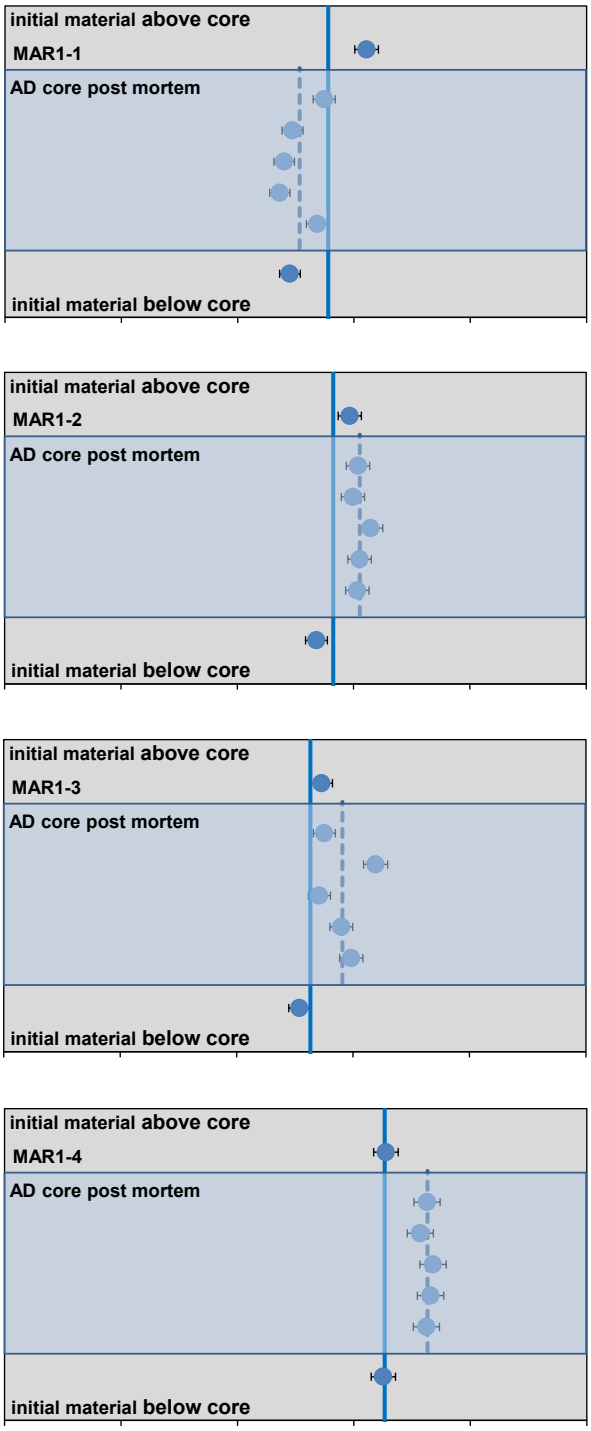

Fig. 4.7-3: Details of water content measurements before and after AD experiments

MAR1-1 = MAR1-1-521.06 («Park.-Württ.-Sch.»); MAR1-2 = MAR1-1-576.32 (Wedelsandstein Formation); MAR1-3 = MAR1-1-645.48 (Opalinus Clay); MAR1-4 = MAR1-1-702.40 (Opalinus Clay); MAR1-5 = MAR1-1-708.51 (Staffelegg Formation); MAR1-6 = MAR1-1-736.79 (Staffelegg Formation); MAR1-7 = MAR1-1-788.85 (Klettgau Formation); MAR1-8 = MAR1-1-996.55 (Kaiseraugst Formation). Average values are indicated for pre-characterisation (solid line) and post-mortem characterisation (dashed line). Error bars refer to measurement uncertainty of 2%.

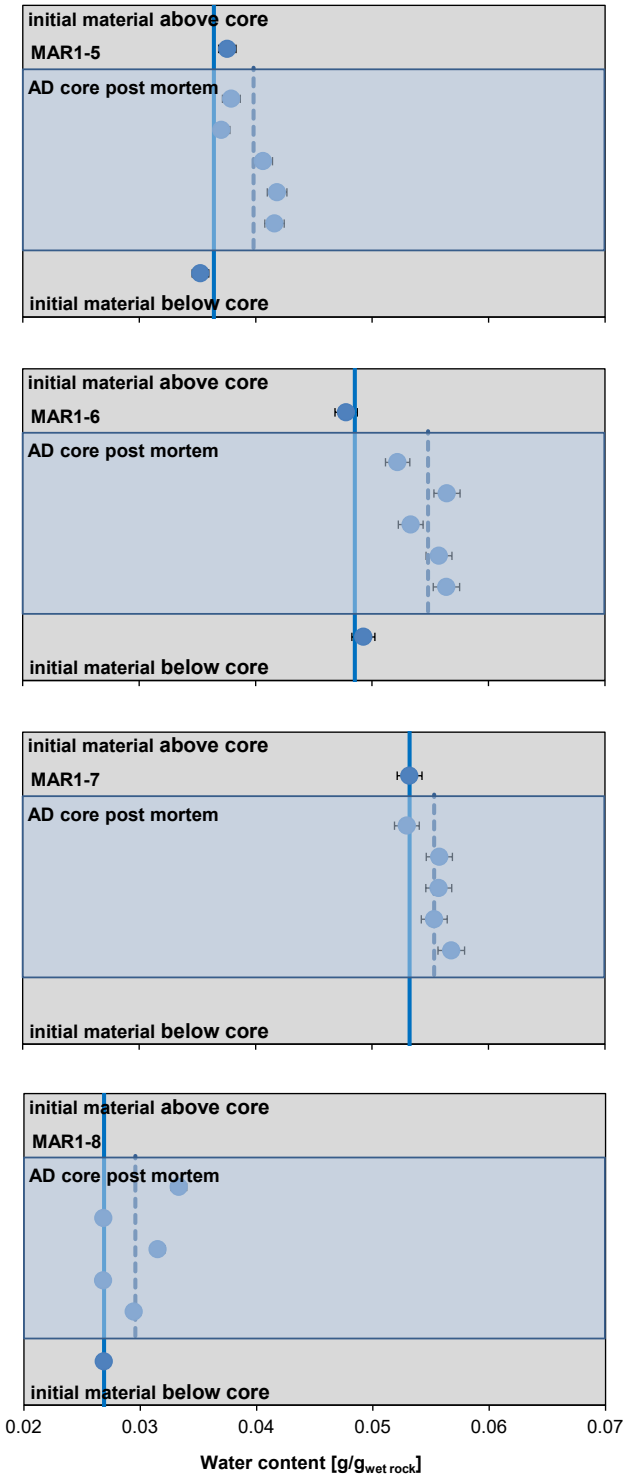

Fig. 4.7-3: continued

4.7.4 Aqueous extracts, CEC and cation selectivity of AD samples

Aqueous extracts, CEC and cation selectivity determinations were carried out within the pre-characterisation (except MAR1-7: no pre CEC/ cation selectivity) and post-mortem analysis. Detailed analyses are provided in Appendix C. Methods are the same as used for other core samples (Waber ed. 2020), with the exception of sample masses that may have been smaller than used for regular core sample analysis. Averaged data – also used for integrative data plots – are presented in this Section. Averaging refers to aqueous extraction measurements of pieces above and below the segment used for the AD experiments (indicated in Fig. 4.7-2 and Tab. 4.7-5). For CEC/cation selectivity, the pieces were combined in equal proportions and analysed as one sample.

Tab. 4.7-5: Composition of aqueous extract solutions from pre-characterisation

Parameter	**Unit**	**MAR1-1**	**MAR1-2**	**MAR1-3**	**MAR1-4**	**MAR1-5**	**MAR1-6**	**MAR1-7**	**MAR1-8**
Depth	[m]	521.06	576.32	645.48	702.40	708.51	736.79	788.85	996.55
Geol. unit		«Parkinsoni-Württem-bergica-Sch.»	Wedel-sandstein Fm.	Opalinus Clay	Opalinus Clay	Staffelegg Fm.	Staffelegg Fm.	Klettgau Fm.	Kaiser-augst Fm.
averaging		top+base (1+1)	top+base (1+1)	top+base (1+1)	top+base (1+1)	top+base (1+1)	top+base (1+1)	top (1)	base (1)
1/WCw*L/Sw		21.54	21.70	21.56	19.61	28.75	21.66	19.85	38.66
Rock wet	[g]	31.18	30.47	31.65	30.75	29.87	30.14	30.12	29.52
Water	[g]	30.50	30.39	30.11	30.09	30.16	30.20	30.22	30.46
WC_w	[g/g_{wet}]	0.048	0.048	0.046	0.053	0.036	0.049	0.053	0.027
S/L (S_d/(L+PW))		0.928	0.910	0.956	0.919	0.921	0.906	0.896	0.918
pH at Titration		9.060	9.180	8.645	8.630	8.745	8.970	9.310	8.600
Na	[mg/L]	256	257	291	302	286	238	346	402
NH_4	[mg/L]	2.3	3.0	1.9	1.7	2.3	1.7	4.2	< 1
K	[mg/L]	9.3	9.8	9.2	8.6	9.6	8.7	19.4	11.3
Ca	[mg/L]	3.4	3.4	3.9	4.4	5.3	2.3	5.5	4.1
Mg	[mg/L]	0.7	0.7	0.8	0.8	1.1	0.4	0.8	0.5
Sr(OES)	[mg/L]	0.1	0.2	0.1	0.1	0.2	0.1	0.1	0.1
Ba (OES)	[mg/L]	< 0.025	< 0.025	< 0.025	< 0.025	< 0.025	< 0.025	< 0.025	< 0.025
F	[mg/L]	4.9	2.2	2.2	4.0	3.4	6.8	4.3	5.7
Cl	[mg/L]	196	243	174	171	137	80	205	380
Br	[mg/L]	0.26	0.21	0.20	0.18	0.16	0.10	0.21	0.19
NO_3	[mg/L]	0.36	0.40	0.41	0.27	0.45	0.35	0.82	6.32
SO_4	[mg/L]	156	168	178	229	307	206	412	227
I	[mg/L]	< 0.4	< 0.4	< 0.4	< 0.4	n.a.	n.a.	n.a.	n.a.
Alk (tit)	[meq/L]	2.81	1.74	n.a.	n.a.	n.a.	n.a.	1.80	2.53
Alk as HCO_3	[mg/L]	171.5	106.2	n.a.	n.a.	n.a.	n.a.	103.1	144.4
TOC	[mg/L]	12.70	11.40	17.95	19.95	19.60	19.90	5.97	11.20
TIC	[mg/L]	31.4	19.6	47.9	42.4	29.0	41.4	20.3	28.4
Lactate	[mg/L]	< 2	< 2	< 2	< 2	< 2	< 2	1.470	< 20
Acetate	[mg/L]	2.94	4.01	4.90	4.40	4.24	3.01	4.10	< 20
Propionate	[mg/L]	< 2	< 2	< 2	< 2	< 2	< 2	< 0.4	< 20
Formate	[mg/L]	< 2	< 2	< 2	< 2	< 2	< 2	1.530	< 20

n.a.: not analysed

All averaged aqueous extract solutions (Tab. 4.7-5) from pre-characterisation processed at S/L ≈ 1 contain low concentrations of NH_4 (up to 4.2 mg/L) and NO_3 (0.27 – 0.82 mg/L, but 6.3 mg/L in MAR1-8). Iodide content was analysed in four samples, but not detected. The factor (1/WCw·L/Sw) refers to the scaling factor required to scale aqueous concentrations for conservative components to porewater concentrations (i.e. at water-loss porosity).

Characteristic molar ion ratios (Tab. 4.7-6) do not follow a systematic trend with depth, except Ca/Mg, which increases with depth.

Tab. 4.7-6: Cation ratios and details of carbon system in aqueous extract solutions from pre-characterisation

Parameter	**Unit**	**MAR1-1**	**MAR1-2**	**MAR1-3**	**MAR1-4**	**MAR1-5**	**MAR1-6**	**MAR1-7**	**MAR1-8**
Depth	[m]	521.06	576.32	645.48	702.40	708.51	736.79	788.85	996.55
Geol. unit		«Parkinsoni-Württem-bergica-Sch.»	Wedel-sandstein Fm.	Opalinus Clay	Opalinus Clay	Staffelegg Fm.	Staffelegg Fm.	Klettgau Fm.	Kaiser-augst Fm.
Br/Cl*1000	[mol/mol]	0.58	0.38	0.51	0.45	0.52	0.57	0.45	0.22
SO_4/Cl	[mol/mol]	0.29	0.25	0.38	0.49	0.82	0.95	0.74	0.22
Ca/Mg	[mol/mol]	2.81	2.74	3.06	3.22	3.05	3.73	3.98	4.71
Ca/Sr	[mol/mol]	50	43	58	69	54	98	120	124
(Ca+Mg)/(Na+K)	[eq/eq]	0.015	0.015	0.015	0.016	0.021	0.011	0.018	0.011
Alk (tit)	[meq/L]	2.81	1.74	n.a.	n.a.	n.a.	n.a.	1.80	2.53
TIC	[meq/L]	2.61	1.63	3.99	3.53	2.41	3.45	1.69	2.36
Acetate	[meq/L]	0.05	0.07	0.08	0.07	0.07	0.05	0.07	< 0.03
TOC	[mg/L]	12.7	11.4	18.0	20.0	19.6	19.9	6.0	11.2
Acetate (as C)	[mg/L]	1.20	1.63	1.99	1.79	1.73	1.23	1.67	< 0.814

n.a.: not analysed

Tab. 4.7-7 shows that the aqueous extract solutions are at or very close to calcite saturation, and not far from dolomite saturation. Extracts are distinctly undersaturated with respect to sulphates and strontianite. TIC was used as input for the carbon system, because the titrated alkalinity would also include acetate.

Tab. 4.7-7: Saturation indices calculated for aqueous extract solutions from pre-characterisation

Parameter	**Unit**	**MAR1-1**	**MAR1-2**	**MAR1-3**	**MAR1-4**	**MAR1-5**	**MAR1-6**	**MAR1-7**	**MAR1-8**
Depth	[m]	521.06	576.32	645.48	702.40	708.51	736.79	788.85	996.55
Geol. unit		«Parkinsoni-Württem-bergica-Sch.»	Wedel-sandstein Fm.	Opalinus Clay	Opalinus Clay	Staffelegg Fm.	Staffelegg Fm.	Klettgau Fm.	Kaiser-augst Fm.
Charge	[eq/kgw]	-1.9E-04	-5.4E-04	3.9E-04	2.8E-04	1.8E-04	2.0E-04	-5.6E-04	-2.6E-04
%-Error		-0.84	-2.26	1.51	1.03	0.71	0.94	-1.75	-0.73
Acetate	[eq/kgw]	5.0E-05	6.8E-05	8.3E-05	7.4E-05	7.2E-05	5.1E-05	6.9E-05	< 3.0E-05
Ionic strength	[mol/kgw]	0.013	0.014	0.015	0.016	0.016	0.013	0.020	0.020
tot_alk	[eq/kg]	2.89E-03	1.90E-03	4.14E-03	3.66E-03	2.55E-03	3.71E-03	2.09E-03	2.44E-03
pH		9.06	9.18	8.65	8.63	8.75	8.97	9.31	8.60
log(pCO_2)	[bar]	-3.91	-4.25	-3.30	-3.34	-3.63	-3.70	-4.40	-3.49
SI(calcite)		0.158	0.070	0.015	-0.025	-0.001	0.017	0.309	-0.270
SI(dolomite)		0.01	-0.16	-0.32	-0.43	-0.37	-0.40	0.14	-1.09
SI(gypsum)		-2.81	-2.77	-2.70	-2.56	-2.36	-2.86	-2.30	-2.63
SI(celestite)		-2.43	-2.33	-2.40	-2.34	-2.03	-2.77	-2.30	-2.66
SI(strontianite)		-0.73	-0.75	-0.94	-1.06	-0.93	-1.15	-0.95	-1.56
SI(anhydrite)		-3.03	-3.00	-2.92	-2.78	-2.58	-3.09	-2.52	-2.85

Nagra PSI 2012 thermodynamic data base, calculated in PHREEQC for 25°C, using ordered dolomite; kgw=kg water; charge=Σ(cation charge) – ıΣ(anion charge)ı ;%-error= 100*charge/ (Σ(cation charge) + ıΣ(anion charge)ı)

Aqueous extracts of all cores were produced after termination of the experiments. A thin disc (10 – 17 mm) from the top and base of each core were processed according to the protocols used for pre-characterisation. The base of the core represents the inlet of the artificial porewater, whereas the top represents the outflow to sampling. The two may yield different results depending on the overall progress of fluid percolation (different concentrations in inlet sample compared to outlet), and averaging is therefore meaningless. Results (Tab. 4.7-8) show that Br (not present in the APW) was effectively flushed out of each core, whereas other minor anionic components were buffered to some extent (e.g. F, NO_3). The initially observed elevated TOC and acetate was partially flushed out. Cation concentrations decreased in general, but cation fractions need to be interpreted in more detail considering ion-exchange processes. Sr concentrations decreased, except in MAR1-4. A more in-depth analysis will be required to reconcile differences between extracts from pre-characterisation and post-mortem.

Calculation of speciation and saturation indices (Tab. 4.7-9) of the aqueous extract solutions from Tab. 4.7-8 are close to calcite saturation, and not far from dolomite saturation. Extracts are distinctly undersaturated with respect to sulphates and strontianite. TIC was used as input for the carbon system.

Cation exchange capacities and cation selectivities determined by the Ni-en method (Waber ed. 2020) were performed on the same subset of sample material as used for aqueous extracts. The results are also presented and interpreted in Section 4.5. Tab. 4.7-10 shows uncorrected (for porewater contribution and mineral dissolution/precipitation) capacities of 71 – 120 meq/kg (dry rock) with errors of up to ~ ± 5%. Ni consumptions is up to 5% higher than the sum of cations, whereas for the Kaiseraugst and one Staffelegg Formation samples Ni consumption was markedly lower. Ammonium was not measured but is expected to be present on the exchanger judged by the presence of up to 4 mg/L of NH_4 in the aqueous extracts performed at the same S/L ratio (Tab. 4.7-5).

Tab. 4.7-8: Composition of aqueous extract solutions from post-mortem characterisation

Parameter	**Unit**	**MAR1-1**		**MAR1-2**		**MAR1-3**	
Depth	[m]	521.06		576.32		645.48	
Geol. unit		«Parkinsoni-Württembergica-Schichten»		Wedelsandstein Fm.		Opalinus Clay	
Position		Top post-mortem	Base post-mortem	Top post-mortem	Base post-mortem	Top post-mortem	Base post-mortem
1/WCw*L/Sw		22.33	22.87	21.37	20.75	21.89	19.86
Rock wet	[g]	30.19	29.86	29.42	30.38	30.03	30.71
Water	[g]	30.54	30.60	30.20	30.19	29.81	28.87
WC_w	[g/g_{wet}]	0.05	0.05	0.05	0.05	0.05	0.05
S/L (S_d/(L+PW))		0.90	0.89	0.88	0.91	0.92	0.96
pH at Titration		8.91	8.77	9.31	8.97	8.70	8.80
Na	[mg/L]	230.00	243.00	245.00	247.00	251.00	268.00
NH_4	[mg/L]	2.01	2.30	3.49	2.92	1.90	1.68
K	[mg/L]	8.28	9.54	9.72	9.55	8.52	7.84
Ca	[mg/L]	2.91	3.02	3.11	3.27	2.94	3.13
Mg	[mg/L]	0.64	0.67	0.64	0.78	0.61	0.77
Sr(OES)	[mg/L]	0.13	0.14	0.15	0.14	< 0.25	< 0.25
Ba (OES)	[mg/L]	n.a.	n.a.	< 0.025	< 0.025	< 0.025	< 0.025
F	[mg/L]	4.44	4.28	2.31	1.97	2.32	2.30
Cl	[mg/L]	146.00	153.00	187.00	191.00	134.00	141.00
Br	[mg/L]	< 0.16	< 0.16	< 0.16	< 0.16	< 0.16	< 0.16
NO_3	[mg/L]	0.57	0.36	1.30	1.40	0.81	1.54
SO_4	[mg/L]	140.00	179.00	196.00	189.00	190.00	196.00
I	[mg/L]	n.a.	n.a.	n.a.	n.a.	n.a.	n.a.
Alk (tit)	[meq/L]	3.08	2.64	1.81	1.76	3.75	3.90
Alk as HCO3	[mg/L]	187.70	161.10	104.30	91.50	198.80	211.50
TOC	[mg/L]	5.69	5.31	8.60	6.77	17.30	18.30
TIC	[mg/L]	41.70	34.40	20.50	18.00	39.10	41.60
Lactate	[mg/L]	< 2	< 2	1.47	1.47	< 20	< 20
Acetate	[mg/L]	4.34	2.32	4.64	2.80	24.80	< 20
Propionate	[mg/L]	< 2	< 2	1.08	< 0.4	< 20	< 20
Formate	[mg/L]	< 2	< 2	1.50	1.60	< 20	< 20

n.a.: not analysed

Tab. 4.7-8: continued

Parameter	**Unit**	**MAR1-4**					**MAR1-5**	
Depth	[m]	702.40					708.51	
Geol. unit		Opalinus Clay					Staffelegg Fm.	
Position		Top post-mortem	Mid1 post-mortem	Mid2 post-mortem	Mid3 post-mortem	Base post-mortem	Top post-mortem	Base post-mortem
1/WCw*L/Sw		19.01	19.08	18.80	18.92	18.65	26.88	24.72
Rock wet	[g]	30.03	30.23	30.08	29.96	30.59	30.69	30.51
Water	[g]	30.45	30.44	30.41	30.37	30.35	30.11	30.12
WC_w	[g/g_{wet}]	0.06	0.06	0.06	0.06	0.06	0.04	0.04
S/L (S_d/(L+PW))		0.88	0.89	0.88	0.88	0.90	0.94	0.93
pH at Titration		8.37	8.44	8.52	8.51	8.47	8.81	8.59
Na	[mg/L]	281.00	274.00	267.00	263.00	264.00	292.00	270.00
NH_4	[mg/L]	1.82	1.77	1.66	1.61	1.70	2.93	2.88
K	[mg/L]	9.78	8.79	8.18	7.99	9.67	12.40	11.60
Ca	[mg/L]	3.69	3.53	3.50	3.34	3.45	6.59	5.69
Mg	[mg/L]	0.74	0.70	0.68	0.68	0.81	1.39	1.27
Sr(OES)	[mg/L]	0.12	0.12	0.11	0.11	0.10	0.29	0.24
Ba (OES)	[mg/L]	n.a.	n.a.	n.a.	n.a.	n.a.	< 0.025	< 0.025
F	[mg/L]	3.91	3.81	3.89	3.93	3.83	3.03	3.04
Cl	[mg/L]	145.00	142.00	138.00	137.00	145.00	114.00	127.00
Br	[mg/L]	< 0.16	< 0.16	< 0.16	< 0.16	< 0.16	< 0.16	< 0.16
NO_3	[mg/L]	0.42	0.27	0.31	0.26	0.43	86.70	19.80
SO_4	[mg/L]	215.00	219.00	197.00	196.00	212.00	294.00	290.00
I	[mg/L]	n.a.	n.a.	n.a.	n.a.	n.a.	n.a.	n.a.
Alk (tit)	[meq/L]	3.56	3.82	3.95	3.84	3.54	2.48	2.57
Alk as HCO_3	[mg/L]	217.30	233.10	241.20	234.40	216.00	133.40	142.20
TOC	[mg/L]	< 5	9.82	8.11	5.93	5.73	21.20	12.80
TIC	[mg/L]	48.40	47.10	49.80	50.20	46.70	26.30	28.00
Lactate	[mg/L]	< 2	< 2	< 2	< 2	< 2	< 2	< 2
Acetate	[mg/L]	< 2	< 2	< 2	< 2	< 2	4.97	2.69
Propionate	[mg/L]	< 2	< 2	< 2	< 2	< 2	< 2	< 2
Formate	[mg/L]	< 2	< 2	< 2	< 2	< 2	< 2	< 2

n.a.: not analysed

Tab. 4.7-8: continued

Parameter	**Unit**	**MAR1-6**		**MAR1-7**		**MAR1-8**	
Depth	[m]	736.79		788.85		996.55	
Geol. unit		Staffelegg Fm.		Klettgau Fm.		Kaiseraugst Fm.	
Position		Top post-mortem	Base post-mortem	Top post-mortem	Base post-mortem	Top post-mortem	Base post-mortem
1/WCw*L/Sw		20.04	18.64	19.85	20.01	31.53	35.09
Rock wet	[g]	30.35	30.36	30.12	29.91	29.84	30.14
Water	[g]	30.16	30.19	30.22	30.13	30.36	30.27
WC_w	[g/g_{wet}]	0.05	0.06	0.05	0.05	0.03	0.03
S/L (S_d/(L+PW))		0.91	0.90	0.90	0.89	0.92	0.94
pH at Titration		8.66	8.85	9.31	9.24	8.68	8.78
Na	[mg/L]	268.00	263.00	346.00	265.00	332.00	264.00
NH_4	[mg/L]	1.55	1.76	4.24	2.09	0.00	0.00
K	[mg/L]	10.80	11.70	19.36	14.64	9.26	7.96
Ca	[mg/L]	2.89	2.74	5.53	3.29	3.15	2.43
Mg	[mg/L]	0.50	0.51	0.84	0.62	0.36	0.29
Sr(OES)	[mg/L]	0.08	0.07	0.10	0.06	0.05	0.03
Ba (OES)	[mg/L]	< 0.025	< 0.025	< 0.025	0.00	n.a.	n.a.
F	[mg/L]	5.68	6.06	4.27	4.00	4.35	4.77
Cl	[mg/L]	93.50	132.00	205.00	163.00	234.00	125.00
Br	[mg/L]	< 0.16	< 0.16	0.21	< 0.16	< 0.16	< 0.16
NO_3	[mg/L]	71.90	17.40	0.82	0.82	4.18	1.03
SO_4	[mg/L]	189.00	192.00	412.00	240.00	226.00	199.00
I	[mg/L]	n.a.	n.a.	n.a.	n.a.	n.a.	n.a.
Alk (tit)	[meq/L]	4.30	3.82	1.80	1.72	2.82	3.37
Alk as HCO_3	[mg/L]	235.30	212.80	103.10	111.90	172.30	205.40
TOC	[mg/L]	16.40	12.80	5.97	11.65	< 5	< 5
TIC	[mg/L]	46.30	41.90	20.30	22.00	39.10	46.00
Lactate	[mg/L]	< 2	< 2	1.47	< 2	< 2	< 2
Acetate	[mg/L]	4.09	2.14	4.10	4.04	3.13	< 2
Propionate	[mg/L]	< 2	< 2	< 0.4	< 2	< 2	< 2
Formate	[mg/L]	< 2	< 2	1.53	< 2	< 2	< 2

n.a.: not analysed

Tab. 4.7-9: Saturation indices calculated for aqueous extract solutions obtained post-mortem

Parameter	**Unit**	**MAR1-1**		**MAR1-2**		**MAR1-3**	
Depth	[m]	521.06		576.32		645.48	
Geol. unit		«Parkinsoni-Württembergica-Schichten»		Wedelsandstein Fm.		Opalinus Clay	
Position		Top post-mortem	Base post-mortem	Top post-mortem	Base post-mortem	Top post-mortem	Base post-mortem
Charge	[eq]	-4.6E-04	-1.4E-04	-2.5E-04	2.7E-04	1.8E-04	3.2E-04
%-Error		-2.18	-0.65	-1.11	1.23	0.78	1.35
Ionic strength	[mol/kgw]	0.012	0.013	0.013	0.013	0.013	0.014
tot_alk	[eq/kg]	3.72E-03	3.02E-03	2.06E-03	1.66E-03	3.39E-03	3.65E-03
pH		8.91	8.77	9.31	8.97	8.70	8.80
log(pCO_2)	[bar]	-3.63	-3.57	-4.38	-4.06	-3.44	-3.52
SI(calcite)		0.09	-0.11	0.15	-0.16	-0.14	0.00
SI(dolomite)		-0.125	-0.529	-0.033	-0.603	-0.614	-0.265
SI(gypsum)		-2.90	-2.78	-2.76	-2.72	-2.77	-2.75
SI(celestite)		-2.51	-2.39	-2.33	-2.37	Sr b.d.	Sr b.d.
SI(strontianite)		-0.77	-0.98	-0.68	-1.07	Sr b.d.	Sr b.d.
SI(anhydrite)		-3.13	-3.01	-2.98	-2.94	-3.00	-2.98

Tab. 4.7-9: continued

Parameter	**Unit**	**MAR1-4**					**MAR1-5**	
Depth	[m]	702.40					708.51	736.79
Geol. unit		Opalinus Clay					Staffelegg Fm.	
Position		Top post-mortem	Mid1 post-mortem	Mid2 post-mortem	Mid3 post-mortem	Base post-mortem	Top post-mortem	Base post-mortem
Charge	[eq]	-4.4E-05	-2.9E-04	-3.1E-04	-4.8E-04	-6.2E-04	3.9E-04	7.3E-05
%-Error		-0.17	-1.16	-1.26	-1.98	-2.52	1.49	0.29
Ionic strength	[mol/kgw]	0.015	0.015	0.014	0.014	0.015	0.016	0.015
tot_alk	[eq/kg]	4.09E-03	4.00E-03	4.25E-03	4.28E-03	3.97E-03	2.35E-03	2.42E-03
pH		8.37	8.44	8.52	8.51	8.47	8.81	8.59
log(pCO_2)	[bar]	-3.01	-3.09	-3.15	-3.14	-3.13	-3.73	-3.47
SI(calcite)		-0.28	-0.24	-0.14	-0.17	-0.23	0.11	-0.13
SI(dolomite)		-0.917	-0.848	-0.648	-0.679	-0.737	-0.122	-0.573
SI(gypsum)		-2.64	-2.65	-2.70	-2.72	-2.67	-2.29	-2.34
SI(celestite)		-2.40	-2.40	-2.47	-2.48	-2.49	-1.92	-1.99
SI(strontianite)		-1.29	-1.25	-1.17	-1.19	-1.30	-0.78	-1.04
SI(anhydrite)		-2.86	-2.88	-2.92	-2.94	-2.90	-2.51	-2.57

Tab. 4.7-9: continued

Parameter	**Unit**	**MAR1-6**		**MAR1-7**		**MAR1-8**	
Depth	[m]	788.85	996.55	n.a.	n.a.	n.a.	n.a.
Geol. unit		Klettgau Fm.	Kaiseraugst Fm.				
Position		Top post-mortem	Base post-mortem	Top post-mortem	Base post-mortem	Top post-mortem	Base post-mortem
Charge	[eq]	2.8E-04	1.7E-04	2.9E-04	-3.0E-04	-1.1E-04	-1.1E-04
%-Error		1.36	0.70	1.22	-1.29	-0.39	-0.46
Ionic strength	[mol/kgw]	0.013	0.014	0.015	0.014	0.017	0.014
tot_alk	[eq/kg]	3.61E-03	4.00E-03	2.13E-03	1.60E-03	3.38E-03	4.01E-03
pH		9.03	8.66	9.24	9.39	8.68	8.78
log(pCO_2)	[bar]	-3.78	-3.33	-4.27	-4.59	-3.43	-3.45
SI(calcite)		0.04	-0.12	0.13	0.05	-0.16	-0.09
SI(dolomite)		-0.289	-0.656	-0.119	-0.238	-0.916	-0.757
SI(gypsum)		-2.88	-2.80	-2.67	-2.75	-2.72	-2.86
SI(celestite)		-2.77	-2.64	-2.70	-2.81	-2.79	-3.01
SI(strontianite)		-1.12	-1.22	-1.17	-1.27	-1.49	-1.50
SI(anhydrite)		-3.10	-3.02	-2.89	-2.98	-2.94	-3.08

Nagra PSI 2012 thermodynamic data base, calculated in PHREEQC for 25°C, using ordered dolomite;
kgw = kg water; charge = Σ(cation charge) – |Σ(anion charge)| ; %-error = 100*charge / (Σ(cation charge) + |Σ(anion charge)|).

The low Br concentrations agree well with the low or non-detectable Br concentrations in aqueous extracts. Interestingly, the SO_4/Cl ratios are significantly and systematically lower in the Ni-en solutions compared to the aqueous extracts, suggesting that there is either a sulphate source in the aqueous extracts or a sink in the Ni-en solutions.

The cation occupancies (selectivities) derived from Ni-en extracts and applying a correction for the porewater contribution are presented in Section 4.5.

Ni-en extracts were also determined post-mortem from discs at the top and base of a sample core (Tab. 4.7-11). The sum of displaced (uncorrected) cations and Ni consumption obtained post-mortem agree with the sum of cations determined for pre-characterisation for homogeneous samples, whereas differences between top and base discs of the same core indicate a heterogeneous clay-mineral content. One would have to compare corrected values for a more in-depth analysis because the ionic strength of the porewater at post-mortem time is significantly less than that of the initial porewater. The sulphate concentrations in the Ni-en extracts post-mortem are similar to those from pre-characterisation, but can differ between top and base. The chloride concentrations are much less post-mortem (resembling the injected fluid) such that the SO_4/Cl ratios are much larger post-mortem, and also well above that of the injected fluid.

Tab. 4.7-10: Composition of Ni-en extract solutions and related parameters from pre-characterisation

Parameter	**Unit**	**MAR1-1**	**MAR1-2**	**MAR1-3**	**MAR1-4**
Depth	[m]	521.06	576.32	645.48	702.40
Geol. unit		«Parkinsoni-Württemb.-Sch.»	Wedelsandstein Fm.	Opalinus Clay	Opalinus Clay
Averaging		1 averaged sample	1 averaged sample	1 averaged sample	1 averaged sample
1/WCw*L/Sw		22.49	21.76	22.54	20.37
Rock wet	[g]	29.60	30.34	30.52	29.94
Solution	[g]	30.39	30.39	30.47	30.52
WC_w	[g/g_{wet}]	0.05	0.05	0.05	0.05
S/L (S_d/(L+PW))		0.89	0.91	0.91	0.88
pH (initial)		8.35	8.35	8.35	8.35
Ni (initial)	[mg/L]	5777	5777	5787	5787
pH (final)		8.42	8.51	8.33	8.38
Na	[mg/L]	845	730	989	1149
K	[mg/L]	214	187	226	236
Mg	[mg/L]	157	134	157	173
Ca	[mg/L]	545	498	595	777
Sr	[mg/L]	36.6	33.6	33.7	35.3
Ba	[mg/L]	0.31	1.08	0.72	0.55
Fe	[mg/L]	< 0.05	0.30	< 0.05	< 0.05
Ni	[mg/L]	2'960	3'250	2'667	2'231
F	[mg/L]	0.88	0.51	0.59	0.93
Cl	[mg/L]	167	222	152	149
Br	[mg/L]	0.21	0.33	0.18	< 0.16
NO_3	[mg/L]	12'480	12'487	12'500	12'401
SO_4	[mg/L]	105	120	114	147
TDS	[mg/L]	17'511	17'663	17'435	17'299
Na	[meq/kgd]	41.5	35.0	47.1	56.6
K	[meq/kgd]	6.2	5.3	6.3	6.8
Mg	[meq/kgd]	14.6	12.1	14.2	16.1
Ca	[meq/kgd]	30.7	27.4	32.5	43.9
Sr	[meq/kgd]	0.94	0.85	0.84	0.91
Ba	[meq/kgd]	0.005	0.017	0.012	0.009
Fe	[meq/kgd]	< 0.002	0.01	< 0.002	< 0.002
SumCat	[meq/kgd]	93.9	80.7	101.0	124.3
SumCat_err	[meq/kgd]	3.90	3.30	4.20	5.20
Ni_cons	[meq/kgd]	98.4	85.0	106.9	126.2
Ni_cons_err	[meq/kgd]	4.80	4.80	4.60	4.60
Br/Cl	[mol/mol*1000]	0.6	0.7	0.5	-
SO_4/Cl	[mol/mol]	0.23	0.20	0.28	0.36

kgd = kg dry rock

Tab. 4.7-10: continued

Parameter	**Unit**	**MAR1-5**	**MAR1-6**	**MAR1-7**	**MAR1-8**
Depth	[m]	708.51	736.79	788.85	996.55
Geol. unit		Staffelegg Fm.	Staffelegg Fm.	Klettgau Fm.	Kaiseraugst Fm.
Averaging		1 averaged sample	1 averaged sample	Not measured	1 base sample
1/WCw*L/Sw		27.44	21.69		40.02
Rock wet	[g]	31.42	30.06		30.08
Solution	[g]	30.25	30.17		32.15
WC_w	[g/g_{wet}]	0.04	0.05		0.03
S/L (S_d/(L+PW))		0.96	0.90		0.89
pH (initial)		8.37	8.37		8.24
Ni (initial)	[mg/L]	5800	5800		5818
pH (final)		8.39	8.37		8.33
Na	[mg/L]	715	1242		880
K	[mg/L]	155	268		220
Mg	[mg/L]	118	139		51
Ca	[mg/L]	464	712		312
Sr	[mg/L]	23.5	26.9		6.9
Ba	[mg/L]	0.63	0.29		0.21
Fe	[mg/L]	< 0.05	< 0.05		< 0.05
Ni	[mg/L]	3'687	2'340		3'951
F	[mg/L]	0.58	1.29		0.27
Cl	[mg/L]	143	73		351
Br	[mg/L]	< 0.16	< 0.16		< 0.16
NO_3	[mg/L]	13'033	12'579		13'140
SO_4	[mg/L]	196	137		158
TDS	[mg/L]	18'536	17'518		19'070
Na	[meq/kgd]	32.2	59.7		43.2
K	[meq/kgd]	4.1	7.6		6.3
Mg	[meq/kgd]	10.1	12.6		4.7
Ca	[meq/kgd]	24.0	39.3		17.6
Sr	[meq/kgd]	0.56	0.68		0.18
Ba	[meq/kgd]	0.010	0.005		0.003
Fe	[meq/kgd]	< 0.002	< 0.002		< 0.002
SumCat	[meq/kgd]	71.0	119.9		71.9
SumCat_err	[meq/kgd]	3.00	5.10		3.30
Ni_cons	[meq/kgd]	67.2	120.3		66.1
Ni_cons_err	[meq/kgd]	4.70	4.50		5.30
Br/Cl	[mol/mol*1000]	-	-		-
SO_4/Cl	[mol/mol]	0.51	0.69		0.17

kgd = kg dry rock

Tab. 4.7-11: Composition of Ni-en extract solutions and related parameters obtained post-mortem

Parameter	**Unit**	**MAR1-1**		**MAR1-2**		**MAR1-3**		**MAR1-4**	
Depth	[m]	521.06		576.32		645.48		702.40	
Geol. unit		«Parkinsoni-Württembergica-Schichten»		Wedelsandstein Fm.		Opalinus Clay		Opalinus Clay	
Position		Top post-mortem	Base post-mortem	Top post-mortem	Base post-mortem	Top post-mortem	Base post-mortem	Top post-mortem	Base post-mortem
1/WCw* L/Sw		22.67	23.14	20.71	21.17	22.81	21.18	19.15	19.21
Rock wet	[g]	30.15	29.95	30.41	29.75	30.47	30.14	30.34	30.31
Solution	[g]	30.99	31.07	30.20	30.19	31.59	30.31	30.99	31.03
WC_w	[g/g_{wet}]	0.05	0.05	0.05	0.05	0.05	0.05	0.06	0.06
S/L (S_d / (L+PW))		0.89	0.88	0.91	0.89	0.88	0.90	0.88	0.87
pH (initial)		8.37	8.39	8.28	8.28	8.30	8.30	8.31	8.33
Ni (initial)	[mg/L]	6'278	6'278	5'966	5'966	5'970	5'970	6'278	6'278
pH (final)		8.27	8.27	8.40	8.45	8.25	8.25	8.27	8.27
Na	[mg/L]	980	905	950	792	918	923	1'290	1'242
K	[mg/L]	184	177	209	189	200	202	195	189
Mg	[mg/L]	148	135	153	143	145	157	152	152
Ca	[mg/L]	480	449	535	518	610	608	708	628
Sr	[mg/L]	34.6	30.8	35.8	24.4	33.1	29.9	30.0	21.2
Ba	[mg/L]	0.25	0.27	0.81	0.94	0.65	0.56	0.40	0.45
Fe	[mg/L]	30.50	32.80	< 0.05	< 0.05	0.09	< 0.05	24.10	25.60
Ni	[mg/L]	3'453	3'608	3'205	3'523	2'879	2'762	2'739	2'947
F	[mg/L]	< 0.16	< 0.16	0.56	0.50	0.58	0.58	< 0.16	0.17
Cl	[mg/L]	127	137	177	173	120	122	129	126
Br	[mg/L]	< 0.16	< 0.16	< 0.16	< 0.16	< 0.16	< 0.16	< 0.16	< 0.16
NO_3	[mg/L]	12'351	12'322	12'760	12'796	13'231	12'784	12'299	12'352
SO_4	[mg/L]	99	125	137	143	115	116	130	120
TDS	[mg/L]	17'887	17'923	1'8163	18'302	18'252	17'706	17'697	17'804
Na	[meq/kgd]	48.1	44.8	45.4	38.6	45.5	44.6	64.1	61.8
K	[meq/kgd]	5.3	5.2	5.9	5.4	5.8	5.8	5.7	5.5
Mg	[meq/kgd]	13.8	12.7	13.8	13.2	13.6	14.3	14.3	14.3
Ca	[meq/kgd]	27.0	25.5	29.3	29.0	34.6	33.7	40.3	35.8
Sr	[meq/kgd]	0.89	0.80	0.90	0.63	0.86	0.76	0.78	0.55
Ba	[meq/kgd]	0.004	0.005	0.013	0.015	0.011	0.009	0.007	0.007
Fe	[meq/kgd]	1.23	1.34	< 0.002	< 0.002	< 0.002	< 0.002	0.99	1.05
SumCat	[meq/kgd]	96.3	90.2	95.3	86.9	100.4	99.2	126.0	119.1
SumCat_err	[meq/kgd]	4.10	3.80	4.00	3.60	4.20	4.10	5.50	5.20
Ni_cons	[meq/kgd]	98.0	93.0	92.6	82.6	109.8	110.8	125.0	117.2
Ni_cons_err	[meq/kgd]	5.30	5.40	4.90	5.10	5.00	4.80	5.10	5.20
Br/Cl	[mol/mol* 1000]	-	-	-	-	-	-	-	-
SO_4/Cl	[mol/mol]	0.29	0.34	0.29	0.31	0.35	0.35	0.37	0.35

Tab. 4.7-11: continued

Parameter	**Unit**	**MAR1-5**		**MAR1-6**		**MAR1-7**		**MAR1-8**	
Depth	[m]	708.51		736.79		788.85		996.55	
Geol. unit		Staffelegg Fm.		Staffelegg Fm.		Klettgau Fm.		Kaiseraugst Fm.	
position		Top post-mortem	Base post-mortem	Top post-mortem	Base post-mortem	Top post-mortem	Base post-mortem	Top post-mortem	Base post-mortem
1/WCw* L/Sw		27.77	25.13	19.91	18.26	21.11	19.66	32.14	36.05
Rock wet	[g]	29.57	29.88	30.38	30.79	29.69	29.92	29.91	30.07
Solution	[g]	30.01	30.01	29.98	29.97	31.64	31.72	31.04	31.05
WC_w	[g/g_{wet}]	0.04	0.04	0.05	0.06	0.05	0.06	0.03	0.03
S/L (S_d / (L+PW))		0.91	0.92	0.91	0.92	0.85	0.84	0.90	0.91
pH (initial)		8.27	8.27	8.27	8.27	8.28	8.28	8.41	8.39
Ni (initial)	[mg/L]	5'852	5'852	5'852	5'852	6'024	6'024	6'278	6'278
pH (final)		8.33	8.28	8.32	8.34	8.43	8.50	8.27	8.27
Na	[mg/L]	754	1395	1350	692	959	976	988	831
K	[mg/L]	189	334	350	186	362	370	173	168
Mg	[mg/L]	117	160	144	121	108	126	40	45
Ca	[mg/L]	523	842	774	488	608	610	256	254
Sr	[mg/L]	23.8	29.2	28.8	21.1	11.3	9.0	5.4	4.7
Ba	[mg/L]	0.39	0.31	0.29	0.45	0.25	0.16	0.16	0.17
Fe	[mg/L]	< 0.05	< 0.05	< 0.05	< 0.05	< 0.05	< 0.05	39.80	40.60
Ni	[mg/L]	3'666	2'010	2'112	3'771	3'210	3'160	4'568	4'598
F	[mg/L]	< 0.16	0.26	0.28	< 0.16	0.21	0.22	0.20	0.17
Cl	[mg/L]	110	121	89	118	143	162	219	107
Br	[mg/L]	< 0.16	< 0.16	< 0.16	< 0.16	< 0.16	< 0.16	< 0.16	< 0.16
NO_3	[mg/L]	1'2963	12'858	12'510	12'832	12'790	12'832	12'644	1'2590
SO_4	[mg/L]	179	129	132	180	173	145	145	110
TDS	[mg/L]	18'525	17'879	17'490	18'409	18'365	18'391	19'079	18'747
Na	[meq/kgd]	35.9	66.3	64.4	32.9	49.3	50.3	47.6	39.5
K	[meq/kgd]	5.3	9.3	9.8	5.2	10.9	11.2	4.9	4.7
Mg	[meq/kgd]	10.5	14.4	13.0	10.9	10.5	12.3	3.7	4.0
Ca	[meq/kgd]	28.6	45.8	42.4	26.6	35.8	36.1	14.1	13.8
Sr	[meq/kgd]	0.60	0.73	0.72	0.53	0.30	0.24	0.14	0.12
Ba	[meq/kgd]	0.006	0.005	0.005	0.007	0.004	0.003	0.003	0.003
Fe	[meq/kgd]	< 0.002	< 0.002	< 0.002	< 0.002	< 0.002	< 0.002	1.58	1.59
SumCat	[meq/kgd]	80.8	136.5	130.3	76.0	106.9	110.0	72.0	63.8
SumCat_err	[meq/kgd]	3.40	5.80	5.50	3.10	4.40	4.50	3.50	3.00
Ni_cons	[meq/kgd]	73.7	134.3	128.8	65.5	101.8	103.2	57.2	56.1
Ni_cons_err	[meq/kgd]	5.00	4.40	4.40	5.00	5.30	5.30	5.70	5.70
Br/Cl	[mol/mol *1000]	-	-	-	-	-	-	-	-
SO_4/Cl	[mol/mol]	0.60	0.39	0.54	0.56	0.45	0.33	0.24	0.38

kgd = kg dry rock

4.7.5 Chemical and isotopic evolution of displaced porewater aliquots

An artificial porewater (APW) composition was injected to force advective displacement. The outflow of each experiment was continuously sampled in small syringes (Waber ed. 2020). These syringe aliquots were analysed for chemical and water isotopic composition. Hydraulic conductivity was evaluated for each sampled aliquot (Darcy's law), and any expelled gas was also recorded, although gas-tightness is commonly good, but cannot be ensured for a syringe sampling system. Most data for each experiment are included in tables and graphs in this Section, and more details are provided in Appendix 4.

According to the method of advective displacement (Mäder 2018), it is expected that the first few sampled aliquots are of similar composition and represent the displaced porewater from the sample core. After this, a gradual breakthrough of the injected APW should be observed, until full breakthrough of conservative components (e.g. Cl, Br), given enough time.

4.7.5.1 Artificial porewater used for advective displacement

In the absence of constraining data, an artificial porewater composition (Tab. 4.7-12) was chosen that was based on work performed for the deep geothermal well in Schlattingen (advective displacement experiments detailed in Mäder & Waber 2017). The composition was calculated with PHREEQC for 25 °C, to be saturated with respect to calcite and dolomite, and a partial pressure of CO_2 of $10^{-2.2}$ bar. This partial pressure was imposed by bubbling with an Ar/CO_2 gas mixture during mixing and again when the fluid reservoir was filled before experiments. A recipe with the appropriate amounts of PA-grade chemicals is given in Tab. 4.7-13.

Deuterium was added as a water tracer for advective-diffusive transport, aiming for a δ^2H of approximately +100‰ (VSMOW). There is no Br contained in the APW and therefore bromide-breakout can be used as an anionic tracer in the case of significant Br concentrations in the porewater. If the Cl concentration in the APW is significantly different from the displaced early aliquots, Cl breakthrough forms an additional anionic tracer for transport.

All eight experiments were fed from PFA-coated fluid tanks containing the APW from the same batch 3. The pressurised head space of the tanks was filled with He after bubbling with the Ar/CO_2 gas mixture mentioned above. The composition of the APW is therefore identical for all experiments.

Tab. 4.7-12: Composition and recipe for the artificial porewater

Parameter	**Unit**	**Recipe**	**Calculated***	**Measured**	**Compounds**
pH		7.19		7.38	
Na	[mg/L]	3'989	3'988	4'059	NaCl; $NaHCO_3$; Na_2SO_4
NH_4	[mg/L]			< 10	
K	[mg/L]	79.4	79.3	78.7	KCl
Ca	[mg/L]	503	504	506	$CaCl_2 \cdot 2H_2O$
Mg	[mg/L]	226	226	208	$MgCl_2 \cdot 6H2O$
Sr(OES)	[mg/L]			< 0.25	
Ba	[mg/L]			< 0.25	
Si	[mg/L]			< 2.5	
Al	[mg/L]			0.279	
F	[mg/L]			< 1.6	
Cl	[mg/L]	5'992	5'986	5'826	$CaCl_2 \cdot 2H_2O$; KCl; $MgCl_2 \cdot 6H_2O$
Br	[mg/L]			< 1.6	
NO_3	[mg/L]			5.25	
SO_4	[mg/L]	2'305	2'303	2'132	Na_2SO_4
I	[mg/L]			n.m	
TOC	[mg/L]			7.4	
TIC	[mg/L]	29.3	29.32	28.0	$NaHCO_3$
lactate	[mg/L]			< 20	
acetate	[mg/L]			< 20	
propionate	[mg/L]			< 20	
formate	[mg/L]			< 20	
$\delta^{18}O$	[‰ VSMOW]		-11.43	-11.52	
$\delta^{2}H$	[‰ VSMOW]	100	91.9	90.8	D_2O

* calculated from the weighed-in chemical compounds; pH measured; CO_2-Ar bubbling not taken into account

Tab. 4.7-13: Recipe for the artificial porewater for a 2-litre batch

Chemical	**Manufacturer**	**Grade**	**Recipe**		**Weighed in** [g/2L)
			[g/kgw]	[g/2kgw]	
$NaHCO_3$	Merck	p.a.	0.2051	0.4101	0.4102
$CaCl_2 \cdot 2H_2O$	Merck	p.a.	1.8465	3.6930	3.6944
KCl	Merck	p.a.	0.1514	0.3029	0.3026
$MgCl_2 \cdot 6H_2O$	Merck	p.a.	1.8907	3.7814	3.7827
NaCl	Merck	p.a.	7.1916	14.3831	14.3838
Na_2SO_4	AnalaR NORAMAPUR	Ph.Eur.	3.4089	6.8177	6.8114
D_2O (100%)	Roth	> 99.8%D	0.0310	0.0620	0.0607

4.7.5.2 Physical conditions, hydraulic conductivity, sampling, and pore volume equivalents

All core samples were subjected to 63 – 65 bar hydraulic confining pressure, and an infiltration pressure of initially around 48 bar set by a He headspace. The infiltration pressure was gradually decreasing with time (displaced APW, and any small He leak), and was replenished repeatedly until the end of the last experiment. The pressure range covered 45 – 49 bar.

Temperature conditions were stable without diurnal fluctuations, ranging seasonally from 21.5 to 25.5 °C. Critical temperature-sensitive measurements, such as electric conductivity, pH and hydraulic conductivity, were temperature-compensated, either intrinsically or explicitly (details in Waber ed. 2020).

Hydraulic conductivity referenced to 25 °C was evaluated for all sampled aliquots based on sample mass and Darcy's law (detailed data in Appendix C, method in Waber ed. 2020). Earliest aliquots commonly show low apparent hydraulic conductivities due to the expulsion of gas from the dead volume in the outflow, and any small unsaturated volume in the sample core itself. All cores (Fig. 4.7-4) share an increasing hydraulic conductivity, followed by a slight decrease to a steady-state value, if sufficient run-time was provided. The exceptionally low conductivity of MAR1-2 at 0.4 pore volume is associated with a large volume of expelled gas at that time. The values for the early conductivity and that measured towards the end of the experiments (Tab. 4.7-14) span a relatively narrow range from $0.2 – 3.6 \cdot 10^{-13}$ m/s. This conductivity refers to a direction perpendicular to bedding and a sample length of 8 – 9 cm, measured at very large hydraulic gradients (Tab. 4.7-2). A gradual but rather minor decrease after an early maximum value may be due to slow sample consolidation, and this was also observed in earlier work (Mäder 2018). These latter values are most representative for in situ conditions, although the confining stress of 60 bar (6 MPa) in the experiments is still considerably less than the lithostatic stress at 500 – 1'000 m depth.

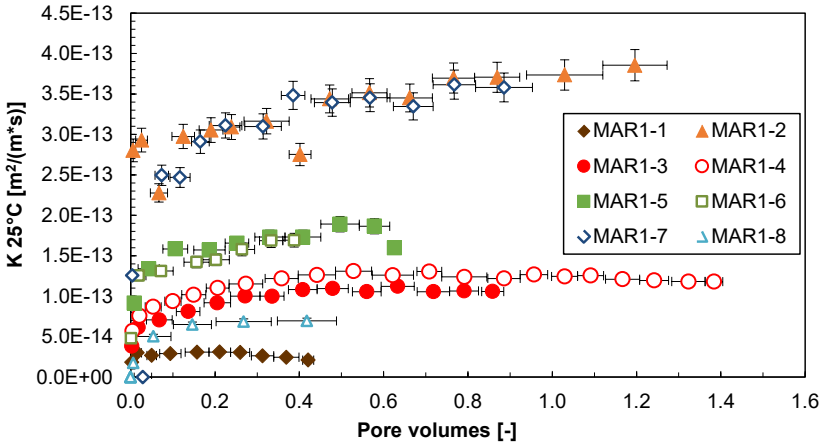

Fig. 4.7-4: Evolution of hydraulic conductivity during advective displacement experiments

MAR1-1 = MAR1-1-521.06 («Parkinsoni-Württem¬bergica-Schichten»); MAR1-2 = MAR1-1-576.32 (Wedelsandstein Formation); MAR1-3 = MAR1-1-645.48 (Opalinus Clay); MAR1-4 = MAR1-1-702.40 (Opalinus Clay); MAR1-5 = MAR1-1-708.51 (Staffelegg Formation); MAR1-6 = MAR1-1-736.79 (Staffelegg Formation); MAR1-7 = MAR1-1-788.85 (Klettgau Formation); MAR1-8 = MAR1-1-996.55 (Kaiseraugst Formation). Pore volume fractions relate to transport time based on water content. Experiment duration is 62 – 257 days. Horizontal length of symbol bar covers the sampling interval, vertical bars are an estimate of combined uncertainties.

Tab. 4.7-14: Hydraulic conductivity of AD samples

Parameter	**Unit**	**MAR1-1**	**MAR1-2**	**MAR1-3**	**MAR1-4**
Depth	[m]	521.06	576.32	645.48	702.40
Geol. unit		«Parkinsoni-Württembergica-Schichten»	Wedelsandstein Fm.	Opalinus Clay	Opalinus Clay
Early_K (25 °C)	[m/s]	3.08E-14	3.05E-13	8.11E-14	1.02E-13
Late_K (25 °C)	[m/s]	2.10E-14	3.85E-13	1.54E-13	1.18E-13
Parameter	**Unit**	**MAR1-5**	**MAR1-6**	**MAR1-7**	**MAR1-8**
Depth	[m]	708.51	736.79	788.85	996.55
Geol. unit		Staffelegg Fm.	Staffelegg Fm.	Klettgau Fm.	Kaiseraugst Fm.
Early_K (25 °C)	[m/s]	1.58E-13	1.42E-13	2.91E-13	6.49E-14
Late_K (25 °C)	[m/s]	1.60E-13	1.69E-13	3.58E-13	6.94E-14

The time axis for all data representations of sequential fluid aliquots is converted to pore volume fractions by dividing the cumulative sample mass (volume) by the water content of the core. In this way, experiments with very different hydraulic conductivities or different water contents can be represented in a meaningful way for transport. There may be some minor ambiguities in case where water contents from pre-characterisation deviate from the true water content of a sample core, or if a significant initial unsaturated porosity fraction would be present. The chosen approximation is sufficient for a visual presentation of data.

Sampled aliquots (mass) plotted versus pore volume fraction (time) provides an overview of all syringe samples taken for all eight AD experiments (Fig. 4.7-5). Up to 21 samples were collected.

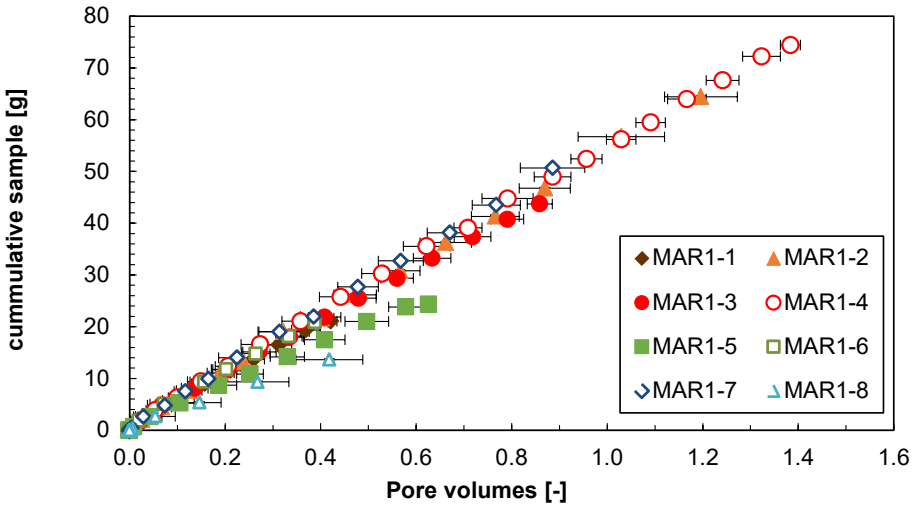

Fig. 4.7-5: Sampling schedule and sample volumes taken

MAR1-1 = MAR1-1-521.06 («Parkinsoni-Württembergica-Schichten»); MAR1-2 = MAR1-1-576.32 (Wedelsandstein Formation); MAR1-3 = MAR1-1-645.48 (Opalinus Clay); MAR1-4 = MAR1-1-702.40 (Opalinus Clay); MAR1-5 = MAR1-1-708.51 (Staffelegg Formation); MAR1-6 = MAR1-1-736.79 (Staffelegg Formation); MAR1-7 = MAR1-1-788.85 (Klettgau Formation); MAR1-8 = MAR1-1-996.55 (Kaiseraugst Formation). Each data point represents a syringe aliquot taken, with the horizontal bar indicating the duration for sampling, here convetred to pore volume fraction percolated. Different slopes reflect different volumetric flow rates scaled by porosity.

4.7.5.3 Inline measurement of electric conductivity and pH

Electric conductivity (EC) was continuously monitored in all experiments (Fig. 4.7-6; Waber ed. 2020, for method). Conductivity cells were initially calibrated but may show a drift to varying extent over time due to electrode corrosion, commonly resulting in low apparent readings. Therefore, electric conductivity values are only meant to provide an indication of salinity but are not used quantitatively.

The electric conductivities generally show a maximum in the early percolated pore volumes ranging from 20 to 30 mS/cm (22 °C laboratory reference), and over 50 mS/cm in case of the Kaiseraugst Formation. The injected artificial porewater has a lower conductivity compared to the displaced porewater. The value of the APW is gradually approached with progress of advective displacement if sufficient run-time is provided. Values below APW presumably are due to corrosion effects of the electrode as mentioned above, or constant exfiltration of gas. Corrosion may not only affect the inner surface of the flow-through electrodes but may also lead to diffusion-dominated short-circuits between the two electrodes. Similar calibration offsets were already established between pre-and post-experiment calibrations performed in earlier experiments (Mazurek et al. 2021).

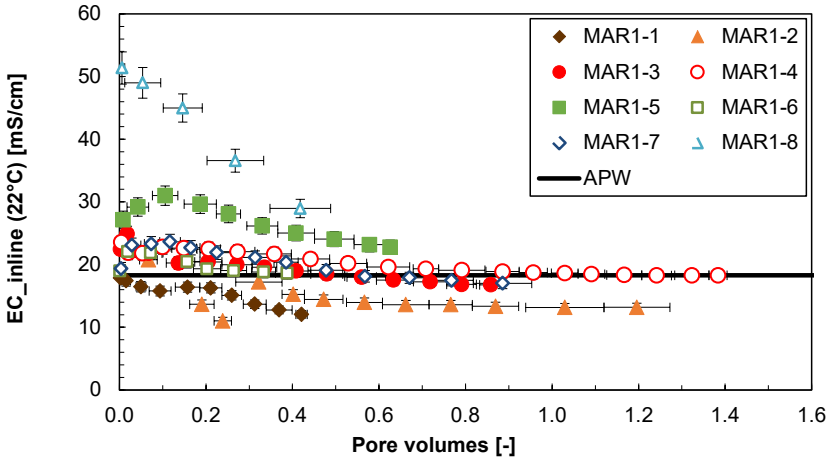

Fig. 4.7-6: Evolution of electric conductivity (22 °C) during advective displacement experiments

MAR1-1 = MAR1-1-521.06 («Parkinsoni-Württembergica-Schichten»); MAR1-2 = MAR1-1-576.32 (Wedelsandstein Formation); MAR1-3 = MAR1-1-645.48 (Opalinus Clay); MAR1-4 = MAR1-1-702.40 (Opalinus Clay); MAR1-5 = MAR1-1-708.51 (Staffelegg Formation); MAR1-6 = MAR1-1-736.79 (Staffelegg Formation); MAR1-7 = MAR1-1-788.85 (Klettgau Formation); MAR1-8 = MAR1-1-996.55 (Kaiseraugst Formation). Pore volume fractions relate to transport time based on water content. Experiment duration is 62 – 257 days. Horizontal length of symbol bar covers the sampling interval, vertical bars are an estimate of combined uncertainties.

The aim was to measure pH inline three times before/after sampling of the first four aliquots, and less frequently at later times (method in Waber ed. 2020). Measurements took 12 – 24 hrs in most cases, to ensure that the dead volume of the very small flow-through pH cell was sufficiently flushed given the very slow flow rates of the experiments. The micro-electrode was left installed in the flow-through cell and was checked before and after each pH measurement period with a standard solution. The initial calibration was made at pH 7 and 9, and simple drift checks and corrections were made with a standard solution at pH 7. The electrode slope was checked from time to time and was found to remain remarkably stable. In most cases, drift corrections over 12 – 24 hrs were ≤ 0.1 pH units. The overall uncertainty is difficult to assess because these small electrodes may respond to manipulations at the flow-through cell (response to small strains) and also small gas bubbles may temporarily affect readings. It is estimated that an error of ± 0.2 pH units is appropriate for most measurements. pH values of early aliquots are also tabulated below.

These in-line pH measurements (Fig. 4.7-7) are rather tricky and require careful handling of equipment. Criteria to accept a value include a small drift and a reasonably well-defined pH-plateau, as well as a stable non-zero electric conductivity (no gas bubbles). It cannot be excluded that for long measurement durations some effect from outgassing or in-gassing may influence the readings. The measurements for each experiment span a range of less than 0.5 pH units and point to a systematic trend over the experimental duration of each experiment, thus indicating that random errors or disturbed signals are not a dominant feature. More details are discussed further below.

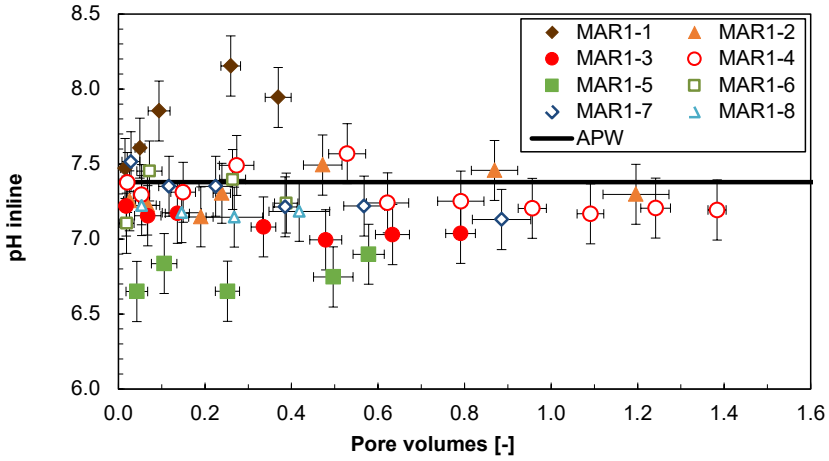

Fig. 4.7-7: Evolution of inline pH during advective displacement experiments

MAR1-1 = MAR1-1-521.06 («Parkinsoni-Württembergica-Schichten»); MAR1-2 = MAR1-1-576.32 (Wedelsandstein Formation); MAR1-3 = MAR1-1-645.48 (Opalinus Clay); MAR1-4 = MAR1-1-702.40 (Opalinus Clay); MAR1-5 = MAR1-1-708.51 (Staffelegg Formation); MAR1-6 = MAR1-1-736.79 (Staffelegg Formation); MAR1-7 = MAR1-1-788.85 (Klettgau Formation); MAR1-8 = MAR1-1-996.55 (Kaiseraugst Formation). Pore volume fractions relate to transport time based on water content. Experiment duration is 62 – 257 days. Horizontal length of symbol bar covers the sampling interval, vertical bars are an estimate of combined uncertainties.

4.7.5.4 Evolution of major and minor components

Evolution of concentrations with progress of percolation are shown in Figs. 4.7-8 to 4.7-13. Select analytical data for the first two aliquots sampled are summarised in Tab. 4.7-15 further below, with full details in Appendix C. The composition of the earliest aliquots displaced from the core samples are the most representative for the pore fluid extracted, and this is highlighted and interpreted in a separate Section 4.7.5.5.

Major components (Cl, SO_4, Na, Ca, Mg) displaced initially are all more concentrated than in the APW (Fig. 4.7-8) except for sulphate in case of MAR1-1 to MAR1-6, that elutes initially at or slightly below the APW concentration, and MAR1-6 (lower Staffelegg Formation) that elutes at chlorinities below that of the APW. Chloride concentrations form an early plateau in experiments from Opalinus Clay and higher lithologies (within uncertainty), but less so in deeper units where gradual changes start right after the first sample. Concentrations tend to converge to APW concentrations with progress of percolation attesting to an ion-exchanger population in situ that is compatible with ion ratios in the APW (but different in ionic strength). An exception is Mg that tends to decrease with time (pore volume) to concentrations below the APW, largely compensated by Na concentrations (detailed in Fig. 4.7-9). Ion-exchange equilibrium with the APW across the entire sample core is not yet reached in the experiments and this would require several more pore volumes of percolation. Elevated Ca in MAR1-5 to MAR1-7 compensates the exceptionally high nitrate, both decreasing with ongoing percolation (also see Tab. 4.7-10). Sr concentrations are shown further below at an expanded scale.

The same information as depicted in Fig. 4.7-8 is summarised for select components for all eight experiments (Fig. 4.7-9), this visualises some differences in the evolution of the early porewater aliquots. In AD experiments, several components show a relatively small change with time over

the first 2 – 3 aliquots, which is interpreted to represent the porewater composition displaced from the core sample at the imposed physical conditions. A choice was made to use average compositions of the first two analysed aliquots to represent the porewater composition. The resulting porefluid compositions are summarised in Tab. 4.7-15 (Section 4.7.5.5) and are also used in the integrative plots in Chapter 5.

Nitrate forms a major component at least in early eluted samples from MAR1-5 to MAR1-7 (Staffelegg Formation and below) and so forms a major carrier for anion charge, along with chloride and sulfate. This is less so for the deepest sample, MAR1-8 (Kaiseraugst Formation). Details are discussed further and depicted in the next Section. These nitrate-rich samples also show initially distinct elevated Ca concentrations compared to APW.

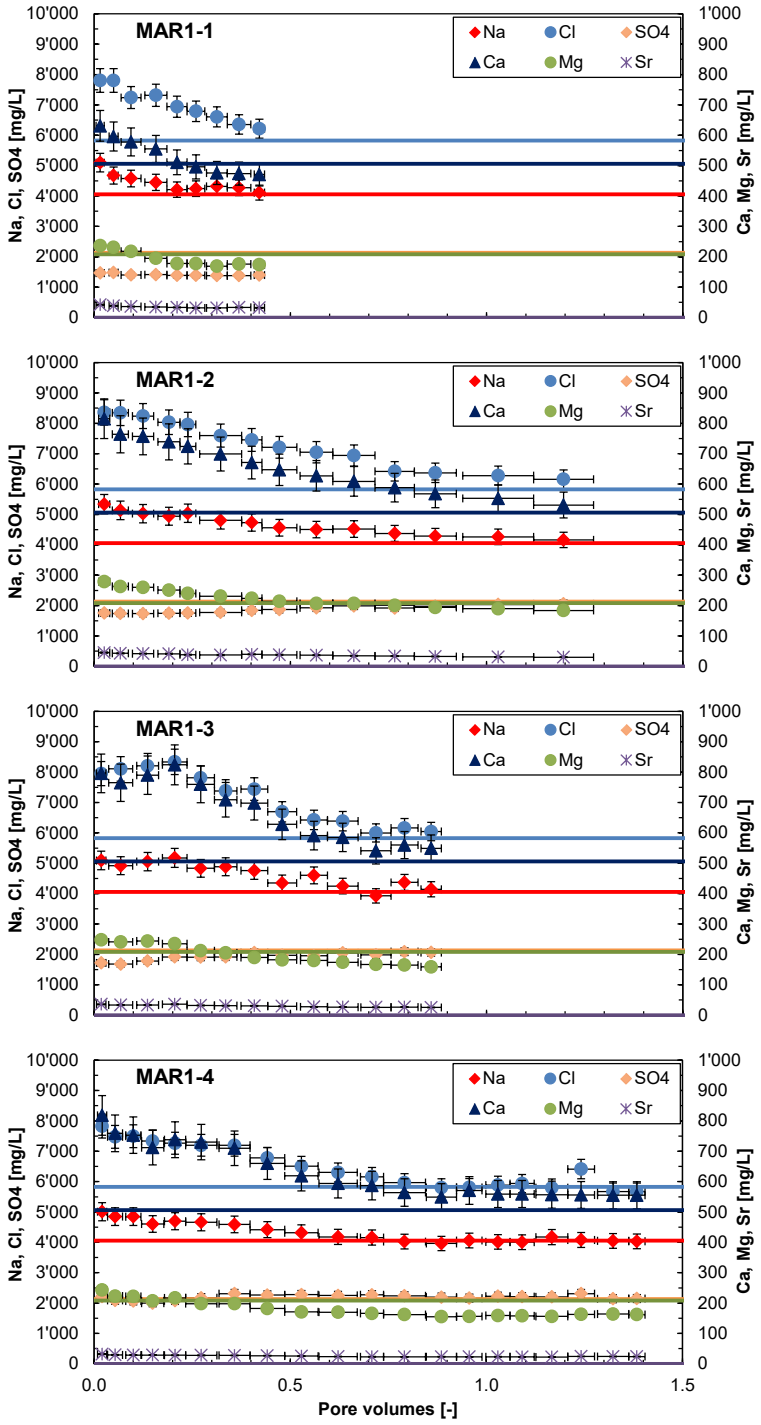

Fig. 4.7-8: Evolution of major components during advective displacement experiments

MAR1-1 = MAR1-1-521.06 («Parkinsoni-Württembergica-Schichten»); MAR1-2 = MAR1-1-576.32 (Wedelsandstein Formation); MAR1-3 = MAR1-1-645.48 (Opalinus Clay); MAR1-4 = MAR1-1-702.40 (Opalinus Clay); MAR1-5 = MAR1-1-708.51 (Staffelegg Formation); MAR1-6 = MAR1-1-736.79 (Staffelegg Formation); MAR1-7 = MAR1-1-788.85 (Klettgau Formation); MAR1-8 = MAR1-1-996.55 (Kaiseraugst Formation). Pore volume fractions relate to transport time based on water content. Experiment duration is 62 – 257 days. Horizontal length of symbol bar covers the sampling interval, vertical bars are an estimate of combined uncertainties. Horizontal lines represent the composition of the injected APW.

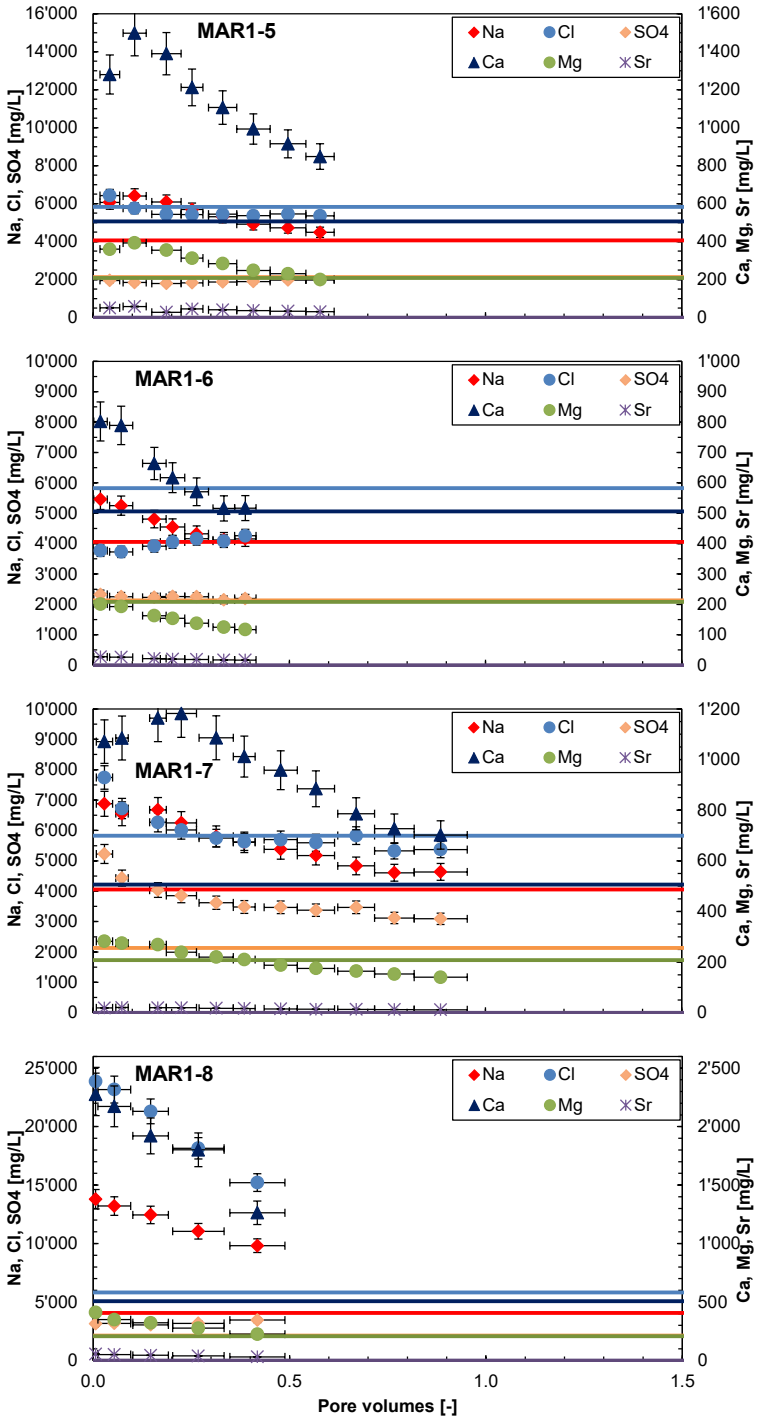

Fig. 4.7-8: continued

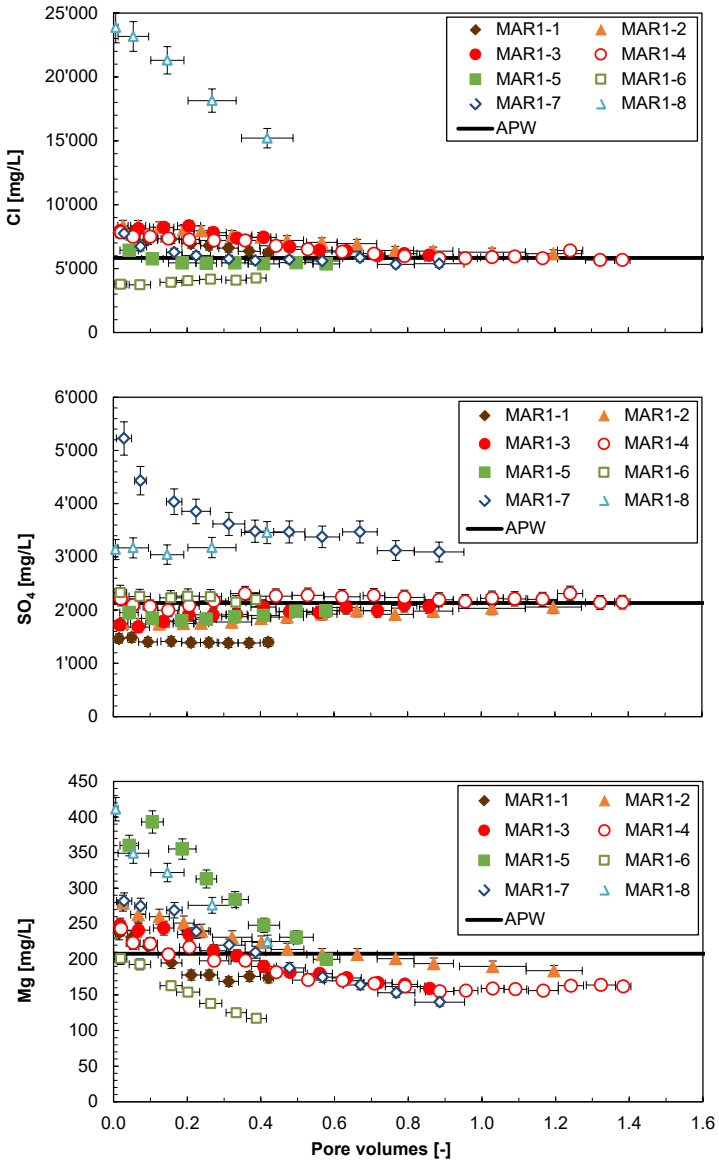

Fig. 4.7-9: Evolution of Cl, SO_4 and Mg during advective displacement experiments

MAR1-1 = MAR1-1-521.06 («Parkinsoni-Württembergica-Schichten»); MAR1-2 = MAR1-1-576.32 (Wedelsandstein Formation); MAR1-3 = MAR1-1-645.48 (Opalinus Clay); MAR1-4 = MAR1-1-702.40 (Opalinus Clay); MAR1-5 = MAR1-1-708.51 (Staffelegg Formation); MAR1-6 = MAR1-1-736.79 (Staffelegg Formation); MAR1-7 = MAR1-1-788.85 (Klettgau Formation); MAR1-8 = MAR1-1-996.55 (Kaiseraugst Formation). Pore volume fractions relate to transport time based on water content. Experiment duration is 62 – 257 days. Horizontal length of symbol bar covers the sampling interval, vertical bars are an estimate of combined uncertainties. Horizontal lines represent the composition of the injected APW.

Of the **minor components (Br, NO_3, K, Sr, Si)**, only potassium is present in the injected APW. Its evolution differs from core to core, clearly affected by transient ion-exchange with major cations not reaching equilibrium (Fig. 4.7-10). Strontium and bromide are gradually decreasing in all experiments (details in Fig. 4.7-11), bromide being flushed out almost completely. This can be used as a reversed break-through of an anionic tracer (see below). Dissolved silica elutes around 3 – 6 mg/L, in some cases slightly decreasing with time.

Nitrate is a major component in the early aliquots in experiments MAR1-5 (Staffelegg Formation) to MAR1-7 (Klettgau Formation), and to a much lesser extent in MAR1-8 (Kaiseraugst Formation). For these samples, the maximum values are up to 10 g/L, but not necessarily in the first aliquot samples, followed by a regular decrease (Fig. 4.7-10, Tab. 4.7-15, Appendix C).

The elution behaviour of NO_3 is variable (Fig. 4.7-10, Tab. 4.7-15, Appendix C): samples from overlaying formations («Brauner Dogger» and Opalinus Clay) provide early values up to 120 mg/L and decrease to well below 6 mg/L or below detection, within 0.3 pore volumes.

The origin of nitrate is still unknown, but a reactive nitrogen phase is suspected, which is not mobilised during comparably short and anaerobic aqueous extracts. There, only samples from the Kaiseraugst Formation show exceptionally high nitrate concentrations of 6 mg/L (other formations < 1 mg/L, Tab. 4.7-5). But aqueous extracts of post-mortem samples from AD experiments from the Staffelegg Formation and deeper show nitrate concentrations up to 87 mg/L (Tab. 4.7-8), generally higher at the outlet side than at the inlet of the core. This indicates a nitrogen mobilisation during the AD experiment. Ammonium (NH_4) is near or below a detection limit of 10 mg/L. Note also that nitrate does not get notably mobilised during porewater squeezing experiments that are carried out over a much shorter time period.

Ba and Al were measured by ICP-OES but always below detection limits. The detection limits depend on dilution factors and were 0.25 – 1 mg/L for Ba, and 1 – 2 mg/L for Al (10 mg/L in some cases with large dilutions).

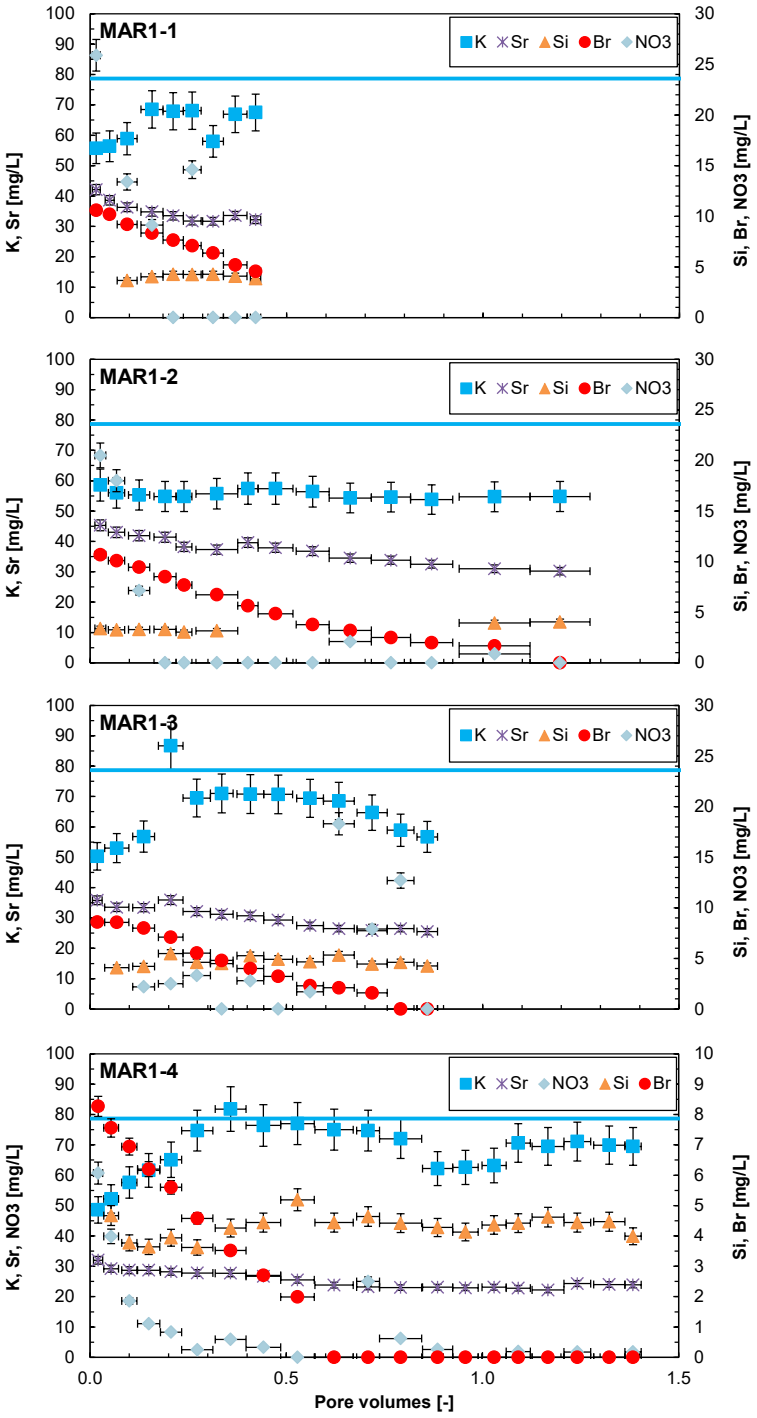

Fig. 4.7-10: Evolution of minor components during advective displacement experiments

MAR1-1 = MAR1-1-521.06 («Parkinsoni-Württembergica-Schichten»); MAR1-2 = MAR1-1-576.32 (Wedelsandstein Formation); MAR1-3 = MAR1-1-645.48 (Opalinus Clay); MAR1-4 = MAR1-1-702.40 (Opalinus Clay); MAR1-5 = MAR1-1-708.51 (Staffelegg Formation); MAR1-6 = MAR1-1-736.79 (Staffelegg Formation); MAR1-7 = MAR1-1-788.85 (Klettgau Formation); MAR1-8 = MAR1-1-996.55 (Kaiseraugst Formation). Pore volume fractions relate to transport time based on water content. Experiment duration is 62 – 257 days. Horizontal length of symbol bar covers the sampling interval, vertical bars are an estimate of combined uncertainties. Horizontal line represent the composition of the injected APW for K (0 for others).

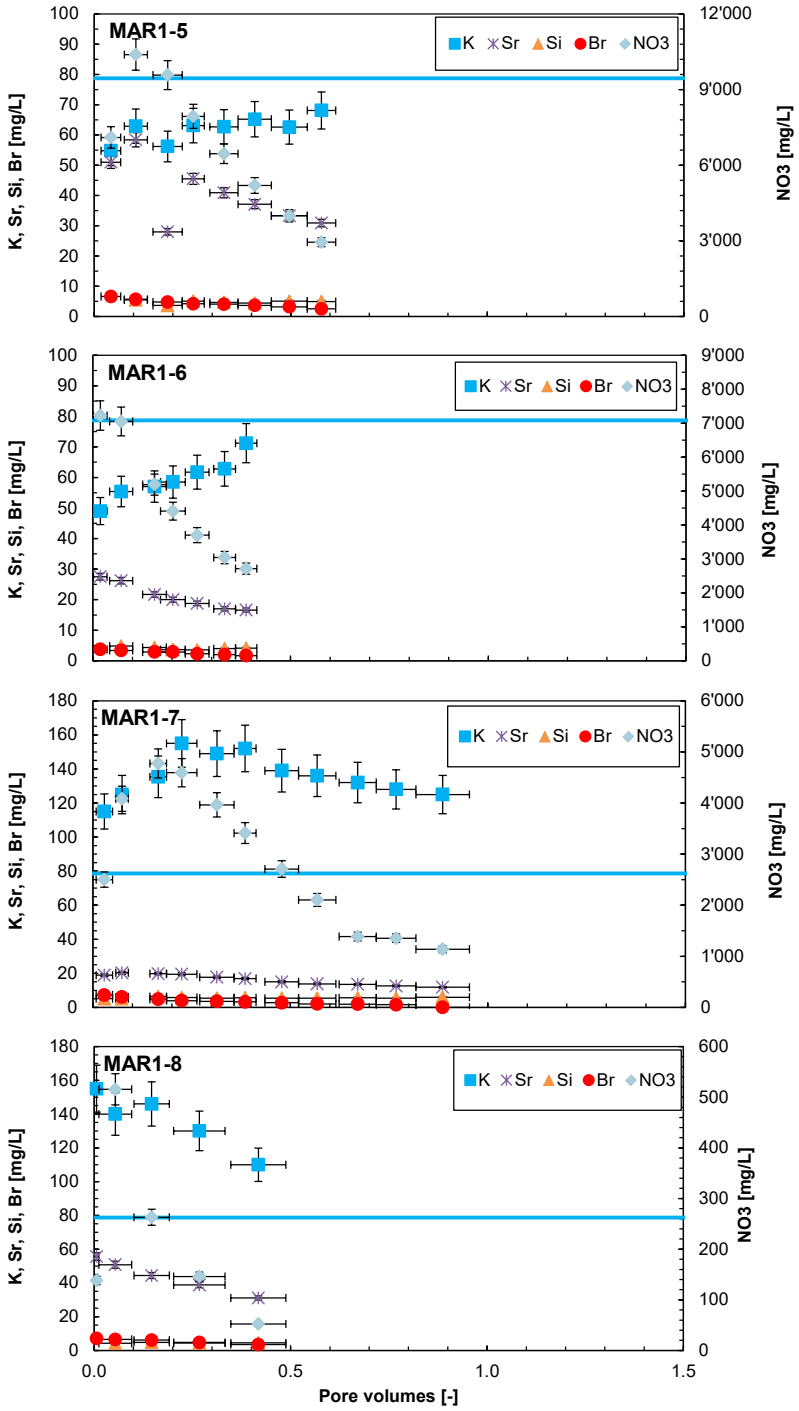

Fig. 4.7-10: continued

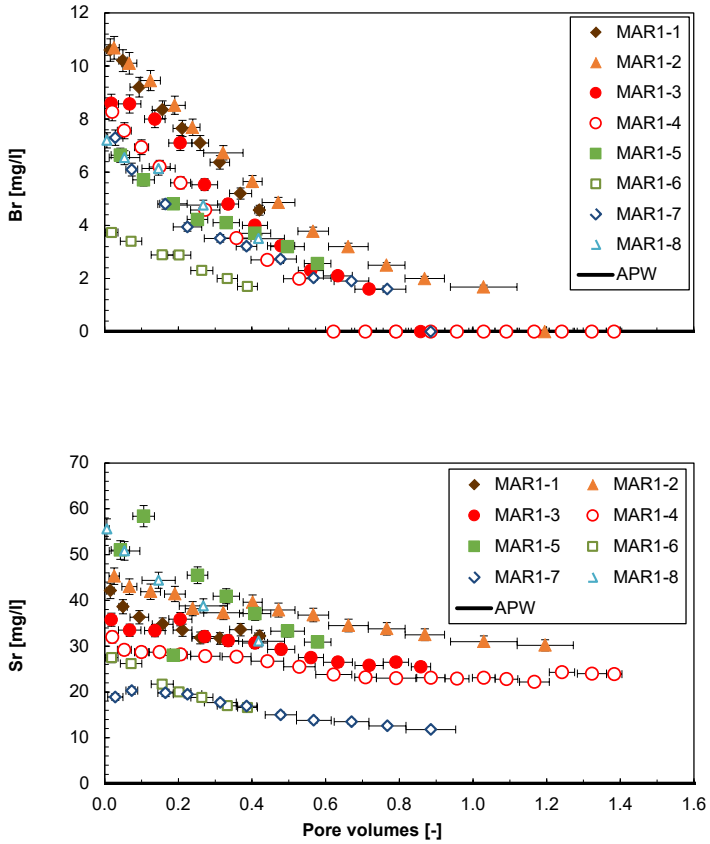

Fig. 4.7-11: Evolution of select minor components during advective displacement experiments

MAR1-1 = MAR1-1-521.06 («Parkinsoni-Württembergica-Schichten»); MAR1-2 = MAR1-1-576.32 (Wedelsandstein Formation); MAR1-3 = MAR1-1-645.48 (Opalinus Clay); MAR1-4 = MAR1-1-702.40 (Opalinus Clay); MAR1-5 = MAR1-1-708.51 (Staffelegg Formation); MAR1-6 = MAR1-1-736.79 (Staffelegg Formation); MAR1-7 = MAR1-1-788.85 (Klettgau Formation); MAR1-8 = MAR1-1-996.55 (Kaiseraugst Formation). Pore volume fractions relates to transport time based on water content. Experiment duration is 62 – 257 days. Horizontal length of symbol bar covers the sampling interval, vertical bars are an estimate of combined uncertainties. Br and Sr in the APW are 0. Br concentrations below detection are plotted at 0.

The **carbon system (TIC, TOC, TC, lmwoa)** shares as a common feature that relatively large TOC concentrations are eluted initially (150 – 900 mg/L) that gradually decrease to 30 – 100 mg/L with progressive percolation (Fig. 4.7-12; Tab. 4.7-15 shows averages of first 2 aliquots). TOC clearly dominates the dissolved carbon inventory (TC) at early times. Up to 25% of TOC is explained by low-molecular-weight organic acids (LMWOA), namely acetate and very minor formate. Acetate concentrations of up to 700 mg/L (Fig. 4.7-12 shows acetate as carbon equivalents, Fig. 4.7-13 in mg/L) were measured in the Wedelsandstein Formation sample (MAR1-2). Aqueous extracts (Tab. 4.7-5) imply TOC values of 100 – 400 mg/L when scaled to porewater content which covers the range seen in the early aliquots. Aqueous extracts carried out post-mortem (Tab. 4.7-8) show a clear depletion of TOC compared to the initial state. These observations are similar to previous work, with samples from the Schlattingen-1 geothermal well (Mäder & Waber 2017) and also TBO borehole BUL1-1.

TIC elutes initially at much lower concentrations than TOC, but covers a wide range of concentrations, and trends for each experiment are dissimilar to some extent (Figs. 4.7-12 and 4.7-13). Microbial activity might influence TIC/TOC, either in the syringe itself (i.e. during sampling/ storage) or at the surface of the core sample, whereby a part of organic carbon is oxidised to inorganic carbon, e.g. coupled with sulphate reduction.

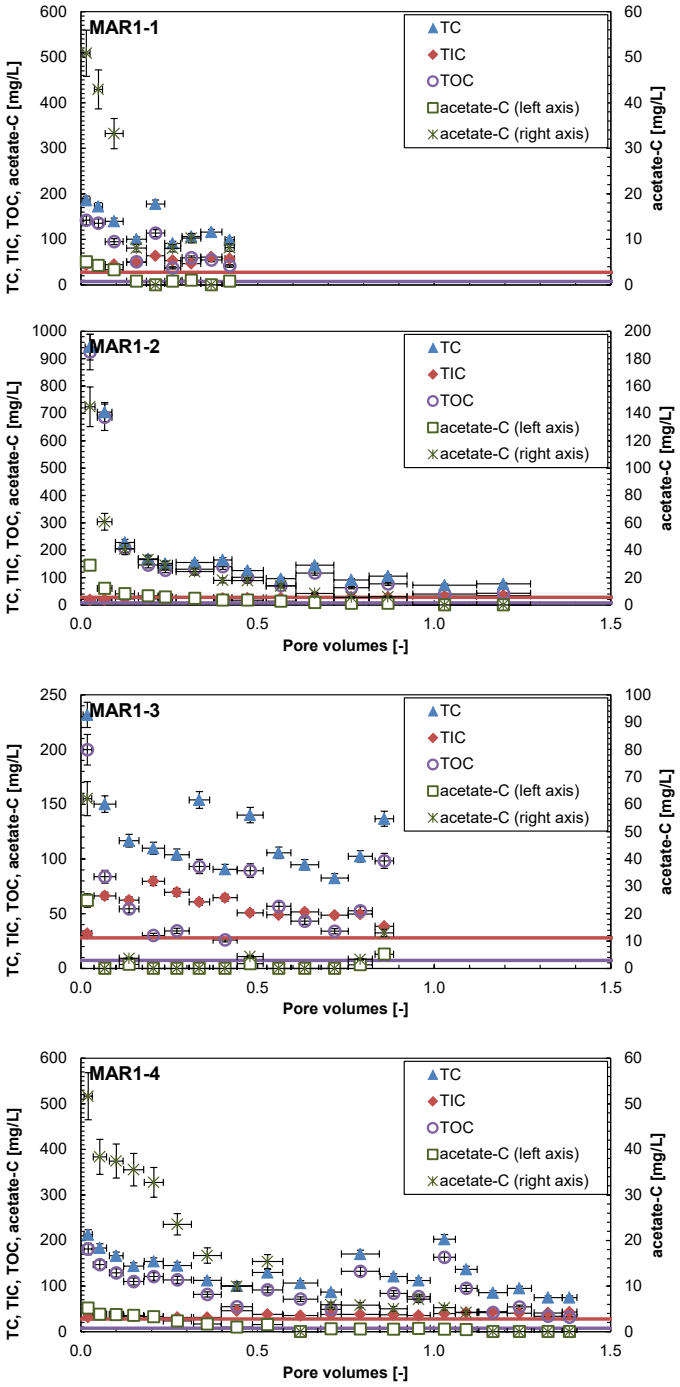

Fig. 4.7-12: Evolution of carbon system during advective displacement experiments

MAR1-1 = MAR1-1-521.06 («Parkinsoni-Württembergica-Schichten»); MAR1-2 = MAR1-1-576.32 (Wedelsandstein Formation); MAR1-3 = MAR1-1-645.48 (Opalinus Clay); MAR1-4 = MAR1-1-702.40 (Opalinus Clay); MAR1-5 = MAR1-1-708.51 (Staffelegg Formation); MAR1-6 = MAR1-1-736.79 (Staffelegg Formation); MAR1-7 = MAR1-1-788.85 (Klettgau Formation); MAR1-8 = MAR1-1-996.55 (Kaiseraugst Formation). Pore volume fractions relate to transport time based on water content. Experiment duration is 62 – 257 days. Horizontal length of symbol bar covers the sampling interval, vertical bars are an estimate of combined uncertainties. Horizontal lines represent the composition of the injected APW.

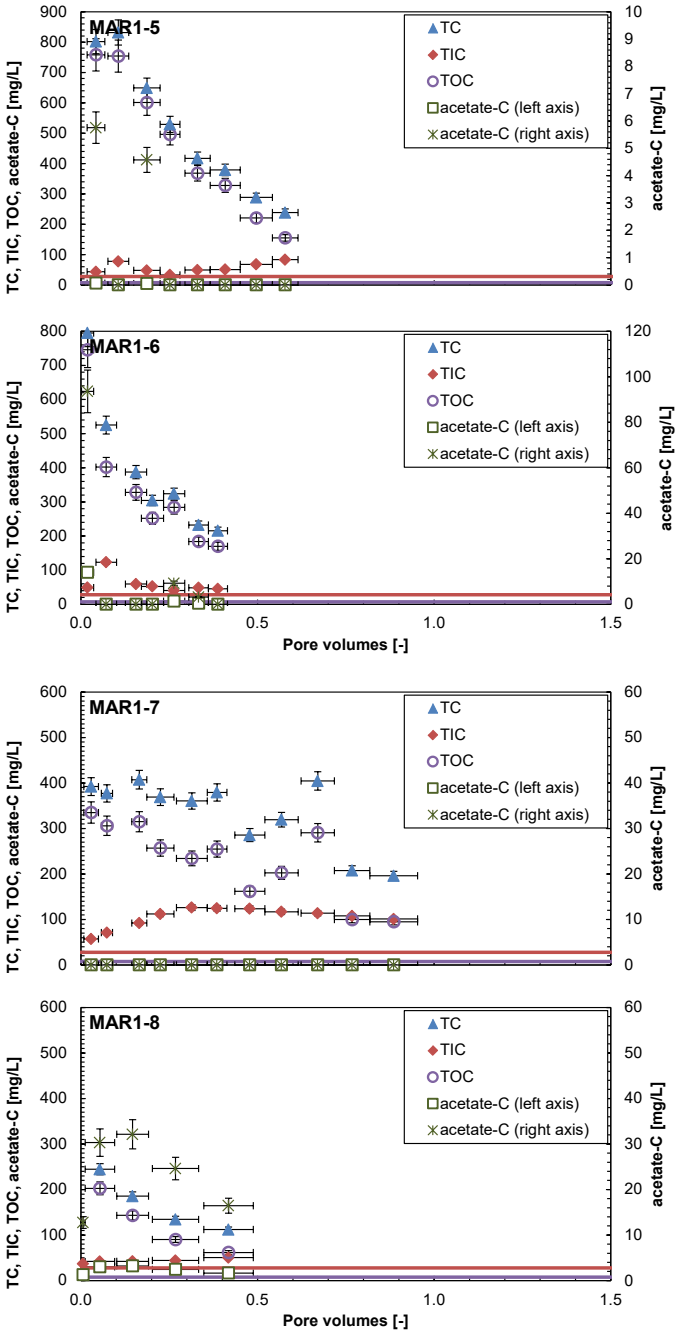

Fig. 4.7-12: continued

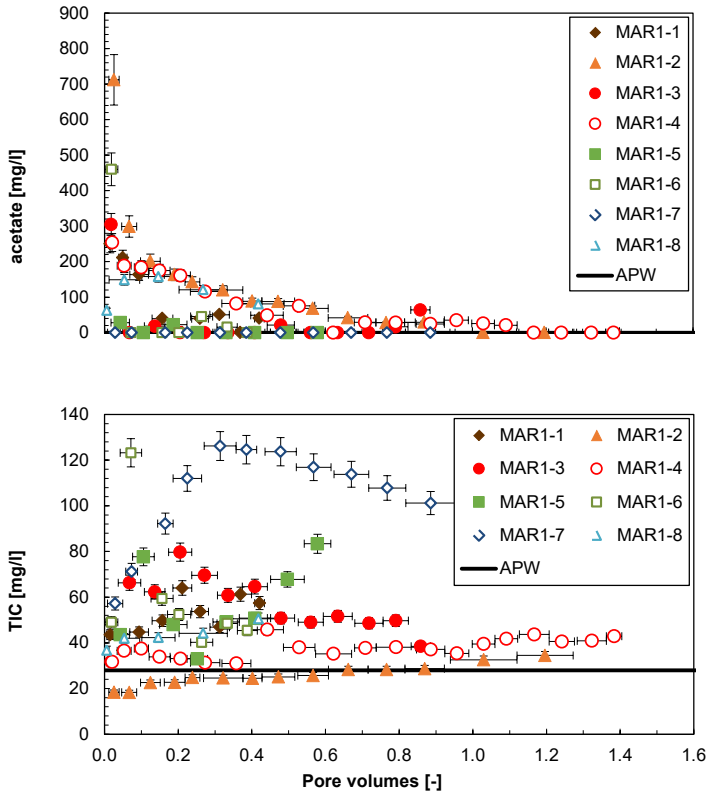

Fig. 4.7-13: Evolution of select carbon components during advective displacement experiments

MAR1-1 = MAR1-1-521.06 («Parkinsoni-Württembergica-Schichten»); MAR1-2 = MAR1-1-576.32 (Wedelsandstein Formation); MAR1-3 = MAR1-1-645.48 (Opalinus Clay); MAR1-4 = MAR1-1-702.40 (Opalinus Clay); MAR1-5 = MAR1-1-708.51 (Staffelegg Formation); MAR1-6 = MAR1-1-736.79 (Staffelegg Formation); MAR1-7 = MAR1-1-788.85 (Klettgau Formation); MAR1-8 = MAR1-1-996.55 (Kaiseraugst Formation). Pore volume fractions relate to transport time based on water content. Experiment duration is 62 – 257 days. Horizontal length of symbol bar covers the sampling interval, vertical bars are an estimate of combined uncertainties. Horizontal lines represent the composition of the injected APW. Concentrations below detection (acetate) are plotted at 0.

The **measurement of pH** was performed in-line between some of the sampling intervals (setup in Waber ed. 2020) and in the laboratory when syringe aliquots were prepared/preserved for analysis. The latter was done in most cases very shortly after sampling (one to a few hours), or after a few days of cold storage. The total range covered for all samples, in-line and laboratory, is 6.7 – 8.2 (Fig. 4.7-14), with laboratory values showing more spread than the in-line measurements.

The in-line pH series define relatively smooth trends with percolation progress, but not a very systematic behaviour. The spread is relatively small, ranging from 0.2 – 0.5 pH units. Some of the low apparent pH values measured in syringe samples (MAR1-4) may relate to sample storage issues, including microbial activity. The partial pressure of CO_2 is larger than atmospheric in the aliquots, and this bears the potential for outgassing and resultant supersaturation with respect to calcite, and a possibility for some loss of Ca and TIC by precipitation.

It should be noted that in samples with the large initial nitrate concentrations (MAR1-5 to MAR1-7) there is some uncertainty as to the generation of this dissolved nitrate. Depending on the processes, this could also affect pH values. While the pH may still be representative of the porewater of the experiment it may be deviated from the undisturbed state.

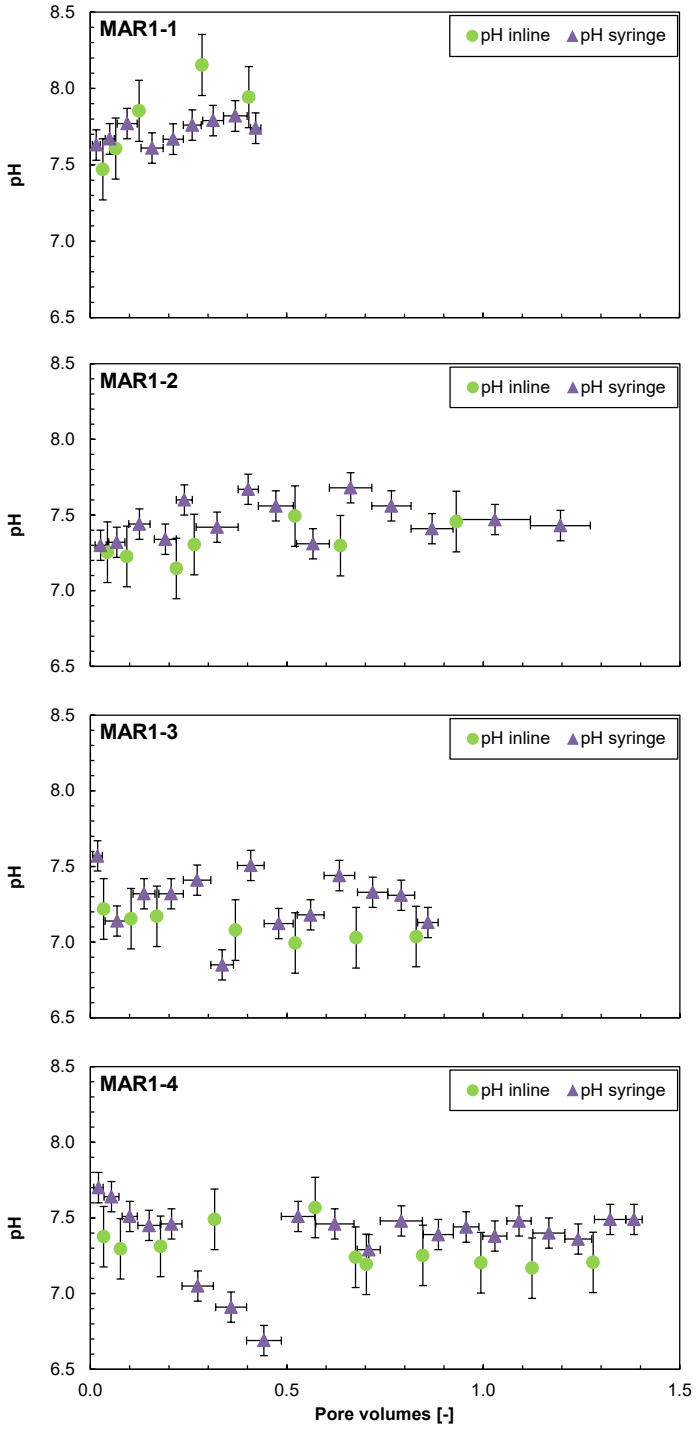

Fig. 4.7-14: Evolution of pH during advective displacement experiments

MAR1-1 = MAR1-1-521.06 («Parkinsoni-Württembergica-Schichten»); MAR1-2 = MAR1-1-576.32 (Wedelsandstein Formation); MAR1-3 = MAR1-1-645.48 (Opalinus Clay); MAR1-4 = MAR1-1-702.40 (Opalinus Clay); MAR1-5 = MAR1-1-708.51 (Staffelegg Formation); MAR1-6 = MAR1-1-736.79 (Staffelegg Formation); MAR1-7 = MAR1-1-788.85 (Klettgau Formation); MAR1-8 = MAR1-1-996.55 (Kaiseraugst Formation). Pore volume fractions relate to transport time based on water content. Experiment duration is 62 – 257 days. Horizontal length of symbol bar covers the sampling interval, vertical bars are an estimate of combined uncertainties.

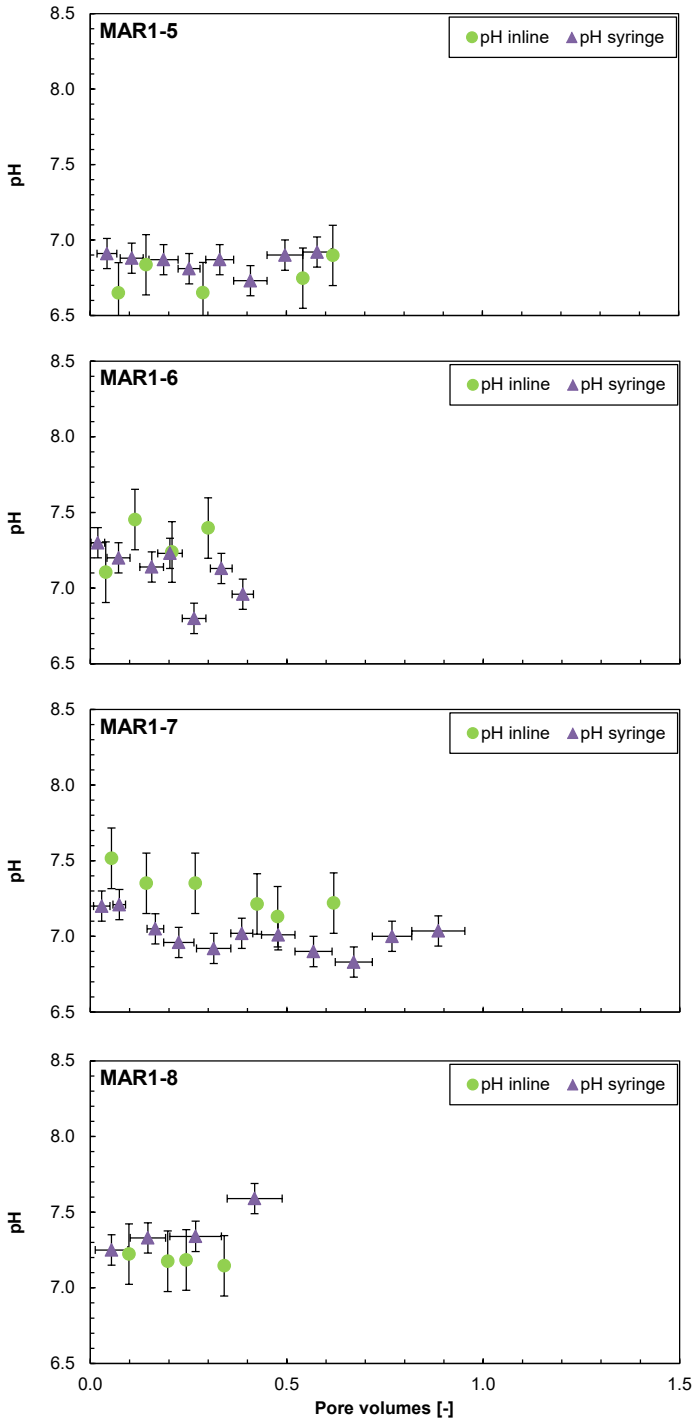

Fig. 4-7-14: continued

4.7.5.5 Early displaced aliquots representing the porewater composition

Early displaced aliquots were generally obtained by averaging the first two measured samples (Tab. 4.7-15). Interpretation of these early displaced aliquots as being representative of the in situ porewater contained in the core at the time of the experiment requires integration and interpretation of the entire dataset supported with geochemical calculations. Comprehensive reactive transport simulations are expected to further restrict the initial porewater compositions, as well as the transport properties of the cores. Only speciation calculations are included in this data report for the early compositions. Speciation calculations for all individual syringes are provided in Appendix B. The laboratory pH values were used for the speciation calculations. TIC was used as constraint for inorganic carbon.

The speciation calculations (Tab. 4.7-16) reveal a cation charge surplus (positive 'Charge', not observed in MAR1-8) that is not large and partially explained by significant acetate concentrations that were not included in the speciation. TIC was used as constraint for inorganic carbon. The aliquots are all significantly oversaturated with respect to calcite and also dolomite. Such oversaturation may result from shifts in pH linked to potential in-gassing or outgassing of CO_2 during sampling and storage. Alternatively, the large TOC (and TC) contents pose analytical difficulties to obtain TIC and associated errors may be larger than commonly assigned to TIC measurements.

Saturation is also reached or slightly exceeded for celestite, but for gypsum only in the lowermost formations (Klettgau and Kaiseraugst, MAR1-7 and MAR1-8). The implication is that the ion-activity products ($[Sr]\cdot[SO_4]$) and ($[Ca]\cdot[SO_4]$) are controlling factors, but this does not necessarily mean that these minerals are also present in the core before the experiments. There is only a small difference between sulphate concentrations in the APW and the early aliquots (Fig. 4.7-8) for MAR1-1 to MAR1-6, but Sr (Fig. 4.7-11) is eluted initially at higher concentrations compared to the APW and is decreasing quite rapidly. To maintain above mentioned ion-activity product at the value of the equilibrium constant, the decreasing Sr concentration is compensated by increasing activity coefficients as a function of decreasing ionic strength. The cation trend is therefore coupled to the relatively rapid breakthrough of the anions that dictate the evolution of the ionic strength. A more in-depth analysis and interpretation will have to be carried out, including reconstructions by geochemical modelling.

Sample MAR1-8 (near top of Kaiseraugst Formation) is just underlying the massive sulfate beds (anhydrite) of the Zeglingen Formation, and also just below this sample there is another anhydrite-rich layer mapped. Anhydrite was not decteted in the sample by XRD, but one might expect porewater conditions to approach anhydrite saturation in this region, as seen in the data.

Tab. 4.7-15: Composition of earliest aliquots from advective displacement experiments

Parameter	**Unit**	**MAR1-1**	**MAR1-2**	**MAR1-3**	**MAR1-4**
Depth	[m]	521.06	576.32	645.48	702.40
Geol. unit		«Parkinsoni-Württembergica-Schichten»	Wedelsandstein Fm.	Opalinus Clay	Opalinus Clay
pH inline	[-]	7.54	7.24	7.19	7.34
pH lab	[-]	7.65	7.31	7.36	7.67
Na	[mg/L]	4'887.5	5'237	5'005.5	4'929
NH_4	[mg/L]	< 10	< 10	< 10	< 10
K	[mg/L]	56.05	57.30	51.65	50.40
Ca	[mg/L]	613.5	790	781	789
Mg	[mg/L]	234	271	244.5	233
Sr	[mg/L]	40.35	44.15	34.65	30.6
Ba	[mg/L]	< 0.5	< 0.25	< 0.25	< 0.25
Si	[mg/L]	#N/A	3.325	4.08	4.67
Al	[mg/L]	< 5	< 2.5	< 2.5	< 2.5
F	[mg/L]	< 1.6	< 1.6	< 1.6	< 1.6
Cl	[mg/L]	7'803	8'353.5	8'028.5	7'651.5
Br	[mg/L]	10.4	10.39	8.58	7.915
NO_3	[mg/L]	33.1	19.25	89.335	50.28
SO_4	[mg/L]	1'475	1'747.5	1'702	2'150.5
I	[mg/L]				
TOC	[mg/L]	138.7	805	141.8	164.1
TIC	[mg/L]	40.15	18.35	49.05	34.1
lactate	[mg/L]	< 20	< 20	< 20	< 20
acetate	[mg/L]	230.5	505.5	305	221.25
propionate	[mg/L]	< 20	< 20	< 20	24.2
formate	[mg/L]	< 20	< 20	< 20	< 20
$\delta^{18}O$	[‰VSMOW]	-4.60	-4.12	-5.81	-6.50
$\delta^{2}H$	[‰VSMOW]	-43.9	-40.7	-46.5	-47.0

Tab. 4.7-15: continued

Parameter	**Unit**	**MAR1-5**	**MAR1-6**	**MAR1-7**	**MAR1-8**
Depth	[m]	708.51	736.79	788.85	996.55
Geol. unit		Staffelegg Fm.	Staffelegg Fm.	Klettgau Fm.	Kaiseraugst Fm.
pH inline	[-]	6.74	7.28	7.52	7.22
pH lab	[-]	6.90	7.25	7.21	7.25
Na	[mg/L]	6'233.5	5'352	6'715	13'500.5
NH_4	[mg/L]	< 10	< 10	< 10	< 10
K	[mg/L]	58.85	52.20	120.00	147.5
Ca	[mg/L]	1389	796	1078	2224.5
Mg	[mg/L]	376.5	197	278.5	380
Sr	[mg/L]	54.7	26.85	19.6	53.2
Ba	[mg/L]	< 0.25	< 0.25	< 0.25	< 0.25
Si	[mg/L]	5.49	4.82	5.12	4.23
Al	[mg/L]	< 2.5	< 2.5	< 2.5	< 2.5
F	[mg/L]	2.38	< 1.6	1.7	2.09
Cl	[mg/L]	6'090.5	3'749.5	7'233	23'519
Br	[mg/L]	6.175	3.565	6.7	6.875
NO_3	[mg/L]	8'744	7'136	3'291.5	326.75
SO_4	[mg/L]	1'900	2'291.5	4'829	3'154.5
I	[mg/L]				
TOC	[mg/L]	756.1	573.9	320.5	202.6
TIC	[mg/L]	60.65	86.1	64.2	39.35
lactate	[mg/L]	< 20	35.8	14.7	< 20
acetate	[mg/L]	28.3	460	< 4.0	105.85
propionate	[mg/L]	< 20	< 20	9.18	< 20
formate	[mg/L]	44.5	49.1	< 4.0	< 20
$\delta^{18}O$	[‰VSMOW]	-7.01	-8.15	-7.67	-9.84
$\delta^{2}H$	[‰VSMOW]	-50.6	-55.0	-50.9	-71.10

Tab. 4.7-16: Saturation state of earliest aliquots from advective displacement experiments

Parameter	**Unit**	**MAR1-1**	**MAR1-2**	**MAR1-3**	**MAR1-4**
Depth	[m]	521.06	576.32	645.48	702.40
Geol. unit		«Parkinsoni-Württembergica-Schichten»	Wedelsandstein Fm.	Opalinus Clay	Opalinus Clay
Charge	[eq]	1.02E-02	1.84E-02	1.18E-02	1.08E-02
%-Error		2.02	3.35	2.23	2.08
Ionic strength	[mol/kgw]	0.28	0.31	0.30	0.30
tot_alk	[eq/kg]	3.37E-03	1.47E-03	3.96E-03	2.87E-03
pH		7.65	7.31	7.36	7.67
log(pCO_2)	[bar]	-2.51	-2.53	-2.15	-2.61
SI(calcite)		0.71	0.11	0.58	0.74
SI(dolomite-o)		1.33	0.09	1.00	1.28
SI(dolomite-d)		0.78	-0.46	0.45	0.73
SI(gypsum)		-0.41	-0.26	-0.27	-0.17
SI(celestite)		0.13	0.20	0.09	0.13
SI(strontianite)		-0.02	-0.69	-0.32	-0.22
SI(anhydrite)		-0.63	-0.48	-0.49	-0.39
Parameter	**Unit**	**MAR1-5**	**MAR1-6**	**MAR1-7**	**MAR1-8**
Depth	[m]	708.51	736.79	788.85	996.55
Geol. unit		Staffelegg Fm.	Staffelegg Fm.	Klettgau Fm.	Kaiseraugst Fm.
Charge	[eq]	1.78E-02	1.57E-02	9.85E-03	-3.16E-03
%-Error		2.51	2.88	1.45	-0.22
Ionic strength	[mol/kgw]	0.41	0.31	0.39	0.80
tot_alk	[eq/kg]	4.47E-03	6.83E-03	5.09E-03	3.28E-03
pH		6.90	7.25	7.21	7.25
log(pCO_2)	[bar]	-1.66	-1.80	-1.90	-2.20
SI(calcite)		0.40	0.70	0.58	0.82
SI(dolomite-o)		0.58	1.13	0.90	1.20
SI(dolomite-d)		0.03	0.58	0.35	0.65
SI(gypsum)		-0.06	-0.15	0.20	0.28
SI(celestite)		0.26	0.10	0.18	0.40
SI(strontianite)		-0.55	-0.32	-0.71	-0.35
SI(anhydrite)		-0.27	-0.37	-0.02	0.08

Nagra PSI 2012 thermodynamic data base, calculated in PHREEQC for 25°C; dolomite-o: ordered dolomite; dolomite-d: disordered dolomite; charge=Σ(cation charge) –|Σ(anion charge)| ;%-error= 100*charge/ (Σ(cation charge) + |Σ(anion charge)|)

4.7.5.6 Initial values and evolution of the composition of stable water isotopes

Common to all eight experiments (Fig. 4.7-15) is a relatively smooth evolution of $\delta^{18}O$ towards the APW value with progress of percolation. Unlike some major chemical components (e.g., chloride), the breakthrough trend starts immediately with the first sample aliquot. In most cases, a relative plateau is visible within the first 0.5 pore volumes, or even a slight increase (not in MAR1-1 and MAR1-8).

The behaviour for $\delta^{2}H$ is distinctly different and shows initially a reverse trend (more negative) that goes through a minimum after percolation of 0.15 – 0.25 pore volumes. The extent of breakthrough is much less compared to $\delta^{18}O$ for reasons that may not be intuitively obvious and are not yet resolved in detail.

One hypothesis is that there is an effect from dry cutting the core surfaces during sample preparation. This may induce evaporation of small amounts of porewater in the close vicinity of the cut surfaces, thus, enriching the residual porewater in heavy isotopes. Percolation would then first yield isotopically heavy signatures, which are then gradually mixed with the unaffected porewater signature, and increasingly also affected by the breakthrough of the traced APW (ca. +100‰ VSMOW for $\delta^{2}H$ and -11.5‰ VSMOW for $\delta^{18}O$). This would explain the observed trends for $\delta^{2}H$. In case of the oxygen isotopes the APW is significantly lighter than the in situ porewater and accordingly, the trend of $\delta^{18}O$ will always decrease as a function of replaced pore volumes (i.e. first by mixing with the non-evaporated and heavier porewater and later with the APW). This could explain the apparent immediate breakthrough behaviour. The suspected evaporation effect on $\delta^{18}O$ would be less compared to $\delta^{2}H$ due to the prevalence of kinetic isotope fractionation during evaporation. In laboratory experiments a slope of a = 4.34 was observed for the relationship $\delta^{2}H = a\ \delta^{18}O - c$ (Cappa et al. 2003). In the $\delta^{2}H$ vs. $\delta^{18}O$ plot (Fig. 4.7-16) the early samples of the experiment, prior to the start of APW breakthrough follow a trend with a similar slope. A more in-depth analysis is attempting to quantify this process. In older studies, wet cutting was used rather than dry cutting, and this led to a small component of contamination by tap water for the early extracted water isotopes (Mäder & Waber 2017). The high concentrations of DOC may also influence the water isotopic system, or any microbial activity, as well as any precipitation of hydrous minerals that may be induced by advective displacement.

The observed differences between $\delta^{18}O$ and $\delta^{2}H$ concerning the extents of breakthrough are discussed below.

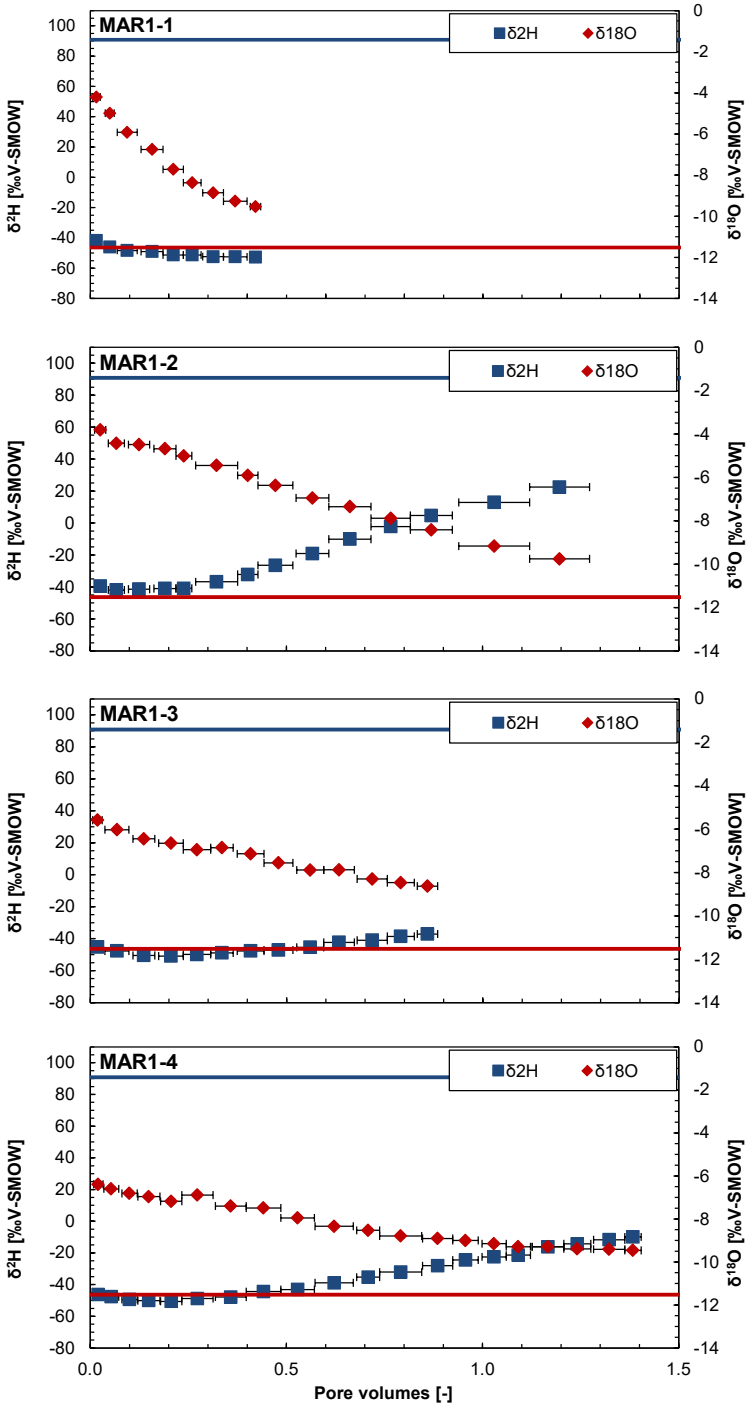

Fig. 4.7-15: Evolution of δ^2H and $\delta^{18}O$ during advective displacement experiments

MAR1-1 = MAR1-1-521.06 («Parkinsoni-Württembergica-Schichten»); MAR1-2 = MAR1-1-576.32 (Wedelsandstein Formation); MAR1-3 = MAR1-1-645.48 (Opalinus Clay); MAR1-4 = MAR1-1-702.40 (Opalinus Clay); MAR1-5 = MAR1-1-708.51 (Staffelegg Formation); MAR1-6 = MAR1-1-736.79 (Staffelegg Formation); MAR1-7 = MAR1-1-788.85 (Klettgau Formation); MAR1-8 = MAR1-1-996.55 (Kaiseraugst Formation). Pore volume fractions relate to transport time based on water content. Experiment duration is 62 – 257 days. Horizontal length of symbol bar covers the sampling interval. Measurement errors are 1.5‰ for δ^2H and 0.1‰ for $\delta^{18}O$.

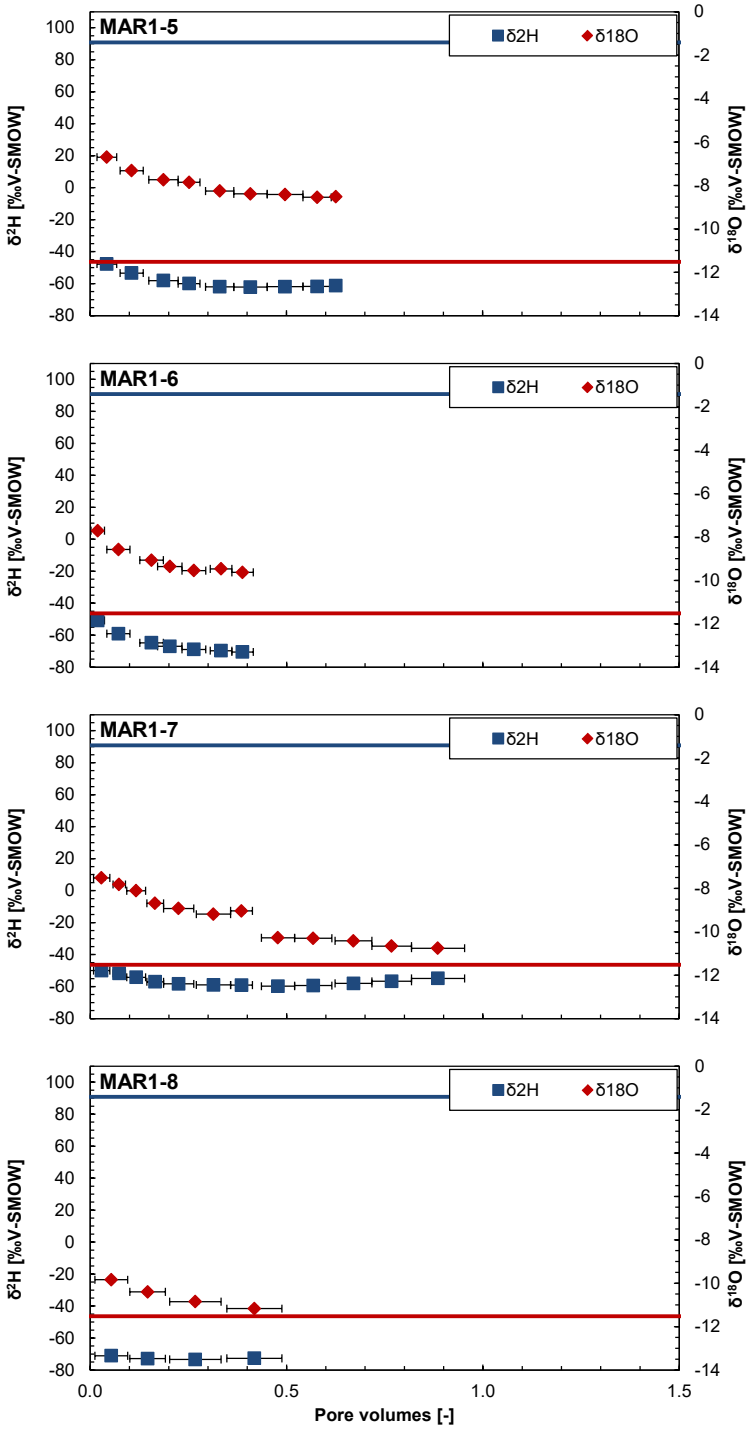

Fig. 4.7-15: continued

The compositions of stable isotopes in $\delta^{18}O$ vs $\delta^{2}H$ coordinates (Fig. 4.7-16) display a slightly curved data array for each experiment extending from the earliest and isotopically light ($\delta^{2}H$) or heaviest ($\delta^{18}O$) extracts towards the APW isotopic composition. Earliest aliquots of experiment (on right side of arrays) define a trend distinctly below the global meteoric water line but plot rather on the GMWL with increasing sample depth. This is compared to other data sources in more details in Chapter 5.

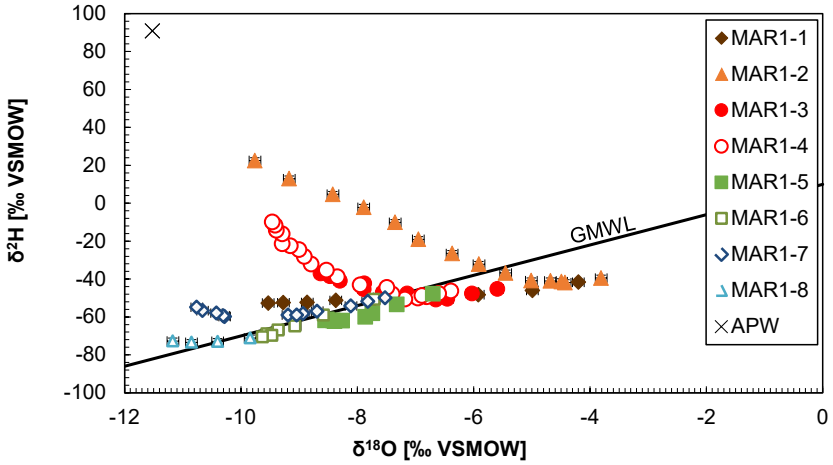

Fig. 4.7-16: Composition stable isotopes of aliquots from advective displacement experiments

MAR1-1 = MAR1-1-521.06 («Parkinsoni-Württembergica-Schichten»); MAR1-2 = MAR1-1-576.32 (Wedelsandstein Formation); MAR1-3 = MAR1-1-645.48 (Opalinus Clay); MAR1-4 = MAR1-1-702.40 (Opalinus Clay); MAR1-5 = MAR1-1-708.51 (Staffelegg Formation); MAR1-6 = MAR1-1-736.79 (Staffelegg Formation); MAR1-7 = MAR1-1-788.85 (Klettgau Formation); MAR1-8 = MAR1-1-996.55 (Kaiseraugst Formation). Measurement errors are 1.5‰ for $\delta^{2}H$ and 0.1‰ for $\delta^{18}O$. GMWL is the global meteoric water line. 1st aliquots are located the furthest to the right, and evolve towards the left.

4.7.6 Derivation of anion-accessible porosity

There are several ways by which chloride- and bromide-accessible porosity fractions may be obtained. The principle is the same: namely the ratio between the anion concentrations obtained from aqueous extracts up-scaled to porewater content divided by that obtained from earliest extracts from the advective displacement experiments (discussions in Waber ed. 2020 and Mäder 2018). There are some variants depending on how water contents were measured and averaged, or how inferred water losses may be corrected. In the case where a full or well-advanced break-through in chloride is captured, such a ratio may also be obtained by post-mortem aqueous extracts (top and base) and the latest aliquots sampled before the end of the experiments (for the outlet / top), or the injected APW (for the inlet / base). Normally, bromide drops below detection and only the chloride data can be evaluated. The bromide data commonly is more 'noisy' due to concentrations that may be quite close to the detection limit (marked in red).

The top two data lines (Tab. 4.7-17) list the average concentrations (Cl, Br) for the first two displaced aliquots as shown in Tab. 4.7-15. The third line lists the concentration of Cl in the last syringe sampled (for post-mortem evaluation). The following three lines list different Cl concentrations up-scaled to water content: for the sample from above the AD core (_upscaled_top), for the sample from below (_upscaled_base) and a corrected and averaged value (top and base).

The correction compensates for a small amount of water loss (unsaturated volume) commonly observed and evaluated from a measured net water uptake. The net water uptake is the measured water uptake (mass gain of the core during the experiment) corrected for a commonly measured volume increase during the experiment (Section 4.7.3 and Tab. 4.7-4). The correction hinges on the assumption that sample treatment for the AD core and the off-cuts share the same history (core handling, storage, sample preparation) and therefore also potentially underwent similar water losses. These corrections are rather small, with small net water uptakes, except for MAR1-8 where a low water content results in a correction of nearly 10% (relative) for chloride. The following three lines contain the same data for Br. The observed range in up-scaled concentrations is an indication of heterogeneity, mainly in the clay-mineral content. A homogeneous sample with respect to the degree of anion exclusion should yield the same up-scaled Cl and Br concentrations, despite differences in the water content. A consistent proportion of anion-accessible porosity would then be evaluated regardless of choosing a sample from the top or from the base as a reference for the early displaced aliquots. The two data lines for Cl suffixed with _p-m are the up-scaled chloride concentrations evaluated post-mortem from aqueous extracts from the top of the core (outlet to sampling) and the base of the core (APW inlet).

The final data block (Tab. 4.7-17) lists the accessible porosity fraction obtained by various combinations and averaging. The first four lines list values that are derived without knowledge of the net water uptake. Marked in italics are the 'best' values for chloride after applying a correction for net water uptake as mentioned above. The data line below is the same for bromide. The last two data lines represent the post-mortem evaluations of the top of the core (outlet) and the base of the core (inlet). There is good agreement and a high degree of consistency among the different ways of evaluation and data derived from pre-characterisation and post-mortem characterisation for chloride, except for MAR1-8. The latter sample has a low water content and thus a large scaling factor for the aqueous extract concentrations that may contribute to a larger uncertainty. The post-mortem evaluation also yields quite a spread (MAR1-8) evaluated for the top and base sections, and the anion-exclusion effect is therefore not well constrained.

In case of MAR1-2, the discrepancy between Cl- and Br-accessible porosity fractions is caused by an exceptionally low Br concentration in the aqueous extract of the top sample, which leads to a low Br-AqEx-upscaled_top. If only the base value is used for the calculation of Br-AqEx_ave_corr / Br-AD_ave, the resulting Br-accessible porosity fraction equals 0.62, very close to the Cl value. The generally higher Br-accessible porosity fractions compared to Cl values in MAR1-5 and cores further below result from very low Br concentrations in the eluting samples (Fig. 4.7-10). These measurements, as well as the corresponding aqueous extract Br concentrations, approach the detection limit of the methods.

The experiments with Opalinus Clay span a range of an accessible porosity fraction for chloride from 0.43 to 0.46, and 0.42 to 0.49 for bromide. This is quite consistent with earlier work from Opalinus Clay and «Brauner Dogger». Chloride-accessible porosity fractions calculated for the two samples with lower clay-mineral contents (29 – 38 wt.-%) from the «Brauner Dogger» are significantly higher, ranging from 0.52 to 0.60 for chloride (but similar for bromide). The two samples from the Staffelegg Formation (33 and 59 wt.-% clay minerals) yield anion-accessible porosity proportions of 0.63 and 0.45, respectively, in proportion to the clay-mineral content, as expected. The sample from the Klettgau Formation with 56 wt.-% clay shows a chloride-accessibility porosity proportion of 0.54.

The accuracy is limited by the basic assumptions underlying the approach and by sample heterogeneity to some degree, mainly in the clay-mineral content. The combined measurement uncertainties are dominated by the analytical error associated with Cl and Br concentrations, but are probably not more than ± 10%, with one clay-poor outlier (MAR1-8).

Tab. 4.7-17: Chloride and bromide-accessible porosity fractions

Parameter	**Unit**	**MAR1-1**	**MAR1-2**	**MAR1-3**	**MAR1-4**
Depth	[m]	521.06	576.32	645.48	702.40
Geol. unit		«Parkinsoni-Württembergica-Sch.»	Wedelsandstein Fm.	Opalinus Clay	Opalinus Clay
Cl-AD_ave (1-2)	[mg/L]	7'803	8'354	8'029	7'652
Br-AD_ave (1-2)	[mg/L]	10.40	10.39	8.58	7.92
Cl_AD_last	[mg/L]	6'216	6'157	6'044	5'669
Cl-AqEx-upscaled_top	[mg/L]	4'186	5'158	3'828	3'382
Cl-AqEx-upscaled_base	[mg/L]	4'251	'5359	3'656	3'319
Cl-AqEx-upscaled_ave_corr	[mg/L]	**4'085**	**4'987**	**3'665**	**3'273**
Br-AqEx-upscaled_top	[mg/L]	5.4	2.7	4.1	3.4
Br-AqEx-upscaled_base	[mg/L]	5.6	6.5	4.5	3.4
Br-AqEx-upscaled_ave_corr	[mg/L]	5.3	4.3	4.2	3.3
Cl-AqEx-upscaled_top_p-m	[mg/L]	3'260	3'997	2'933	2'757
Cl-AqEx-upscaled_base_p-m	[mg/L]	3'499	3'964	2'800	2'704
Cl-AqEx_top / Cl-AD_ave		0.54	0.62	0.48	0.44
Br-AqEx_top / Br-AD_ave		0.52	0.26	0.48	0.43
Cl-AqEx_ave / Cl-AD_ave		0.54	0.63	0.47	0.44
Br-AqEx_ave / Br-AD_ave		0.53	0.44	0.50	**0.43**
Cl-AqEx_ave_corr / Cl-AD_ave		*0.52*	*0.60*	*0.46*	*0.43*
Br-AqEx_ave_corr / Br-AD_ave		0.51	0.42	0.49	0.42
Cl_AqEx_p-m_top / Cl_last_AD		0.52	0.65	0.49	0.49
Cl_AqEx_p-m_base / Cl_APW		0.60	0.68	0.48	0.46

In bold: preferred values; in italics: 'best' values for chloride after applying a correction for net water uptake; empty cells: no sample taken due to limited core size; red values: Br measurement close to detection limit.

Tab. 4.7-17: continued

Parameter	**Unit**	**MAR1-5**	**MAR1-6**	**MAR1-7**	**MAR1-8**
Depth	[m]	708.51	736.79	788.85	996.55
Geol. unit		Staffelegg Fm.	Staffelegg Fm.	Klettgau Fm.	Kaiseraugst Fm.
Cl-AD_ave (1-2)	[mg/L]	6'091	3'750	7'233	23'519
Br-AD_ave (1-2)	[mg/L]	6.18	3.57	6.70	6.88
Cl_AD_last	[mg/L]	5'358	4'258	5'371	15'212
Cl-AqEx-upscaled_top	[mg/L]	3'767	1"761	4069	
Cl-AqEx-upscaled_base	[mg/L]	4'130	1'713		14'692
Cl-AqEx-upscaled_ave_corr	[mg/L]	**3'849**	**1'695**	**3'905**	**13'523**
Br-AqEx-upscaled_top	[mg/L]	4.5	2.3	4.2	
Br-AqEx-upscaled_base	[mg/L]	4.7	2.3		7.3
Br-AqEx-upscaled_ave_corr	[mg/L]	4.5	2.2	4.0	6.8
Cl-AqEx-upscaled_top_p-m	[mg/L]	3'064	1'873	3'262	7'379
Cl-AqEx-upscaled_base_p-m	[mg/L]	3'139	2'460	3'651	4'387
Cl-AqEx_top / Cl-AD_ave		0.62	0.47	0.56	
Br-AqEx_top / Br-AD_ave		0.73	0.65	0.62	
Cl-AqEx_ave / Cl-AD_ave		0.65	0.46	0.56	0.62
Br-AqEx_ave / Br-AD_ave		0.75	0.63	0.62	1.07
Cl-AqEx_ave_corr / Cl-AD_ave		*0.63*	*0.45*	*0.54*	*0.57*
Br-AqEx_ave_corr / Br-AD_ave		0.73	0.61	0.60	0.98
Cl_AqEx_p-m_top / Cl_last_AD		0.57	0.44	0.61	0.49
Cl_AqEx_p-m_base / Cl_APW		0.54	0.42	0.63	0.75

In bold: preferred values; in italics: 'best' values for chloride after applying a correction for net water uptake; empty cells: no sample taken due to limited core size; red values: Br measurement close to detection limit.

4.7.7 Transport properties marked by breakthrough of δ^2H, $\delta^{18}O$, Cl and Br

There are four components that can be used to elucidate on transport properties by their breakthrough behaviour, namely Cl, Br, and the water isotopes δ^2H and $\delta^{18}O$. Chloride is a good tracer in the experiments MAR1-1, MAR1-2, MAR1-3, MAR1-4, MAR1-7, and MAR1-8, because the APW is distinctly less saline than the in situ porewater (negative breakthrough). It is a breakthrough tracer in MAR1-6, the APW being more concentrated than the early sampled aliquots. The resolution towards a full breakthrough is diminished because small differences between large concentrations can no longer be resolved. Bromide is a break-out tracer that is gradually flushed out of the core (no Br in the APW). Again, as a full break-out is approached, bromide concentrations tend to fall below the detection limit. Water tracers also feature a considerable contrast between the in situ porewater (Tab. 4.7-15) and the APW.

For comparison (Fig. 4.7-15) all breakthrough data are normalised to 1 and the breakout of chloride (except MAR1-6 with initial Cl below APW) and bromide is inverted to mimic a breakthrough behaviour. The normalised breakthrough of chloride, for example, is given by $1-(Cl-Cl_{APW})/(Cl_{PW}-Cl_{APW})$, where Cl_{PW} refers to the value of the early aliquots representing the in situ porewater composition (Tab. 4-7.15). Chloride and bromide breakthrough are similar in MAR1-1 to MAR1-4, and MAR1-8. This same behaviour was illustrated in earlier work by Mäder (2018), where a slightly faster breakthrough for Br was observed. MAR1-5 shows an initial Cl concentration above the APW and deceasing rapidly below the APW concentration, and this is not in line with a normal conservative breakthrough behaviour. Here, and in MAR1-6 and MAR1-7, very high nitrate concentrations may disturb a normal breakthrough, and even Cl elution may be somewhat disturbed. The exact processes and their effects are a subject of further clarification but may need a numerical modelling analysis of multicomponent transport. Bromide breakthrough cannot be tracked beyond the percolation progress where it drops below detection (seemingly missing points in Fig. 4.7-17). There is some ambiguity in dealing with data scatter that may be present in the first few syringe compositions (e.g. Br, Cl), and the choice made to define the initial value that is used for normalisation of breakthrough curves. Different choices may shift curves somewhat, but this is a minor effect for these relatively smooth data trends.

Fig. 4.7-18 illustrates the breakthrough behaviour of the Br/Cl molal ratio vs. time (pore volume fraction). Plotting the ratio, removes some of the data scatter of the individual data series and illustrates similarities between the different experiments, and thus also highlights any differences. MAR1-5 is the only experiment that does not plot on a set of nearly parallel curves. This is also the experiment with the largest nitrate elution (production) as illustrated in the lower graph of Fig. 4.7-18, but it is not entirely clear if this is really the cause for the somewhat aberrant trend. The trends of decreasing Br/Cl ratios are mainly caused by the washing out of bromide (no Br in the injected APW) and to a minor extent by the small observed difference of Br transport vs. Cl transport properties (mentioned above).

$\delta^{18}O$ is expected to break through more slowly compared to the anions Br and Cl, and this is observed in Opalinus Clay cores MAR1-3 and MAR1-4. δ^2H displays an anomalous behaviour during the early breakthrough, possibly for reasons discussed in Section 4.7.5. Deuterium lags considerably behind oxygen suggesting some sort of retardation mechanism that is presently not well understood. The two water tracers may interact differently with the accessible porewater volumes and mineral surfaces. This behaviour was also observed with samples from the Schlattingen-1 geothermal well (Mäder & Waber 2017) and also for samples from the BUL1-1 borehole (Mazurek et al. 2021)

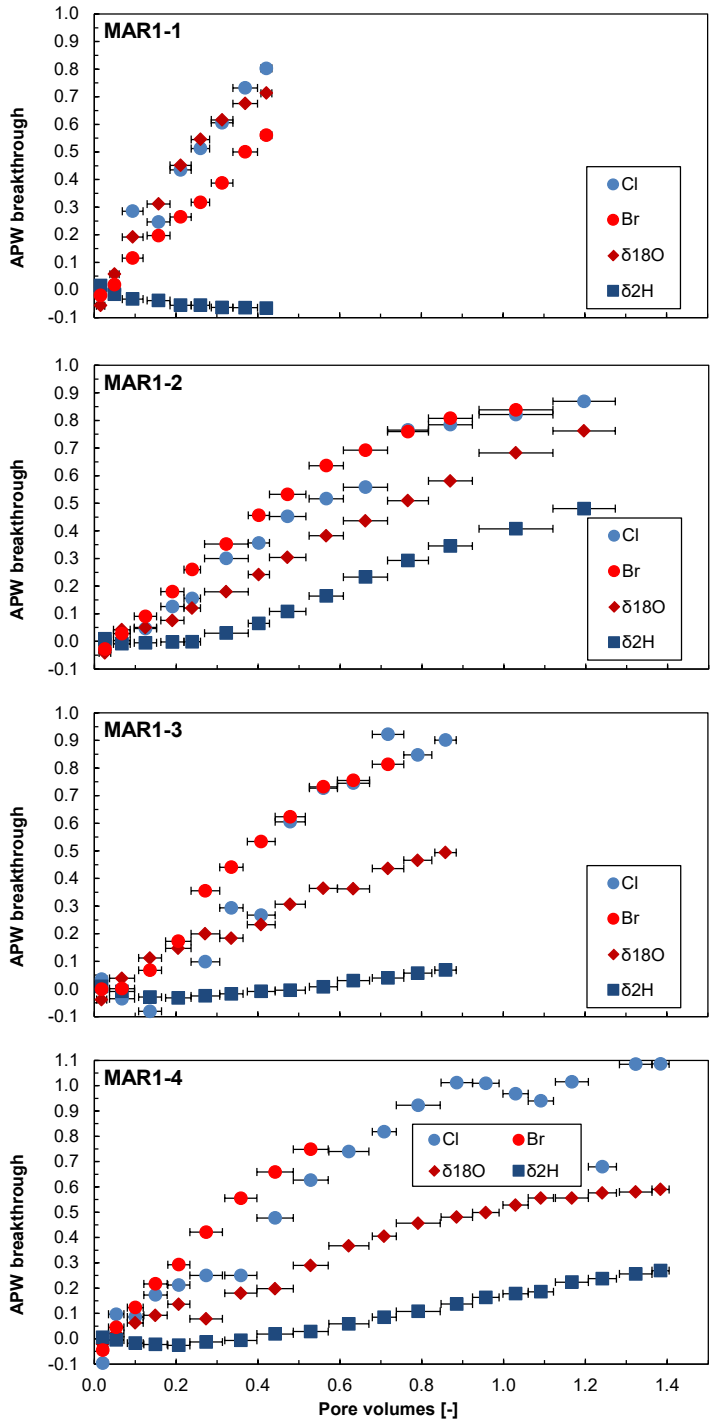

Fig. 4.7-17: Breakthrough of Cl, Br, δ^2H and $\delta^{18}O$ during advective displacement experiments

MAR1-1 = MAR1-1-521.06 («Parkinsoni-Württembergica-Schichten»); MAR1-2 = MAR1-1-576.32 (Wedelsandstein Formation); MAR1-3 = MAR1-1-645.48 (Opalinus Clay); MAR1-4 = MAR1-1-702.40 (Opalinus Clay); MAR1-5 = MAR1-1-708.51 (Staffelegg Formation); MAR1-6 = MAR1-1-736.79 (Staffelegg Formation); MAR1-7 = MAR1-1-788.85 (Klettgau Formation); MAR1-8 = MAR1-1-996.55 (Kaiseraugst Formation). Pore volume fractions relate to transport time based on water content. Experiment duration is 62 – 257 days. Horizontal length of symbol bar covers the sampling interval.

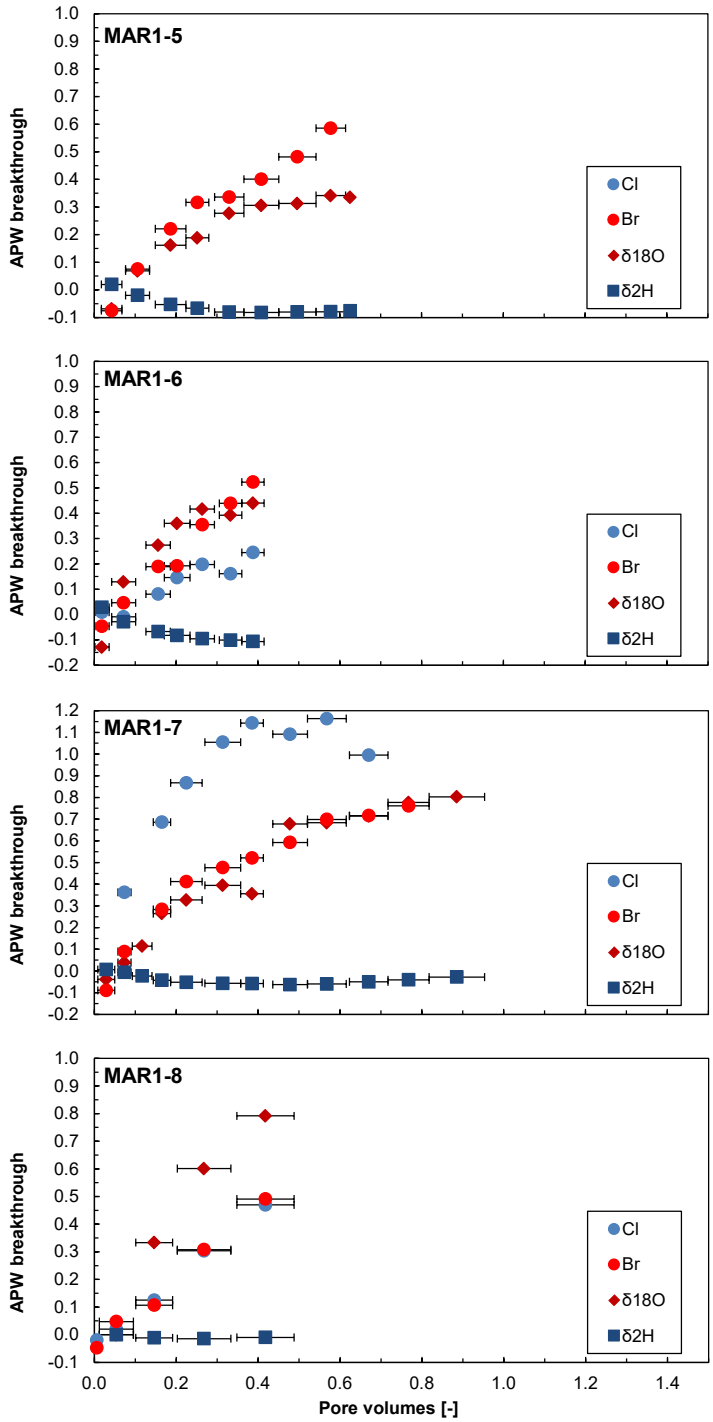

Fig. 4.7-17: continued

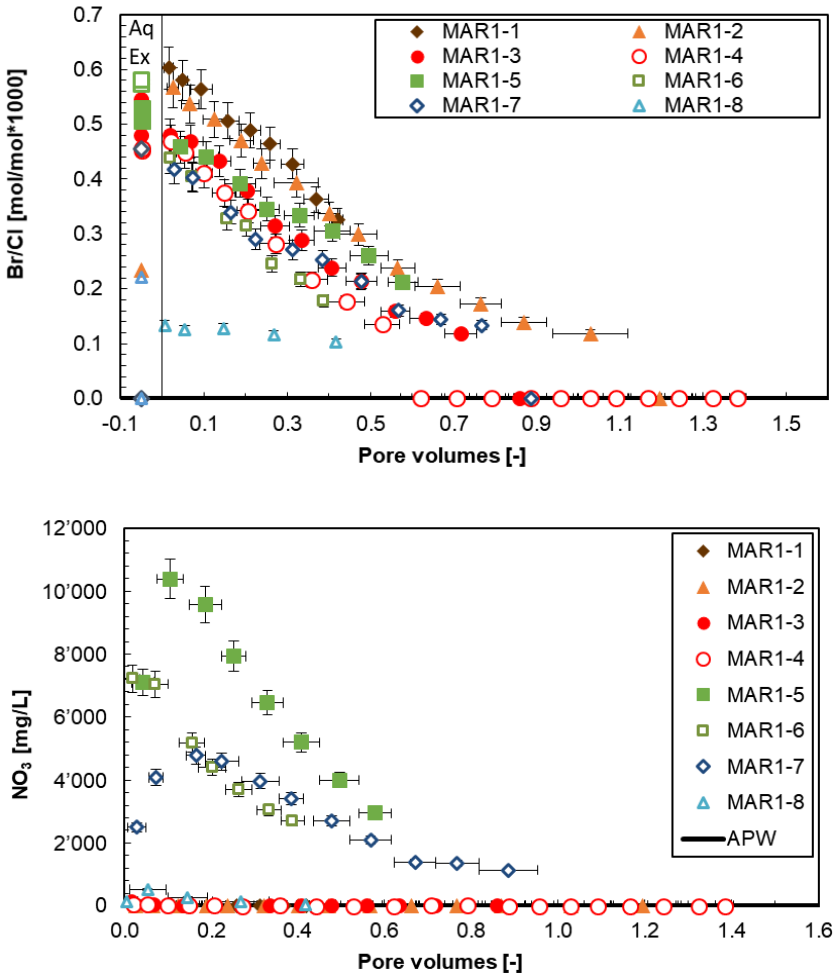

Fig. 4.7-18: Breakthrough of Cl/Br and NO_3 during advective displacement experiments

Data on left side (top graph, 'Aq Ex') are the ratios measured in the aqueous extracts perfomed for pre-characterisation. Ratios plotted at 0 correspond to later aliquots where Br concentration drops below detection. MAR1-1 = MAR1-1-521.06 («Parkinsoni-Württembergica-Schichten»); MAR1-2 = MAR1-1-576.32 (Wedelsandstein Formation); MAR1-3 = MAR1-1-645.48 (Opalinus Clay); MAR1-4 = MAR1-1-702.40 (Opalinus Clay); MAR1-5 = MAR1-1-708.51 (Staffelegg Formation); MAR1-6 = MAR1-1-736.79 (Staffelegg Formation); MAR1-7 = MAR1-1-788.85 (Klettgau Formation); MAR1-8 = MAR1-1-996.55 (Kaiseraugst Formation); APW = artificial porewater. Pore volume fractions relate to transport time based on water content. Horizontal length of symbol bar covers the sampling interval.

4.7.8 Concluding remarks and open issues

Eight successful advective displacement experiments were conducted on samples from the clay-rich Dogger units and lower Liassic, Keuper and Muschelkalk, especially focussing on the derivation of constraints for a representative porewater composition, and with less emphasis on transport properties. Thus, experimental duration was in general shorter than for BUL1-1 (Mazurek et al. 2021). Nevertheless, a systematic and consistent dataset on petrophysical and geochemical properties was obtained not only of value for the specific site characterisation but also for interpretation of porewater chemistry and chloride- / bromide-accessible porosity fractions across all TBO drilling sites.

Advective displacement experiments on samples from the clay-rich confining units supplied a large amount of systematic, consistent and plausible data on petrophysical and geochemical properties of high quality. Samples covered a clay-mineral content of 29 – 67 wt.-%, with similar proportions of (illite/smectite + smectite) compared to total clay minerals, and a derived anion-accessible porosity proportion of 0.43 – 0.63 for chloride and 0.42 – 0.73 bromide. The hydraulic conductivities are similar for all core samples tested, but porosities differ and thus also volumetric fluxes induced by identical head gradients.

Earliest displaced aliquots are representative of the porewater contained in the sample cores, possibly subject to some artefacts, but these aliquots are not equally representative for the in situ porewater due to issues of drilling, unloading, handling and storage. While derived Cl and Br concentrations are robust with respect to such artefacts, the sulphate system in all aliquots appears to be controlled by celestite equilibrium. This either implies that such a control is imposed by these minerals being initially present, or that a disturbance causes to reach such a solubility-product control. In the latter case, the reconstruction of the porewater sulphate concentration is more challenging, and also influences the carbonate system and clay-exchanger complex by ways of interdependent thermodynamic mass-action equilibria.

Like in all earlier work, there are unusually high concentrations of DOC mobilised in the earliest aliquots, decreasing gradually to values more in line with aqueous extracts, but still at significant concentrations. Remarkably, early aliquots of 3 cores from the Staffelegg and Klettgau Formations show large nitrate concentrations (3'300 – 8'700 mg/L, averages of first two aliquots, from Tab. 4.7-15) that gradually decrease at later sampling times, a feature not observed in samples from BUL1-1 and TRU1-1. Corresponding aqueous extracts from post-mortem samples show still increased nitrate not completely flushed out, but not the normal aqueous extracts from pre-characterisation. The origin of this nitrate is likely the kerogenous solid organic matter, but the mechanisms of its mobilisation or liberation are not known. There is relatively little data and experience to compare such findings.

An interesting feature – not yet well understood – is the observed delayed breakthrough of deuterium (δ^2H traced in the APW) compared to δ^{18}O that elutes more regularly as expected for a water tracer. However, compared to observations from more clay rich units in the BUL1-1 borehole (Mazurek et al. 2021), the delay in deuterium breakthrough determined here for the Wedelsandstein Formation is less pronounced.

An initial decreasing trend of deuterium isotopic signatures in early displaced aliquots is suspected to be the result of evaporation from the surface during dry cutting of the core. Alternatively – or in addition – a very early but limited APW breakthrough along a preferential flow path (unsaturated core surface) might lead to an initial increase in deuterium, but also a decrease in δ^{18}O.

There are no fundamental adaptations to the methods prompted by this study. The mechanical, hydraulic and electronic or sensor aspects of the experimental setup reliably performed for the duration of the experiments and even longer. Likewise, the analytical procedures were already optimised and adequate, naturally limited by very small sample volumes for some cases.

The large gas volumes exfiltrating mainly at the beginning of the experiments (Tab. 4-7-2), but in some cases continuing throughout the entire percolation period, cannot be explained by initial dead volumes, initially undersaturated porosity in the core, or He dissolved in the APW at infiltration pressure (45 – 49 bar, hydraulic head) and outgassing due to pressure decrease to 1 bar. During MAR1 and following experiments, selective gas analyses revealed considerable volumes of Ar in the exfiltrating gas, which originates from the core confinement water, where Ar was used in the pressurised headspace. Therefore, a gas-free confining pressure system was installed starting with samples from TBO Stadel. However, both Ar and He in the exfiltrating system do not significantly influence the solution composition.

4.8 Water-isotope data from diffusive-exchange experiments

Lukas Aschwanden & H. Niklaus Waber

The porewater isotope composition ($\delta^{18}O$, $\delta^{2}H$) was derived by isotope diffusive-exchange experiments conducted on core material of 93 samples collected across an interval of 464.9 – 1'053.6 m. The obtained highly resolved profiles for $\delta^{18}O$ and $\delta^{2}H$ cover the lithologies from the «Felsenkalke» + «Massenkalk» of the Malm to the Permian Weitenau Formation.

Isotope diffusive-exchange experiments were conducted in two different laboratories for reasons of quality assurance and optimisation of data production time. The latter became an issue when the first lockdown due to COVID-19 initially posed some uncertainty on efficient sample processing at Uni Bern. Hydroisotop GmbH conducted experiments and analyses on 23 samples between 615.6 and 745.3 m, whereas 37 and 33 samples were investigated by the University of Bern in the intervals of 464.9 – 609.1 m and 754.10 – 1'053.6 m, respectively.

The dataset of Hydroisotop GmbH is provided in their data report in Appendix C. The relevant data produced at the University of Bern are included in the Excel summary sheet (Appendix A).

4.8.1 Data evaluation

4.8.1.1 Experimental and analytical data

Both laboratories followed the experimental and analytical protocol given in Waber (ed.) (2020) and Appendix C (report by Hydroisotop GmbH). The evaluation of the experimental and analytical data underlying the derivation of the composition of stable isotopes of the in situ porewater followed a standardised procedure as detailed below.

In order to qualify for a successful isotope diffusive-exchange experiment the following criteria had to be met (within the propagated analytical uncertainties) by the two conjugate experiments (so-called LAB[7] and NGW or ICE[8] experiments) conducted for one core sample:

- Equal mass of experiment container including rock and test water before and after an experiment (i.e. ± 0.04 g; indicating no severe leakage, otherwise the experiment is considered as failed).
- Equal mass of rock + test water before and after the experiment: Small differences might not be detectable outside the analytical error in the total mass of the set-up, but might indicate minor evaporation of the porewater – test water mixture for which a correction can be applied.
- Evaporation of < 10% of the porewater – test water mixture by leakage of the experiment container: This can reasonably be corrected by applying Rayleigh-distillation calculations to the measured isotope value before calculating the porewater isotope ratio.

---

[7] LAB: Experiments with laboratory tap water used as test water (same terminology for experiments performed at the University of Bern and Hydroisotop GmbH).

[8] NGW and ICE: Experiments using test water depleted in ^{18}O and ^{2}H (melt water of Antarctic ice cores). Different terminology for experiments performed at the University of Bern (NGW) and Hydroisotop GmbH (ICE).

- Reasonable mass ratio of porewater to test water yielding a change in the isotope signal of the test water after equilibration outside the propagated analytical uncertainty. Porewater to test water ratios as low as 0.1 – 0.2 render the calculated isotope composition of the porewater less reliable, whereas at porewater to test water ratios of < 0.1 it becomes unreliable. The mass of porewater in an experiment is defined by the mass of rock and its gravimetric water content. The latter is not known when starting an experiment.
- Limited transfer of test water to rock or vice versa due to excessive salinity difference between test water and porewater.
- Limited transfer of test water to rock because of hydrating mineral phases (e.g. anhydrite, halite).
- Stable isotope analyses of test water solutions within the required accuracy.

Of the 93 investigated samples (or 186 experiments) 9 experiment couples and 4 individual (LAB or NGW/ICE) experiments did not pass these criteria, mainly owing to 1) transfer of porewater to the testwater, 2) porewater to testwater ratios smaller than 0.1 (mainly concerning rocks with low water contents such as some carbonates in the Malm and the Triassic), 3) leakage of the container (i.e. evaporation of the porewater – testwater mixture during the experiments), and 4) a large transfer of testwater to rock for an anhydrite-rich sample from the Zeglingen Formation (i.e. anhydrite hydration; Tab. 4.8-1). Porewater isotope compositions calculated from these experiments are unreliable and will not be shown in the following graphs.

For 6 samples the experimental data resulted in an elevated uncertainty of the calculated isotope composition of the in situ porewater. Three of these experiment couples show minor evaporation of the porewater – test water mixture (corrected by Rayleigh-distillation calculations), the remaining three samples show low porewater to test water ratios of 0.1 – 0.2 (Tab. 4.8-1). Porewater isotope compositions calculated from these experiments are afflicted by somewhat larger uncertainties. These data are shown but marked with black circles in the following graphs.

4.8.1.2 Calculation of porewater composition

Porewater $\delta^{18}O$ and $\delta^{2}H$ values were calculated using equation 76 in Appendix A in Waber (ed.) (2020) considering the ratio *q* of the gravimetric water contents of the individual subsamples used in the experiments (for details see Appendix A in Waber ed. 2020). The robustness of the calculated porewater $\delta^{18}O$ and $\delta^{2}H$ values is further tested according to the following criteria:

1. A relative difference of less than 20% between the water contents calculated from $\delta^{18}O$ and $\delta^{2}H$ data derived from the experiments with test water depleted in ^{18}O and ^{2}H (NGW/ICE subsamples).
2. A relative difference of less than 20% between the average water content calculated by isotope mass balance from $\delta^{18}O$ and $\delta^{2}H$ data and the average of the gravimetric water content of the two subsamples used in the experiments.

If the relative difference in the different water contents is larger than 20% the calculated porewater $\delta^{18}O$ and $\delta^{2}H$ values are considered less reliable. Such data may still be used for further interpretation by accepting the larger propagated uncertainty (Tab. 4.8-1); they are marked with black circles in the following graphs.

Of the 80 samples that passed the experimental quality criteria (*cf.* Section 4.8.1.1; including samples with elevated experimental uncertainties) 2 samples do not pass criterion 1 above (Fig. 4.8-1), 6 samples do not pass criterion 2 (Fig. 4.8-2) and 2 samples fail both criteria. Five of the samples that fail the comparison of the water contents are afflicted by larger uncertainties

from the experiments themselves, i.e. minor evaporation of the porewater – test water mixture or low porewater-to-test water ratios (i.e. 0.1 – 0.2). In these cases, the failure of criterion 1 and/or criterion 2 is due to experimental artefacts. The other 5 samples that fail the comparison of the water contents do not show any experimental irregularities. In these cases, the reason for the difference between the water contents calculated from $\delta^{18}O$ and $\delta^{2}H$ data is likely due to interactions between test water and rock mineralogy, which are not quantifiable at the current state of knowledge. In turn, the differences between the average of the water contents derived by isotope mass balance and the average of the gravimetric water content of the two subsamples likely reflect lithological heterogeneity of the different subsamples used in the two experiments. Note that in anhydrite-bearing lithologies hydration of anhydrite during the isotope diffusive-exchange experiments also plays a role, although its effect is unknown at this stage.

All samples that pass the above criterion 2 display a consistent, previously observed relationship between the average water content derived by isotope mass balance and the average of the gravimetric water content of the subsamples used in the experiments, the former being around 10% larger than the latter (Fig. 4.8-2). As the water content is generally well correlated with the clay-mineral content of the rocks (*cf.* Chapter 4.3), it was postulated that this difference might be associated with minor exchange with water of different isotope composition adsorbed on clay minerals (e.g. Pearson et al. 2003).

Contamination of some samples by drilling fluid – even in the central parts of the core material – was identified on the basis of aqueous extract solutions (*cf.* Section 4.4). This mainly concerns clay-poor samples from the Muschelkalk, as well as two samples from the Bänkerjoch Formation. The isotope data of these samples are marked with a grey circle in the following plots. The reliability of such data is further discussed in Section 5.8.

Tab. 4.8-1: Summary of samples which do not fulfil the quality criteria of the isotope diffusive-exchange experiments of MAR1-1

Porewater isotope compositions calculated from these experiments are unreliable and are not shown in graphs (m_{pw}: mass porewater, m_{tw}: mass test water). All samples analysed at University of Bern.

Sample ID	**Formation**	**Leakage of container**	**Transfer of porewater to test water**	**Transfer of testwater to rock**	**Ratio m_{pw}/m_{tw}**
MAR1-1-609.06-RP	Opalinus Clay	×			> 0.2
MAR1-1-771.18-PW	Klettgau Fm.		×		> 0.2
MAR1-1-782.61-PW	Klettgau Fm.	×			> 0.2
MAR1-1-852.75-PW	Bänkerjoch Fm.				< 0.1
MAR1-1-885.59-PW	Schinznach Fm.		×		> 0.2
MAR1-1-908.68-PW	Schinznach Fm.		×		0.1 – 0.2
MAR1-1-918.04-PW	Schinznach Fm.		×		> 0.2
MAR1-1-922.60-PW	Schinznach Fm.				< 0.1
MAR1-1-963.33-PW	Zeglingen Fm.				< 0.1
MAR1-1-972.31-PW	Zeglingen Fm.			×	0.1 – 0.2
MAR1-1-981.01-PW	Zeglingen Fm.				< 0.1
MAR1-1-988.60-PW	Zeglingen Fm.				< 0.1
MAR1-1-1053.55-PW	Weitenau Fm.		×		> 0.2

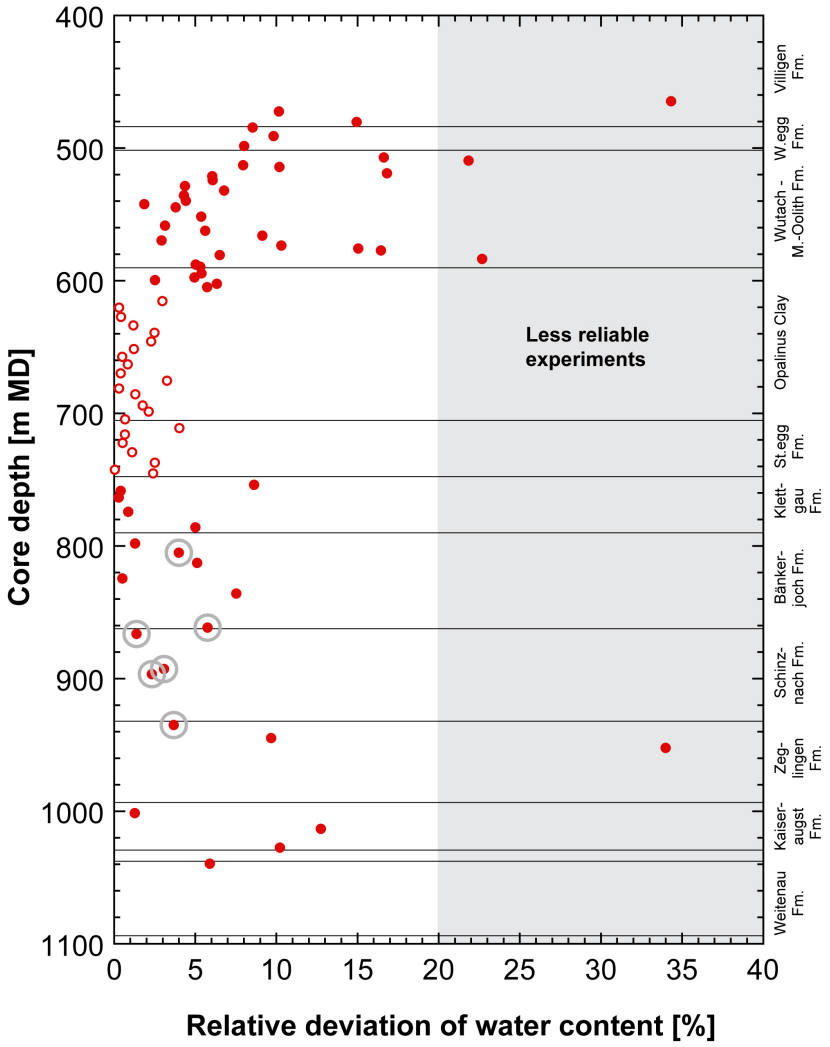

Fig. 4.8-1: Relative deviation of water contents obtained from $\delta^{18}O$ and $\delta^{2}H$ mass balance

The relative deviation is defined as the difference between the water contents calculated from the equilibrated $\delta^{18}O$ and $\delta^{2}H$ values, respectively, of the experiments with testwater depleted in ^{18}O and ^{2}H (NGW or ICE, respectively) divided by the water content based on $\delta^{2}H$. Grey area: Relative deviation of water contents obtained from $\delta 1^{8}O$ and $\delta^{2}H$ mass balance is > 20%. For samples within this area the calculated porewater $\delta^{18}O$ and $\delta^{2}H$ values are considered less reliable. Samples with grey circles show some signs of contamination by drilling fluid (*cf.* Section 4.4).

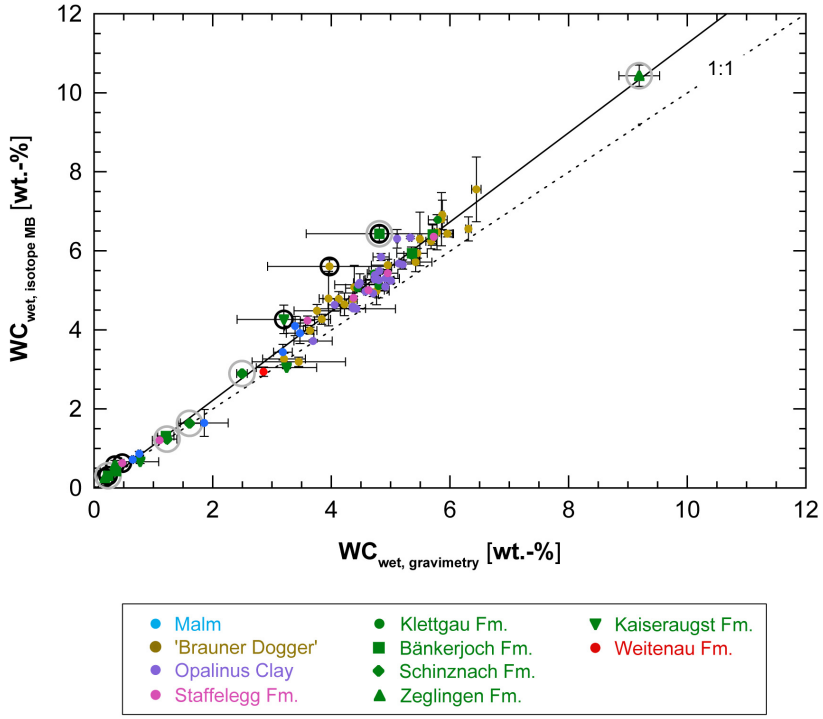

Fig. 4.8-2: Average water content obtained by water-loss at 105 °C ($WC_{wet,\ gravimetry}$) of subsamples LAB and NGW/ICE vs. average water content calculated from $\delta^{18}O$ and $\delta^{2}H$ mass balance from NGW/ICE diffusive-exchange experiments ($WC_{wet,\ isotope\ MB}$)

Samples with black circles show differences larger than 20% between the average water content derived by isotope mass balance and the average gravimetric water content of the two subsamples used in the experiment. Samples with grey circles show signs of contamination by drilling fluid (*cf.* Section 4.4).

4.8.2 $\delta^{18}O$ and $\delta^{2}H$ values of porewater

4.8.2.1 Data comparison University of Bern – Hydroisotop GmbH

All the porewater isotope data that pass the various quality criteria are illustrated in Fig. 4.8-3 as a function of depth. It can be observed that the general trend of porewater $\delta^{18}O$ and $\delta^{2}H$ values produced at Hydroisotop GmbH perfectly links the isotope trends of University of Bern.

4.8.2.2 Depth profiles of porewater isotope composition

Both $\delta^{18}O$ and $\delta^{2}H$ values of the porewater show well defined, curved profiles across the investigated depth interval (Fig. 4.8-3). Although both tracers indicate the same general trends, minor differences exist. $\delta^{18}O$ values of the porewater remain constant (at around -3.7‰ VSMOW) across the lower parts of the Villigen Formation down to the «Humphriesioolith Formation». From there the $\delta^{18}O$ values of the porewater increasingly become more negative across the lower parts of the «Brauner Dogger», the Opalinus Clay and the Staffelegg Formation approaching a local minimum of -8.0‰ VSMOW at around 763 m in the Klettgau Formation. In contrast, $\delta^{2}H$ values of the porewater remain remarkably constant across the lower parts of the Villigen Formation down to the base of the Opalinus Clay (at around -40‰ VSMOW) where they start to decrease towards the same local minimum as is indicated by $\delta^{18}O$ values in the Klettgau Formation ($\delta^{2}H$ at around -53‰ VSMOW). The different shapes of the $\delta^{18}O$ and $\delta^{2}H$ profiles are also illustrated in Fig. 4.8-4, which shows the depth profile of deuterium excess (defined as $\delta^{2}H - 8 \times \delta^{18}O$; deuterium excess is +10‰ for a sample that lies on the GMWL, lower values of deuterium excess reflect sample positions to the right of the GMWL in a plot of $\delta^{18}O$ vs. $\delta^{2}H$; note that the deuterium excess as used at this stage carries no genetic implications about the origin of H_2O, e.g. on palaeo-climate at the time of infiltration). Deuterium excess shows constant values of around -10‰ across the lower parts of the Villigen Formation down to the «Humphriesioolith Formation» from where it steadily increases across the lower parts of the «Brauner Dogger», the Opalinus Clay and the Staffelegg Formation approaching a general maximum of +10.0‰ at around 763 m in the Klettgau Formation.

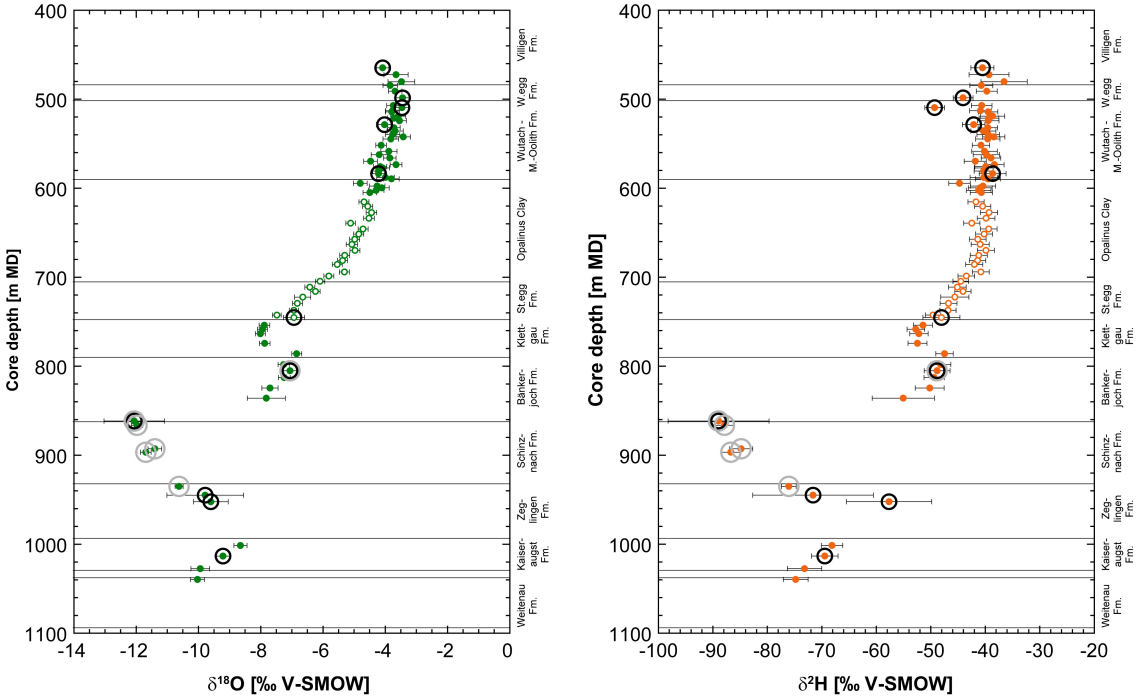

Fig. 4.8-3: Depth distribution of accepted porewater $\delta^{18}O$ and $\delta^{2}H$ values obtained from isotope diffusive-exchange experiments

Closed symbols: samples investigated at University of Bern; open symbols: samples investigated at Hydrosisotop GmbH; samples in circles are less reliable owing to experimental artefacts (black circles; see text) and/or possible contamination by drilling fluid (grey circles; *cf.* Section 4.4).

From the local minimum in the Klettgau Formation both $\delta^{18}O$ and $\delta^{2}H$ values of the porewater first increase towards local maxima near the top of the Bänkerjoch Formation (reaching values of -6.9 and -47.5‰ VSMOW, respectively) and then steadily decrease towards its base before sharply dropping to a general minimum in the water-conducting zone at the top of the Schinznach Formation at around 872 m ($\delta^{18}O$ and $\delta^{2}H$ values around -12.1 and -89.1‰ VSMOW, respectively). Isotope profiles in the underlying Muschelkalk, Buntsandstein and 'Rotliegendes' (Weitenau Formation) are less well defined, mainly owing to the comparatively larger sample spacing and experimental difficulties associated with these samples (e.g. hydration of anhydrite, low water contents; *cf.* Section 4.8.1). Nevertheless, the general trends show an increase in $\delta^{18}O$ and $\delta^{2}H$ values of the porewater across the Schinznach Formation into the Zeglingen Formation where a trend reversal is indicated. From there, both $\delta^{18}O$ and $\delta^{2}H$ decrease to values as low as -10.1 and -88.6‰ VSMOW, respectively at the top of the Weitenau Formation. Deuterium excess slightly decreases from its maximum of around 10.0‰ in the Klettgau Formation to values of around 4.5‰ at the base of the profile, with a likely outlier marked as a less reliable datum.

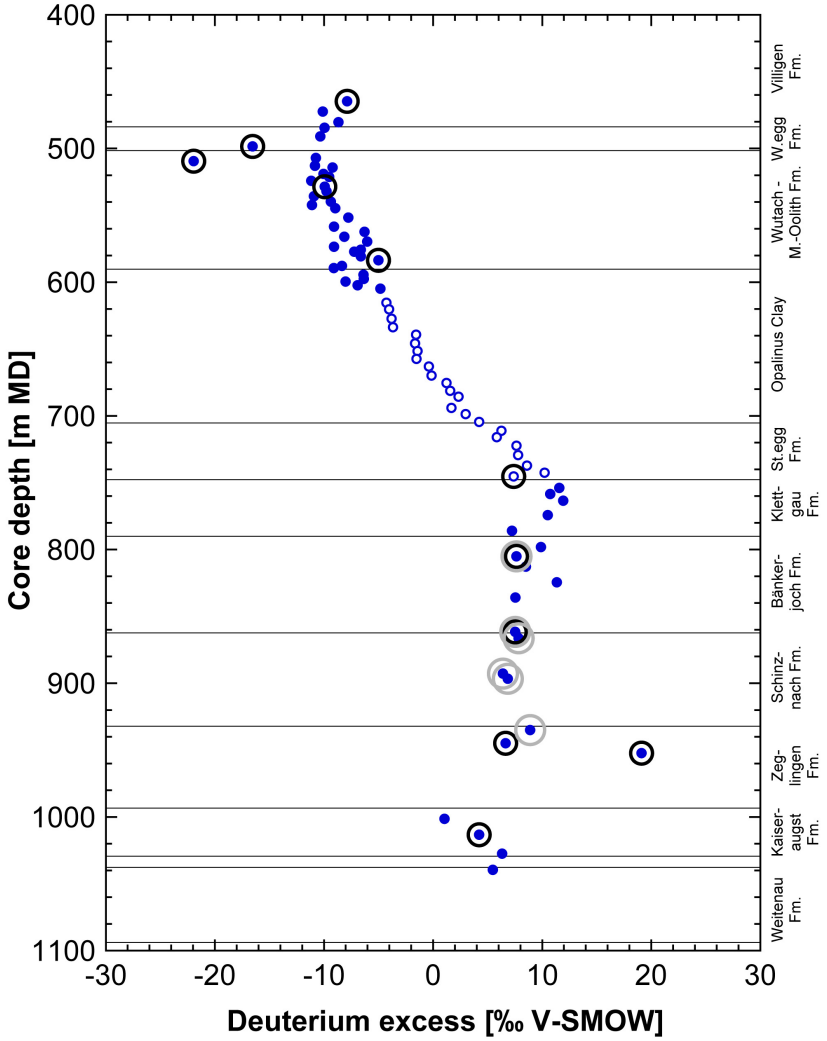

Fig. 4.8-4: Depth trend of deuterium excess in porewater based on the isotope diffusive exchange technique

Deuterium excess is +10‰ for a sample that lies on the GMWL. Lower values of deuterium excess reflect sample positions to the right of the GMWL in a plot of $\delta^{18}O$ vs. $\delta^{2}H$. Note that the deuterium excess as used at this stage carries no genetic implications about the origin of H_2O, e.g. on palaeoclimate at the time of infiltration. Closed symbols: samples investigated at the University of Bern; open symbols: samples investigated at Hydroisotop GmbH; samples in circles are less reliable owing to experimental artefacts (black circles; see text) and/or possible contamination by drilling fluid (grey circles; *cf.* Section 4.4).

In the $\delta^{18}O$-$\delta^{2}H$-diagramm (Fig. 4.8-5) some remarkably regular and linear trends can be observed. From the Malm to the Staffelegg Formation the porewater isotope composition evolves from $\delta^{18}O$ and $\delta^{2}H$ values that fall to the right of the Global Meteoric Water Line (GMWL) towards values that plot on the GMWL, the latter values indicating a dominant meteoric component in the latter porewaters. Similarly, the isotope compositions of the porewater in the Klettgau Formation and the Bänkerjoch Formation have a meteoric signature. At the base of the Bänkerjoch Formation, porewater $\delta^{18}O$ and $\delta^{2}H$ values sharply evolve to more negative values in the water-conducting zone of the Schinznach Formation (see Chapter 5.8 for further discussion), but still plotting on the GMWL. Porewaters in the underlying Zeglingen (one outlier) and Kaiseraugst Formation again show less negative isotope signatures plotting close to or (neglecting the single outlier) slightly to the right of the GMWL.

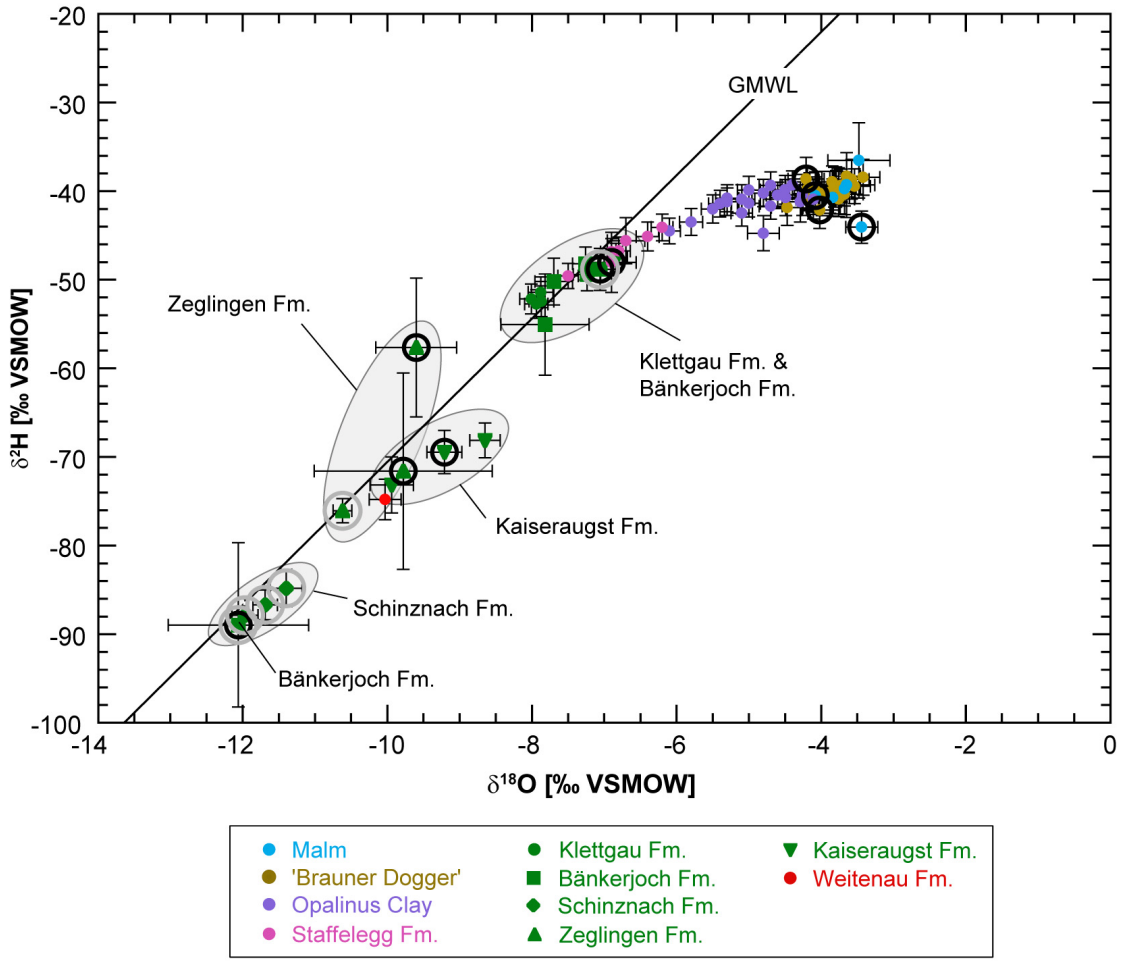

Fig. 4.8-5: $\delta^{18}O$ vs. $\delta^{2}H$ values of porewater obtained from isotope diffusive-exchange experiments

GMWL = Global Meteoric Water Line ($\delta^{2}H = 8 \times \delta^{18}O + 10$‰ VSMOW), samples in circles are less reliable owing to experimental artefacts (black circles; see text) and/or possible contamination by drilling fluid (grey circles; *cf.* Section 4.4).

5 Discussion of porewater data

5.1 Chloride data and estimation of chloride- and bromide-accessible porosity

Paul Wersin & Martin Mazurek

Chloride, a major compound in the porewater, has been determined by squeezing (Section 4.6), advective displacement (Section 4.7) and aqueous extraction (Section 4.4). This anion is considered to behave as a conservative species with no or very limited interaction with the minerals. The same can be said for bromide, which occurs at much lower concentrations in the porewater. In argillaceous rocks, anions are repelled from the negative structural charge of the clay-mineral surfaces and are thus affected by ion exclusion. In other words, they only 'see' part of the total water-filled porosity, the fraction of which is often termed anion-accessible porosity (Pearson et al. 2003). Ion exclusion is not complete according to theory and depends on distance from charged surfaces, but here this simplifying assumption is made for adopting a simplest possible model.

Knowing the concentration of Cl and/or Br in a sample from aqueous extraction ($C_{Cl\ in\ bulk\ porewater}$), the Cl-accessible porosity fraction, f_{Cl}, can be estimated from Cl and/or Br measurements in squeezing ($C_{Cl\ in\ squeezed\ water}$) or advective displacement ($C_{Cl\ in\ adv.\ displaced\ water}$) experiments:

$$f_{Cl} = \frac{n_{anion-accessible}}{n_{total}} = \frac{C_{Cl\ in\ bulk\ pore\ water}}{C_{Cl\ in\ squeezed\ or\ adv.displaced\ water}}$$

$C_{Cl\ in\ bulk\ porewater}$ is calculated from

$$C_{Cl\ in\ bulk\ pore\ water} = \frac{C_{Cl\ in\ aq.extract}}{WC_{dry}\ {}^{S}/_{L}}$$

with C = concentration [mg/L], n = porosity [–], WC_{dry} = water content relative to dry rock mass [g/g], S/L = solid/liquid ratio of aqueous extraction experiment [g/g]. The Br-accessible porosities are derived in an analogous fashion.

The anion-accessible porosities have been derived according to the above equation for squeezed and advectively displaced porewaters (Tabs. 4.6-7 and 4.7-14). In the case of the squeezed waters it is assumed that the waters squeezed at the lowest pressure reflect the in situ porewater (Mazurek et al. 2015, Wersin et al. 2016). For the advectively displaced waters, the first two aliquots are assumed to be the most representative of the in situ porewater (Section 4.7).

The derived values of the Cl-accessible porosity fraction (f_{Cl}) for the two datasets are shown as a function of the clay-mineral content in Fig. 5.1-1 (left). Consistent porosity fractions are obtained from the two different methods, yielding values of 0.42 – 0.55 (48 – 84 wt.-% clay) for squeezing samples, and 0.43 – 0.63 (29 – 67 wt.-% clay) for advective displacement samples. Most samples display high clay-mineral contents of > 40 wt.-%. Sampling for squeezing focussed on the more clay-rich lithologies for better squeezability, whereas this is not a limiting factor for advective displacement. Three AD-samples with a clay content of ~ 30 wt.-% (Wedelsanstein Formation 576.32 m, Staffelegg Formation 708.51 m, Kaiseraugst Formation 996.55 m) show higher f_{Cl} values of ~ 0.6. This supports the general trend of increasing anion-accessibility with

decreasing clay-mineral content observed in the TRU1-1 borehole. In that borehole, additional f_{Cl} data from through-diffusion experiments (Van Loon & Glaus *in prep.*) are available. Due to the proximity of the TRU1-1 borehole and the similar geological setting, these diffusion data together with squeezing and advective displacement data are illustrated in Fig. 5.1-1 (right) for comparison. This comparison underlines the consistency of the MAR1-1 and TRU1-1 AD and SQ data on the one hand and the similarity of these data with through-diffusion data (DI) from TRU1-1 on the other. The mean f_{Cl} value for clay-mineral contents > 40 wt.-% derived for the AD and SQ datasets from MAR1-1 is 0.483 ± 0.0546 (1σ). Taking the ensemble of MAR1-1 and TRU1-1 data (AD, SQ, DI), the mean f_{Cl} value for clay-mineral contents > 40 wt.-% is 0.461 ± 0.082. These values are somewhat lower than the corresponding mean f_{Cl} values that were derived for the Schlattingen-1 borehole (0.52 ± 0.05; Wersin et al. 2016) or the BUL1-1 borehole (0.52 ± 0.06; Mazurek et al. 2021) but very similar to the TRU1-1 borehole (0.45 ± 0.06).

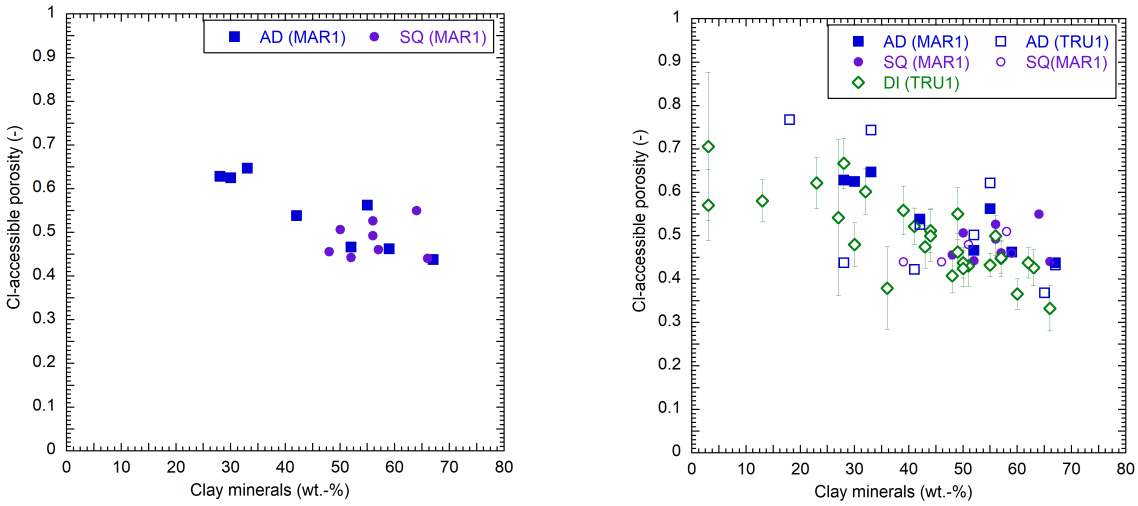

Fig. 5.1-1: Cl-accessible porosity fraction as a function of the clay-mineral content

Error bars on diffusion data indicate propagated analytical errors. Left: data from MAR1-1 only; right: dta from MAR1-1 and TRU1-1.

Within the interval between the Malm and Keuper aquifers, the lithologies in the MAR1-1 profile vary substantially. In order to derive a porewater profile for Cl, the anion accessibility in these lithologies must be known or assumed. On the basis of the f_{Cl} -clay-mineral content trend, a f_{Cl} value of 0.46 is used for clay-mineral contents ≥ 40 wt.-%.

Below a clay content of 40 wt.-%, an increasing trend of fCl with decreasing clay-mineral content is noted. This trend is expressed by the AD and SQ data which suggest a linear correlation between these two variables (Fig. 5.1-1) but is constrained only to clay-mineral contents of 30 wt.-% (MAR1-1) or 20 wt.-% (TRU1-1). The diffusion data from TRU1-1, however, display more scatter and do not appear to be entirely consistent with the trend suggested by the AD and SQ data, especially at very low clay-mineral contents. It should be noted that in this region only three samples with clay-mineral contents < 20 wt.-% (two from the Malm unit and one from the Wedelsandstein Formation) were measured by the through-diffusion method, suggesting rather low f_{Cl} values compared to the trend outlined above. The reason for the scatter of the DI data and apparent discrepancy with the available AD and SQ data at lower clay-mineral contents is not clear. At this stage, the limited amount of measurements and their inherent experimental uncertainty do not enable to draw a firm conclusion in this regard. Being aware of this uncertainty, a linear increase

towards 1.0 is assumed to derive the Cl concentrations from aqueous extracts for the range from 40 to 0 wt.-% clay-mineral content, which is based on the extrapolated trend suggested by the AD und SQ data. The same procedure was adopted for the TRU1-1 borehole (Aschwanden et al. 2021). In addition, an alternative Cl profile based on formation-specific trends is tested (see below).

An uncertainty range of ±20% is considered for f_{Cl}, which is probably sufficient for clay-rich lithologies but may still be an underestimation for clay-poor rocks. This uncertainty propagates into the calculated Cl concentrations in the anion-accessible porewater, i.e., an error of ±20% must be considered in addition to the propagated analytical error. The fact that f_{Cl} shows such a wide range when plotted against the clay-mineral content suggests that the latter is not the only parameter that determines anion accessibility. Correlations with individual clay minerals (e.g. illite or smectite end-members) are not better than those with the total clay-mineral content. Mean grain size, grain-size distribution, fabric and other factors are expected to affect anion accessibility as well. Furthermore, according to theory, anion accessibility also varies with the salinity and composition of the porewater, i.e., it is not just a material property. All these partly interdependent effects cannot be properly quantified at this stage, which severely limits the application of theoretical models.

There is a difference between data obtained from squeezing and from advective displacement. The Cl concentrations obtained from squeezing are systematically lower than those from advective displacement, by 15 – 20% (best seen in the Opalinus Clay section where gradients are small). Despite this, the anion-exclusion effect is derived to be the same, in both cases related to the bulk concentration, derived either from aqueous extracts (AD) or from the reconstructed inventory of all squeezed aliquots and the residual chloride (SQ). With the anion-exclusion effect adopted as detailed above, the chloride concentrations in depth profiles (Section 5.2) recalculated to porewater content and including the anion-exclusion effect yield average concentrations that are 15 – 20% more concentrated than the aliquots squeezed at lowest pressures. This issue is presently not resolved and is further discussed in Section 5.9.2.

For Br, only advective displacement data are available. The derived f_{Br} values as a function of the clay-mineral content are illustrated in Fig. 5.1-2. These exhibit a larger scatter than the corresponding f_{Cl} values, in particular at a lower clay-mineral content. The mean f_{Br} value at a clay-mineral content > 40 wt.-% is 0.52 ± 0.08. The reason for the large scatter in f_{Br} data is probably related to larger analytical errors (concentrations are frequently close to detection limit in aqueous extracts). Note in this context that the sample from Kaiseraugst Formation displays a rather large f_{Br} value of 0.98, thought to be not realistic. The values obtained for Opalinus Clay are better constrained and consistent with Cl-data, with fractions of 0.49 and 0.43.

Fig. 5.1-3 illustrates the Cl-accessible porosity fraction as a function of depth for the MAR1-1 data (left) and the combined MAR1-1/TRU1-1 data (right). The upper confining unit, the «Brauner Dogger», exhibits large variations in f_{Cl} values, which is likely due to the large mineralogical and textural heterogeneity within this unit. The f_{Cl} values for the Opalinus Clay show constant values (mean value 0.449 ± 0.012 considering AD/SQ of MAR1-1 and 0.436 ± 0.038 considering all MAR1-1 and TRU1-1 data) with no clear depth trend. In the underlying Staffelegg Formation the f_{Cl} data suggest a jump in the uppermost sample, followed by a sharply decreasing trend with depth, remarkably similar to what was observed for TRU1-1 and BUL1-1. In parallel, the clay-mineral content of the samples from this formation shows a tendency to increase with depth (see Section 4.2). This may suggest the influence of clay mineral charge on the anion-accessible porosity. On the other hand, the porewater chloride concentrations and salinity (see next Section) also show a strong decrease with depth in the Staffelegg Formation, which may affect the anion-accessible porosity as indicated from through-diffusion experiments

(Wigger & Van Loon 2017). Those results showed that the Cl-accessible porosity fraction increased from 0.35 to 0.6 when increasing the ionic strength from 0.1 to 1 molal.

Data suggest that the spread and uncertainty in the anion-exclusion effect is smaller for Opalinus Clay than for the other units. Consistent f_{Cl} values of ~ 0.44 between the MAR1-1 and TRU1-1 boreholes with a spread of about 10% and no effect of depth have been obtained for the Opalinus Clay. The average value derived from all samples with a clay-mineral content ≥ 40 wt.-% is 0.46. This is very close to the average values obtained for the Opalinus Clay samples.

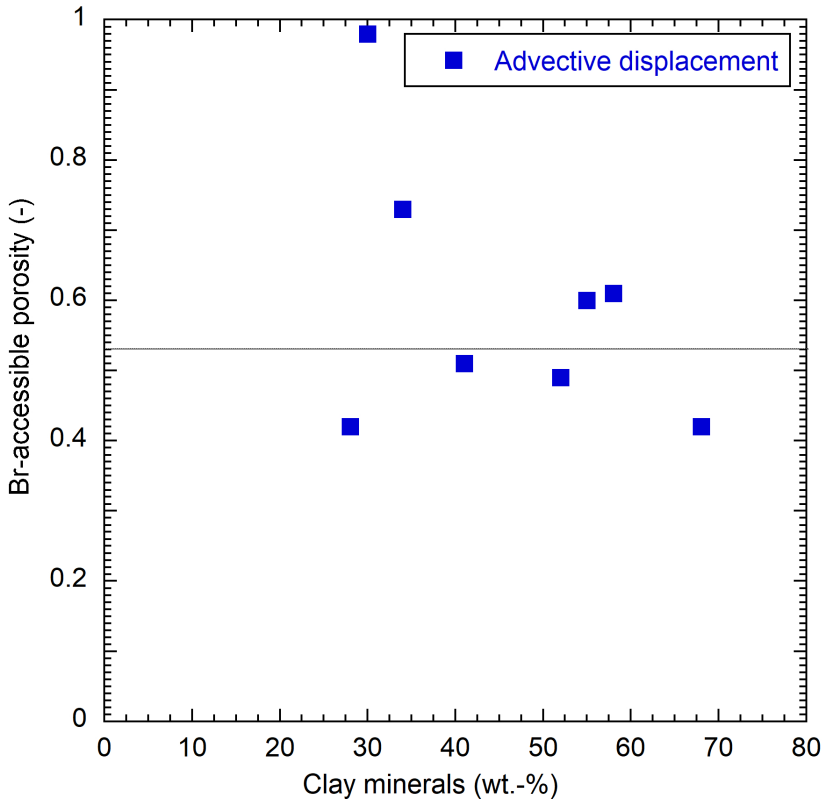

Fig. 5.1-2: Br-accessible porosity fraction as a function of the clay-mineral content

Line: average f_{Br} value for a clay-mineral content > 40 wt.-%.

It appears that the locations in the lower «Brauner Dogger» (e.g. Wedelsandstein Formation) and near the top of the Staffelegg Formation (e.g. Rietheim Member = 'Posidonienschiefer' and overlying unit) are locations that repeatedly display large variations in chloride-accessible porosity fractions, well outlined in the diffusion tests from TRU1-1 (Fig. 5.1-3) and one AD experiment for the Wedelsandstein Formation, and similarly for the top of the Staffelegg Formation. These excursions appear to reflect variations in the accessible porosity rather than in porewater chloride concentration. Contrary to the Opalinus Clay, the underlying Staffelegg Formation displays a clear trend of decreasing f_{Cl} values with depth, also seen in the BUL1-1 borehole. A more detailed evaluation of the variability of f_{Cl} follows in the next Section (see also Fig. 5.2-2b right).

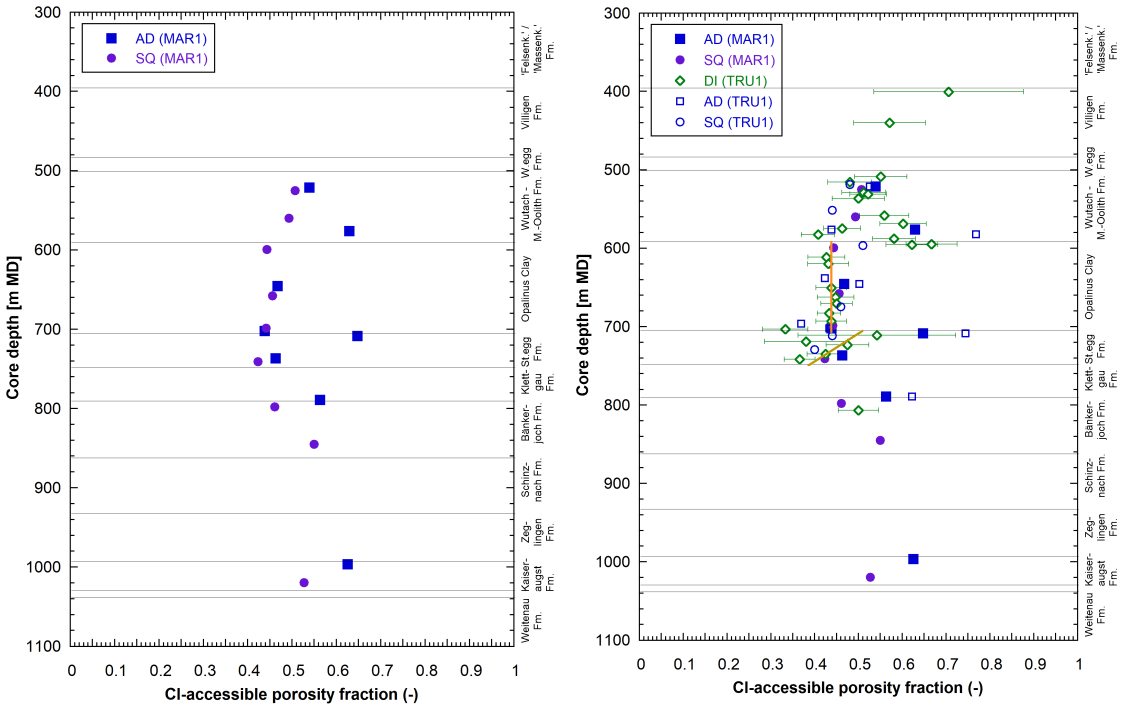

Fig. 5.1-3: Cl-accessible porosity fraction (f_{Cl}) as a function of depth; left: MAR1-1 data; right: MAR1-1 and TRU1-1 data

Formation boundaries in TRU1-1 were adjusted to correspond to those of the MAR1-1 borehole. Orange trend lines are discussed in Section 5.2. Error bars on the through-diffusion data indicate propagated analytical errors.

5.2 Chloride, bromide and Br/Cl profiles

Paul Wersin, Martin Mazurek & Carmen Zwahlen

The chloride profile depicted in Fig. 5.2-1 includes aqueous extraction data re-calculated to in situ conditions assuming the relationship between clay-mineral content and f_{Cl} as discussed in Section 5.1. The Cl data based on squeezing and advective displacement, as well as those for the groundwaters in the Malm and in the Muschelkalk, are also shown. The error bars include the propagated analytical uncertainty and an additional 20% that reflect the uncertainty related to f_{Cl} (see Section 5.1, Fig. 5.1-1).

Data from all three methods are consistent within the extended error bars. Note that contamination for select components (e.g. Si, K) by drilling fluid was identified or at least suspected in a number of samples from the Bänkerjoch and Schinznach Formations used for aqueous extraction (Section 4.4). These samples are nevertheless included in the profile because no obvious reason could be found why such a contamination would significantly affect Cl or Br concentrations (Section 4.4).

The Cl profile between the Malm und the Keuper aquifers is curved, with the highest Cl concentrations in the upper Opalinus Clay and lower «Brauner Dogger» of 8 – 9 g/L, decreasing towards the upper and lower aquifers, respectively. A similar Cl profile was derived for the Benken borehole (Gimmi & Waber 2004) and the TRU1-1 borehole (Aschwanden et al. 2021) from the same siting area, and for the nearby Schlattingen-1 borehole (Wersin et al. 2013). The Cl concentrations were generally slightly lower in the latter two boreholes, with maximum concentrations of ~ 7 g/L, but slightly higher in the TRU1-1 borehole (~ 10 g/L). Based on transport modelling, the Cl profiles in the Benken and Schlattingen-1 boreholes could be explained by diffusive exchange between the low permeability sequence of the Staffelegg Formation – Opalinus Clay – «Brauner Dogger» and bounding aquifers having occurred during the last 0.5 – 1 Ma (Gimmi & Waber 2004, Wersin et al. 2021). Note that for the MAR1-1 borehole no water samples in the upper Keuper could be extracted, contrary to TRU1-1. However, the very similar Cl and water isotope profiles (Section 5.8) strongly suggest the presence of an active aquifer system in the upper Klettgau Formation also in the area of the MAR1-1 borehole.

A general steady upward increase of Cl concentration starting at the level of the (expected) Keuper aquifer (~ 780 m depth) is observed. Thus, Cl concentrations increase from ~ 1 g/L near the Keuper aquifer to ~ 9 g/L in the central part of the Opalinus Clay (~ 640 m depth), above which concentrations remain constant up to the top of the formation (580 m depth). The Cl profile in the heterogeneous «Brauner Dogger» displays some scatter, owing to the uncertainty related to water content and, more importantly, to the uncertainty related to the anion-accessible porosity. Cl levels start decreasing in the Wildegg Formation, a trend that continues in the lower part of the Villigen Formation, reaching about 3 g/L in the top sample at 465 m depth. The sampled groundwater located in the «Felsenkalke» + «Massenkalk» about 100 m above displays about 2 g/L. Note that no samples are available within this 100 m interval. Given the fact that the Cl concentration in the uppermost sample from the Villigen Formation is low and similar to that of the groundwater sample extracted about 100 m above, it is tentatively hypothesised that an interconnected fracture network exists in the limestones of the «Felsenkalke» + «Massenkalk» and upper Villigen Formation that propagates the groundwater signal within this interval (see further discussion in the isotope Section 5.8).

In summary, a consistent Cl profile between the Malm and Keuper aquifers is obtained from squeezing, advective displacement and aqueous extraction data. The profile shape is similar to those derived for the other boreholes of the siting area (Benken, TRU1-1). A well-defined profile is identified with some scatter in the «Brauner Dogger» and near the Opalinus Clay / Staffelegg Formation boundary. This scatter is related predominantly to the uncertainty in anion-accessible porosity and to a lesser extent to the uncertainty in the water content. In this analysis, a simple relationship of the anion-accessible porosity with the clay-mineral content (as proxy of surface charge) based on through-diffusion, squeezing and advective displacement data was used. It is worth noting that other relationships with the clay-mineral content (e.g. linear extrapolation from clay-mineral content < 20 wt.-%, < 30 wt.-%, or < 50 wt.-%) resulted in a slightly larger scatter in the data. Also, considering relationships between f_{Cl} and smectite or illite content did not result in less data scatter.

In view of the general uncertainty related to the anion-accessible porosity and the formation-specific trends noted in the Opalinus Clay and the Staffelegg Formation (Fig. 5.1-3), an alternative Cl profile for these formations based on a f_{Cl} – depth relationship shown in Fig. 5.1-3 is illustrated in Fig. 5.2-2 (right). A comparison of aqueous extraction data with the corresponding profile obtained from the 'standard' method (Fig. 5.2-2 left) reveals a similar behaviour, but with more scatter. Specifically, for the sample at 622.45 m with a comparatively low clay-mineral content of 33 wt.-% in the Opalinus Clay, the assumption of constant f_{Cl} across the entire formation induces a somewhat higher Cl concentration relative to the overall trend. For the sample 712.92 m in the uppermost part of the Staffelegg Formation, the 'kink' in the profile is augmented compared to the 'standard' profile. Overall, the approach based on simple formation-specific trends leads to more scatter in the Cl profile compared to the procedure based on the clay-mineral content.

The Cl profile in the Klettgau Formation exhibits low concentrations < 1 g/L in the upper part down to about 780 m depth, and increasing from there towards the bottom to ~ 10 g/L. The profile in the underlying Bänkerjoch Formation suggests a slightly decreasing trend, approaching the groundwater concentration in the uppermost Muschelkalk. Below this sampled aquifer, the profile shows a tendency of strongly increasing Cl concentrations down to the Zeglingen Formation, where they reach a maximum of ~ 150 g/L in the 'Obere Sulfatzone'. It should be noted that there are no indications of the presence of rock salt in this depth interval (or anywhere else). From there, they steadily decrease to ~ 2 g/L in the Dinkelberg Formation and upper Weitenau Formation. The data from the AD and SQ samples in the Kaiseraugst Formation are consistent with AqEx data. Note that the error bars are large, in particular in the Zeglingen Formation, arising from the large uncertainties in water contents in these low porosity rocks combined with the error on the anion-accessible porosity fraction. Thus, the scatter of the data must not be over-interpreted.

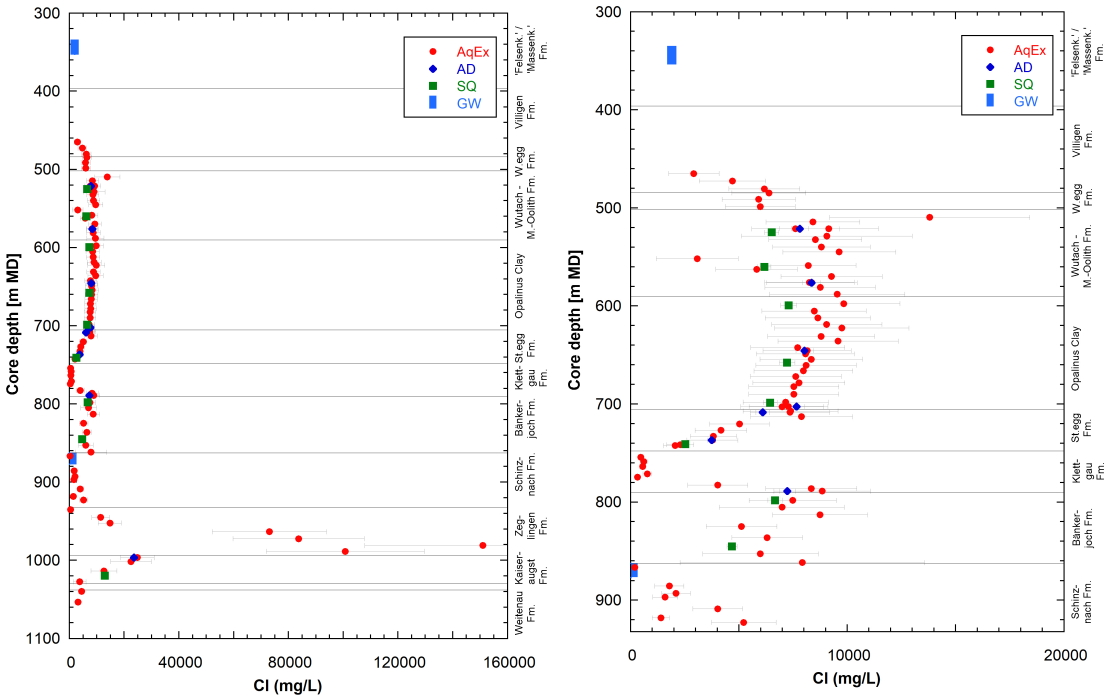

Fig. 5.2-1: Cl profiles at different depth scales with data from squeezing, advective displacement, aqueous extraction, and groundwater samples

Aqueous extraction data re-calculated to Cl-accessible porosity assuming the relationship between accessibility and clay-mineral content as discussed in Section 5.1. Error bars on the data from aqueous extraction include propagated analytical uncertainty plus another 20% that reflect the uncertainty related to f_{Cl}. The propagated uncertainty for SQ data assumes the same analytical uncertainty as for the other samples (4% for Cl).

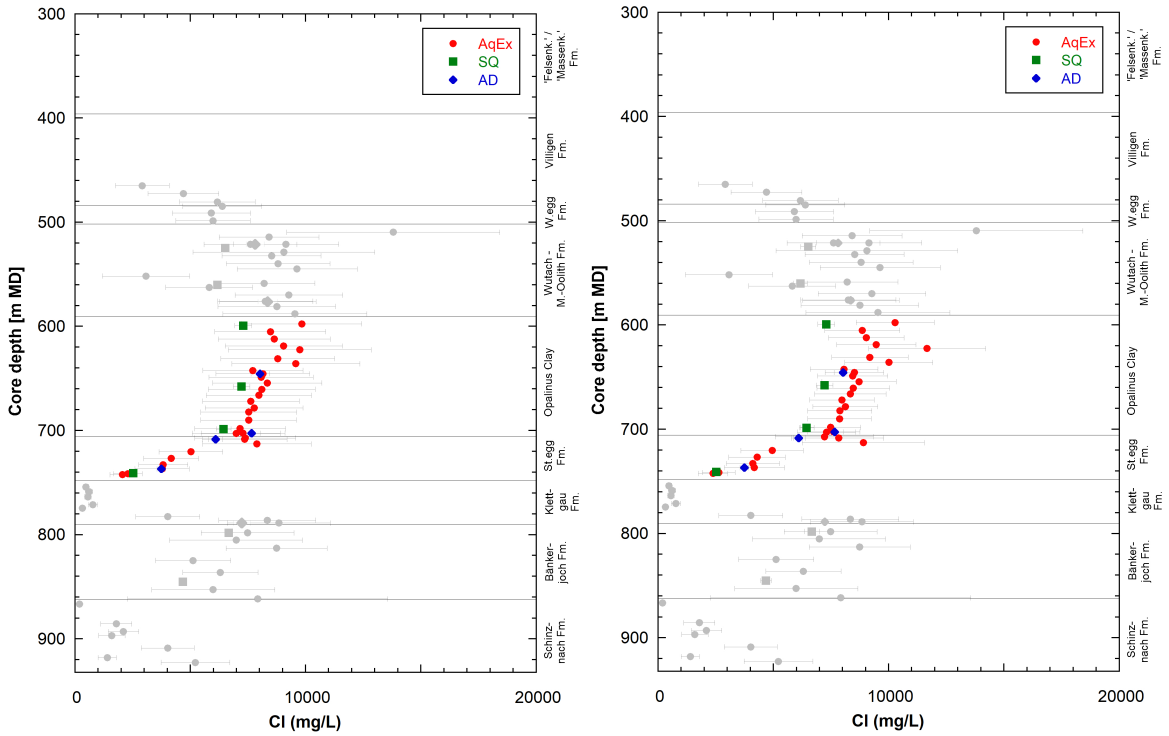

Fig. 5.2-2: Cl profiles using 'standard'procedure (left) and alternative approach (right), see text

Alternative approach: The Cl-accessible porosity fraction f_{Cl} of aqueous extraction data was derived from the trend lines illustrated in Fig. 5.1-3. Error bars from aqueous extraction for Opalinus Clay in right graph include propagated analytical uncertainty plus 10%, reflecting uncertainty related to f_{Cl}. For all other aqueous extraction data, the uncertainty in f_{Cl} is assumed to be 20%. The propagated uncertainty for SQ data assumes the same analytical uncertainty as for the other samples (4% for Cl).

The Br profile shows an increasing trend from the Keuper aquifer up to the top of the Opalinus Clay (Fig. 5.2-3). Within the «Brauner Dogger» this trend continues, but there is more scatter towards lower values. There is one apparent outlier in the Variansmergel Formation at a depth 509.68 m which displays a higher value, also observed in the Cl concentration. At the top of the Dogger lithologies the profile displays a decreasing trend continuing into the Malm units. The Br profile is thus similar to the Cl profile. In the Triassic, data scatter is substantial, at least partially related to analytical issues (low porosity, Br contents close to the limit of detection, potential sample contamination).

The similarity between Br and Cl is also illustrated in the Br/Cl ratios, which are remarkably constant in the interval Staffelegg Formation – «Brauner Dogger», with only a slight upward increase in the «Brauner Dogger», continuing into the Villigen Formation (Fig. 5.2-4). On the other hand, Br/Cl ratios strongly increase from the Lias/Keuper boundary down to the Schinznach Formation from where they steadily drop, reaching a minimum at the Zeglingen/Kaiseraugst Formation boundary. From there an increasing signal is noted down to the lowest sample in the Weitenau Formation. Note that the Br/Cl ratio of the sampled groundwater in the top Muschelkalk is not compatible with those of the corresponding porewaters. The distinct minimum at the base of the Zeglingen Formation is remarkable, as no hydraulic boundary is expected at this depth. Also note that the Dinkelberg Formation, which typically hosts the Buntsandstein aquifer, finds no expression in the profile.

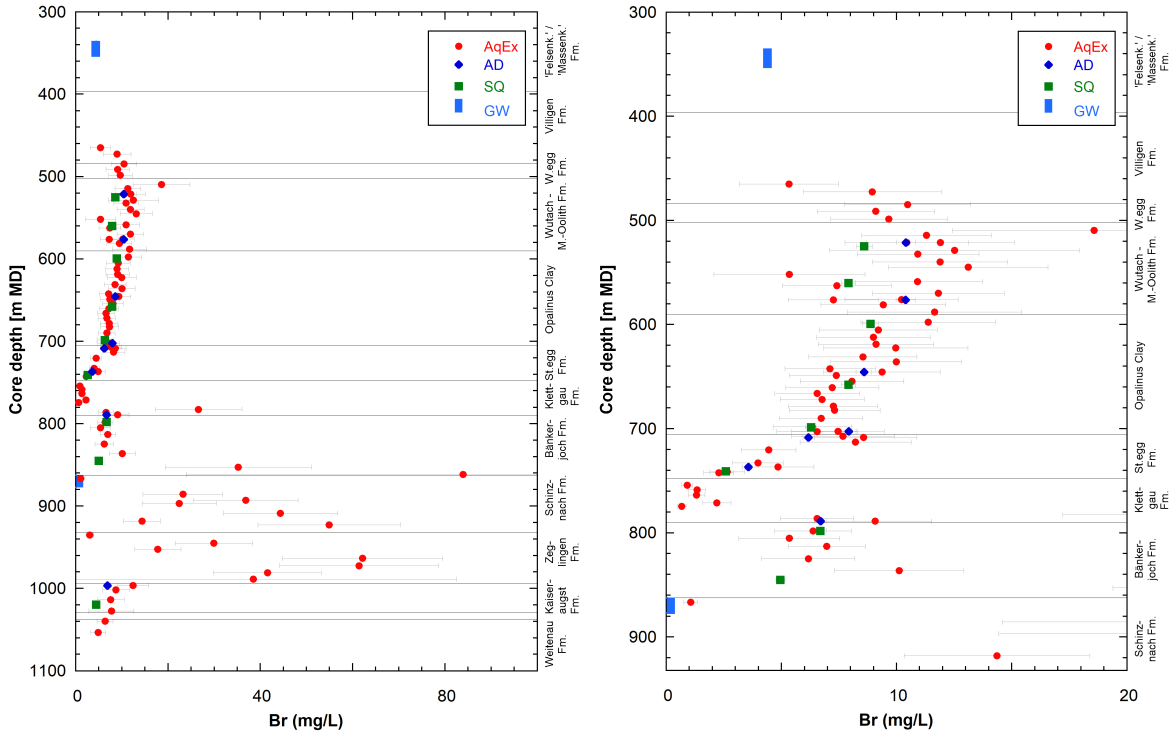

Fig. 5.2-3: Br with data at two different depth scales from squeezing, advective displacement, aqueous extraction and groundwater samples

Aqueous extraction data in the Br profile re-calculated to Br-accessible porosity assuming the relationship between accessibility and clay-mineral content as discussed in Section 5.1. Error bars on the data from aqueous extraction include propagated analytical uncertainty plus another 20% that reflect the uncertainty related to f_{Br}.

The Br/Cl profile reveals a remarkable consistency between the three datasets. The much smaller scatter of the Br/Cl profile when compared to the profiles of Cl and Br is because rock heterogeneity and uncertainty related to anion-accessibility and water content do not affect the Br/Cl ratio, contrary to the individual concentrations.

The (1000*Br/Cl) (molar units) ratio in the Opalinus Clay and confining units increases upwards roughly from 0.4 to 0.6 and shows a more pronounced rise in the lower Malm units to 0.85, approaching the ratio of the groundwater sample in the «Felsenkalke» + «Massenkalk» (1.0). In any case, these Br/Cl ratios a far below that of modern seawater (~ 1.55).

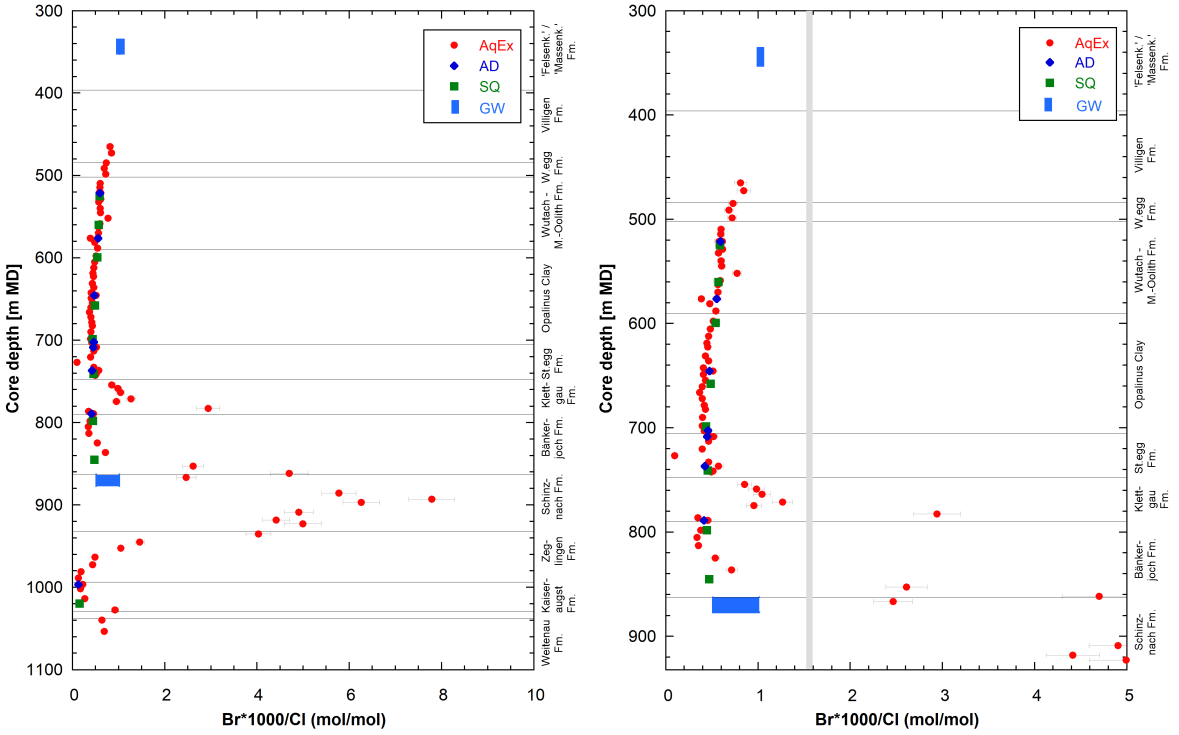

Fig. 5.2-4: Br*1000/Cl ratios (mol/ mol) at two different depth scales with data from squeezing, advective displacement, aqueous extraction and groundwater samples

Grey bar: range of modern seawater. The propagated uncertainty for SQ data assumes the same analytical uncertainty as for the other samples (4% for Cl).

5.3 Sulphate and SO_4/Cl profiles

Paul Wersin & Martin Mazurek

Sulphate data from squeezing, advective displacement, aqueous extraction and groundwaters are illustrated in logarithmic and linear scales in Fig. 5.3-1. Data from aqueous extraction were recalculated to concentrations in bulk porewater assuming conservative behaviour of sulphate. This assumption is not true at least in anhydrite-bearing lithologies in the Bänkerjoch and Zeglingen Formations where mineral dissolution contributed to SO_4 concentrations in the extracts. Anion exclusion has not been considered at this stage. Note that the groundwater concentrations of sulphate are not corrected for drilling fluid contamination, which, however, is considered to be minor for the sampled Muschelkalk groundwater (Lorenz et al. 2021).

From a qualitative perspective, the highest sulphate levels based on aqueous extraction are observed in the Klettgau, Bänkerjoch and Zeglingen Formations. Below the latter formation, SO_4 concentrations strongly decrease with depth, reaching about 1 g/L in the Weitenau Formation. Above the Zeglingen Formation, also a decreasing trend within the Schinznach Formation. towards the sampled Muschelkalk aquifer is observed (note however that these samples are potentially affected by drilling fluid contamination, but most likely not for SO_4 as outlined in Section 4.4). The concentrations sharply decrease from the upper Bänkerjoch Formation to the Klettgau Formation from where a weak and steady decrease up to the top of the Dogger is found.

The very high SO_4 concentrations obtained for the re-calculated aqueous extracts in the Bänkerjoch, Zeglingen and one sample from the Klettgau Formation are not meaningful because of anhydrite dissolution during extraction (Fig. 5.3-1 left). High concentrations are also exhibited in some samples in the Schinznach and Kaiseraugst Formations, although no anhydrite or gypsum could be detected by XRD in these samples. Such phases might, however, be present below the detection limit of XRD.

SO_4 concentrations based on squeezing and advective displacement yield distinctly lower and less scattered values (with only two values from the Bänkerjoch Formation) in comparison to the re-calculated data from aqueous extraction. A closer look at the Opalinus Clay and the underlying and overlying confining units (Staffelegg Formation and «Brauner Dogger») reveals consistent concentrations between squeezing and advective displacement data and a slightly increasing trend with depth, from about 1 g/L to 2 g/L (Fig. 5.3-2 right). Conversely, the re-calculated aqueous extraction data exhibit systematically higher and more variable concentrations. The discrepancy between aqueous extraction and squeezing/advective displacement data becomes even larger when anion exclusion is considered, e.g. by assuming the same relationship between anion-accessible porosity and clay-mineral content as that applied for Cl (Fig. 5.3-2). However, it should be noted that the anion-exclusion effect of SO_4 in the considered rocks is not well known. From double layer theory, the exclusion of SO_4 in clayrocks is predicted to be higher because of its higher charge (Gimmi & Alt-Epping 2018). On the other hand, SO_4 has a larger tendency to form weak complexes, such as with alkaline earths, thus partly compensating the charge effect.

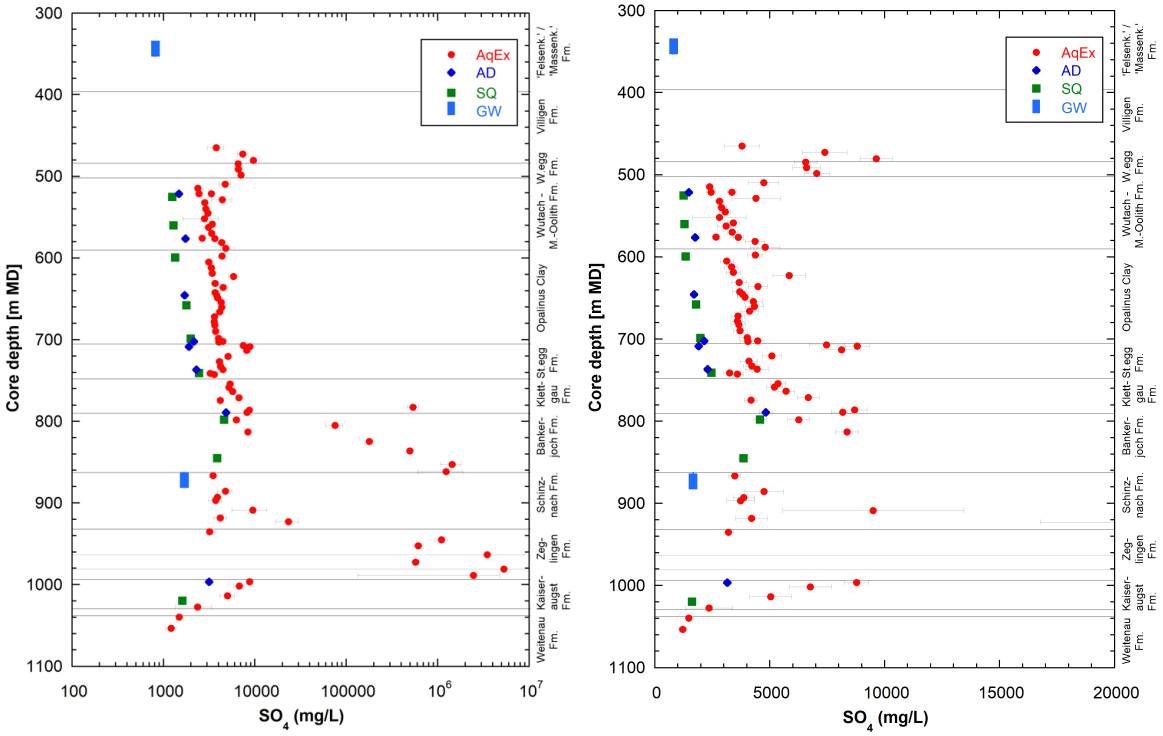

Fig. 5.3-1: SO_4 profiles (logarithmic and linear scales) with data from squeezing, advective displacement, aqueous extraction, Ni-en extraction and groundwater samples; left: entire data (logarithmic scale); right: data with SO_4 concentrations < 20 g/L (linear scale)

Aqueous extraction data re-calculated to contents in bulk porewater using water content. The propagated uncertainty for SQ data assumes the same analytical uncertainty as for the other samples (4% for Cl).

A similar discrepancy between squeezing/advective displacement data on the one hand and aqueous extraction data on the other has been observed for other boreholes, such as Schlattingen-1 (Wersin et al. 2013), the BUL1-1 borehole (Mazurek et al. 2021), the TRU1-1 borehole (Aschwanden et al. 2021) as well as in in the Mont Terri Rock Laboratory (Wersin et al. 2021). In the latter case, waters sampled from packed-off boreholes exhibit similar sulphate concentrations and SO_4/Cl ratios as waters squeezed from nearby drillcores. All porewaters from squeezed and advectively displaced samples are close to equilibrium with regard to celestite. Celestite could be identified in some samples of the matrix of the Opalinus Clay and «Brauner Dogger» samples at Mont Terri and Schlattingen-1 by a combined SEM/microprobe study (Jenni et al. 2019). In the case of BUL1-1, where in view of the higher sulphate levels, higher amounts of sulphate phases such as anhydrite and celestite could be expected, no such phase (with grain sizes of > 3 µm) could be identified by SEM analysis so far. Samples from advective displacement and squeezing are generally undersaturated with regard to gypsum, and gypsum is not thought to play a role in this issue.

The reason for the higher sulphate levels derived from aqueous extraction compared to squeezing/advective displacement data is not understood at this stage, in spite of a recent systematic aqueous extraction study on Opalinus Clay including Mont Terri and BUL1-1 samples (Debure & Gailhanou 2019, Aschwanden & Wersin 2020). Interestingly, the SO_4 concentrations obtained

from re-calculated Ni-en extracts used for obtaining cation exchange parameters are systematically lower than those obtained from aqueous extraction, but still higher than those displayed by squeezing/advective displacement data (Fig. 5.3-2). The reason for this difference is not known at this point.

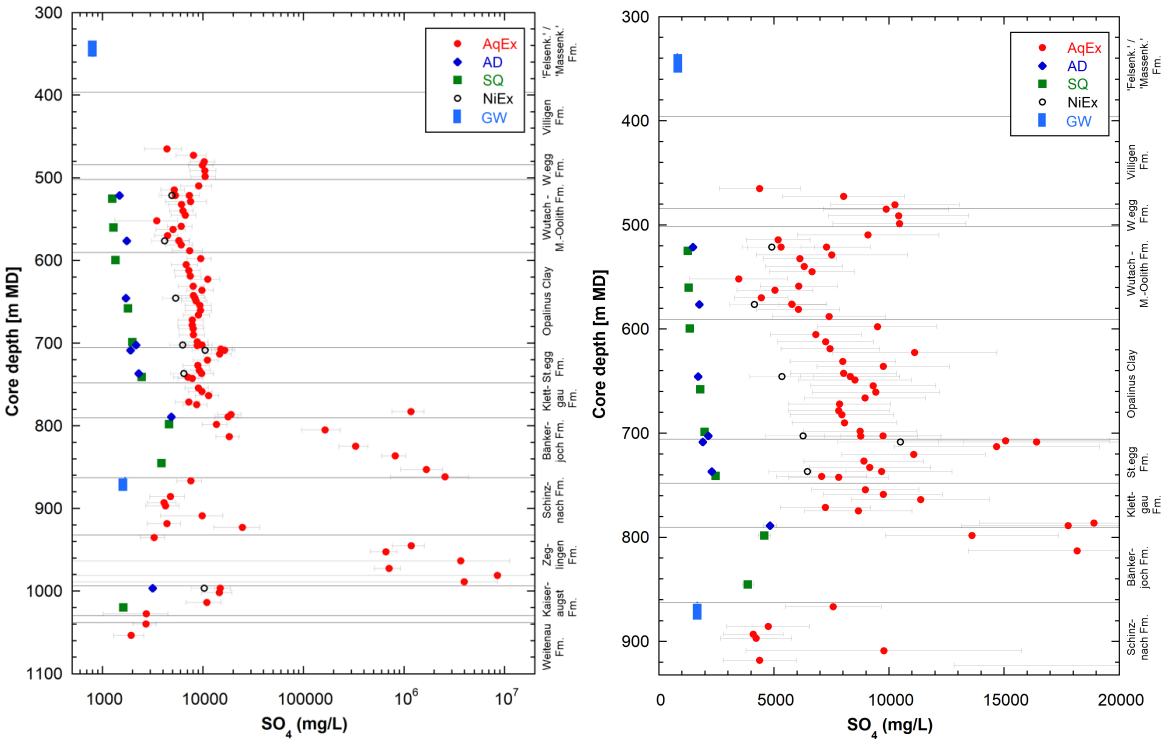

Fig. 5.3-2: SO_4 profile at two different depth scales with data from aqueous and Ni-en extraction, compared with squeezing, advective displacement and groundwater data

Aqueous and Ni-en extraction data re-calculated to SO_4-accessible porosity assuming the same relationship between accessibility and clay-mineral content as applied above for Cl. Samples potentially affected by drilling-fluid contamination (Section 4.4) are shown as open symbols. The propagated uncertainty for SQ data assumes the same analytical uncertainty as for the other samples (4% for Cl).

The depth profile of SO_4/Cl ratios (Fig. 5.3-3) shows similar trends as the SO_4 profile. The high molar SO_4/Cl ratios up to more than 10 in aqueous extracts from anhydrite-bearing units in the lower sequence of the profile point to the dissolution of sulphate-bearing mineral phases during extraction. In the central part, SO_4/Cl ratios remain below 1, whereby the values obtained from squeezing and advective displacement are clearly lower. A strong drop with decreasing depth in the Staffelegg Formation, followed by a more gradual decrease in the Opalinus Clay and rather constant ratios in the «Brauner Dogger» are seen both in the AD/SQ and AqEx data. Note that the SO_4/Cl profile in the interval Staffelegg Formation – «Brauner Dogger» is well defined and shows less scatter than the profiles of the individual solutes, likely because anion accessibility plays no role in the case of ion ratios. AqEx data data suggest a sharp increase and a spread from the top Dogger to the lower Malm strata. As noted in the previous section, these data may not reflect the in situ porewater concentrations for reasons not yet understood. The SO_4/Cl ratios decrease down to ~ 0.4 in the Muschelkalk groundwater sample. The sampled Malm groundwater displays a ratio of 0.15.

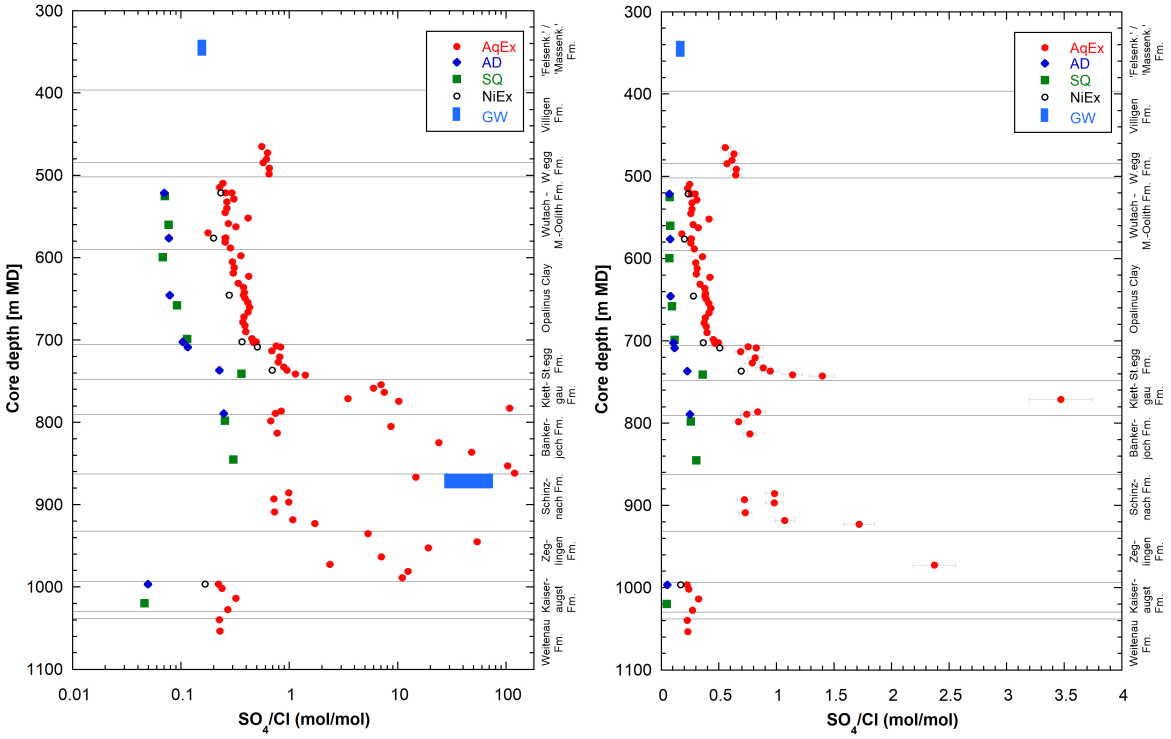

Fig. 5.3-3: Profiles showing molar SO_4/Cl ratios obtained from different methods in logarithmic and linear scales

Data from aqueous extracts not shown for some samples from sequence below the Staffelegg Formation in the right graphic (many points fall out of the plotted range).

5.4 Cation concentrations in porewaters

Urs Mäder

5.4.1 General considerations

Deriving cation concentrations in porewaters involves a discussion about controlling processes and disturbing effects (mineral dissolution/precipitation, cation exchange, oxidation, others) that operate invariably when handling drill core samples, in our case for performing aqueous extractions, Ni-en extractions, porewater squeezing and advective displacement experiments. These overreaching discussion topics are elaborated in Section 5.9.

The seemingly least-affected cation is Na (no mineral source except for halite if present), not because it does not interact, but because it is in most units the major positive charge-carrying cation and thus is not sensitive to small relative changes, and a priori correlates well with chloride concentrations where chloride is the major anion charge-carrier. With increasing sulphate concentrations (and ionic strength), however, charge compensation may increasingly also relate to Ca concentrations, and Na forms an important ligand for sulphate complexation ($NaSO_4^-$) and is no longer a quasi-conservative component. In some porewater models, Na is used to top up cation charge to balance the sum of anionic charge, with other major cation concentrations and ratios constrained by mineral equilibria and measured exchanger composition.

All cations interact to variable degrees with the clay exchanger, an inventory that far exceeds the dissolved load (except in very clay-poor limestones), and disturbances are thus interlinked. Some cations are directly involved in mineral saturation equilibria (calcite, dolomite, sulphates where present), and all are directly or indirectly linked to the carbonate system (detailed in Section 5.5) that also forms a sliding pH buffer.

Some limited data were obtained for minor or trace cations such as Ba and Si. These are not drivers for interactions but may be controlled by mineral saturation equilibria. A minor cation of some significance is ammonium (NH_4) that is known to be present in porewater and on the clay exchanger, but relatively few data exist. The Fe-system is analytically not well-constrained for the solutes and exchanger concentrations due to the inherent sensitivity of Fe to redox processes: it is normally constrained by modelling and linked to the more reactive Fe-bearing minerals pyrite and Fe-carbonates. Fe was not measured. It was below a detection limit of 0.025 mg/L in 22 aqueous extract samples from the TRU1-1 borehole. Little comprehensive data exists on trace cations (e.g. transition metals) and none were measured in this study.

5.4.2 Constraints from aqueous extract data

A comprehensive dataset is available for MAR1-1, comparable to BUL1-1, but including only aqueous extracts performed at the University of Bern (78 PW samples, 8 AD samples).

Aqueous extracts are affected by mineral dissolution of calcite to saturation, by dolomite to a variable degree, and by anhydrite where present (Bänkerjoch Formation, Zeglingen Formation), as detailed in Section 4.4.2.4. This adds Ca and some Mg to the extract solutions, in addition to a releas from the exchanger due to dilution, charge-compensated by alkalinity and sulphate in case of anhydrite. Ionic strength is low in aqueous extracts compared to porewater, and this is causing a much stronger preference for the divalent cations relative to Na and K to populate the clay exchanger. This combined disturbance renders all cation concentrations to be non-conservative and therefore they cannot be scaled to porewater concentrations (by water content). This is occasionally done for Na, but as discussed above, it is an approximation, and likely fails for porewaters that are not of Na-Cl type.

It may be possible to perform modelling calculations to back-track mineral dissolution contributions during aqueous extraction and the dilution induced by the added water, and so arrive at a model porewater composition. This has not yet been rigorously attempted and it remains to be demonstrated that it is possible to constrain a unique reaction pathway for back-calculation.

5.4.3 Constraints from porewater squeezing and advective displacement data

The two so-called direct sampling methods, porewater squeezing (9 SQ samples) and advective displacement (8 AD samples), aim at obtaining sample aliquots that are porewater like. Both approaches mobilise porewater and it is thought that this mobile part is more kin to the free porewater (charge-neutral, not affected by electrostatic effects / charged clay surfaces and interlayers). Past experience and comparison to through-diffusion experiments attest some degree of consistency to this end. One method implies high-pressure deformation and destruction of the rock fabric to squeeze porewater, the other applies large hydraulic gradients and an artificial porewater to displace the in situ porewater. The two methods are therefore quite contrasting regarding the mechanism of extraction, and some method-specific artefacts may be expected. Both methods show some agreement in a subset of characteristic porewater parameters. Also important are additional constraints for certain parameters by independent methods to identify any systemic short comings.

Most significant for porewater composition are the squeezed aliquots at lowest pressures (Tabs. 4.6-3 and 4.6-4) and the first 1 – 3 small sample aliquots from advective displacement (Tab. 4.7-15, average of first 2 aliquots, Appendix 4 for all data). The small sample volumes available typically allow not for analysing all parameters, and it may lead to high detection limits for some parameters due to required dilution, and analytical uncertainties may be larger than commonly adopted for standard analytical procedures. The aliquots squeezed at lowest pressures – in contrast to earlier work (BUL1-1, TRU1-1) – include pH measurements and information on TIC/TOC.

The measured concentrations of major and some minor cations in squeezing aliquots from lowest pressure and the average concentration from the first two aliquots from advective displacement (Figs. 5.4-1 and 5.4-2) are discussed below. Data interpretation is on-going, and data below thus represent squeezed or displaced aliquot concentrations (rather than in situ porewater), potentially subject to experimental artefacts as indicated below.

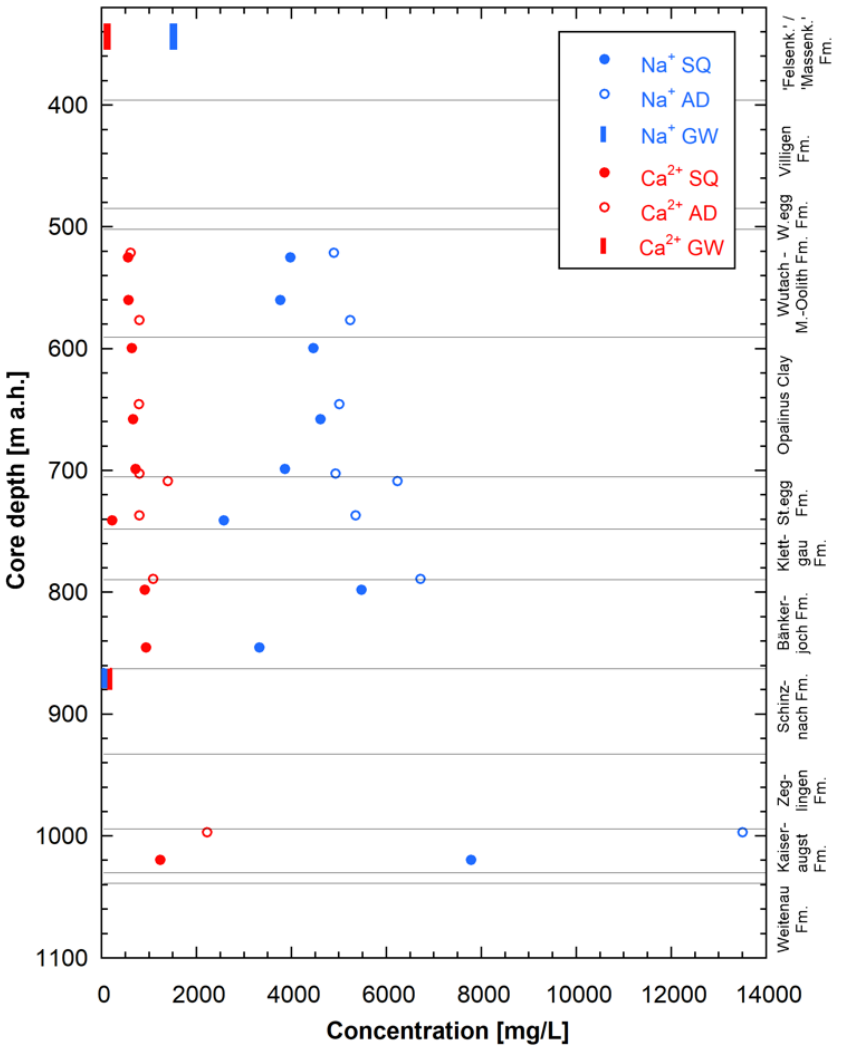

Fig. 5.4-1: Concentrations of Na and Ca in aliquots from squeezing experiments and advective displacement experiments

Only aliquots squeezed at lowest pressures are shown, and average values for the first two aliquots obtained from advective displacement.

Ca concentrations are quite comparable for the two methods, but different where steep salinity gradients exist and mask a direct comparison (towards Keuper aquifer in top Klettgau Formation). Na concentrations are systematically lower in SQ samples compared to AD samples. The reason for this is that SQ samples are less saline compared to AD samples, despite that the derived anion-exclusion effect is quite similar. This is further discussed in Section 5.9. The relatively large difference near the base of the Staffelegg Formation is in part due to the steep gradient to low salinities in the Keuper aquifer and adjacent porewater (Cl profile, Fig. 5.2-1). The same holds true for the AD and SQ sample in the Kaiseraugst Formation, where salinity is sharply decreasing towards the Permian strata (see Cl profile, Fig. 5.2-1). Note that the two AD experiments are characterised by unusually large initial nitrate concentrations (8.7 and 7.1 g/L) and this leads to some distortion also of the cation concentrations (Section 4.7.5.5, Tab. 4.7-15). The reason for nitrated generation is not yet known, but may be related to the organic-rich nature of parts of the Staffelegg Formation (e.g. 'Posidonienschiefer' / Rietheim Member).

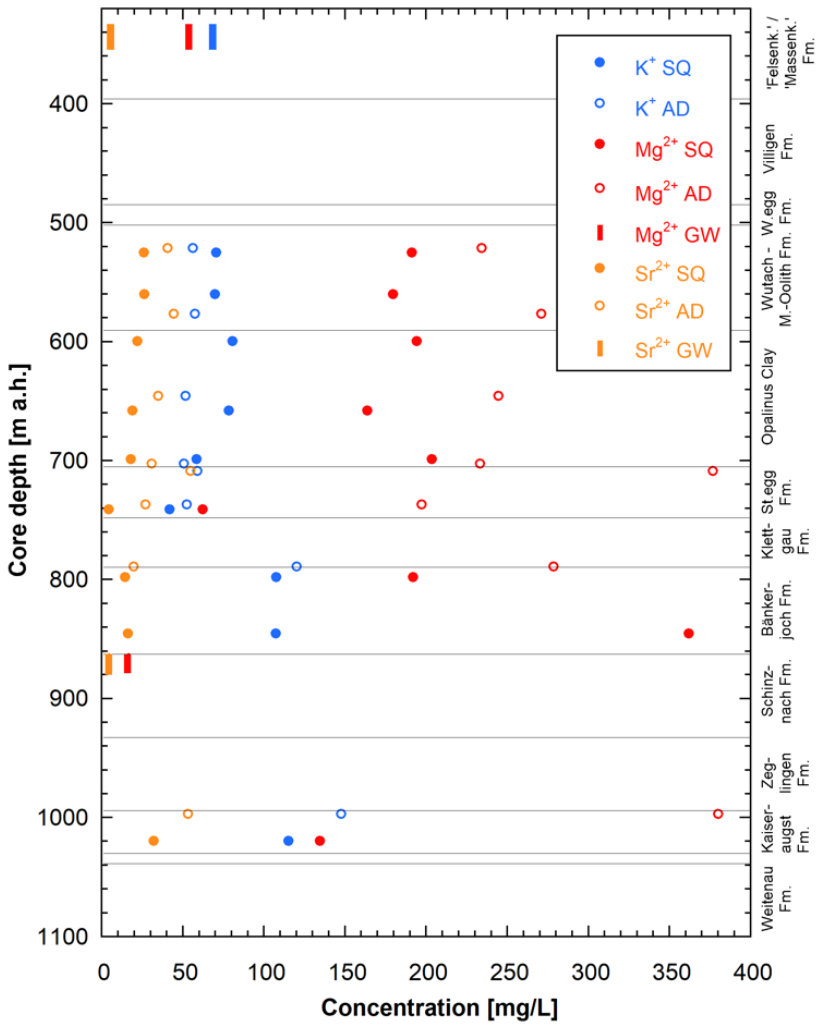

Fig. 5.4-2: Concentrations of K, Mg and Sr in aliquots from squeezing experiments and advective displacement experiments

Only aliquots squeezed at lowest pressures are shown, and average values for the first two aliquots obtained from advective displacement.

As is the case for Na, also Mg and Sr concentrations are systematically lower in SQ samples compared to AD samples. Again, this correlates with the lower salinities obtained by squeezing compared to advective displacement. The cation ratios are rather similar. The excursions to elevated Mg and Sr concentrations in AD samples from the Staffelegg Formation are likely related to the nitrate issue discussed in the previous paragraph. In contrast, K concentrations are larger in squeezing samples compared to advective displacement. The reason for this contrasting behaviour is not understood.

5.4.4 Significance of sample aliquots from advective displacement and squeezing for cation concentrations in porewater

The so-called direct porewater sampling methods, squeezing and advective displacement, are subject to a number of similar artefacts, and some method-specific differences. These differences and artefacts include:

- Aliquots are significantly or even strongly supersaturated with respect to calcite (SI > 1 in some cases) and dolomite (Tabs. 4.7-16 and 4.6-5).
- Aliquots show a Ca/Mg molar ratio that is larger than permissible by simultaneous calcite-dolomite equilibrium.
- Aliquots are saturated or supersaturated with respect to celestite (Tabs. 4.7-16 and 4.6-5). This may or may not be an artefact, depending if celestite is indeed present.
- Substantial dissolved organic carbon species are mobilised in earliest AD aliquots and decrease strongly in subsequent aliquots (see also Section 5.5; Fig. 4.7-12, Tab. 4.6-3).
- Aliquots show systematically lower pH values in advectively displaced aliquots compared to squeezed aliquots (8.3 – 8.7 vs. 7 – 8, respectively; Fig. 4.7-14, Tab. 4.6-3).
- Ionic strength (salinity) is systematically higher in advectively displaced aliquots compared to squeezed aliquots (by 10 – 20%).

While a detailed analysis to reconcile artefacts and differences is beyond the scope of this data report, it is quite clear that these direct samples obtained from advective displacement or squeezing do not strictly represent the porewater composition contained in the experimental cores at laboratory conditions, nor at in situ conditions in the rock formation. Some components may reasonably represent porewater conditions, others may have been modified significantly from in situ conditions as a result of drilling, unloading, handling, storage, sample preparation and artefacts induced by the experimental method. Section 5.9 includes a more detailed discussion of some of these and more general issues. A number of approaches to correct for some of these artefacts have already been elaborated in earlier work (Wersin et al. 2021, Wersin et al. 2013, Mäder & Waber 2017). Other issues will require a more in-depth data analysis.

5.5 Dissolved carbon species (inorganic, organic), alkalinity, pH and pCO_2

Urs Mäder

5.5.1 General considerations

The carbonate system (dissolved inorganic species/alkalinity, carbonate minerals, pCO_2) plays a pivotal role for porewater composition as it links measurable parameters like pH, alkalinity/TIC (total inorganic carbon) to difficult-to-measure quantities like partial pressure of CO_2. Inorganic carbon species in combination with the solid carbonate system (calcite, dolomite, etc.) intimately link dissolved Ca and Mg to the exchange complex that contains an inventory of cations that far exceeds the dissolved load (except for pure limestones). Via this link to the exchanger, also Sr, K and to a lesser extent Na are interlinked. Due to potentially solubility-limiting sulphates (anhydrite, gypsum, celestite), there is also a link to the sulphate system. With other words: the controlling carbonate equilibria, or any disturbing effects to the carbonate system, affect the entire porewater composition. By the same token, the exchanger capacity has a buffering effect on external disturbances, and also the carbonate system itself forms a sliding pH buffer (buffering along a curved surface in pH – pCO_2) alkalinity space, constrained by calcite – dolomite saturation).

Constraining the in situ porewater composition – or even that of the porewater chemical state of a sample core after drilling – involves different levels of data interpretation based on geochemical equilibrium models (like PHREEQC) and cannot be simply derived from aqueous extracts by scaling (like for conservative anions) or from a one-to-one adoption of concentrations in advective-displacement or squeezing aliquots. This data report does not include such modelling interpretation and therefore can only elucidate on some aspects of porewater composition.

The dissolved organic carbon species pose analytical challenges, cannot be characterised to any degree of completeness by the methods used here, and the measured TOC (total dissolved organic carbon) contents seem to be dependent on sample handling and sampling techniques. There is evidence that some TOC components may readily get involved in microbial processes. The link of TOC to the solid organic matter or its generation from solid organic matter are not well understood.

We use solely TOC in referring to dissolved organic carbon, and not TOC and DOC, with the latter being designated to filtrated solutions. In most cases, our TOC concentrations represent DOC values. Filtration was commonly applied to aqueous extract samples (0.2 µm), but not to small aliquots from squeezing or advective displacement experiments, except for few cases where suspended particles were visible after dilution. In-line filtration was involved in IC analysis for low-molecular-weight organic acids.

5.5.2 Organic carbon

Available data includes (LMWOA: low-molecular-weight organic acids):

1. TOC in aqueous extracts associated with AD experiments (8 samples)
2. TOC in aliquots from AD (8) and SQ (9) experiments
3. Organic C in rock samples (PW samples, AD, SQ, GM)

4. LMWOA in 8 AD aqueous extract samples
5. LMWOA in direct samples of 8 AD experiments
6. TIC and TOC concentrations are available for the Malm aquifer waters (and titrated alkalinity), but LMWOA were not measured. The samples from the Muschelkalk aquifer are too contaminated to be useful for constraining the carbon system.

Organic C in rock samples (Fig. 5.5-1) show consistent and typical values near 1 wt.-% organic carbon for Opalinus Clay (average of 1.11 wt.-%, range of 0.78 – 1.41, Tab. 4.2-1), and lower values on average, but more variable, in the «Brauner Dogger» and Staffelegg Formation. The deeper parts of the profile (Klettgau Formation to Weitenau Formation) contain low concentrations of organic carbon, with only one sample of 1.3 wt.-% from the uppermost Schinznach Formation (Asp Member). Highest values of 5 – 7 wt.-% are associated with two samples from the Rietheim Member ('Posidonienschiefer') in the Staffelegg Formation. There were no specific analyses performed for further characterisation of the solid organic matter.

Organic carbon in liquid samples (TOC) has either been determined by direct measurement (NPOC, non-purgeable organic carbon), or by difference (total carbon – TIC). Almost all TOC determinations for this study were performed by difference.

TOC (DOC) measurements for earliest sample aliquots from advective displacement (AD) contain elevated TOC of 140 – 800 mg/L for the clayey sequence (Fig. 5.5-2), and 320 and 200 mg/L in the Klettgau Formation and Kaiseraugst Formation, respectively. Data are also available for aliquots squeezed at lowest pressures, and these range from 130 to 250 mg/L, and show significantly less spread compared to AD samples, but overlap in ranges.

TOC values from aqueous extracts from AD samples (pre-characterisation, 11 – 20 mg/L) range from 120 – 430 mg/L when up-scaled to porewater content. Such an upscaling may be subject to debate because the nature of the organic species is mostly not known, except that a portion is present as acetate (see below). Acetate is expected to show some kind of anion-exclusion effect, resulting in higher calculated concentrations in the anion-accessible part of the porewater. A value of 19 mg/L for TOC measured in groundwater samples from the Muschelkalk aquifer is reported (Lorenz et al. 2021), but this value is most likely too elevated due to contamination by drilling fluid, that is difficult to correct for in case of organic carbon. This value is shown in Fig. 5.5-2 but does likely not represent the groundwater composition.

Low-molecular-weight organic acids (LMWOA) that are detectable by our IC separation column include acetate, formate, lactate and propionate. These acids were only analysed in aqueous extracts from eight AD samples and in aliquots from AD experiments. Of these acids, acetate was present in aqueous extracts above a detection limit of 2 mg/L at concentrations of 3 – 5 mg/L, and lactate and formate was only detected in one sample at 1.5 mg/L, each (Klettgau Formation; Tab. 4.7-5). Early aliquots from AD experiments contain 30 – 500 mg/L acetate (below 4 mg/L in one sample, Klettgau Formation) and other acids mostly below a detection limit of 20 mg/L, with some exceptions (Tab. 4.7-15). The conecntrations decrease rapidly in subsequent AD aliquots and drop below those scaled from aqueous extracts. Organic acids were not evaluated in aqueous extracts from PW samples, or in SQ samples.

Note that an upscaling of concentrations in aqueous extracts to the chloride-accessible porosity proportion is not necessarily correct because these organic acids are not only subject to purely electrostatic effects, but also to interactions specific to functional groups of surfaces. It should be viewed as an illustration.

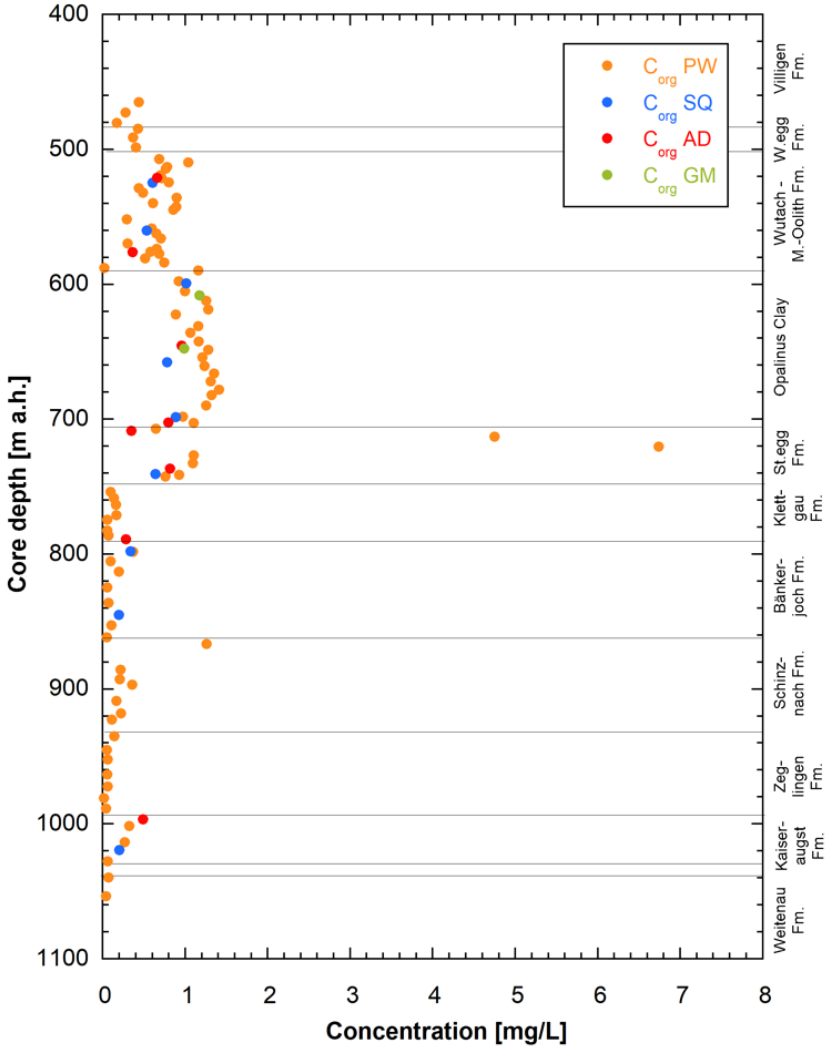

Fig. 5.5-1: Organic carbon in rock samples

Colour coding is according to sample type.

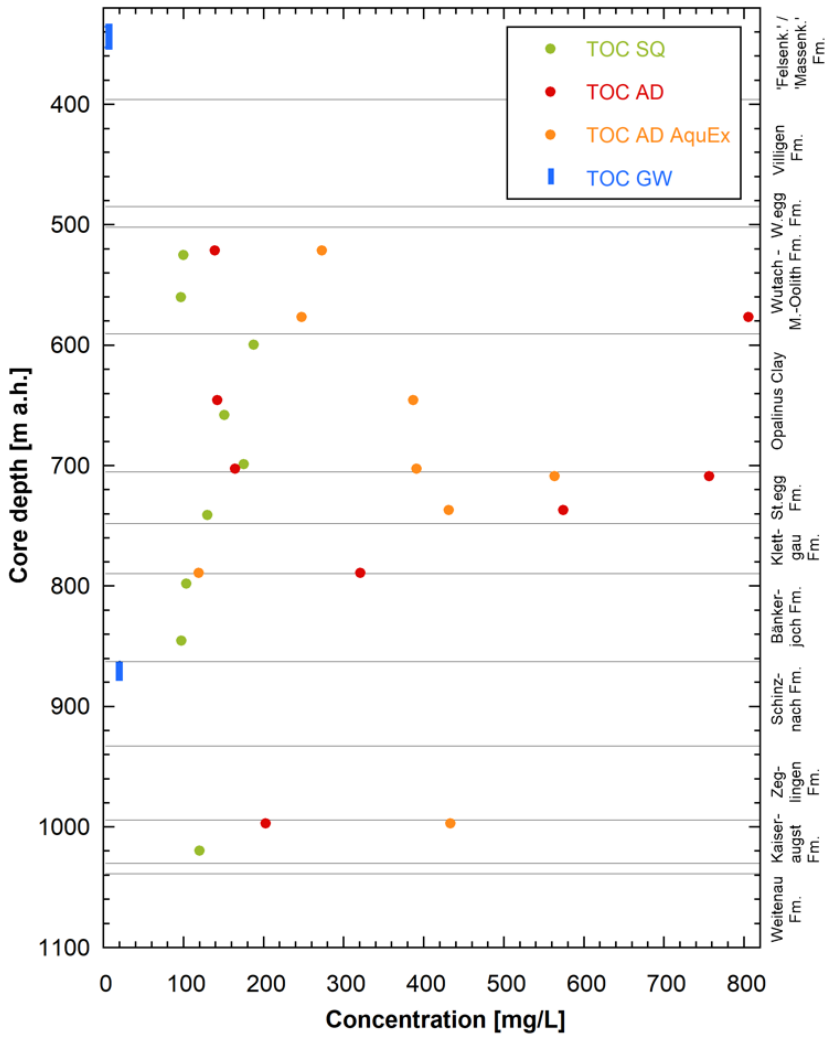

Fig. 5.5-2: TOC in aliquots from AD, upscaled from aqueous extracts, and aquifers

Aqueous extract samples from AD samples are scaled to water content (TOC_WC). The groundwater sample for the Muschelkalk aquifer is contaminated by drilling fluid and is not representative for the groundwater composition.

Acetate concentrations recalculated to water content (aqueous extracts of AD samples, Tab. 4.7-5) range from 60 to 115 mg/L and may be significant in the clayey sequence («Brauner Dogger» – Opalinus Clay – Staffelegg Formation). These up-scaled concentrations (to water content) overlap with the lower range of concentrations seen in earliest AD aliquots (30 to 500 mg/L).

It is rather difficult to interpret or transfer this data directly to in situ porewater conditions. The process of aqueous extraction, porewater squeezing and advective displacement seem to mobilise TOC and LMWOA above values that have been determined from long-term in situ sampling (e.g. at Mont Terri Rock Laboratory). Furthermore, TOC concentrations strongly decrease with progress of advective displacement (Section 4.7) and the advection process seems to wash out this labile initial TOC pool. Likewise, TOC concentrations also decrease with increasing squeezing pressure (Section 4.6, Tab. 4.6-3), and seem to be preferentially mobilised during early squeezing stages (observed for BUL1-1 samples and earlier work). It seems certain, however, that

TOC and LMWOA are part of the clay-porewater system, presumably in some kind of long-term disequilibrium situation with the solid organic matter and the inorganic carbon system. Apparently, any disturbance (drilling, sampling, EDZ, experiments, etc.) is able to mobilise TOC significantly.

TOC in the aquifers is only constrained at a low concentration of 2.2 mg/L (Lorenz et al. 2021) in the Malm aquifer but is dominated by drilling fluid contamination in the Muschelkalk aquifer (20 mg/L).

5.5.3 Dissolved inorganic carbon, alkalinity

Inorganic carbon species are either analysed directly as TIC or titrated as alkalinity. The latter is a summation parameter for all acids that can be protonated to a pH of ~ 4.3, such that it would also include most acetate, for example.

The inorganic carbon system in aqueous extracts is affected by calcite/dolomite dissolution induced by dilution and does not reflect porewater composition. Alkalinity in these samples largely represents the carbonate alkalinity. Because calcite/dolomite dissolution evolves in a closed and initially CO_2-free system during extraction, the pH rises strongly (pH 8 – 10 for Malm to Staffelegg Formation, for example) and bears no similarity to porewater pH.

The sample aliquots from advective displacement and porewater squeezing potentially may yield information on porewater TIC. TIC analyses were conducted within hours after sample collection for AD-sample aliquots, and after some weeks including an air-freight transport for the SQ aliquots. Alkalinity titration is not advisable for early aliquots because it may be dominated by organic acids (acetate) and thus overestimates carbonate alkalinity, and alkalinity titration also requires more sample volume than is commonly available. TIC concentrations in earliest AD aliquots range from 18 to 86 mg/L for the clayey sequence (Tab. 4.7-15). Straight speciation of these AD aliquots results in significant supersaturation with respect to calcite with SI values of 0.1 to 0.8 (Tab. 4.7-16), such that a geochemical modelling interpretation to restore calcite saturation may adjust some of these TIC values. TIC measurements were possible for samples squeezed at lowest pressures and thus also saturation states for carbonates could be evaluated (Tab. 4.6-5). TIC concentrations range from 26 – 45 mg/L for the clayey sequence and are near 10 mg/L for the Bänkerjoch Formation (Tab. 4.6-15). Squeezing aliquots are strongly supersaturated with respect to calcite, with SI values ranging from 1.3 – 1.5 for the clayey sequence, and values near 1.1 for the Bänkerjoch Formation.

In summary, a rather large range in inorganic carbon is covered by AD and SQ sample aliquots, but this range may also be due to method-specific artefacts, and this will have to be further constrained by geochemical modelling analysis.

TIC and alkalinity are well constrained for the Malm aquifer (10.6 meq/L total alkalinity), but potentially masked by drilling fluid contamination in the Muschelkalk aquifer.

5.5.4 pH and partial pressure of CO_2

Like for carbonate alkalinity, it is not possible to adopt pH and calculated partial pressures of CO_2 from aqueous extract solution as representative for porewater conditions for reasons explained above.

pH measurements were done for advective displacement experiments, both in-line during sampling and shortly after sampling (one to few hours) on aliquots collected in closed syringes. Earliest in-line measurements range from 7.2 – 7.5 for the clayey sequence («Brauner Dogger» – Opalinus Clay – Staffelegg Formation), except for one value of 6.7 for one sample from the Staffelegg Formation (Fig. 4.7-14, Tab. 4.7-15), and laboratory measurements range from pH 7.3 – 7.7, except for the same sample with a value of 6.9 (Fig. 4.7-14, Tab. 4.7-12). pH values for the two deeper samples (Klettgau Formation, Kaiseraugst Formation) are 7.2 – 7.5 for in-line and laboratory meausrements. pH measurements for aliquots squeezed at lowest pressures are distinctly elevated, ranging from 8.3 – 8.7 for the clayey sequence, and 8.4 – 8.6 for samples from the Bänkerjoch Formation and Kaiseraugst Formation. A reason may be a pronounced strain-induced calcite dissolution leading also to the observed strong calcite supersaturation.

Calculated partial pressures of CO_2 in log bar units from first AD aliquots range from -1.7 to -2.5 based on straight speciation calculations, without restoration of calcite equilibrium at this stage. Depending on how calcite saturation is restored (CO_2 in/outgassing or adjustments to carbonate alkalinity) this will somewhat adjust both pH and pCO_2 values. The calculated partial pressures of CO_2 for samples from porewater squeezing are distinctly smaller, ranging from -3.2 to -3.5 for the clayey sequence, and approximately -4 for the deeper samples (Bänkerjoch Formation, Kaiseraugst Formation). This difference is mainly related to the much higher pH value measured for squeezed aliquots.

The ranges for pH and calculated pCO_2 observed for AD samples in this study are quite comparable to those obtained from the BUL1-1 and TRU1-1 borehole using the same method, and to other sites (Mont Terri Rock Laboratory, Schlattingen-1 geothermal well), although only a more limited dataset was available for the latter. The large acetate concentrations measured for some AD samples have not yet been rigorously addressed in the modelling interpretations but may have some impact on the carbonate system and pH control (buffering processes). The exact process of liberation of acetate is at present poorly constrained, and so are potential interactions. Apart from effects discussed above, there are also potentially disturbing processes involved that are common to all methods, namely related to drilling, unloading, sample handling and cooling from in situ temperature. Also, these processes will have to be included in restoring in situ porewater compositions.

5.6 External surface area and pore-size distribution

No author

No BET measurements (N_2 adsorption) had been performed for samples from the MAR1-1 borehole.

5.7 Cation exchange capacity and exchangeable cation population

Paul Wersin & Martin Mazurek

5.7.1 Corrected exchangeable cation data

As mentioned in Section 4.5, in order to obtain the exchangeable cation concentrations, the extracted cation data need to be corrected for cations dissolved in the porewater and the cations released from (potential) mineral dissolution. As shown from previous work (e.g. Hadi et al. 2019) and also indicated from speciation calculation presented in Section 4.5 (Tab. 4.5-4), carbonate mineral dissolution is minimised with the appropriate S/L ratio, extraction time and pH conditions. Such conditions were applied to the Uni Bern dataset.

Two correction methods were applied based on the concentrations of the main anions chloride and sulphate (Bradbury & Baeyens 1998, Hadi et al. 2019). The first correction method ($NaCl/Na_2SO_4$) attributes dissolved Cl and SO_4 from the Ni-extracts to Na and leaves the other cations unchanged. The second method ($NaCl/CaSO_4$) attributes Cl to Na and SO_4 to Ca, leaving the other cations unchanged. In both methods, the CEC is calculated from the sum of cations (ΣCAT) minus the concentrations (normalised to meq/kg_{dry_rock}) of Cl and SO_4. The corresponding data are shown in Tab. 5.7-1.

The relative difference between the uncorrected and corrected sums of extracted cations (ΣCAT) is within 7 – 21%. The largest difference is noted for the sample at 996.55 m depth from the Kaiseraugst Formation.

The graphic of Ni consumption vs. ΣCAT (Fig. 5.7-1) illustrates the good correlation between these two parameters. The values for the corrected ΣCAT is close to those of Ni consumption, albeit slightly lower by -16 to -5%. The good match between the two datasets supports the validity of the correction procedure for deriving the CEC based on the sum of cations. Further, Fig. 5.7-2 indicates a good correlation between clay-mineral content and CEC parameters, except for the data < 40 wt.-% clay-mineral content which display a considerable scatter.

The exchangeable cations are expressed as cation occupancies (in equivalent fractions) in Tab. 5.7-1. Na and Ca are the main exchangeable cations, followed by Mg and K. The Sr occupancies are considerably lower (0.3 – 1% of the CEC).

Tab. 5.7-1: Sum of cations and cation occupancies obtained from Ni-en extraction after correction (Uni Bern data)

First line for each sample indicates fractional cation occupancies (fr. oc.) obtained by the $NaCl/Na_2SO_4$ correction method, the second line those obtained by the $NaCl/CaSO_4$ method.

Type	**Depth** [m]	**Formation**	**Clay-mineral content** [wt.-%]	**ΣCAT raw** [meq/kg_{rock}]	**ΣCAT corr.** [meq/kg_{rock}]	**Na**	**K**	**Ca**	**Mg**	**Sr**
						Fractional occupancy (equivalent units)				
AD	521.06	«Parkinsoni-Würtembergica-Sch.»	42	93.9	86.1	0.39	0.07	0.36	0.17	0.011
						0.42		0.33		
AD	576.32	Wedelsandstein Fm.	28	80.7	71.0	0.36	0.07	0.39	0.17	0.012
						0.42		0.35		
AD	645.48	Opalinus Clay	52	101.0	93.7	0.42	0.07	0.35	0.15	0.009
						0.45		0.32		
AD	702.40	Opalinus Clay	67	124.3	116.1	0.42	0.06	0.38	0.14	0.008
						0.45		0.35		
AD	708.51	Staffelegg Fm.	33	71.0	62.6	0.38	0.07	0.38	0.16	0.009
						0.45		0.32		
AD	736.79	Staffelegg Fm.	59	119.9	114.5	0.47	0.07	0.34	0.11	0.006
						0.50		0.32		
AD	996.55	Kaiseraugst Fm.	30	71.9	57.0	0.50	0.11	0.31	0.08	0.003

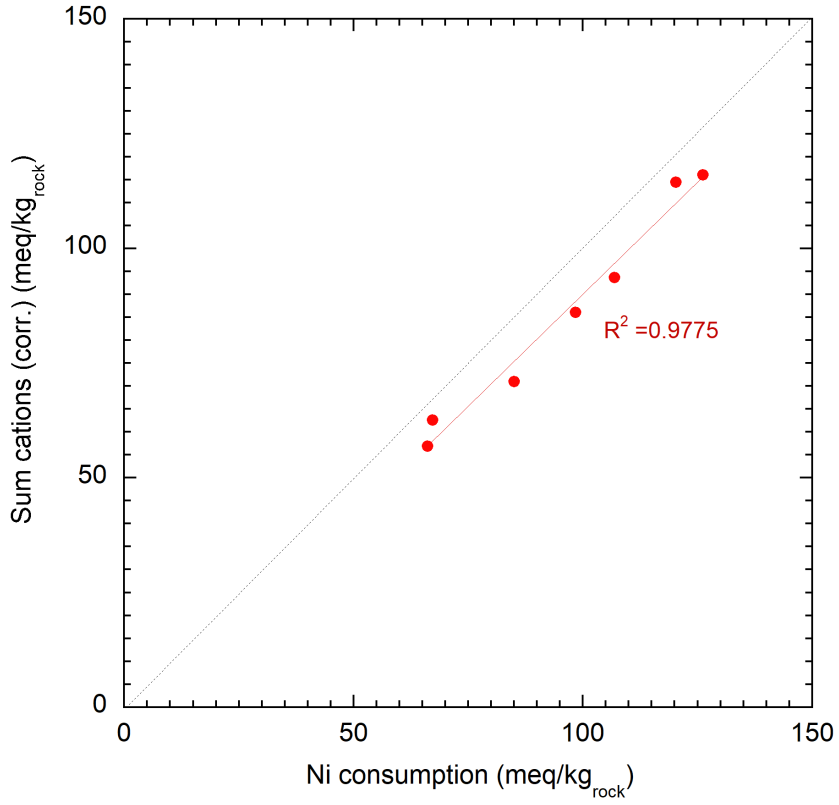

Fig. 5.7-1: Ni consumption vs. corrected sum of cations (data of Uni Bern)
Dashed line: 1:1 relationship.

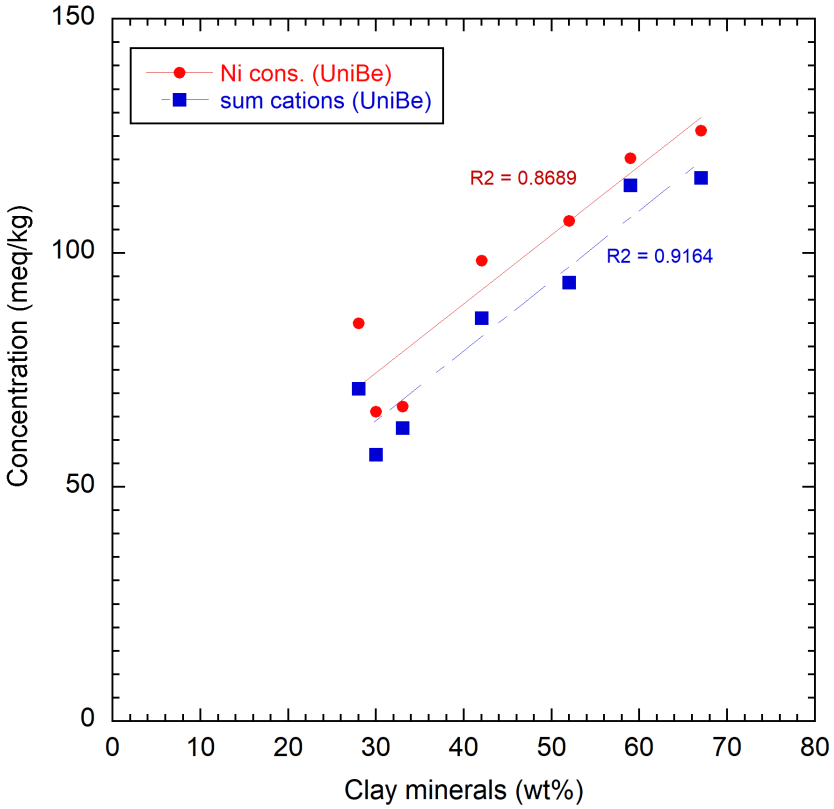

Fig. 5.7-2: CEC parameters as a function of the clay-mineral content (data of Uni Bern)

5.7.2 Comparison with data from PSI

A dataset including 20 samples from the MAR1-1 borehole was elaborated by PSI (Marques Fernandes & Baeyens *in prep.*). Samples originated from the Opalinus Clay and confining units («Brauner Dogger» and Staffelegg Formation).

In a first step, the CEC at PSI was estimated for all samples from Ni consumption with the Ni-en extraction method. Subsequently, the main dataset was generated via CsCl extraction, from which the CEC and the exchanger population were obtained. The CEC was derived by subtracting the anions (Cl, SO_4, HCO_3/CO_3) from the cations (Na, Ca, Mg, K, NH_4, Sr). The exchanger population was derived by two correction methods: (1) attributing Cl and SO_4 to Na and TIC to Ca, and (2) attributing Cl to Na and SO_4 and TIC to Ca. Note that these two methods are analogous to the ones used for the Uni Bern samples presented above, except for the additional consideration of TIC. The contribution of the latter is less relevant in the case of the Uni Bern data (see Tab. 4.5-4) because of the much higher solid/liquid ratios and thus a lower contribution of mineral dissolution to measured cation concentrations.

The conditions applied in the different extraction methods of PSI and Uni Bern are compared in Tab. 5.7-2. Important differences of the PSI methods relative to that of the Uni Bern are (i) the lower solid/liquid ratios, (ii) the smaller amount of solid mass and (iii) the more variable concentration of the index cation depending on the expected CEC. It should be noted that extraction conditions at PSI differed from those applied in boreholes BUL1-1 and TRU1-1. Thus, CsCl instead of $CsNO_3$ was used and the extract solution concentration was lowered by a factor of about 1.3 (Marques & Fernandes Baeyens *in prep.*). The use of CsCl made it necessary to determine the originally present Cl indirectly from aqueous extraction.

Tab. 5.7-2: Extraction conditions applied by Uni Bern and PSI

	University of Bern	**PSI**	**PSI**
Extraction method	Ni-ethylenediamine	Ni-ethylenediamine	CsCl
Extract solution concentration	98 – 107 mmol/L [a]	3.3 mmol/L	26 – 27 mmol/L
Solid/liquid ratio	~ 0.9 kg/L	~ 0.033 kg/L	0.04 – 0.19 kg/L
Amount of solid used	~ 30 g	~ 1 g	~ 1.5 – 8 g [a)]
Extraction time	24 h	24 h	24 h
Final pH	8.3 – 8.5	8.3 – 8.4	7.6 – 8.4
Sample disaggregation	Disintegration by hand to a few mm^3 pieces	Milled and passed through 1 mm sieve	Milled and passed through 1 mm sieve
Sample storage time prior to preparation	1 – 14 days	Several months	Several months
Extraction in glovebox	Yes	No	Yes

[a] S/L ratio adjusted to obtain the expected index cation consumption-to-CEC ratio.

Cation exchange capacity and corrected sum of extracted cations

The Ni-en consumption and the corrected ΣCAT data (the latter from Ni-en extraction in the case of Uni Bern and CsCl in the case of PSI) are shown in Fig. 5.7-3. From the comparison of these two datasets, the following findings can be derived:

- The CEC values obtained from Ni consumption exhibit consistent values for both datasets. In this context, it should be noted that the two datasets were not performed on the same samples, thus CEC variations at similar depths due to mineralogical variation can be expected. Comparing neighbouring samples, such as for example at depths of about 521 m, 580 m, 702 and 707 m, reveals remarkable agreement within the analytical uncertainties between the two datasets.
- The CEC values obtained from the corrected sum of cations also indicates consistency between Uni Bern and PSI but displays a slightly larger difference compared to the Ni consumption data. Comparison of neighbouring samples suggests slightly lower values for Uni Bern data.
- Both datasets indicate approximate consistency between Ni consumption and corrected ΣCAT data, the latter however being systematically lower. The difference relative to Ni consumption data is -16 to -5% for Uni Bern data (Fig. 5.7-1) and -10 to +3% for PSI data.
- In general, both datasets show the expected positive trend between clay-mineral content and CEC, both for Ni consumption and (corrected) sum of cations (Fig. 5.7-4). At a lower clay-mineral content, however, the correlation between these two parameters is rather poor, as illustrated in particular by the PSI dataset. Note that the correlations between CEC and the illite end-member or smectite end-member are generally not better than those of the total clay-mineral content.
- Both Ni consumption and corrected ΣCAT data from the two laboratories are thought to be representative measures of the CEC in view of the overall data consistency. The difference between these data is largely within the analytical error, although it should be noted that ΣCAT data tend to yield slightly lower values for Uni Bern data whereas the values for PSI are slightly higher.
- The scatter in CEC at a lower clay-mineral content is paralleled by that of the smectite end-member content (Fig. 5.7-5 left). It appears that below a clay-mineral content of about 40 wt.-%, the sampled rocks display a larger variation in smectite content with a tendency of increasing smectite/total clay ratio toward a lower clay-mineral content (Fig. 5.7-5, right).

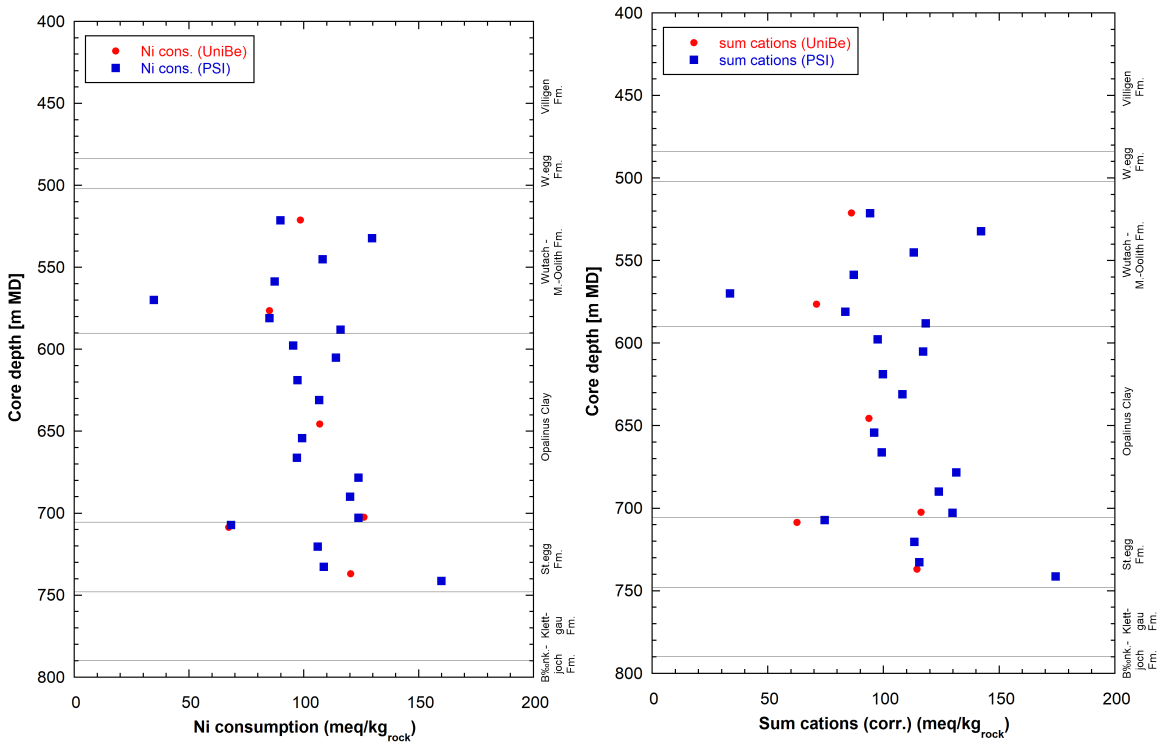

Fig. 5.7-3: Comparison of CEC data from Uni Bern and from PSI; Ni consumption data (left) and (corrected) sum of cations data (right)

The lowest Uni Bern sample at 996.55 m is not shown.

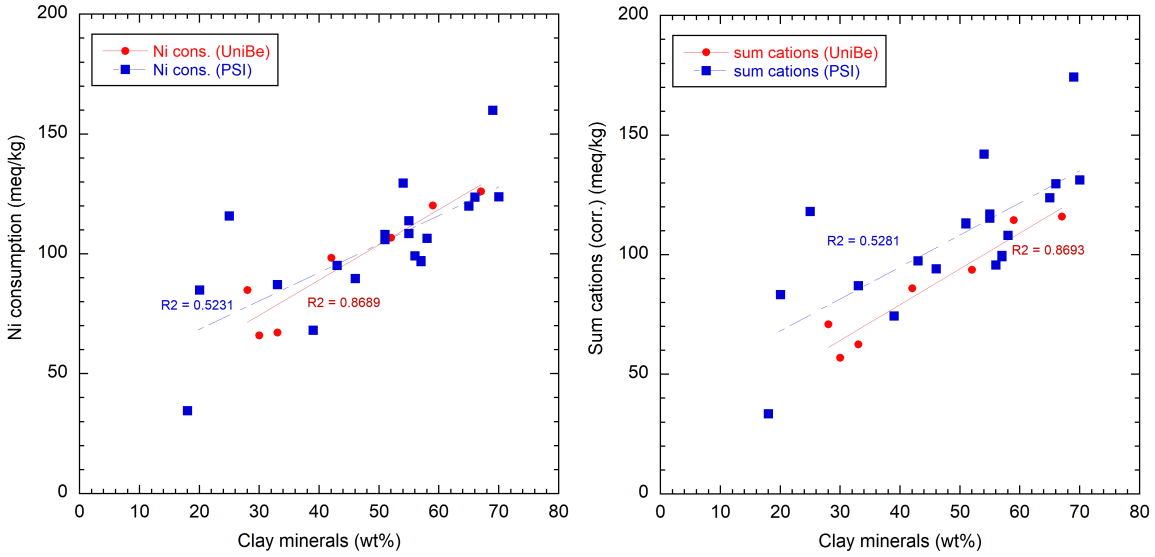

Fig. 5.7-4: CEC data as function of the clay-mineral content; left: Ni consumption data; right: Corrected sum of cations

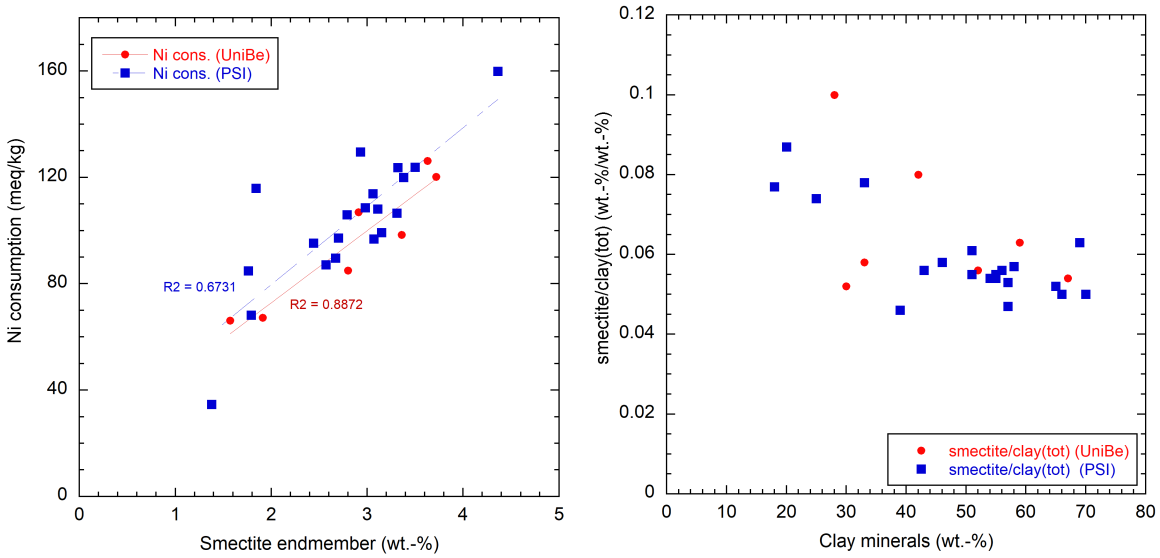

Fig. 5.7-5: Ni consumption as function of the smectite end-member (left) and smectite end-member/clay-mineral content ratio as a function of the clay-mineral content (right)

Exchangeable cation occupancies

The advantage of comparing fractional cation occupancies rather than the extracted cation concentrations is that they are normalised to the sum of cations (as proxy for the CEC) and do not directly depend on the clay-mineral content of the sample.

Fig. 5.7-6 shows the Na and Ca occupancies derived from the two correction methods. Note that in method 1 Cl and SO_4 are attributed to Na, whereas in method 2, SO_4 and, in the case of PSI data, also TIC is attributed to Ca. Thus, the Na fraction is minimised in method 1 and maximised in method 2, while the opposite is true for Ca.

Comparison of Uni Bern and PSI data illustrates consistent trends for all measured exchangeable cations (Na, Ca, Mg, K, Sr) as illustrated in Figs. 5.7-6 to 5.7-8. There is one sample at a depth of 569.87 m from the Wedelsandstein Formation from the PSI set that falls off the general trend, exhibiting lower Na, higher Ca/Na ratio, higher K and as well as higher amounts of extracted Cl. Disregarding this sample, the two datasets reveal similar fractional occupancies for all measured cations except for K (see below).

The occupancies for the main cations Na and Ca indicate a weak increase with depth for Na and an even weaker decrease for Ca across the «Brauner Dogger»-Staffelegg Formation sequence, i.e. a decreasing Ca/Na ratio (Fig. 5.7-8, right). The Mg and K profiles are flat, whereas the Sr profile shows a notable decrease with depth.

Regarding K, the dataset from PSI systematically shows higher fractional occupancies (by a factor of slightly below two) than those obtained from Uni Bern samples. The same feature was observed for the Bülach-1 and Trüllikon-1 boreholes (Mazurek et al. 2021, Aschwanden et al. 2021). This suggests that an additional pool of K present in illite (possibly from the interlayer) is mobilised by Cs in the case of PSI, which is less the case for the Ni method used by Uni Bern.

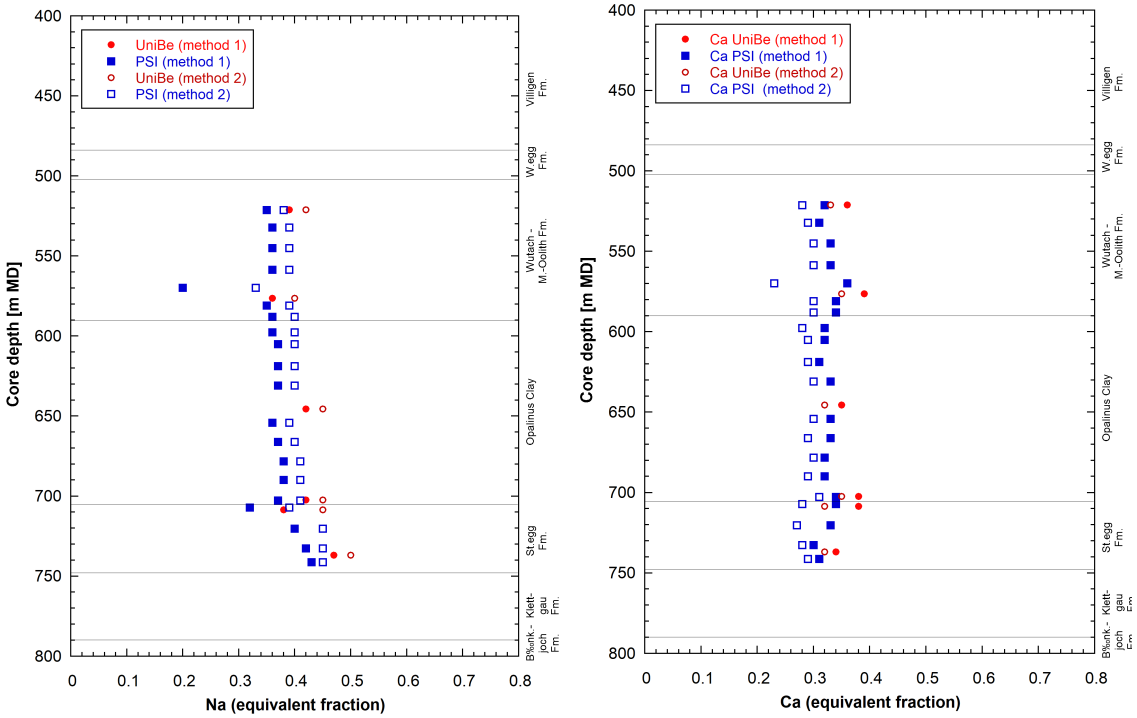

Fig. 5.7-6: Na (left) and Ca (right) occupancies according to Uni Bern and PSI data

The lowest Uni Bern sample at 996.55 m is not shown.

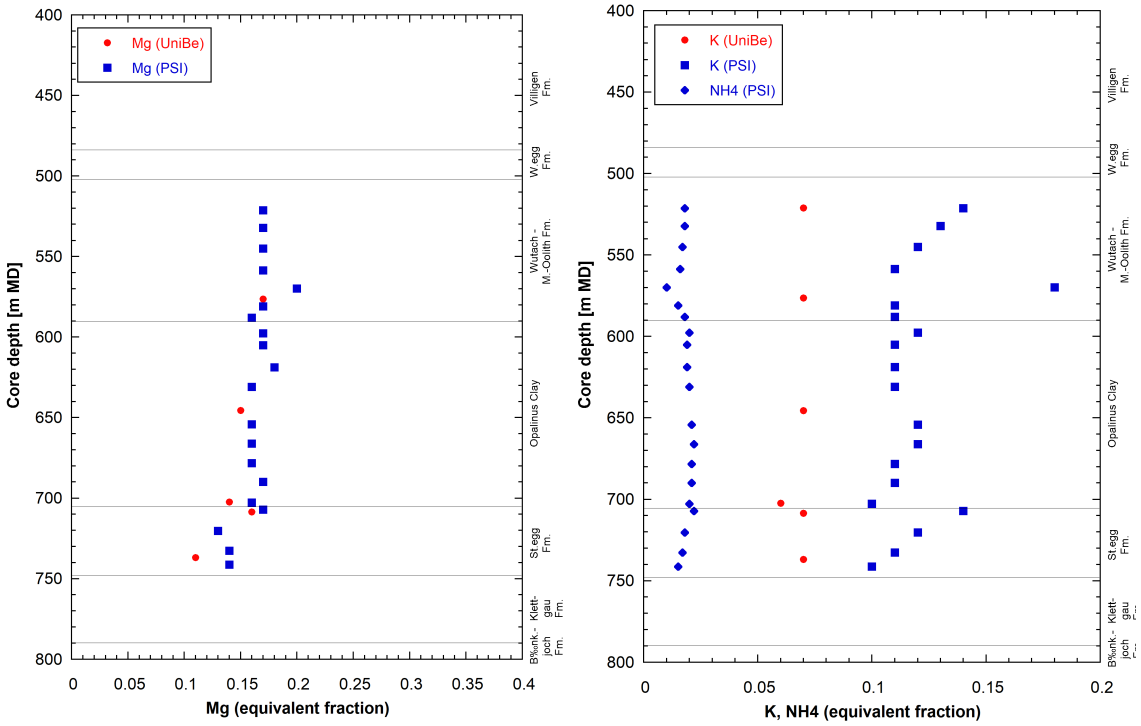

Fig. 5.7-7: Mg (left) and K, NH_4 (right) occupancies according to Uni Bern and PSI data
The lowest Uni Bern sample at 996.55 m is not shown.

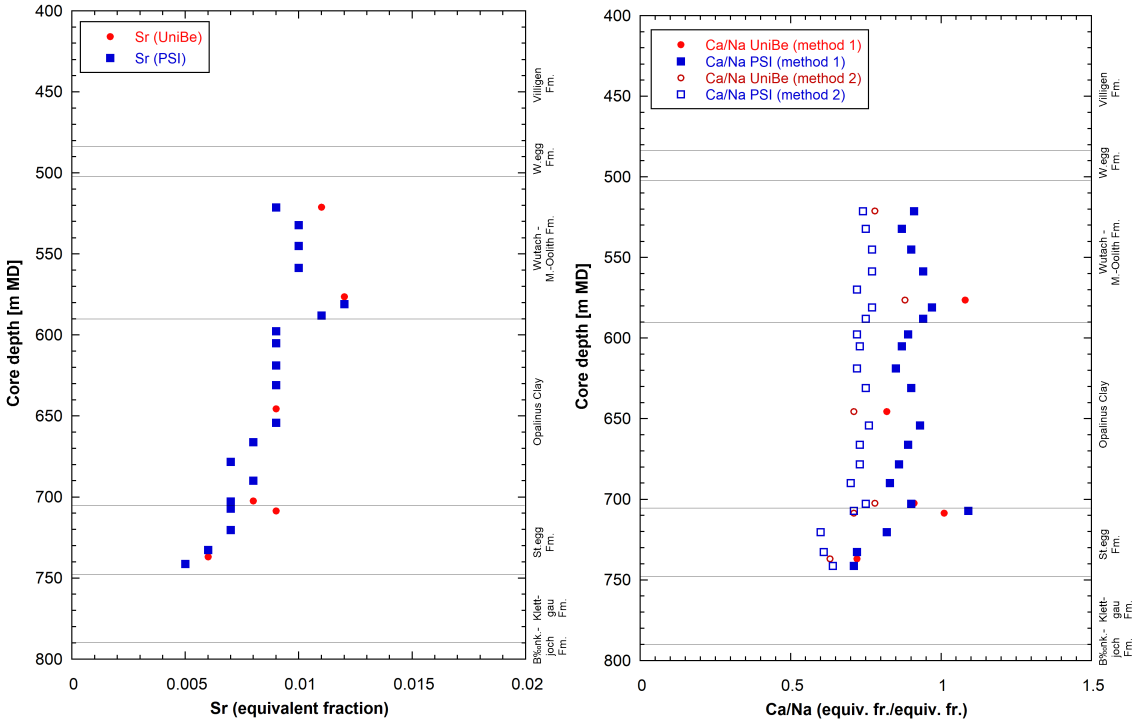

Fig. 5.7-8: K occupancies (left) and Ca/Na ratios (right) according to Uni Bern and PSI data

The lowest Uni Bern sample at 996.55 m is not shown.

Extracted anions

The amounts of Cl and SO_4 extracted are consistent between the two datasets of PSI and Uni. Bern except for the higher amount of Cl extracted from sample 569.87 m by PSI (see above; Fig. 5.7-9). This outlier is possibly due to contamination from fluid inclusions released from quartz (58 wt.-%) from this siltstone sample. Note that PSI passed the sample material through a 1 mm sieve after milling, while Uni Bern only mildly disintegrated its rock samples and used larger particles for analysis (see Tab. 5.7-2) – and so minimised this type of contamination. The Cl data indicate a decreasing trend with depth within the Opalinus Clay and Staffelegg Formation, in line with data from aqueous extraction (Section 4.4). Sulphate exhibits more constant levels in these two units.

Total inorganic carbon (TIC) measured in the PSI extracts is 5 – 10 mmol/$kg_{dry\ rock}$ except for sample 569.87 m with 2 mmol/$kg_{dry\ rock}$ (not shown). This is higher than expected for Uni Bern extracts. TIC was not measured in the latter but calculated to be below 1 mmol/$kg_{dry\ rock}$ based on the assumption of calcite equilibrium (data not shown). The higher TIC in the PSI extracts is explained by the lower S/L ratio which induces a higher proportion of dissolved carbonate from carbonate minerals.

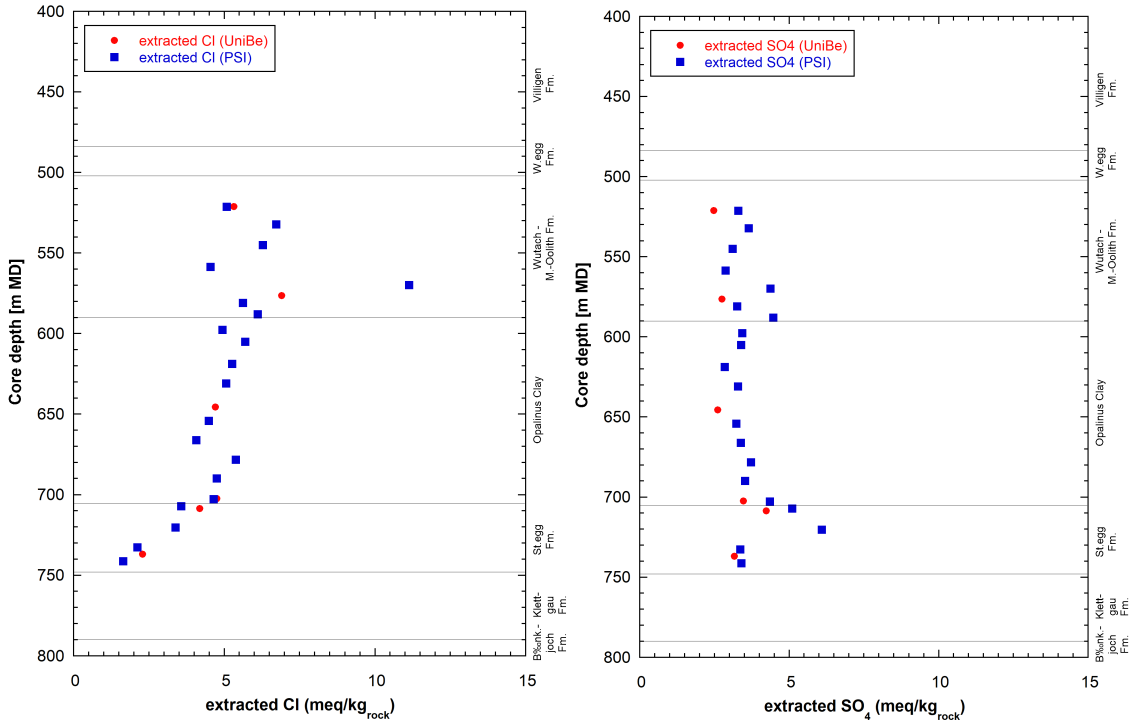

Fig. 5.7-9: Extracted Cl (left) and SO_4 (right) according to Uni Bern and PSI data
The lowest Uni Bern sample at 996.55 m is not shown.

5.8 Stable water isotopes

Lukas Aschwanden & H. Niklaus Waber

5.8.1 Comparison between different methods for the determination of porewater compositions of stable isotopes

The porewater oxygen and hydrogen isotope compositions were determined using three different methods including the isotope diffusive-exchange (Section 4.8), advective displacement (Section 4.7) and high-pressure squeezing (Section 4.6) methods. Data of the three techniques are available for the sections 520 – 800 m and 990 – 1'020 m where clay-rich rocks dominate, and all methods can be applied. For the clay-poor rocks of the Malm, Keuper and the Muschelkalk only data from isotope diffusive-exchange experiments are available. For the advective displacement technique, the average of the first two displaced solution aliquots is considered as being most representative for the in situ porewater. For the squeezed water, the one obtained at the lowest squeezing pressure (200 MPa or 300 MPa) is considered as being most representative for the in situ porewater.

All the porewater isotope data, together with those for the two groundwater samples from the Malm and the Muschelkalk aquifer (*cf.* Section 2.3), are shown in Fig. 5.8-1 as a function of depth. For isotope data from isotope diffusive-exchange experiments the error bars reflect the propagated experimental and analytical uncertainty, however, for isotope data from advective displacement and high-pressure squeezing experiments only the analytical error is illustrated. In general, there is a good agreement (within the uncertainty) between porewater $\delta^{18}O$ and $\delta^{2}H$ values obtained from isotope diffusive-exchange experiments and high-pressure squeezing, whereas most of the isotope data from advective displacement show lower values. The reason for this is currently unknown.

5.8.2 Comparison with groundwater data and depth profiles

The groundwater in the Malm aquifer («Felsenkalke» + «Massenkalk») was sampled at a depth of 335.6 – 352.6 m. At this shallow depth no porewater isotope data is available for comparison. The porewater isotope profile starts at the base of the Villigen Formation at a depth of 464.9 m where the porewater shows $\delta^{18}O$ and $\delta^{2}H$ values of around -4 and -40‰ VSMOW, respectively. These values are distinctly enriched in the heavy isotopes compared to the groundwater in the «Felsenkalke» + «Massenkalk» 110 m further up ($\delta^{18}O$ = -8.72 and $\delta^{2}H$ = -68.5‰ VSMOW, respectively; Lorenz et al. 2021). Owing to the lack of porewater isotope data in the upper Malm it cannot be evaluated to what extent the groundwater exchanged with the adjacent porewater and how they relate to the porewater at the base of the Villigen Formation (e.g. continuous evolution or water of different origin/evolution).

The porewater isotope composition shows a continuous evolution in $\delta^{18}O$ and $\delta^{2}H$ from the base of the Villigen Formation down to the Seebi Member in the Klettgau Formation where a local minimum is indicated. This minimum coincides with a distinct trend reversal in the profile of deuterium excess (Fig. 4-8.5). Although no groundwater sample could be collected in the Keuper of MAR1-1 (owing to a low hydraulic conductivity of 2.9×10^{-10} m/s; see Dossier VII), the shapes of the isotope and deuterium excess profiles indicate that exchange with water bodies located in the Seebi Member of the Klettgau Formation plays a role for the evolution of porewater $\delta^{18}O$ – $\delta^{2}H$ signatures in the interval Villigen Formation – Staffelegg Formation.

The $\delta^{18}O$ and $\delta^{2}H$ values of groundwater from the Muschelkalk aquifer agree well with those of the porewater obtained from the sample in the packed-off interval and from the nearby sample at the base of the Bänkerjoch Formation. The Muschelkalk groundwater appears to represent minima of $\delta^{18}O$ and $\delta^{2}H$ and the adjacent porewaters indicate remarkably steep gradients towards heavier values up- and downwards. Such steep gradients indicate either that the isotope signal in the groundwater is geologically young, and/or the diffusion coefficients in the clay-poor Schinznach Formation are very low.

As indicated by aqueous extracts, all drill core samples from the Schinznach Formation plus two other samples, one in the underlying Zeglingen Formation and one in the overlying Bänkerjoch Formation, show variable degrees of contamination by drilling fluid (*cf.* Section 4.4). In the Muschelkalk the drilling fluid is enriched in ^{18}O (-8.97‰ VSMOW) and even more in ^{2}H (-49.6‰ VSMOW; Lorenz et al. 2021) compared to the in situ porewater. The good agreement between the isotope composition of the groundwater and the porewater derived from contaminated samples in or in the direct vicinity of the packed-off interval indicates that for these samples the contamination by drilling fluid does not measurably affect the porewater isotope composition. For the contaminated samples outside the packed-off interval it can be noted that an e.g. 10% admixture of drilling fluid to a porewater with isotope signatures similar to those at the top of the Schinznach Formation ($\delta^{18}O$ = -11.97‰ VSMOW; $\delta^{2}H$ = -87.9‰ VSMOW) – i.e. porewaters isotopically most different to the drilling fluid – would shift their $\delta^{18}O$ and $\delta^{2}H$ values by 0.3 and 3.5‰ VSMOW, respectively, towards heavier values (based on mixing calculations of drilling fluid and the calculated isotope composition of the porewater). These are relatively small shifts considering the overall large variability of the porewater isotope signatures in the interval Bänkerjoch Formation – Zeglingen Formation and thus, this gives confidence in the observed isotope trends in this section of the profile.

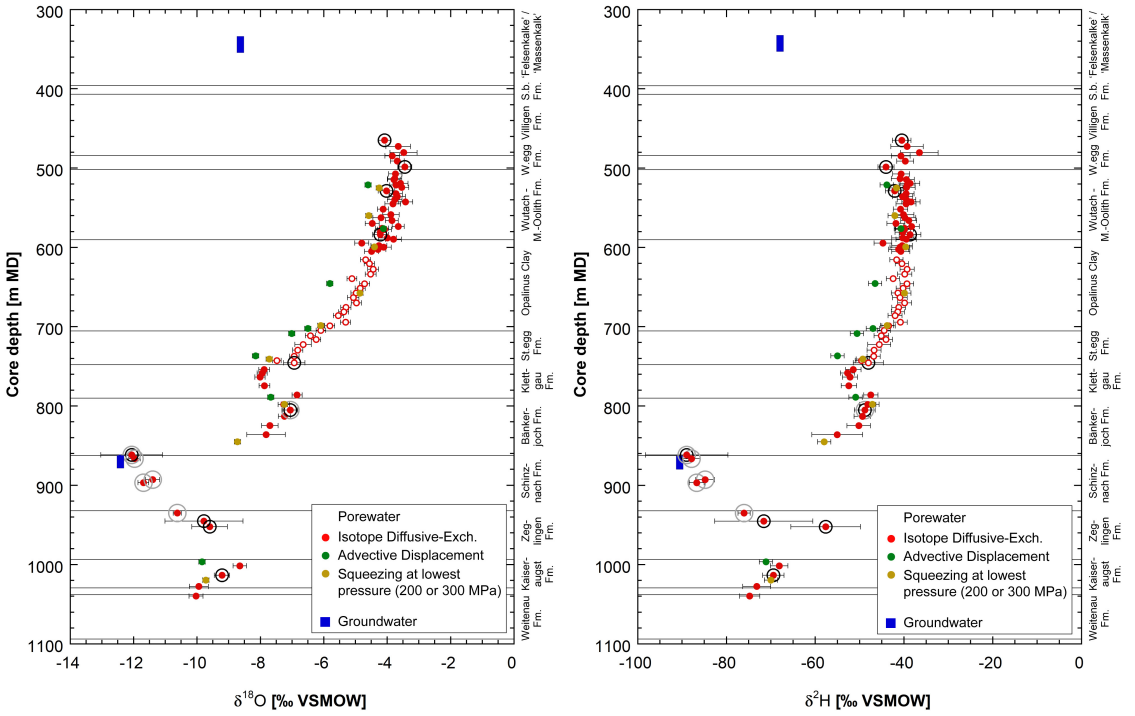

Fig. 5.8-1: Depth trends of $\delta^{18}O$ and $\delta^{2}H$ in groundwater and porewater derived by all techniques

Bars indicate propagated analytical errors (diffusive exchange) or simple analytical errors (squeezing, advective displacement). Groundwater data are from Lorenz et al. (2021). Samples in circles are less reliable owing to experimental artefacts (black circles; *cf.* Section 4.8) and/or possible contamination by drilling fluid (grey circles; *cf.* Section 4.4).

5.8.3 $\delta^{18}O$ versus $\delta^{2}H$ and comparison with Global Meteoric Water Line

Fig. 5.8-2 illustrates all data in a $\delta^{18}O$ vs. $\delta^{2}H$ diagram. Such diagrams provide information, e.g. on climatic conditions during recharge and indications on water – rock interactions or mixing of different water components. The isotope composition of the groundwater collected in the «Felsenkalke» + «Massenkalk» plots slightly to the right of the GWML in the $\delta^{2}H$ range of modern recharge. The deviation from the GMWL is likely due to mixing with isotopically different water components and/or water – rock interactions. Interestingly, 110 m further down at the base of the Villigen Formation, porewaters are distinctly enriched in ^{2}H and ^{18}O and their isotope composition plots far to the right of the GMWL. As outlined above, the significance of the groundwater in the «Felsenkalke» + «Massenkalk» for the evolution of porewater $\delta^{18}O$ and $\delta^{2}H$ values further down in the sequence cannot be assessed owing to the lack of porewater isotope data in the upper Malm (indicated by the stippled red arrow 1 in Fig. 5.8-2).

Shown by the solid red arrow 2 in Fig. 5.8-2, the porewater isotope composition shows a continuous evolution in $\delta^{18}O$ and $\delta^{2}H$ from the base of the Villigen Formation to the base of the Staffelegg Formation, starting with $\delta^{18}O$ and $\delta^{2}H$ porewater values far to the right of the Global Meteoric Water Line towards values that fall on the GMWL in the lower parts of the Staffelegg Formation. This suggests a significant meteoric component in the latter porewaters. The pronounced deviation of the porewater $\delta^{18}O$ – $\delta^{2}H$ signatures with respect to the Global Meteoric Water Line in the upper part of the section indicates long residence times of these porewaters, with values affected by exchange with groundwater in over- and underlying water-conducting zones, and possibly by water-rock interactions. The evolution of the isotope signatures from the Villigen Formation down to the base of the Staffelegg Formation is dominated by exchange with groundwater in the underlying water-conducting zones. The $\delta^{18}O$ and $\delta^{2}H$ profiles with their negative excursions in the Klettgau Formation suggest the presence of mobile groundwater at these depths (see Section 5.8.2).

Similar to the porewater at the base of the Staffelegg Formation, isotope signatures of porewater in the Klettgau Formation and in most of the Bänkerjoch Formation also plot along the GMWL indicating the presence of a significant meteoric component. The $\delta^{18}O$ and $\delta^{2}H$ values of these porewaters are heavier than those of modern recharge. At the base of the Bänkerjoch Formation and in the Schinznach Formation the groundwater and porewater still fall on the GMWL, however, they show distinctly more negative $\delta^{18}O$ and $\delta^{2}H$ values than that of modern recharge, indicating infiltration under colder climate conditions (solid red arrow 3 in Fig. 5.8-2). Following the above hypothesis of exchange between porewater and groundwater in the Seebi Member, exchange in the system Keuper-Muschelkalk seems more advanced than the exchange in the system Keuper – Malm further up in the profile, probably due to the rather short distance between the Keuper and the Muschelkalk groundwaters (ca. 100 m).

Porewater in the underlying Zeglingen and Kaiseraugst Formations again show isotope signatures enriched in ^{18}O and ^{2}H compared the Muschelkalk porewater and plot close to or slightly to the right of the GMWL (the single outlier being a less reliable value) in the range of modern recharge (solid red arrow 4 in Fig. 5.8-2). This might indicate that they either represent warmer climate infiltrates or have been modified by exchange with groundwater that has infiltrated under warmer climatic conditions.

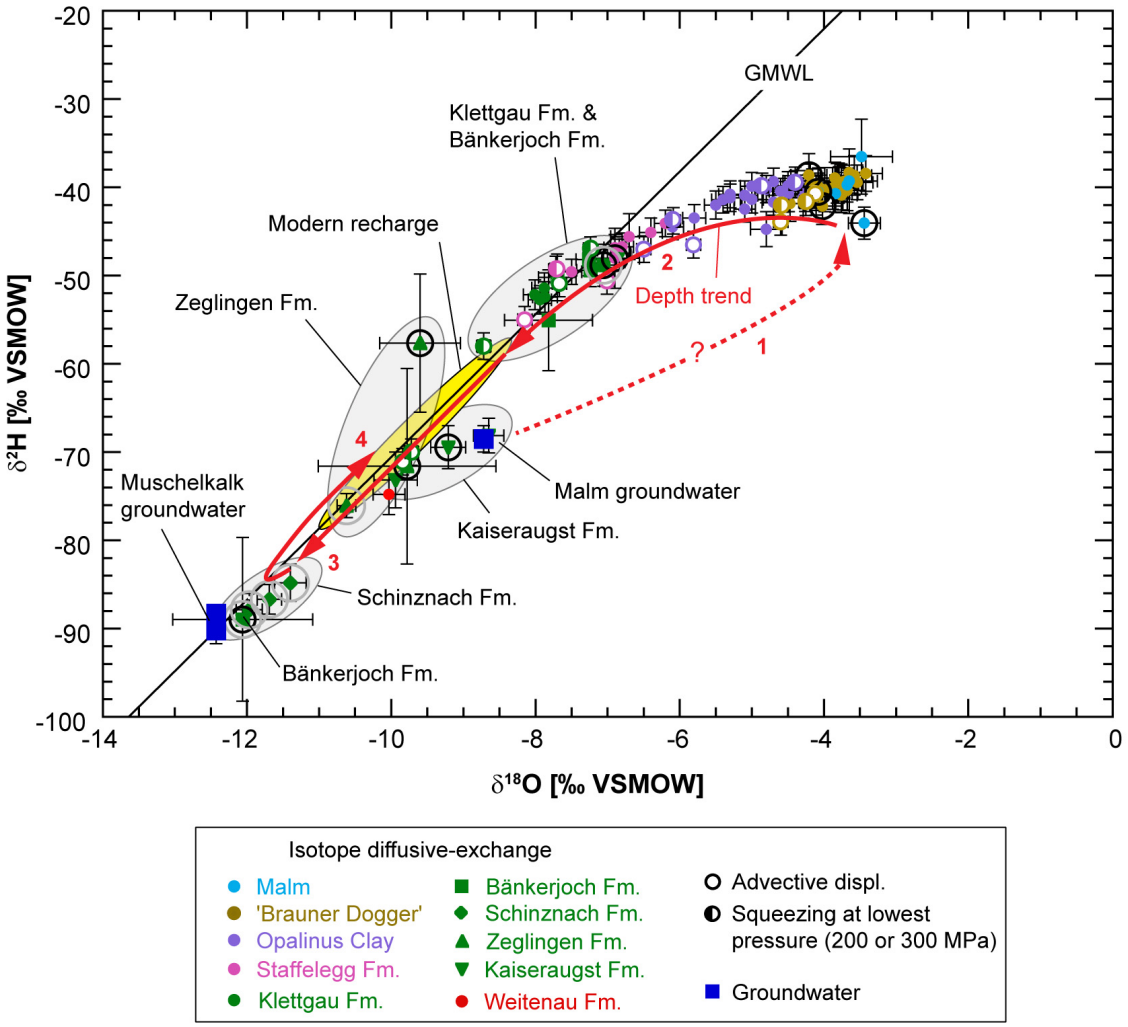

Fig. 5.8-2: $\delta^{18}O$ vs. $\delta^{2}H$ for groundwater and porewater derived by all techniques

Bars indicate propagated analytical errors (diffusive exchange) or simple analytical errors (squeezing, advective displacement). Groundwater data are from Lorenz et al. (2021). GMWL = Global Meteoric Water Line (defined as $\delta^{2}H = 8\ \delta^{18}O + 10$; Craig 1961). Range of modern recharge from Kullin & Schmassmann (1991). Samples in circles are less reliable owing to experimental artefacts (black circles; *cf.* Section 4.8) and/or possible contamination by drilling fluid (grey circles; *cf.* Section 4.4). See text for details on the numbering of red arrows.

5.9 Overreaching topics

Urs Mäder

5.9.1 The porewater – depth profile

There are a number of features in the porewater composition and water isotopic profiles that do not lend themselves to straightforward interpretations. It is beyond the scope of this data report to resolve such issues, but what is evident just from browsing through the combined datasets should be briefly addressed here. In contrast to other TBO boreholes, MAR1-1 offers a continuous dataset from the lower parts of the Malm to the top of the Permian strata. The profile is potentially influenced by aquifers in the Malm («Felsenkalke» + «Massenkalk»), Keuper (Klettgau Formation), Muschelkalk (Schinznach Formation), and the Buntsandstein (Dinkelberg Formation). A summary plot (Fig. 5.9-1) directly compares the depth profiles with paramaters $\delta^{18}O$, Cl and Br/Cl.

The profiles from the base of the Villigen Formation across the clayey confining sequence («Brauner Dogger» – Opalinus Clay – Staffelegg Formation) are well defined and quite similar to the profiles encountered in TRU1-1. The isotope profile evolves from the least negative $\delta^{18}O$ – $\delta^{2}H$ values to the right of the GMWL (Villigen Formation) to the GMWL at the base of the Staffelegg Formation and Klettgau Formation (Fig. 5.8-2). The Br/Cl ratio of this section forms a smooth trend, well below the present-day seawater ratio, gradually decreasing from values near that of the Malm groundwater to a low value in the Staffelegg Formation and increasing to a local maximum in the Klettgau Formation (Figs. 5.9-1 and 5.2-4). The porewater chloride concentration profile (scaled aqueous extracts and direct samples) forms a lopsided bulging curve, from loosely constrained 3 – 6 g/L at the top to a maximum around 7 – 9 g/L in the «Brauner Dogger» and a moderately decreasing trend across the Opalinus Clay, followed by a steep decrease across the Staffelegg Formation to values below 1 g/L in the Klettgau Formation (Figs. 5.9-1 and 5.2-2).

The genetic link between the well-characterised groundwaters of the Malm aquifer and the onset of our porewater geochemical characterisation remains unclear due to the information gap of more than 100 m between water sampling depth and start of coring section (see details in Section 5.8, Fig. 5.8-2, stable water isotopes).

The 'Keuper aquifer' (Klettgau Formation, Seebi Member) could not be sampled due to too low hydraulic conductivities (~ 10^{-10} m/s), but its effect is clearly evident isotopically and chemically. Isotopically, it is seen as local minimum in the $\delta^{18}O$ and $\delta^{2}H$ profiles (Figs. 5.8-1 and 5.9-1), located approximately on the GMWL. It is interesting to note that the chlorinity found in the Keuper aquifer at the TRU1-1 location matches porewaters scaled from the aqueous extracts in this profile, and the major-component chemistry of the groundwater may also be similar.

The next segment of the profile across a lithologically heterogeneous marly sequence (Klettgau/Bänkerjoch Formation) and the upper anhydrite rocks of the Bänkerjoch Formation to the Muschelkalk aquifer at the top of the Schinznach Formation shows local maxima in $\delta^{18}O$ and $\delta^{2}H$ profiles near the top of the Bänkerjoch Formation and a sharp decrease to the absolute minima of the entire profile at the transition to the Schinznach Formation. While the samples from the Bänkerjoch Formation are still near the 'Keuper aquifer' signal on the GMWL, the samples from the top of Schinznach Formation are also on the GMWL but near the Muschelkalk groundwater forming the lowest $\delta^{18}O$ – $\delta^{2}H$ value (Figs. 5.9-1, 5.8-1 and 5.8-2). The chloride concentration forms a relatively sharp bulge with a maximum close to that of water isotopes (uppermost Bänkerjoch Formation), with porewater concentrations ~ 9 g/L near those found in the Opalinus

Clay (Figs. 5.9-1 and 5.2-1). The Br/Cl profile is more complex, with a local minimum at the Klettgau/Bänkerjoch Formation transition, and some elevated values at the Bänkerjoch/Schinznach Formation transition that are at odds with the very low value of the Muschelkalk groundwater (Figs. 5.9-1 and 5.2-4).

The Muschelkalk aquifer bears a meteoric water isotope signature and forms the most negative $\delta^{18}O - \delta^{2}H$ value encountered in the profile. It is not easy to reconcile the extremely low chloride concentration of this groundwater of only 18 mg/L (sampled) or 9 – 22 mg/L (corrected for contamination; Lorenz et al. 2021). As mentioned above, nearest samples from the base of the Bänkerjoch Formation still contain 6'000 mg/L of chloride (aqueous extracts scaled to water content), and those from just below the Muschelkalk aquifer indicate 1'700 – 2'100 mg/L. Only one sample from the very top of the Schinznach Formation yielded a very low chlorinity of 160 mg/L. It should be noted that in this region (868 – 887 m) major fluid losses caused disturbances and also resulted in a switch from potassium-silicate mud to sodium-silicate mud, although these muds should not significantly disturb components like chloride or bromide. There is a scaricity of data in some parts of this profile segment, including some gaps, and this makes interpretation more speculative.

The remainder of the profile extends from below the transmissive zone in the Muschelkalk aquifer across the Schinznach Formation (dolostones, some limestones), the Zeglingen Formation (dolostone at top, anhydrite rocks), the Kaiseraugst Formation (claystones, marls), the Dinkelberg Formation ('Buntsandstein', no sample) to the top of the Weitenau Formation (Permian sandstones, breccias). The stable water isotope profile is based on a more limited number of samples but forms a relatively simple rise to less negative values with a relative maximum in the anhydrite rocks of the Zeglingen Formation and is decreasing somewhat towards the deepest analysed samples (Figs. 5.8-1, and 5.9-1). In a $\delta^{18}O - \delta^{2}H$ cross-plot (Fig. 5.8-2), the porewaters of the lower Schinznach Formation are still near the Muschelkalk groundwater signature, but then move roughly along the GMWL to less negative values, with data spreading a bit off the GMWL (shifted to the left for the Zeglingen Formation, to the right for the Kaiseraugst Formation). A single sample from the Weitenau Formation (Permian) is near the GMWL, in a region of overlap for samples from the Kaiseraugst and Zeglingen Formations, just a bit to the right of present-day recharge. The chloride profile for this section (Figs. 5.9-1 and 5.2-1) is also relatively simple but loosely constrained due to large uncertainties obtained for water content. Chlorinity rises sharply from 1 – 2 g/L in the dolostones of the Zeglingen Formation to a maximum of 150 g/L in the anhydrites of the Zeglingen Formation (with a large uncertainty, see explanation below). It drops also sharply across the Kaiseraugst Formation (constrained additionally by data from squeezing and advective displacement) to 3 – 4 g/L at the base of the Kaiseraugst Formation and in two samples of the Weitenau Formation. The Br/Cl profile (Figs. 5.9-1 and 5.2-4) shows strangely elevated values in the Schinznach Formation at the level of the Muschelkalk aquifer, rises sharply to a maximum in the Schinznach Formation, drops sharply to a minimum at the base of the Zeglingen Formation, and then rises a bit towards the deep end of the profile. The samples of the Schinznach Formation (and top of Zeglingen Formation) also define an entirely different trend in the Br vs. Cl cross-plot (Fig. 4.4-1), located entirely to the left of the seawater line. Some of the scatter in the data may also be due to difficulties in Br analysis.

The region of the Dinkelberg Formation ('Buntsandstein', no sample) and the top of the Permian may represent an aquifer, but there are no samples or hydraulic data available. In the Benken borehole, this aquifer contains 252 mg/L Cl, and a $\delta^{18}O$ of -11.04‰ VSMOV (Gimmi & Waber 2004).

The dissynchrony in the water isotope, chloride and Br/Cl profiles below the Muschelkalk aquifer is presently not understood. The elevated chloride concentrations in the anhydrite rocks are not well constrained in terms of absolute chlorinities, but the anomaly is real, and the source cannot be from leached rock salt during aqueous extraction (halite dissolution would lead to much higher concentrations than seen in the extracts). Data indicate an additional and entirely different source for Br than in all other parts of the profile. Rock salt consisting of halite but not sylvite is supposed to be depleted of bromide relative to chloride, but evidence here suggests that a high-Br source was available in this part of the stratigraphic section. Rock salt is present in the Benken borehole, but not in the MAR1-1 and TRU1-1 boreholes, and so a halite source is available within the Zeglingen Formation at some distance towards Benken. There is presently no Br/Cl data available on this rock salt from Benken, but this would be helpful to resolve some of these issues.

Porewater contents determined in anhydrite rocks may be subject to additional uncertainties than just arising from mass measurements, and therefore also scaling of aqueous extract concentrations to porewater are bearing the same uncertainties. This uncertainty arises because the samples recovered from depth are no longer at porewater equilibrium with anhydrite, and anhydrite will tend to transform to gypsum, the thermodynamically more stable Ca-sulphate at room temperature. Anyhdrite-rich rocks may therefore consume a significant fraction of the porewater solvent. In theory, this gypsum-bound water will be given off again during drying of samples at 105 °C (for several weeks), and so may off-set the aforementioned water consumption. The rates of this water uptake and release at laboratory conditions due to the hydration of anhydrite and dehydration of gypsum are not known at the relevant conditions. Note, that such processes will not affect ion ratios, such as Br/Cl. The anion-exclusion effect in relatively clay-rich anhydrite layers is not known, presently, two such samples from the Zeglingen Formation (824.70 m, 836.13 m) with about 30 wt.-% clay content are responsible for the highest chloride concentrations in the profile (80 g/L from aqueous extract recalculated to water content, and scaled to 150 g/L by the anion-exclusion effect). This maximum chlorinities should therefore be viewed with caution, but the general shape of this preserved 'anomaly' is thought to be valid.

Many samples from the deep part of the profile that displayed unusually large scatter in the water content (determined in triplicate) were re-analysed, using just a single already dried subsample with known water content for aqueous leaching (Section 4.4). The new data agree well with the old data in terms of the Br/Cl ratio, and so attest to the quality of analysis. Several of the new chloride concentrations are associated with much smaller water contents than the average value obtained from the former triplicate determination. This yields a chloride anomaly of up to 80 g/L rather than the previously obtained 40 g/L (and scaled to even larger values by the ion-exclusion effect, see paragraph above). The shape of the new profile is the same, but the concentration uncertainty is much smaller than the previously obtained very large error bars from some of the triplicate samples. The steepness of this chloride anomaly also attests to the tightness of this rock package consisting of the lower part of the Schinznach Formation, the Zeglingen Formation and the Kaiseraugst Formation, because it represents unlikely just a short-lived anomaly.

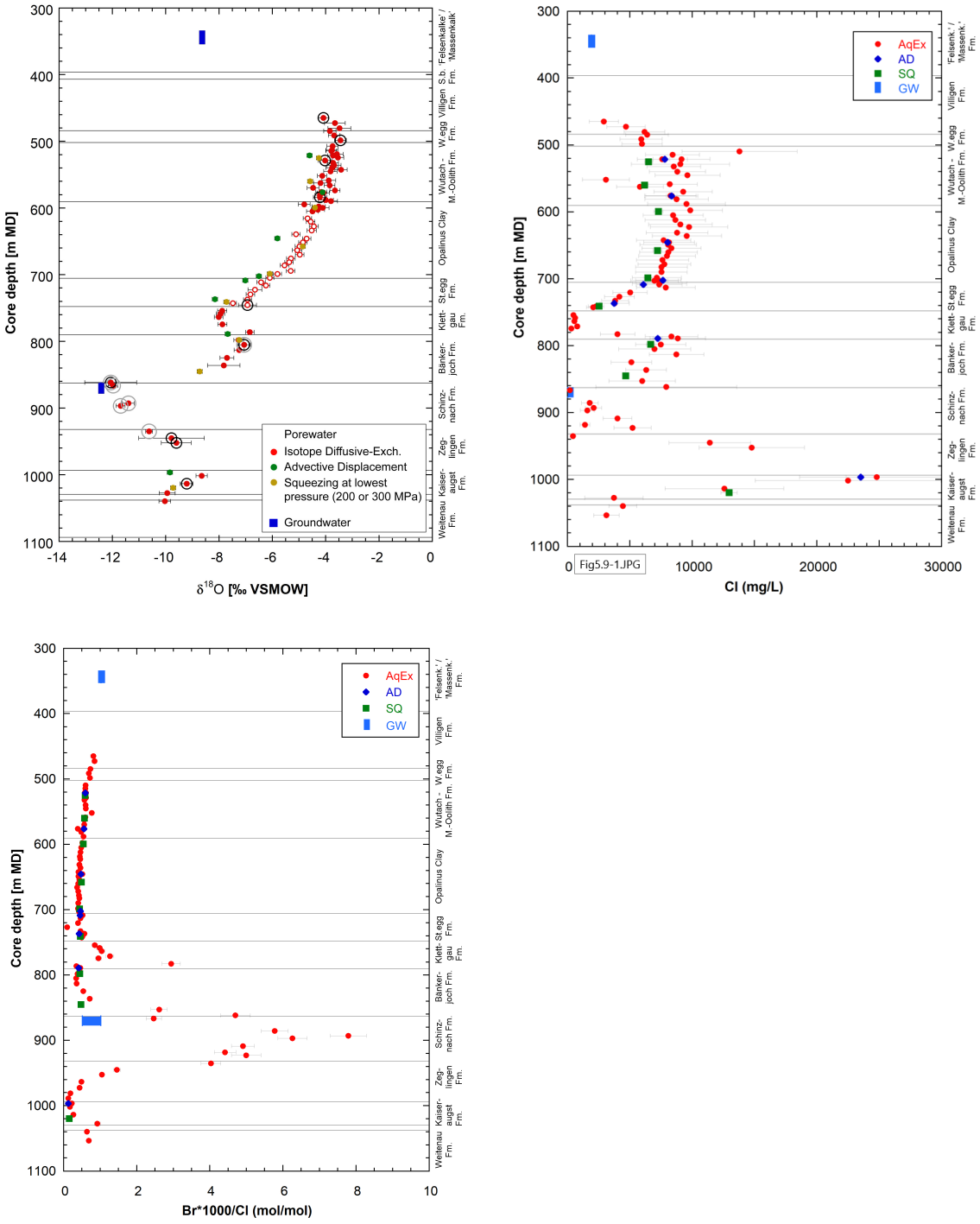

Fig. 5.9-1: Depth profiles for $\delta^{18}O$, Cl and Br/Cl

See Fig. 5.8-1 (left), Fig. 5.2-1 (left) and Fig. 5.2-4 (left) for detailed legend information. The aqueous extracts in the Cl profile are scaled to wtaer content and the chloride-accessible porosity. Some data points in the Cl profile (middle) from the Zeglingen Formation Plot beyond the X-axis range.

5.9.2 Differences and commonalities between porewater aliquots obtained from squeezing and advective displacement

The two so-called direct sampling methods, porewater squeezing (9 SQ samples) and advective displacement (8 AD samples), aim at obtaining sample aliquots that are porewater like. Both approaches mobilise porewater and it is thought that this mobile part is more kin to the free porewater (not affected by electrostatic effects / charged clay surfaces and interlayers). One method implies high-pressure deformation and destruction of the rock fabric to squeeze porewater, the other applies large hydraulic gradients and an artificial porewater to displace the in situ porewater. The two methods are therefore quite contrasting regarding the mechanism of extraction, and some method-specific artefacts may be expected. Most significant for porewater composition are the squeezed aliquots at lowest pressures (Tabs. 4.6-3 and 4.6-4) and the first 1 – 3 small sample aliquots from advective displacement (Tab. 4.7-15, average of first 2 aliquots, Appendix B for all data). Here, a more in-depth discussion is provided compared to the method-specific data presentation.

On close inspection of squeezing (SQ) data (Section 4.6) and advective displacement (AD) data (Section 4.7) the following differences and similarities are obvious or may be derived:

- Chloride concentrations from AD and SQ samples do not suggest significant gradients across «Brauner Dogger» and Opalinus Clay, but a slight curvature with a maximum at the top of the Opalinus Clay: AD samples from Opalinus Clay range from 7'650 – 8'350 mg/L (Tab. 4.7-15), and SQ samples from 6'170 – 7'290 mg/L (Tab. 4.6-4). The SQ aliquots are therefore significantly less saline than the AD aliquots by ~ 15% (Fig. 5.2-1). This is a similar situation as observed for BUL1-1 samples (Mazurek et al. 2021) and TRU1-1 samples (Aschwanden et al. 2021). Further below along the profile, Cl decreases steeply in the Staffelegg Formation towards the inferred Keuper aquifer, also captured by SQ and AD samples. The situation is similar for Br concentrations, and the Br/Cl ratios are the same for AD, SQ and aqueous extract samples (Figs. 5.2-3 and 5.2-4).
- Sulphate concentrations from the same clay-rich section as for chloride are quite similar for AD and SQ samples and are gradually increasing from 1'250 – 1'470 mg/L at the top of the «Brauner Dogger» to 1'980 – 2'150 mg/L at the base of the Opalinus Clay. Sulphate concentrations further increase across the Staffelegg Formation (where chlorinity is concomitantly decreasing) to 2'300 – 2'500 mg/L at its base, and even further to a maximum value in the profile of 4'600 – 4'800 mg/L at the base of the Klettgau Formation/top of Bänkerjoch Formation. The sulphate concentrations in the groundwater samples of the Keuper aquifer from the TRU1-1 borehole are quite similar (also in chlorinity) to what might be inferred from AD and SQ samples encountered in this profile.
- Because the sum of anion charge in SQ samples is ca. 15% smaller than that in AD samples, also the sum of cations is 15% smaller. A comparison value-by-value is therefore not meaningful, and approximately all cation concentrations in SQ samples are smaller than those in AD samples (except for K; Fig. 5.4-2). Ca concentrations are similar, and therefore Ca is enriched in SQ samples relative to Cl and compared to AD samples. This – and also due to the higher pH values in SQ sample – is reflected in generally higher degrees of calcite supersaturation in SQ samples vs. AD samples. Potassium is more concentrated in SQ samples, in contrast to other cations, and this is not understood.

- The carbonate system (details in Sections 4.6, 4.7 and 5.5) in SQ samples squeezed at lowest pressures is characterised by pH values of 8.3 – 8.7, strong supersaturation with respect to calcite (SI 0.8 to 1.5), and a low calculated partial pressure of CO_2 ($\log(pCO_2)$: -3.2 to -4.2, in bar; Tab. 4.6-5). pH values from first AD aliquots range from 6.7 – 7.5, SI values of calcite are 0.1 to 0.8 and $\log(pCO_2)$ in bar ranges from -1.8 to -2.6 (Tab. 4.7-16).
- Dissolved organic carbon contents in SQ samples range from 95 – 190 mg/L in aliquots squeezed at lowest pressures (Tab. 4.6-4), and those measured in AD samples are much higher, ranging from 140 – 800 mg/L (Tab. 4.7-15).
- Saturation indices for celestite are at or slightly above saturation for AD samples (0.09 to 0.40; Tab. 4.7-16), and slightly below saturation for SQ samples (-0.09 to -0.49). This difference is a consequence of the distinctly lower Sr concentrations measured in SQ aliquots but quite similar concentrations for sulphate. The saturation indices for gypsum are below saturation in both datasets, except for AD samples from the Klettgau and Kaiseraugst Formations that are somewhat above gypsum saturation (0.20 to 0.28), and SQ samples from the Bänkerjoch Formation (0.12 to 0.14; Tab. 4.6-5).
- Calculated chloride-accessible porosity fractions obtained from AD samples are 0.46 and 0.43 for Opalinus Clay, 0.60 for a sample from the Wedelsandstein Formation (only 29 wt.-% clays, 45 wt.-% quartz) and 0.52 for a sample from the «Parkinsoni-Württembergica-Schichten» (38 wt.-% clays, 19 wt.-% quartz; Tab. 4.7-17, Fig. 5.1-3). Cl-accessible porosity fractions of 0.44, 0.44 and 0.46 were obtained from squeezing data for Opalinus Clay, and 0.49 for a sample from the Wedelsandstein Formation (56 wt.-% clays, 23 wt.-% quartz) and 0.51 for a sample from the «Parkinsoni-Württembergica-Schichten» (50 wt.-% clays, 21 wt.-% quartz; Tab. 4.6-7, Fig. 5.1-3). There is a perfect match for Opalinus Clay, and a spread correlating with the clay-mineral content in the others.
- One AD sample from the upper Staffelegg Formation with a relatively low clay content yields a chloride-accessible porosity fraction of 0.63 (33 wt.-% clays, 8 wt.-% quartz, 51 wt.-% calcite), another from the lowermost Staffelegg Formation yields a fraction of 0.45 (59 wt.-% clays, 24 wt.-% quartz, 6 wt.-% calcite; Tab. 4.7-17, Fig. 5.1-3). A single, very clay-rich SQ sample from the lower Staffelegg Formation (84 wt.-% clays, 15 wt.-% quartz) results in an accessible porosity fraction of 0.42 (Tab. 4.6-7, Fig. 5.1-3).
- An AD sample from the lowermost Klettgau Formation yields an anion-accessible porosity fraction of 0.54 (56 wt.-% clays, 24 wt.-% quartz, calcite below detection limit; Tab. 4.7-17, Fig. 5.1-3). A very nearby SQ sample from the top of the Bänkerjoch Formation yields a fraction of 0.46 (57 wt.-% clays, 9 wt.-% quartz, 20 wt.-% dolomite), and a sample from the lower Bänkerjoch Formation yields 0.55 (64 wt.-% clays, 14 wt.-% quartz, 14 wt.-% dolomite; Tab. 4.6-7, Fig. 5.1-3). The two SQ samples represent relatively dolomite-rich claystone samples, a lithology normally not encountered in the clayey sequence above the Keuper aquifer.
- An AD sample from the Kaiseraugst Formation gives a chloride-accessible porosity fraction of 0.57 (30 wt.-% clays, 8 wt.-% quartz, 57 wt.-% calcite), quite similar to a SQ sample with a fraction of 0.53 (56 wt.-% clays, 14 wt.-% quartz, 18 wt.-% calcite).
- It is interesting to note that the difference of 15% (on average) in chloride concentration of the aliquots (AD vs. SQ, see second bullet point above) does not lead to different Cl-accessible porosity fractions (best seen in well-defined Opalinus Clay samples, also mentioned in Section 5.1), despite that both methods relate the extracted aliquots to the same basis, namely the initial bulk porewater concentration. The SQ samples therefore also contain systematically less Cl in the bulk reconstructed from mass balance, in comparison to AD samples and regular aqueous extracts of PW samples.

- An as-yet enigmatic feature is the liberation of substantial nitrate concentrations in early aliquots from advective displacement experiments, most obvious in those of the Staffelegg Formation (7 – 9 g/L), but also those from deeper samples (3 g/L, 0.3 g/L), as well as in a much more subdued way in «Brauner Dogger» and Opalinus Clay samples (20 – 90 mg/L; Tab. 4.7-15). This is not seen in sample aliquots obtained from squeezing.

5.9.3 Dependence of chloride-accessible porosity fraction on lithology

The sum of previous work using porewater squeezing, advective displacement and through-diffusion data to obtain the chloride-accessible porosity fraction has demonstrated that there is no simple relationship between this fraction and some simple mineralogical parameters such as the clay-mineral content to cover all rock types encountered. Clearly, there are other factors of importance, such as the geometry of the pore network and pore connectivity as well as textural factors such as clay distribution. There is a relatively poorly defined correlation between a decreasing clay-mineral content and an increasing chloride-accessible porosity fraction at clay-mineral contents below 40 wt.-% (TRU1-1) or 20 wt.-% (BUL1-1). Based on this, a simple model was used for BUL1-1 samples (Mazurek et al. 2021), using a constant fraction at clay-mineral contents > 20 wt.-% matched to averaged data from AD, SQ and through-diffusion (0.52), and a linear extrapolation to 1.0 with clay-mineral contents decreasing towards 0 wt.-%.

The principle shape of the model was also used for TRU1-1, but here data suggested an increasing trend of anion-accessibility already at clay contents < 40 wt.-%, and the baseline at larger clay contents was constrained by data to be 0.45 rather than 0.52 as used for BUL1-1. There are fewer data available for TRU1-1, and particularly the few diffusion data at low clay contents in fact do not support this extrapolation to zero anion exclusion, indicating an anion-exclusion effect even at very low clay contents < 5 wt.-%, but with significant uncertainties. This may be explained by the effect of clay distribution relative to porewater migration pathways. If clays are arranged along preferential pathways, as is evident in certain clay-bearing limestones, even a small clay-mineral content may have a large leverage on anion exclusion. Such a hypothesis has not yet been tested.

In the absence of more insight into the parameter-dependence of anion exclusion, the same principle model as used for BUL1-1 and TRU1-1 was also adopted for MAR1-1, just with the exclusion effect for clay-rich samples fixed at some average value obtained from SQ and AD data (0.46, no diffusion data are available; Section 5.1, Fig. 5.1-1), and maintaining a cut-off level of 40 wt.-% clay as done for TRU1-1 for a linear extrapolation to zero ion exclusion. This trend is in fact supported by the data, but only to ca. 28 wt.-% clay-mineral content and no measurements below this. As an alternative approach, scaling was also performed based on formation-specific dependencies on the clay-mineral content (Sections 5.1 and 5.2), with trends as illustrated in Fig. 5.1-3 (right) for «Brauner Dogger», Opalinus Clay and Staffelegg Formation, and a comparison of the different scaling variants depicted in Fig. 5.2-2. This approach did not lead to a visibly improved reduction of scatter.

This is presently a limiting factor for the ability to scale the aqueous extract data for chloride and bromide reliably to the water content and the anion-accessible porosity fraction. Some of the 'noise' in the concentration profiles across the otherwise well-defined clayey sequence are thought to be due to differences in this anion-exclusion effect that apparently exist even at comparably high clay-mineral contents. Profiles are much more 'noisy' across the «Brauner Dogger» and particularly towards the overlying clayey limestones, and this may also be related to the inability of such a simple model to extrapolate reliably to very low clay contents. It is emphasised that the ion-exclusion effect across the Opalinus Clay section is rather well-behaved and well-constrained,

without indication of much variation for the range of encountered clay-mineral contents. The scaling for Opalinus Clay is essentially done by a constant chloride-accessible porosity fraction (0.46 for MAR1-1, 0.45 for TRU1-1, 0.52 for BUL1-1) because clay-mineral contents are almost invariably > 40 wt.-%.

What emerges from the combined BUL1-1, TRU1-1 and MAR1-1 data on chloride-accessible porosity fraction is that particularly in the Wedelsandstein Formation and the (upper) part of Staffelegg Formation significant differences exist in anion exclusion at short depth-scale. While heterogeneity in the clay-mineral content and quartz content is substantial in the Wedelsandstein Formation and correlates to some extent with these observed differences, the Staffelegg Formation is more consistently clay-rich and sharp differences in anion exclusion are less plausible just from a simplistic mineralogical point of view. Such a likely small-scale variation in ion-exclusion despite elevated clay-mineral contents is indicated in the top part of the Staffelegg Formation, where apparent 'outliers' in chloride concentration (assuming constant scaling) are located in profiles of MAR1-1, TRU1-1 and also BUL1-1. This stratigraphic level also marks the onset of much steeper gradients in chlorinity across the deeper parts of the Staffelegg Formation to the Keuper aquifer.

6 Final remarks and main conclusions

RWI team

Borehole MAR1-1 was the first one for which we faced obstructions by the COVID-19 pandemic happenings that started during March 2020. Work proceeded normally to a depth of 612 m (uppermost Opalinus Clay) with a last sample transport on March 16, 2020. The University of Bern stopped most activities on March 27, and so we had to halt sample processing, but were able to complete the stack of samples already in progress, concluding ongoing measurements and maintaining advective displacement experiments. To minimise the risk of data loss or a diminished data quality, it was decided to delegate a critical section across the Opalinus Clay and Staffelegg Formation to Hydroisotop GmbH for diffusive exchange measurements for the stable water isotopes. Other samples were kept in cold storage at Nagra. Sample shipments to the University of Bern were resumed April 27, 2020, and sample processing was possible as planned from then onwards but complicated by the COVID related safety precautions. This implies that the section across Opalinus Clay (removed March 19 from the drill site) experienced approximately an extra month of cold storage time compared to normal operations. This is similar for the section across the Staffelegg Formation that was removed March 20, 2020, from the drill site, followed by borehole testing until mid-May 2020. There is no indication that data quality may have suffered from this longer storage time.

A change in sample preparation procedures was invoked for the borehole section below the clayey sequence (below the Staffelegg Formation). Up to now, hands-on subsampling and sample processing was performed with active participation by an experienced staff scientist from the RWI team, supported by staff members from the analytical laboratory. From this point onwards, sample processing was performed by a supervised team of well-trained M.Sc. students in order to relieve some of the workload that became too heavy for the senior team members, with an increasing number of simultaneous boreholes, sampling and data processing.

This borehole experienced unusually large and persistent losses of drilling mud related to two fracture zones, one in the Schinznach Formation (868 – 887 m) and one at the transition of the Schinznach Formation to the Zeglingen Formation (932 – 943 m). This led to technical difficulties, some delays, some core loss and the use of Na-silicate drilling mud to replace the exhausted supplies of K-silicate mud. There is no indication that these difficulties had an adverse effect on sample quality or data quality.

The average clay-mineral content of the Opalinus Clay is 57 ± 8 wt.-%, a typical value when compared with other locations. Given the dense sample spacing (typically 6 m), specific depth trends of various parameters within the formation were identified, presumably correlating with depositional cycles. Boundaries of sub-units within the Opalinus Clay as defined by lithostratigraphic core logging generally correlate with discontinuities or trend reversals, best seen for water content and the ratio quartz/clay minerals. Systematic depth trends can also be seen in the Staffelegg Formation. In contrast, less systematic depth trends in mineralogy or water content are observed in the «Brauner Dogger». The composition of the clay-mineral fraction within the Opalinus Clay is remarkably constant. In the overlying «Brauner Dogger» the ratio illite/kaolinite sharply increases and then decreases across the Wedelsandstein Formation and remains low towards the top of the unit.

Porosity of all rock units increases with the clay-mineral content, but the correlation is far from perfect, meaning that parameters other than the clay-mineral content also affect the porosity of a rock sample. In particular, a number of highly porous samples with low clay-mineral contents are found in dolomite-rich lithologies. These were affected by dolomitisation and diagenetic dissolu-

tion to some degree. Thus, their porosity is not the result of compaction and cementation alone. Porosities calculated from diffusive-exchange experiments are systematically larger than those obtained from water-loss measurements and pycnometry. The correlation between water-loss porosity and pycnometer porosity is quite good, with the latter being slightly smaller than the former, on average.

A total of 86 aqueous extracts were performed from the lower Malm to Permian section, and 10 samples (deepest Schinznach Formation and Zeglingen Formation) were reanalysed for chloride content (aqueous extracts, matched to an already known water content). The reanalysis was deemed necessary due to sample heterogeneity that yielded a large spread in water contents (5 samples) obtained from triplicate samples, and an accordingly large error bar for chloride contents scaled to water content or chloride-accessible porosity. Eight samples (anhydrite rocks of Bänkerjoch Formation, dolostones of Schinznach Formation and Zeglingen Formation) were declared as potentially contaminated because they showed elevated concentrations of some components indicative of K-silicate mud: diminished Na/K, elevated Si and pH. In all cases, this contamination does not affect major or critical components such as Cl, Br, SO_4, or the Br/Cl ratio. This contamination was likely caused by some inadvertent contamination by rim material, or in case of porous dolostones, drilling fluid may also have penetrated deeper than normally expected.

The porewater profile of stable isotopes obtained by the diffusive-exchange method was seamlessly pieced together from a top section and a lower section measured at the University of Bern, and a section across the Opalinus Clay and the Staffelegg Formation measured at Hydroisotop GmbH. It is quite similar to the profile obtained from the TRU1-1 borehole but reaches all the way to the top of Permian strata. The isotope composition of the groundwater collected in the «Felsenkalke» + «Massenkalk» (Malm aquifer) plots slightly to the right of the GWML in the δ^2H range of modern recharge. Interestingly, 110 m deeper at the base of the Villigen Formation, porewaters are distinctly enriched in ^2H and ^{18}O and their isotope composition plots far to the right of the GMWL. The significance of the groundwater in the «Felsenkalke» + «Massenkalk» for the evolution of porewater $\delta^{18}O$ and δ^2H values further down in the sequence cannot be assessed owing to the lack of porewater isotope data in the upper Malm. The porewater isotope composition shows a continuous evolution in $\delta^{18}O$ and δ^2H from the base of the Villigen Formation to the base of the Staffelegg Formation, starting with $\delta^{18}O$ and δ^2H porewater values far to the right of the Global Meteoric Water Line towards values that fall on the GMWL in the lower parts of the Staffelegg Formation. This suggests a significant meteoric component in the latter porewaters. The pronounced deviation of the porewater $\delta^{18}O$-δ^2H signatures with respect to the Global Meteoric Water Line in the upper part of the section indicates long residence times of these porewaters, with values affected by exchange with groundwater in over- and underlying water-conducting zones, and possibly by water-rock interactions. The evolution of the isotope signatures from the Villigen Formation down to the base of the Staffelegg Formation is dominated by exchange with groundwater in the underlying water-conducting zones. The $\delta^{18}O$ and δ^2H profiles with their negative excursions in the Klettgau Formation suggest the presence of mobile groundwater at these depths (inferred Keuper aquifer). Similar to the porewater at the base of the Staffelegg Formation, isotope signatures of porewater in the Klettgau Formation and in most of the Bänkerjoch Formation also plot along the GMWL indicating the presence of a dominant meteoric component. The $\delta^{18}O$ and δ^2H values of these porewaters are heavier than those of modern recharge. At the base of the Bänkerjoch Formation and in the Schinznach Formation the groundwater and porewater still fall on the GMWL, however, they show distinctly more negative $\delta^{18}O$ and δ^2H values than that of modern recharge, indicating infiltration under colder climate conditions. Exchange in the system Keuper – Muschelkalk seems more advanced than the exchange in the system Keuper – Malm further up in the profile, probably due to the rather short distance between the Keuper and the Muschelkalk groundwaters (ca. 100 m). Porewaters in the

underlying Zeglingen and Kaiseraugst Formation again show isotope signatures enriched in ^{18}O and ^{2}H compared the Muschelkalk porewater and plot close to or slightly to the right of the GMWL in the range of modern recharge. This might indicate that they have been modified by exchange with groundwater that has infiltrated under warmer climate conditions.

A chloride-accessible porosity fraction of 0.46 was averaged for samples with clay-mineral contents > 40 wt.-% based on porewater squeezing and advective displacement experiments (no through-diffusion tests were performed). This compares to a value of 0.45 derived for TRU1-1 (including through-diffusion tests) and 0.52 for BUL1-1 (including through-diffusion tests). Values just for Opalinus Clay cluster in a narrow range of 0.42 – 0.46 for Trüllikon and Marthalen for both methods, squeezing and advective displacement. The aliquots squeezed at lowest pressures are systematically less saline than those from advective displacement but yield the same anion-exclusion effect. The simple model adopted to scale chloride and bromide from aqueous extracts to porewater concentration uses a fixed anion-accessible porosity fraction at clay-mineral contents > 40 wt.-%, and a linear extrapolation to full accessibility at zero clay-mineral content. This model was inferred mainly from rather scattered through-diffusion data from BUL1-1 but is less supported by data from TRU1-1 at low clay-mineral contents, and there is no data at low clay-mineral contents (< 28 wt.-%) for MAR1-1. How exactly the anion-exclusion effect depends on some measurable parameters is not yet understood: it is a more complex issue than just a dependence on mineralogy. An alternative approach with Formation-specific dependencies on the clay-mineral content (for «Brauner Dogger» – Opalinus Clay – Staffelegg Formation) was also explored but did not lead to an improved chloride profile with less scatter or jumps.

A consistent Cl profile between the Malm and the inferred Keuper aquifers is obtained from squeezing, advective displacement and aqueous extraction data. Highest Cl concentrations in the upper Opalinus Clay and lower «Brauner Dogger» are 8 – 9 g/L, decreasing upwards and downwards. The curved profile shape with a local minimum at the inferred Keuper aquifer is similar to those derived for the other boreholes of the siting area ZNO (Benken, TRU1-1). The Cl profile in the Klettgau Formation exhibits low concentrations < 1 g/L in the upper part down to about 780 m depth, and increasing from there towards the bottom to ~ 10 g/L. The profile in the underlying Bänkerjoch Formation suggests a slightly decreasing trend but stays well above the unusually low groundwater concentration in the uppermost Muschelkalk. Below this sampled aquifer, the profile shows a tendency of strongly increasing Cl concentrations down to the Zeglingen Formation, where they reach a maximum of ~ 150 g/L. From there, they steadily decrease to ~ 3 g/L in the Dinkelberg Formation and upper Weitenau Formation. The data from the AD and SQ samples in the Kaiseraugst Formation are consistent with AqEx data. Note that the error bars are large, in particular in the Zeglingen Formation, arising from the large uncertainties in water contents in these low porosity rocks combined with the error on the anion-accessible porosity fraction.

The Br/Cl profile reveals a remarkable consistency between the three datasets, aqueous extracts, squeezing and advective displacement, and shows less scatter than the individual Cl and Br profiles due to its independence of a scaling factor to porewater concentration. The Br/Cl profile is remarkably constant in the interval «Brauner Dogger» – Opalinus Clay – Staffelegg Formation, with only a slight upward increase in the «Brauner Dogger», continuing into the Villigen Formation. Br/Cl ratios strongly increase from the Lias/Keuper boundary down to the Schinznach Formation from where they steadily drop, reaching a minimum at the Zeglingen /Kaiseraugst Formation boundary. From there onwards an increasing signal is noted down to the lowest sample in the Weitenau Formation. Note that the Br/Cl ratio of the sampled groundwater in the top Muschelkalk is not compatible with those of the corresponding porewaters (ca. 0.11 in groundwater and > 2.5 in aqueous extracts from surrounding rocks, for 1'000·Br/Cl mol/mol).

The sulphate profile based on aqueous extracts scaled to porewater content reveal somewhat elevated concentrations in the Wedelsandstein and Villigen Formations at the top, followed by a drop at the top of «Brauner Dogger» and a slightly increasing trend with depth across Opalinus Clay, Staffelegg Formation, Klettgau Formation and top of Bänkerjoch Formation (top of anhydrite rocks with no information on porewater sulphate). The highest sulphate levels based on aqueous extraction are observed in the Klettgau, Bänkerjoch and Zeglingen Formations. Below the latter formation, SO_4 concentrations strongly decrease with depth, reaching about 1 g/L in the Weitenau Formation. Above the Zeglingen Formation, also a decreasing trend within the Schinznach Formation towards the sampled Muschelkalk aquifer is observed. Sulphate concentrations based on squeezing and advective displacement yield distinctly lower values in comparison to the data from aqueous extracts scaled to porewater content. The Opalinus Clay and the underlying and overlying clayey units (Staffelegg Formation and «Brauner Dogger») reveal consistent concentrations between squeezing and advective displacement data and a slightly increasing trend with depth, from about 1 g/L to 2 g/L. Conversely, the re-calculated aqueous extraction data exhibit systematically higher and more variable concentrations. The discrepancy between aqueous extraction and squeezing/advective displacement data becomes even larger when anion exclusion is considered (note that the anion-exclusion effect of SO_4 in the considered rocks is not well known and is at least partly off-set by aqueous complexation). A similar discrepancy between squeezing/advective displacement data and aqueous extraction data has been observed for other boreholes, such as Schlattingen-1, BUL1-1, TRU1-1 and in the Mont Terri Rock Laboratory. The reason for this difference in sulphate levels derived from aqueous extraction compared to squeezing/advective displacement is not understood at this stage, in spite of recent systematic efforts with aqueous extraction studies on Opalinus Clay and SEM studies.

Seven samples were analysed for cation exchange capacity and cation occupancy at the University of Bern (Ni-en method, 6 from the clayey sequence, and 1 from the Klettgau Formation), and 20 samples were analysed at PSI (Ni-en for pre-characterisation, CsCl method for final dataset, all from the clayey sequence). The consistency for the cation exchange capacity between the two methods, and also between Ni consumption and the sum of released cations (corrected for porewater contribution) is quite good. It scales with the clay-mineral content. The fractional occupancies (corrected for porewater contribution) are comparable except for K that is significantly larger in the CsCl-extracted tests (as observed for BUL1-1 and TRU1-1), and this may indicate that an additional potassium pool is mobilised, possibly from illite, by the CsCl method. PSI also measured ammonium that is ubiquitously present but at a small fractional occupancy of 0.01 to 0.02. There is a slight increase in Na-occupancy with depth across «Brauner Dogger» – Opalinus Clay – Staffelegg Formation, no variation in Ca and Mg, a slight decrease in K, and a marked decrease in Sr-occupancy.

7 References

Alcala, F.J. & Custodio, E. (2004): Use of the Cl/Br ratio as a tracer to identify the origin of salinity in some coastal aquifers of Spain. *In:* Araguas, F.J., Custodio, E. & Manzano, M. (eds.): 18 SWIM, Cartagena 2004, Spain, 471-497.

Alcala, F.J. & Custodio, E. (2008): Using the Cl/Br ratio as a tracer to identify the origin of salinity in aquifers in Spain and Portugal. Journal of Hydrology 359, 189-207.

Allison, J.D., Brown, D.S. & Novo-Gradac, K.J. (1991): MINTEQA2/PRODEFA2, a geochemical assessment model for environmental systems: Version 3.0 user's manual. Environmental Research Laboratory, Office of Research and Development, U.S. Environmental Protection Agency, 106 p.

Aschwanden, L., Camesi, L., Gimmi, T., Jenni, A., Kiczka, M., Mäder, U., Mazurek, M., Rufer, D., Waber, H.N., Wersin, P., Zwahlen, C. & Traber, D. (2021): TBO Trüllikon-1-1: Data Report – Dossier VIII Rock properties, porewater characterisation and natural tracer profiles. Nagra Arbeitsbericht NAB 20-09.

Aschwanden, L. & Wersin, P. (2020): Experimental study of sulphate in the Opalinus Clay: Results from extraction tests. Nagra Arbeitsbericht NAB 20-17.

Bradbury, M.H. & Baeyens, B. (1998): A physicochemical characterisation and geochemical modelling approach for determining porewater chemistries in argillaceous rocks. Geochim. Cosmochim. Acta 62, 783-795.

Cappa, C.D., Hendricks, M.B., DePaolo, D.J. & Cohen, R.C. (2003): Isotopic fractionation of water during evaporation. Journal of Geophysical Research 108/D16.

Craig, H. (1961): Isotopic variation in meteoric waters. Science 133, 1702-1703.

Davis, S.N., Whittemore, D.O. & Fabryka-Martin, J. (1998): Uses of chloride/bromide ratios in studies of potable water. Ground Water 36/2, 338-350.

Debure, M. & Gailhanou, H. (2019): GD experiment: Experimental study of sulphate in Opalinus Clay. Unpubl. Mont Terri Technical. Mont Terri Project, Switzerland.

Gimmi, T. & Waber, H.N. (2004): Modelling of tracer profiles in porewater of argillaceous rock in the Benken borehole: Stable water isotopes, chloride and chlorine isotopes. Nagra Technical Report NTB 04-05.

Gimmi, T. & Alt-Epping, P. (2018): Simulating Donnan equilibria based on the Nernst-Planck equation. Geochim. Cosmochim. Acta 232, 1-13.

Hadi, J., Wersin, P., Mazurek, M., Waber, H.N., Marques Fernandes, M., Baeyens, B., Honty, M., De Craen, M., Frederickx, L., Dohrmann, R. & Fernandez, A.M. (2019): Intercomparison of CEC method within the GD project. Mont Terri Technical Report TR 2017-06. Mont Terri Project, Switzerland.

Isler, A., Pasquier, F. & Huber, M. (1984): Geologische Karte der zentralen Nordschweiz 1:100'000. Herausgegeben von der Nagra und der Schweiz. Geol. Komm.

Jenni, A., Aschwanden, L., Lanari, P., de Haller, A. & Wersin, P. (2019): Spectroscopic investigation of sulphur-containing minerals in Opalinus Clay. Nagra Arbeitsbericht NAB 19-23.

Kullin, M. & Schmassmann, H. (1991): Isotopic composition of modern recharge. *In:* Pearson, F.J., Balderer, W., Loosli, H.H., Lehmann, B.E., Matter, A., Peters, T., Schmassmann, H. & Gautschi, A.: Applied Isotope Hydrogeology – A Case Study in Northern Switzerland. Studies in Environmental Science 43, Elsevier, Amsterdam, 65-89.

Lorenz, G.D., Pechstein, A. & Stopelli, E. (2021): Borehole MAR1-1 (Marthalen): Fluid sampling and analytical hydrochemical data report. Nagra Arbeitsbericht NAB 21-25.

Mäder, U. (2018): Advective displacement method for the characterisation of porewater chemistry and transport properties in claystone. Geofluids 2018/4, 1-11.

Mäder, U. & Waber, H.N. (2017): Results of advective displacement / multi-component transport experiments from claystone samples of the Schlattingen borehole. Nagra Arbeitsbericht NAB 17-16.

Marques Fernandes, M. & Baeyens. B. (*in prep.*): Sorption measurements of Cs, Ni, Eu, Th and U on rock samples of Opalinus Clay and confining geological units from deep boreholes at the potential siting regions for a deep geological repository for radioactive waste in Switzerland: Jura Ost, Nördlich Lägern and Zürich Nordost. Nagra Technical Report NTB 22-02.

Mazurek, M. (2017): Gesteinsparameter-Datenbank Nordschweiz – Version 2. Nagra Arbeitsbericht NAB 17-56.

Mazurek, M. & Aschwanden, L. (2020): Multi-scale petrographic and structural characterisation of the Opalinus Clay. Nagra Arbeitsbericht NAB 19-44.

Mazurek, M., Oyama, T., Wersin, P. & Alt-Epping, P. (2015): Pore-water squeezing from indurated shales. Chemical Geology 400, 106-121.

Mazurek. M., Al, T., Celejewski, M., Clark, I.D., Fernández, A.M., Kennell-Morrison, L., Matray, J.M., Murseli, S., Oyama, T., Qiu, S., Rufer, D., St-Jean, G., Waber, H.N. & Yu, C. (2017): Mont Terri Project: Mont Terri DB-A Experiment: Comparison of pore-water investigations conducted by several research groups on core materials from the BDB-1 borehole. Technical Report for the Nuclear Waste Management Organization, NWMO-TR-2017-09. (also published as Mont Terri TR 2017-01).

Mazurek, M., Aschwanden, L., Camesi, L., Gimmi, T., Jenni, A., Kiczka, M., Mäder, U., Rufer, D., Waber, H.N., Wanner, P., Wersin, P. & Traber, D. (2021): TBO Bülach-1-1: Data Report – Dossier VIII Rock properties, porewater characterisation and natural tracer profiles. Nagra Arbeitsbericht NAB 20-08.

Millero, F.J. (2014): Physico-chemical controls on seawater. *In:* Holland, H.D. & Turekian, K.K. (eds.): Treatise on Geochemistry 8, 1-18. 2nd ed., Elsevier.

Monnier, G., Stengel, P.T. & Fies, J. (1973): Une méthode de mesure de la densité apparente de petits agglomérats terreux – Application à l'analyse des systèmes de porosité du sol. Ann. Agron. 24.

Morris, A.W. & Riley, J.P. (1966). The bromide/chlorinity and sulphate/chlorinity ratio in sea water. Deep Sea Research and Oceanographic Abstracts 13, 699-705

Naef, H., Büchi, M., Bläsi, H.R., Deplazes, G. & Gysi, M. (2019): Lithology Manual – Lithological description of drill cores and cuttings in Northern Switzerland. Nagra Arbeitsbericht NAB 19-11.

Nagra (2008): Vorschlag geologischer Standortgebiete für das SMA- und das HAA-Lager. Geologische Grundlagen. Nagra Technischer Bericht NTB 08-04.

Nagra (2014): SGT Etappe 2: Vorschlag weiter zu untersuchender geologischer Standortgebiete mit zugehörigen Standortarealen für die Oberflächenanlage. Geologische Grundlagen. Dossier II: Sedimentologische und tektonische Verhältnisse. Nagra Technischer Bericht NTB 14-01.

Parkhurst, D.L. & Appelo, C.A.J. (2013): Description of input and examples for PHREEQC version 3: A computer program for speciation, batch-reaction, one-dimensional transport, and inverse geochemical calculations. No. 6-A43. US Geological Survey.

Pearson, F.J., Arcos, D., Bath, A., Boisson, J.Y., Fernandez, A.M., Gäbler, H.E., Gaucher, E., Gautschi, A., Griffault, L., Hernan, P. & Waber, H.N. (2003): Mont Terri project – geochemistry of water in the Opalinus Clay formation at the Mont Terri rock laboratory. Federal Office for Water and Geology Rep. 5, Bern, Switzerland.

Pietsch, J. & Jordan, P. (2014): Digitales Höhenmodell Basis Quartär der Nordschweiz – Version 2013 (SGT E2) und ausgewählte Auswertungen. Nagra Arbeitsbericht NAB 14-02.

Rufer, D. (2019): Field Manual: Drillcore sampling for analytical purposes. Nagra Arbeitsbericht NAB 19-13.

Rufer, D. & Mazurek, M. (2018): Pore-water extraction and characterization: Benchmarking of the squeezing and adapted isotope diffusive exchange methods. NWMO Technical Report NWMO-TR-2018-14, Nuclear Waste Management Organization, Toronto, Canada.

Thoenen, T., Hummel, W., Berner, U. & Curti, E. (2014): The PSI/Nagra Chemical Thermodynamic Database 12/07. PSI Bericht Nr. 14-04, Paul Scherrer Institut, Villigen, Switzerland.

Tournassat, C., Vinsot, A., Gaucher, E.C. & Altmann, S. (2015): Chemical conditions in clayrocks. *In:* Tournassat, C., Steefel, C.I., Bourg, I.C. & Berrgaya, F. (eds.): Natural and engineered clay barriers. Developments in Clay Science 6, Chapter 3, 71-100. Elsevier.

Van Loon, L.R. & Glaus, M.A. (*in prep.*): Diffusion measurements of HTO, $^{36}Cl^-$ and $^{22}Na^+$ on rock samples of Opalinus Clay and confining geological units from deep boreholes at the potential siting regions for a deep geological repository for radioactive waste in Switzerland: Jura Ost, Nördlich Lägern and Zürich Nordost. Nagra Technical Report NTB 22-01.

Waber, H.N. (ed.) (2020): SGT-E3 deep drilling campaign (TBO): Experiment procedures and analytical methods at RWI, University of Bern (Version 1.0, April 2020). Nagra Arbeitsbericht NAB 20-13.

Wersin, P., Mazurek, M., Waber, H.N., Mäder, U.K., Gimmi, T., Rufer, D. & de Haller, A. (2013): Rock and porewater characterisation on drillcores from the Schlattingen borehole. Nagra Arbeitsbericht NAB 12-54.

Wersin, P., Mazurek, M., Mäder, U.K., Gimmi, T., Rufer, D., Lerouge, C. & Traber, D. (2016): Constraining porewater chemistry in a 250 m thick argillaceous rock sequence. Chemical Geology 434, 43-61.

Wersin, P., Pekala, M., Mazurek, M., Gimmi, T., Mäder, U., Jenni, A., Rufer, D. & Aschwanden, L. (2021): Porewater chemistry of Opalinus Clay: Methods, data, modelling and buffering capacity. Nagra Technical Report NTB 18-01.

Wigger, C. & Van Loon, L.R. (2017): Importance of interlayer equivalent pores for anion diffusion in clay-rich sedimentary rocks. Environmental Science & Technology 51, 1998-2006.